Pyunghwa Peace Kim

Reduction Rates of SiMn Slags from Various Raw Materials

Pyunghwa Peace Kim

Doctoral thesis

◻ **NTNU**
Norwegian University of
Science and Technology

◻ **NTNU**
Norwegian University of
Science and Technology

◼ NTNU

Pyunghwa Peace Kim

Reduction Rates of SiMn Slags from Various Raw Materials

Thesis for the Degree of Philosophiae Doctor

Trondheim, September 2018

Norwegian University of Science and Technology
Faculty of Natural Sciences
Department of Materials Science and Engineering

NTNU
Norwegian University of
Science and Technology

Preface

The present doctoral thesis is submitted to the Norwegian University of Science and Technology (NTNU) as a partial fulfillment of the requirements for the degree of Philosophiae Doctor.

The doctoral work has been carried out at the Department of Materials Science and Engineering (DMSE) at the NTNU, Trondheim with Prof. Merete Tangstad as advisor. This Ph.D project has been made possible due to the financial support by the Research Council of Norway and the partners of the SFI Metal Production (Center for Research-based Innovation), grant number 237738. The SFI Metal Production projects encompass contributions from several industrial partners including ERAMET Norway AS and GLENCORE Manganese Norway.

The main aim of the present research work was to investigate the kinetic information in the SiMn process from the melting of raw materials to the production of metal. The raw materials were provided by ERAMET Norway AS, and the experiments were conducted by the author. Collaboration with two master's projects and an internship project was also part of the thesis work. Microprobe analyses were obtained by collaboration with Morten Peder Raanes (DMSE).

A portion of the thesis work was published via international conferences and journal articles.

Pyunghwa Peace Kim

Trondheim, June 5th, 2018

List of Publications

A. Conferences

- P. P. Kim, J. Holtan and M. Tangstad. "Reduction Behavior of Assmang and Comilog Ore in the SiMn Process". Advances in Molten Slags, Fluxes and Salts: Proceedings of The 10th International Conference on Molten Slags, Fluxes and Salts (MOLTEN 16), Seattle, May 2016. 1285-1292.

- P. Kim, T. Larssen, M. Tangstad and R. Kawamoto. "Empirical Activation Energies of MnO and SiO_2 Reduction in SiMn Slag between 1500 and 1650 °C". Applications of Process Engineering Principles in Materials Processing, Energy and Environmental Technologies, The Minerals, Metals & Materials Society 2017 (TMS 17), San Diego, Feb. 2017. 475-483.

- P. P. Kim, T. A. Larssen and M. Tangstad. "Reduction Rates of MnO and SiO_2 in SiMn Slags between 1500 and 1650 °C". The 15th International Ferroalloys Congress (INFACON 15), Cape Town, Feb. 2018.

B. Journal Articles

- P. P. Kim and M. Tangstad. "Kinetic Investigation of SiMn Slags From Different Mn-Sources". Metallurgical and Materials Transactions B, Vol. 49B, Jun. 2018. 1185-1196.

- P. Kim, T. Larrsen and M. Tangstad. "Reduction Rates of MnO and SiO_2 in SiMn Slags between 1500 and 1650 °C". The Southern African Institute of Mining and Metallurgy (SAIMM), 2018 (Submitted)

- P. P. Kim and M. Tangstad. "The Effect of Sulfur on MnO and SiO_2 Reduction in Synthetic Manganese Silicate Slags". Metallurgical and Materials Transactions B (To be submitted).

But he knows the way that I take;
when he has tested me, I will come forth as gold.
– Job 23:10 –

Men han kjenner den veien jeg fulgte.
Prøver han meg, kommer jeg ut som gull.
– Job 23:10 –

나의 가는 길은 오직 그가 아시나니

그가 나를 단련하신 후에는 내가 정금같이 나오리라.

– 욥기 23:10 –

Acknowledgements

Abstract

The kinetic information in the SiMn (Silicomanganese) process from melting of raw materials to production of metal was investigated in this work. This is of interest for the SiMn production industries where the effect of raw materials in the furnace is not well known and is assumed to give impact to the metal producing rates. The doctoral work comprises experimental investigation of industrial and synthetic SiMn charges, where a TGA (ThermoGravimetric Analyzer) under CO atmospheric pressure was used to simulate the industrial SiMn furnace. The kinetic information was observed and confirmed by considering four subsequent research topics.

First, the melting behavior of raw materials with particle sizes between 4 and 20 mm in SiMn charges was initially investigated mainly between 1200 and 1400 °C. Cross-section images and micro-analyses of two different charge compositions with and without HC (High-Carbon) FeMn (Ferromanganese) slag as raw material were compared to observe the slag forming temperatures. The results from the cross-section images proved that the melting of charges materials and completion of liquid slag occur relatively fast and at low temperatures between 1200 and 1400 °C regardless of particle size and of using HC FeMn slag as raw material. In fact, the contact between manganese sources and quartz was the most important factor during the formation of liquid slag, while the individual melting temperatures of each raw material were of less relation. From the micro-analyses, it was observed that the formation of liquid SiMn slag complies to the binary MnO-SiO$_2$ system regardless of the charge composition. The slag phases were mainly composed of the two manganese silicates, Mn$_2$SiO$_4$ and MnSiO$_3$, which were solidified from liquid SiMn slag.

Second, the reduction behavior of SiMn charges were investigated by comparing FeMn charges as reference between 1200 and 1600 °C. Charges with two different particle sizes, $0.6 - 1.6$ and $4.0 - 6.3$ mm, were also compared to observe the effect of particle size on the reduction rate. It was observed that the reduction of SiMn charges had occurred in two stages, while the reduction of FeMn charges was progressive. The two-stage reduction of SiMn charges involved a slow reduction followed by a rapid reduction, where the dividing temperature was approximately 1500 °C. The effect of particle size for reduction was only observed with FeMn charges, where faster reduction was observed from charge with smaller particle sizes. SiMn charges only contained liquid slag regardless of the particle sizes, which was observed from the experiments of the melting behavior of raw materials. Completion of liquid slag before the second reduction stage had nullified the effect of particle sizes on the reduction rate.

Third, the kinetic information of MnO and SiO$_2$ reduction between 1500 and 1650 °C were obtained by using the following rate models:

$$r_{MnO} = k_{MnO} \cdot A \cdot (a_{MnO} - \frac{a_{Mn} \cdot p_{CO}}{K_{MnO} \cdot a_C})$$

$$r_{SiO_2} = k_{SiO_2} \cdot A \cdot (a_{SiO_2} - \frac{a_{Si} \cdot p_{CO}^2}{K_{SiO_2} \cdot a_C^2})$$

The chemical reactions of MnO and SiO$_2$ reduction were assumed to be the rate-determining steps, where the rate and kinetic parameters were calculated by investigating three different SiMn charges: Charges "As" (Assmang ore + quartz + coke), "As/HCS" (Assmang ore + quartz + HC FeMn slag + coke) and "HCS" (quartz + HC FeMn slag + coke), where the manganese bearing materials are Assmang ore (As) and HC FeMn slag (HCS). It was initially observed that SiMn charges containing HC FeMn slag as raw material had faster and higher reduction rates than charges without HC FeMn slag. The use of HC FeMn slag had the apparent effect of the enhanced reduction rates. From the comparison of the rate and kinetic parameters,

it was observed that the reduction rate of MnO was considerably more influenced by the slag properties from the rate constants rather than the driving force ($a_{MnO} - a_{Mn}/K_{MnO}$). The comparison also indicated that the effect of sulfur as impurity element in the charge was superior than the effect of slag viscosity or amount of iron for enhanced reduction rates. In addition, the two rate models were applicable to describe the changing amount of MnO and SiO_2 in various SiMn slags between 1200 and 1650 °C of different reduction degrees.

Finally, the effect of sulfur for enhanced reduction rates was confirmed by experiments with synthetic SiMn charges. A controlled slag system, MnO-SiO_2-CaO, with different amount of sulfur between 0 and 0.9 wt% was studied between 1500 and 1650 °C. Addition of sulfur into the charge has significantly enhanced the reduction rates of MnO and SiO_2, where the threshold amount of sulfur was approximately 0.3 wt%. Also, it was observed that sulfur does not behaves as a catalyst for MnO reduction but was assumed to influence the reduction rate between slag and dissolved carbon in the metal phase by increasing the wetting between the two phases. Similar observation of the effect of sulfur from iron and steel production studies were compared with this work, where the effect of sulfur was further discussed. In addition, the reduction paths of MnO and SiO_2 in the MnO-SiO_2-CaO system between 1200 and 1650 °C were construed by using the two rate models and experimental measurements. It was observed that the initial direction of the reduction was determined by the SiO_2/CaO ratio, but the reduction degree was determined by the amount of sulfur.

Contents

List of Tables

List of Figures

xiv

List of Symbols and Abbreviations

Symbol	Nomenclature	Unit
a_i	Activity of i	–
K	Equilibrium constant	–
p_i	Partial pressure of gas i	atm
r_i	Reduction rate of i	g/min
k_i	Rate constant of i	g/min·cm^2
A	Reaction interface	cm^2
E_a	Activation energy	kJ/mol
k_o	Pre-exponential constant	g/min·cm^2
$k_{Arr.}$	Rate constant (Arrhenius)	g/min·cm^2
R	Gas constant	J/K·mol

Abbreviations	Nomenclature
FeMn	Ferromanganese
SiMn	Silicomanganese
SAF	Sumbered Arc Furnac
FeSi	Ferrosilicon
HC	High-Carbon
TGA	ThermoGravimetric Analysis
EPMA	Electron Probe Micro-Analyzer
BSE	Back Scattered Electron
DF	Drivnig Force
Arr.	Arrhenius
(C+M) / A	(CaO + MgO) / Al_2O_3

Chapter 1: Introduction

1.1 Manganese ferroalloys

Manganese (Mn) is mainly produced in the form of ferroalloys, such as ferromanganese (FeMn) and silicomanganese (SiMn) in submerged arc furnaces (SAF) [1, 2]. These two types of alloys are consumed as important ingredients in the steel producing industries due to their many contributions [1-9]. Manganese is used as a desulfurizing and alloying unit to enhance the strength, toughness and hardness of steel products. Its reaction with residual sulfur in liquid steel forms manganese sulfide to prevent the formation of iron sulfide, which causes the "Hot-Shortness" phenomena. Manganese addition into steel also stabilize the austenite phase, which is beneficial for refined pearlite structures during quenching. In case of SiMn, both manganese and silicon (Si) serve as deoxidizers to prevent porous steel structures [1-9]. As dissolved oxygen in liquid steel causes porous structures during cooling, manganese and silicon are added to form oxides which remove the dissolved oxygen and separate on the top of the steel melt. Due to silicon being a more effective deoxidizer than manganese, SiMn is more favorable than the separate use of FeMn and ferrosilicon (FeSi). Furthermore, SiMn adds less impurity elements, such as phosphorus, carbon, aluminum and nitrogen to steel compared to FeMn [1, 10]. These facts increase the trend for more use of SiMn than FeMn [1, 2], but the production and demand will mostly be determined by the cost and the steel producing technologies.

There are several types of FeMn and SiMn products depending on their alloy content. The example of a typical high-carbon (HC) FeMn and standard SiMn alloys in different grades is described in **Table 1.1**. Such type of alloy production will be affected by the use of raw materials, production/refining process and specific demands from the consumers.

Table 1.1: Chemical requirements of HC FeMn and standard SiMn of different grades by ASTM International standards [wt%] [10]. Note that iron (Fe) consists the rest of the metal compositions.

Type of alloy	Grade	Mn	Si	C_{Max}	P_{Max}	S_{Max}
	A	78 − 82				
HC FeMn	B	76 − 78	1.2	7.5	0.35	0.05
	C	74 − 76				
	A		18.5 − 21	1.5		
Std. SiMn	B	65 − 68	16 − 18.5	2	0.2	0.04
	C		12.5 − 16	3		

1.2 Raw materials

The main raw materials for FeMn and SiMn production can be divided into four categories: Manganese sources, quartz, fluxes and coke. Manganese sources mainly include various manganese ores, agglomerates and high-carbon (HC) FeMn slag from the FeMn process. HC FeMn slag as raw material is only used in the SiMn process. Frequently used fluxes are carbonates, such as limestone ($CaCO_3$) and dolomite ($CaCO_3 \cdot MgCO_3$).

Depending on the geological origin of manganese ores, manganese is deposited as manganese oxides, hydroxides or carbonates. **Table 1.2** shows the typical chemical composition of some commercial manganese ores. Due to the deposition history of the manganese ores, the chemical composition will differ from ore to ore each having similar yet distinctive characteristics.

Table 1.2: Typical chemical composition of some commercial manganese ores (dry basis) [11]. Note that all manganese ores will contain some iron content.

Mn ore	MnO	MnO_2	SiO_2	Fe_2O_3	CaO	MgO	Al_2O_3	CO_2	P	Total [wt %]
Assmang	37.9	34.7	5.5	14.3	4.3	0.7	0.4	0.8	0.04	98.6
Comilog	4.4	76.0	7.4	5.1	0.2	0.3	5.5	0.1	0.11	99.11
Mamatwan	29.8	23.4	4.0	6.6	14.7	3.5	0.5	17.0	0.02	99.5
Gloria	31.3	23.6	5.7	7.2	12.7	3.8	0.3	15.4	0.02	100
Amapa	22.4	38.0	5.9	18.0	0.3	0.1	8.1	3.5	0.11	96.4

Comilog ores typically contain higher amount of higher manganese oxides (MnO_2) and alumina (Al_2O_3) compared to the other manganese ores. Mamatwan and Gloria ores have more calcia (CaO) content due to the higher amount of carbonates. Assmang and Amapa are relatively high in amount of iron oxides (Fe_2O_3). These different chemical compositions of manganese ores are likely to affect the process and final product. Nevertheless, the metallurgical grade manganese ores, which are used to produce FeMn and SiMn, usually contain manganese content between 35 and 50 wt%. Note that all manganese ores have some iron.

Agglomerates are made from utilizing the fines from the mining and transportation of manganese ores. Considerable amount of manganese is lost as small fines during the transportation and beneficiation process of manganese ores [1, 12]. Undersized materials cannot be directly used in the process of alloy production as fines decrease the permeability of gas and clog the furnace charge [1, 13]. The fines are thus made into sinters, briquettes or pellets through a separate process before it is charged into the furnace. The agglomerates will have different properties compared to the ores, such as melting behavior and porosity [1, 12, 13], and the combination of ores and agglomerates will be optimized depending on the furnace performance [1].

HC FeMn slag is the residual slag which is produced from the FeMn process [1]. The slag can contain high amount of manganese monoxide (MnO) as much as 30 to 50 wt%, which is reused as raw material for the SiMn process in the "Duplex Processing" system [1, 14]. Since HC FeMn slag is produced through the FeMn process, its advantages include lower amount of impurities, especially phosphorous, and lower usage of other fluxes. The "Duplex Processing" system will be further explained in **Section 1.3**.

Besides the land-based manganese ore deposits, the largest manganese resources are located on the bottom of the deep-sea ocean as manganese nodules [1, 2]. Manganese nodules contain up to 30 wt% manganese with some appealing amount of nickel (Ni), copper (Cu) and cobalt (Co) varying in different sizes between 5 and 20 cm. However, the mining technology of deep-sea manganese nodules is still at its infancy and territorial disputes between nations make the mining operation less feasible in the current period [15, 16].

Quartz or quartzite as silicon dioxide (SiO_2) is the main source of silicon for the SiMn process. Fluxes such as limestone and dolomite are used to control the slag viscosity. Metallurgical coke, which is a product from the coking process of coal in absence of air [17], is the typical material used as the carbon reductant in the FeMn and SiMn processes. Other carbon sources can also be used as charcoal, char, coal and petroleum

coke. **Table 1.3** describes a typical chemical composition of quartz, limestone, dolomite and metallurgical coke.

Table 1.3: Typical chemical composition of quartz, limestone, dolomite and metallurgical coke (dry basis).

Material	MnO	SiO_2	Fe_2O_3	CaO	MgO	Al_2O_3	C	CO_2	Total [wt%]
Quartz [18]	0.1	96.9	-	0.1	0.1	1.2	-	-	98.4
Limestone [18]	-	1.0	-	54.0	1.0	0.3	-	47.5	103.8
Dolomite [18]	-	0.1	0.5	31.3	21.1	-	-	47.2	100.2
Coke	-	5.6	0.9	0.4	0.2	2.8	87.7	-	97.6

1.3 Production of FeMn and SiMn

There has been an increasing demand for the more use of SiMn along with FeMn in many countries [1, 2]. This makes the "Duplex Processing" system more attractive, where both FeMn and SiMn production are available based on the access of raw materials. HC FeMn slag as raw material can be reused in the SiMn process to minimize the manganese loss. A simple illustration of the "Duplex Processing" system for FeMn and SiMn production is described in **Figure 1.1**.
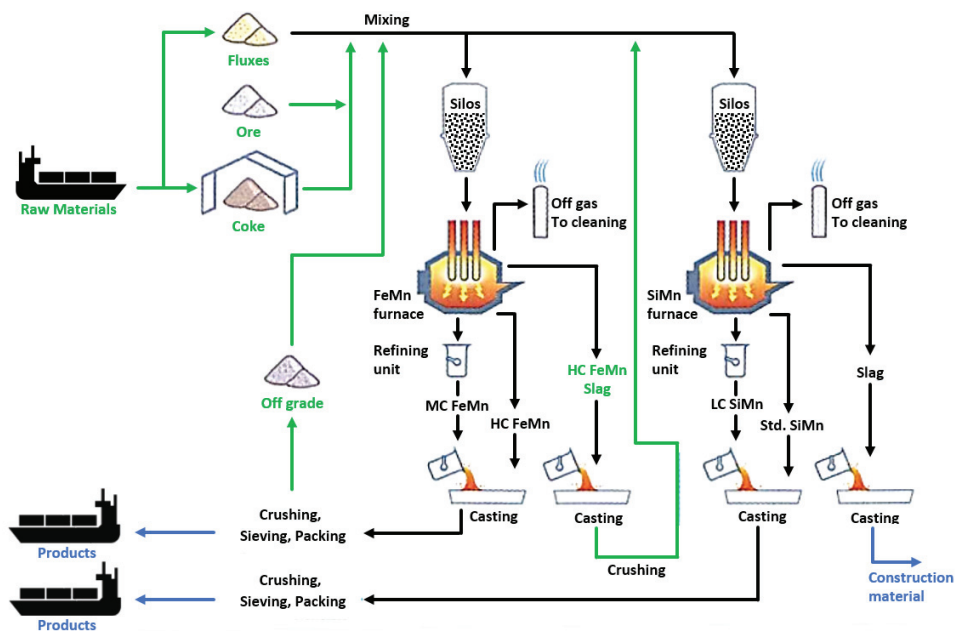
Figure 1.1: Overview of the materials flow in a typical FeMn and SiMn "Duplex Processing" system (re-illustrated) [19]. HC FeMn slag from the FeMn process is reused as raw material in the SiMn process to minimize manganese loss.

The raw materials are initially charged into the FeMn furnace and each amount is controlled according to the product specifications and furnace operation. The process inside the FeMn furnace is complex but can simply be divided into two zones: The pre-reduction zone where raw materials are reduced by ascending hot carbon monoxide (CO) gas, and the high temperature coke-bed zone where metal production occurs [1, 19]. Note that more details regarding the chemistry in the furnace will be further explained in the **Section 1.4**. The tapping of the furnace will give HC FeMn alloy and slag. The initial tapped alloy contains approximately 7 wt% of carbon, but the carbon content can be reduced through separate refining processes [1, 19]. The slag, which still contains high amount of MnO, around 30 to 50 wt% depending on the basicity, is reused as raw material for the SiMn process. The charge materials for SiMn production including HC FeMn slag goes through a similar process inside the SiMn furnace with higher temperatures. Then, the tapping of the SiMn furnace yields standard SiMn alloy, which contains approximately 1 to 2 wt% carbon. The carbon content in the initial standard SiMn alloy can also decrease by going through separate refining processes, and the SiMn slag is further used as construction materials by request. The examples of alloy grades are shown in **Table 1.4**. Note that the refining of HC FeMn and standard SiMn alloys are separate processes and are not included in this study.

Table 1.4: Examples of FeMn and SiMn alloy grade specifications from primary production (HC FeMn and Std. SiMn) and refining (MC FeMn, LC FeMn, LC SiMn and ULC SiMn) [wt%] [1].

Grade	Mn	Si	Fe	C	S	P	Note
HC FeMn	78	0.3	10 − 15	7.5	-	0.20	Primary production
MC* FeMn	80 − 83	0.6	15 − 18	1.5	-	0.20	Refining
LC** FeMn	80 − 83	0.6	15 − 18	0.5	-	0.20	Refining
Std. SiMn	67 − 68	17 − 20	10 − 15	1.5 − 2.0	0.02	0.10 − 0.15	Primary production
LC SiMn	59 − 63	25 − 30	7 − 16	0.1 − 0.5	0.01	0.1	Refining
ULC*** SiMn	58 − 62	27 − 31	7 − 15	0.05	0.01	0.05	Refining

* MC (Medium-Carbon) / ** LC (Low-Carbon) / *** ULC (Ultralow-Carbon)

1.4 Process chemistry

Excavation of FeMn and SiMn furnaces in previous studies had observed that the furnace can be divided into two main zones: Pre-reduction and coke-bed zones [1, 19-22]. The pre-reduction zone is the upper part of the furnace where it consists of pre-reduced solid charge materials, and the coke-bed zone consists mainly liquid slag with coke particles at the lower region. A cross-section illustration of a pilot-scale SiMn furnace dividing the pre-reduction and coke-bed zone is described in **Figure 1.2** [23].
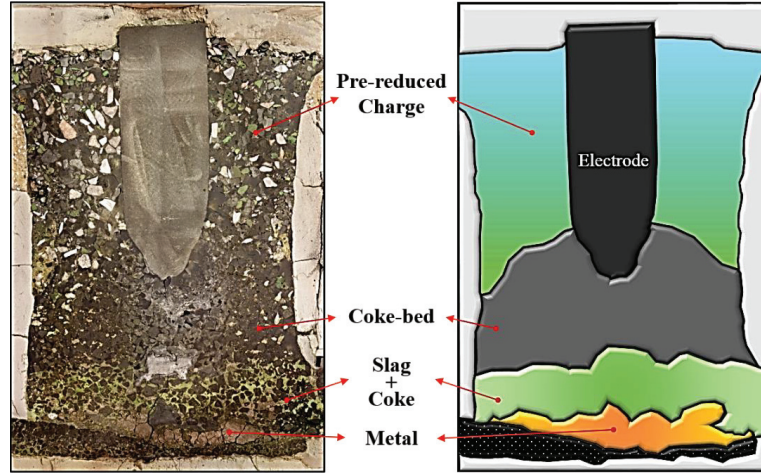
Figure 1.2: Cross-section (left) and sketch (right) of a single electrode pilot-scale SiMn furnace [23]. Pre-reduction zone consists solid charge materials while coke-bed zone mainly consists liquid slag with coke particles.

1.4.1 Pre-reduction zone

The pre-reduction zone is where the charge materials are reduced or decomposed by ascending CO gas and heat from the high temperature coke-bed zone. The temperature at the top part of the pre-reduction zone will vary depending on the furnace performance but it is typically between 200 and 600 °C for closed furnaces [1, 19, 21]. When the raw materials enter the furnace, evaporation of moisture in raw materials will take place. Since the evaporation of water is endothermic, **Reaction (1.1)** [1], the total power consumption will increase with more moisture content in the raw materials.

$$H_2O_{(l)} = H_2O_{(g)} \qquad \Delta H^{\circ}_{298\,K} = +44.0\ kJ \qquad \textbf{(1.1)}$$
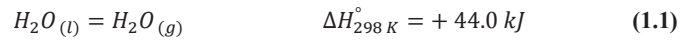
As the charge materials descend towards the coke-bed zone, decomposition of fluxes will also occur. The energies associated with the decomposition of limestone ($CaCO_3$) and dolomite ($CaCO_3 \cdot MgCO_3$) are described in **Reactions (1.2)** and **(1.3)** [1].

$$CaCO_{3\,(s)} = CaO_{(s)} + CO_{2\,(g)} \qquad \Delta H^{\circ}_{298\,K} = +178.3\ kJ \qquad \textbf{(1.2)}$$

$$CaMg(CO_3)_{2\,(s)} = CaO \cdot MgO_{(s)} + 2CO_{2\,(g)} \qquad \Delta H^{\circ}_{298\,K} = +295.4\ kJ \qquad \textbf{(1.3)}$$

The decomposition of these carbonates are also endothermic reactions. Thus, increasing amount of fluxes in the furnace process will increase the power consumption. In carbon dioxide (CO_2) atmospheric pressure ($p_{CO_2} \approx 1atm$), the approximate temperatures for decomposition of limestone and dolomite are 900 and 600 °C, respectively.

The reaction of manganese ores with ascending hot CO gas mainly represents the pre-reduction zone. Manganese sources are mainly composed of higher manganese oxides (MnO_x: x =1.33, 1.5 and 2) with

relatively smaller amount of iron oxides (Fe_2O_3). The relating reactions are described in **Reactions (1.4), (1.5), (1.6) and (1.7)** [1]. An illustration of the solid-state reduction of manganese ore with ascending CO gas is described in **Figure 1.3**. The main part of the reduction of higher manganese oxides reacts topochemically, where the diffusion of CO and CO_2 gas will be the rate-determining steps after the initial reaction.

$$MnO_{2\,(s)} + \frac{1}{2}CO_{(g)} = \frac{1}{2}Mn_2O_{3\,(s)} + \frac{1}{2}CO_{2\,(g)} \qquad \Delta H^\circ_{298\,K} = -99.9\,kJ \qquad (1.4)$$

$$\frac{1}{2}Mn_2O_{3\,(s)} + \frac{1}{6}CO_{(g)} = \frac{1}{3}Mn_3O_{4\,(s)} + \frac{1}{6}CO_{2\,(g)} \qquad \Delta H^\circ_{298\,K} = -31.3\,kJ \qquad (1.5)$$

$$\frac{1}{3}Mn_3O_{4\,(s)} + \frac{1}{3}CO_{(g)} = MnO_{(s)} + \frac{1}{3}CO_{2\,(g)} \qquad \Delta H^\circ_{298\,K} = -6.9\,kJ \qquad (1.6)$$

$$\frac{1}{2}Fe_2O_{3\,(s)} + \frac{3}{2}CO_{(g)} = Fe_{(s)} + \frac{3}{2}CO_{2\,(g)} \qquad \Delta H^\circ_{298\,K} = -12.9\,kJ \qquad (1.7)$$
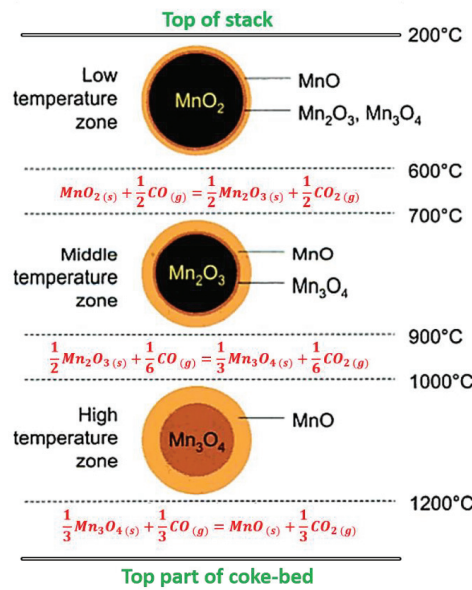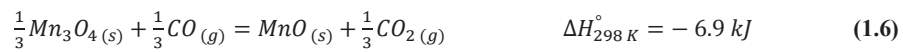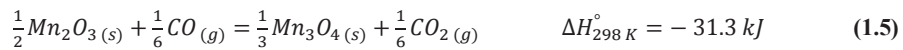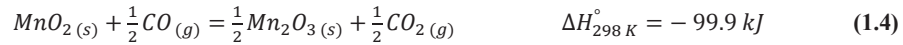
Figure 1.3: Illustration of a progressive solid-state reduction of manganese ore with ascending CO gas in the pre-reduction zone (re-illustrated) [1]. Main part of the reduction of higher manganese oxides reacts topochemically: After the initial reaction, the diffusion of CO and CO_2 gas will be the rate-determining steps.

The pre-reduction of manganese ores are exothermic reactions, which will produce considerable amount of heat. Therefore, manganese ores with higher oxygen ratio, such as Comilog ore, are likely to contribute to reduce the total energy consumption of the process. However, the Boudouard reaction [17], which is shown in **Reaction (1.8)**, should also be considered when the temperature has reached higher than 800 °C. The CO_2 gas from **Reaction (1.6)** will consume coke where the reaction becomes rapid at higher temperatures.

Combining **Reactions (1.6)** and **(1.8)** is the overall reaction of Mn_3O_4 reduction, **Reaction (1.9)**, which is an endothermic reaction [1].

$$\frac{1}{3}C_{(s)} + \frac{1}{3}CO_{2\,(g)} = \frac{2}{3}CO_{(g)} \qquad \Delta H^{\circ}_{298\,K} = +57.5\,kJ \qquad \textbf{(1.8)}$$

$$\frac{1}{3}Mn_3O_{4\,(s)} + \frac{1}{3}C_{(s)} = MnO_{(s)} + \frac{1}{3}CO_{(g)} \qquad \Delta H^{\circ}_{298\,K} = +40.5\,kJ \qquad \textbf{(1.9)}$$

While most iron oxides can be reduced into metallic iron by ascending CO gas during the pre-reduction zone, the reduction of MnO with CO gas is not likely to occur. The stability of MnO is higher than iron monoxide (FeO), and more energy is required to reduce MnO [1, 17, 19]. Beyond the pre-reduction zone where the temperature is higher than approximately 1250 ºC, melting of raw materials will occur and further reduction of MnO and SiO_2 (in case of SiMn process) takes place in the high temperature coke-bed zone from liquid slag. The pre-reduction zone for the FeMn and SiMn process is similar while the coke-bed zone will differ in process chemistry and temperature.

1.4.2 Coke-bed zone

The carbothermic reduction of MnO and SiO_2 occurs in the high temperature coke-bed zone where the temperature is assumed to be higher than 1250 ºC [1, 19, 22, 24]. The metal producing reactions are described in **Reactions (1.10)** and **(1.11)** [1, 19, 20]. In the FeMn process, the reduction of MnO will be the main focus, whereas both MnO and SiO_2 reduction are considered in the SiMn process.

$$MnO_{(l)} + C = Mn_{(l)} + CO_{(g)} \qquad \Delta H^{\circ}_{298\,K} = +252.3\,kJ \qquad \textbf{(1.10)}$$

$$SiO_{2\,(l)} + 2C = Si_{(l)} + 2CO_{(g)} \qquad \Delta H^{\circ}_{298\,K} = +754.9\,kJ \qquad \textbf{(1.11)}$$
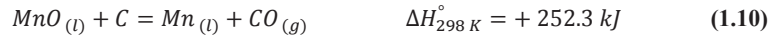
Both reactions imply that considerable amount of electrical energy is required to produce manganese and silicon metal. Generally, the process consumes approximately 70 % of the supplied electric energy for metal production, while the rest is lost in the electrical equipment and as heat loss through the furnace walls [1, 25]. The energy is mainly generated from the electrical resistance of the flowing current between the electrodes and solid/liquid charge materials. Note that most of the current will run through the coke-bed zone due to the large difference in electrical resistivity of the two zones.

Initially, melting of charge materials occurs at the top part of the coke-bed to produce an initial slag phase containing solid coke particles. The temperature is assumed to be higher than 1250 ºC. Recent studies had observed that most of MnO and SiO_2 reduction occurs at the top part of the coke-bed close to the melting of raw materials [20, 22, 23]. Then, the remaining slag and produced metal continuously flow down into the coke-bed, whereas the coke particles will deposit on the top of the coke-bed. The bottom part of the coke-bed will contain more slag than the top layer. A layer of metal is beneath the coke-bed due to the density difference of slag and metal. Previous and recent excavations also observed that coke particles are present in the slag layer due to the weight of the charge materials above [20, 22, 23-28].

1.5 Thesis outline

The main purpose of this thesis is to increase the knowledge and understanding of the kinetic information in the SiMn process by experimental work. More specifically, the research involves the observation of raw materials during melting into liquid slag, the development of a method for measuring the rate of MnO and SiO_2 reduction and pinpointing the crucial aspects by obtained kinetic information. The overall objective is to observe how the raw materials influence the production rate of SiMn alloy.

Chapter 2 will focus on the theoretical background and previous studies related to this work. Details regarding melting of raw materials, manganese thermodynamics and kinetics for manganese ferroalloy production of previous studies are reviewed. In addition, the objectives of this work and four research topics based on the summary of previous studies are described.

Chapter 3 shows the experimental set-ups and procedures of four main research topics: Melting behavior or raw materials, reduction behavior of different SiMn charges, kinetic measurements and confirmation by using synthetic materials. The experimental procedures and conditions are similar among the four main activities, but details are explained separately in this chapter. The parallel studies related to this work are also described.

Chapter 4 presents the experimental results of the four main research topics observed in this study. Several images of the melting of raw materials are shown and the measured weight change from different SiMn charges are described as a function of time and temperature. Then, the reduction behavior between FeMn and SiMn charges are compared from different experimental conditions. The estimation of kinetic information from industrial SiMn charges are also shown in this chapter along with the results from synthetic SiMn charges. Lastly, the results of the parallel studies are described where comparison with this work is made.

Chapter 5 discusses the experimental methods and results of this work. The melting phenomena of raw materials, estimated information from kinetic calculations and validation of methods are discussed, where the critical information is highlighted. The relation between the kinetic information obtained from this work and the industrial furnace is also discussed, where the materials flow with process temperatures and locations in the furnace is illustrated. The effect of sulfur on the reduction rate of MnO is further discussed by comparing the studies of recent iron and steel production and by applying the transition state theory.

Chapter 6 finalizes the main conclusions of the thesis. Key points from the four research topics are summarized in the final chapter. Recommendations for further work are also included.

Chapter 2: Theoretical Background

The following chapter reviews the theories and previous studies related to thermodynamics and kinetics of FeMn and SiMn production. The thermodynamics part mainly consists the SiMn metal and slag systems. The previous studies of raw materials melting are also included. The kinetics section will discuss the rate models, slag viscosity and effects of iron and sulfur based on the findings from previous studies.

2.1 Thermodynamics of FeMn and SiMn production

The thermodynamics of FeMn and SiMn production were studied extensively over the last three decades. In this section, previous studies of the SiMn metal and slag systems, melting of raw materials and the equilibrium distribution of manganese and silicon are summarized and reviewed.

2.1.1 Stability of manganese oxides

The stability relation for the reduction of MnO with carbon is the initial information which should be considered to understand the thermodynamics of FeMn and SiMn production. **Figure 2.1** describes the calculated equilibrium relations in the Mn-C-O system.
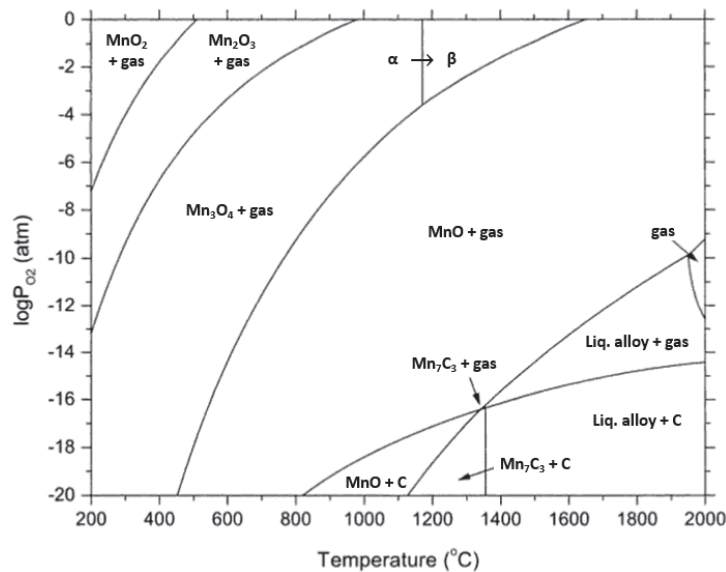
Figure 2.1: Calculated equilibrium relations in the Mn-C-O system [1]. Lowest temperature to produce carbon saturated liquid manganese metal is approximately 1370 °C at $p_{O_2} \approx 10^{-16}$ atm.

In industrial furnaces where carbon is present, the oxygen partial pressure is very low, and the total pressure is $p_{Tot.} \approx p_{CO} = 1\ atm$. This implies that the lowest temperature to produce carbon saturated liquid manganese metal is around 1370 °C at an oxygen partial pressure of $p_{O_2} \approx 10^{-16}\ atm$. An oxygen partial pressure lower than this is not achievable by using CO gas in equilibrium with solid carbon. This

indicates that the thermodynamic option to reduce MnO with carbon is in the liquid state. Thus, the solid-state reduction of MnO with CO gas to form solid manganese metal is not thermodynamically feasible. In addition, **Figure 2.1** also shows that manganese ores with higher oxides will be reduced by CO gas with increasing temperatures. When the oxygen partial pressure is $p_{O_2} \approx 10^{-16}\ atm$, reduction of manganese ores to MnO can be expected at around 600 °C.

2.1.2 The SiMn metal systems

As the main components in SiMn alloys are manganese and silicon, the binary Mn-Si system is shown in **Figure 2.2**. The Fe-Mn system of FeMn alloy is also shown for comparison of the two manganese ferroalloys. One of the main differences between the two systems is the solidified metal product. While both alloys show complete miscibility in the liquid state, FeMn shows a wide range of solid solution while SiMn shows several intermetallic compounds when solidification occurs. This implies that analyzing metal composition for SiMn by scanning electron microscope (SEM) or electron probe micro-analyzer (EPMA) can be difficult due to its many intermetallic compounds.
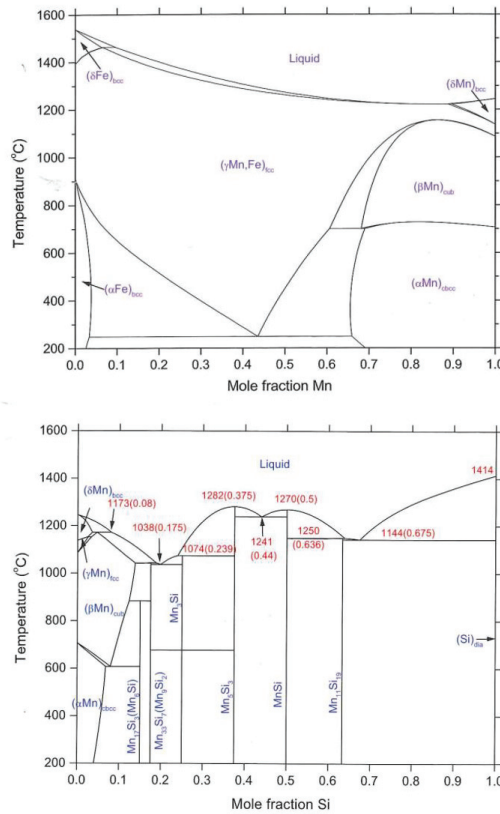
Figure 2.2: Fe-Mn system (top) and Si-Mn system (bottom) [1]. Main difference between the two alloys is the solidified product: A wide range of solid solution for FeMn and several intermetallic compounds for SiMn.

The carbon concentration in the metal phase is important as the production of standard SiMn alloy will consist approximately of 2 wt% carbon depending on the silicon content. There are limited studies on the carbon dissolution kinetics in manganese ferroalloys, but a recent work had observed that the dissolution kinetics of carbon in FeMn with different manganese content were similar with iron [29]. Previous studies of carbon dissolution in liquid iron up to saturation had observed that it occurs relatively fast [30-33]. Manganese is similar with iron and the carbon dissolution is also assumed to reach saturation relatively fast. The Mn-Si-C ternary system at 1500 °C is shown in **Figure 2.3**.
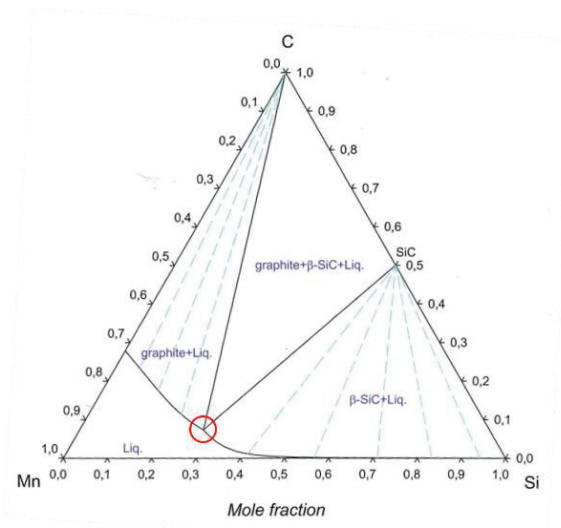
Figure 2.3: Calculated phase relations in the Mn-Si-C system at 1500 °C [1]: Red circle indicates the point where carbon will exist both as graphite and silicon carbide, where the silicon content will determine the carbon stability.

The phase relations at 1500 °C show that the silicon concentration in the metal determines the saturation content of carbon. The saturation phase of carbon changes from graphite to silicon carbide (SiC) as the silicon content in the metal increases. The red circle in **Figure 2.3** shows an example where it indicates the point when carbon is presented as both graphite and silicon carbide. This implies that build-up of silicon carbide can occur with increasing amount of silicon concentration in the metal system, and vice versa with lower silicon content [34, 35].

The previous studies on the solubility of carbon in the Mn-Si-C system between 1400 and 1600 °C are shown in **Figure 2.4** [1, 36-42]. The measured results showed good corresponding fit with the calculated data. This implies that the stability of carbon as graphite increases with increasing temperature at constant amount of silicon. Based on this proposition, the calculated carbon solubility at various temperatures between 1200 and 2400 °C is also shown in **Figure 2.4**. The temperature of the metal is approximately between 1550 and 1650 °C for typical SiMn production [1, 19, 22, 43]. This implies that the silicon content is approximately 18 wt% in the metal when carbon coexists as both graphite and silicon carbide. Thus, silicon carbide will be present at higher amount of silicon.
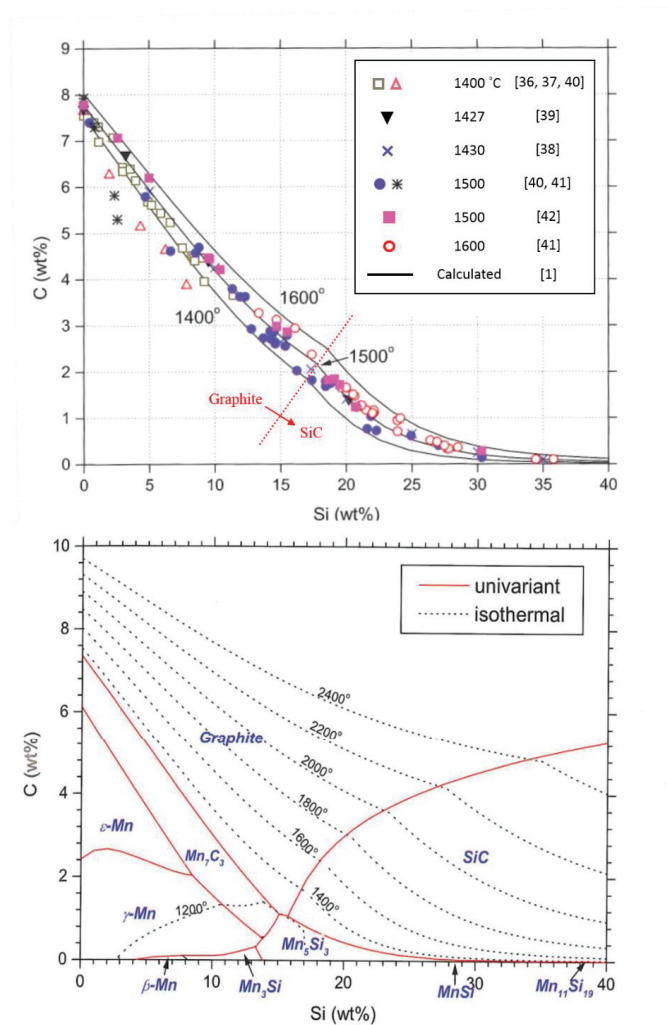
Figure 2.4: Calculated and measured carbon solubility in Mn-Si-C$_{Sat.}$ alloys between 1400 and 1600 °C (top) [1, 36-42] and between 1200 and 2400 °C (bottom) [1]. Stability form of carbon changes from graphite to silicon carbide at approximately 18 wt% between 1550 and 1650 °C.

Since all manganese ores consist of some iron oxides (**Table 1.2**), iron will always be present in the metal. The Mn-Si-Fe-C system becomes the representative system describing the SiMn alloy. The calculated phase relations for the Mn-Si-Fe-C (Mn/Fe = 7) system at 1550 °C are shown in **Figure 2.5**, and the calculated carbon solubility at various temperatures is shown in **Figure 2.6**.

12
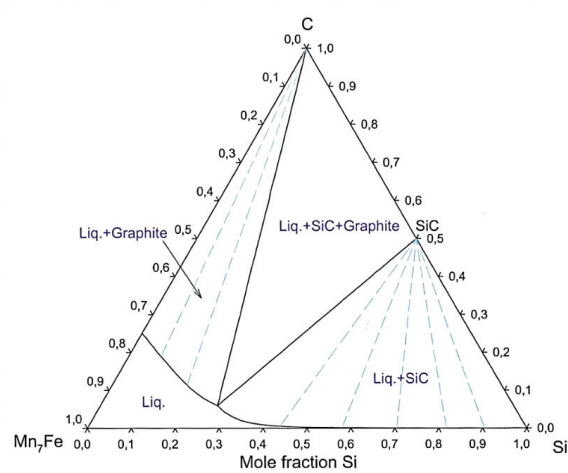
Figure 2.5: Calculated phase relations of the Mn-Si-Fe-C (Mn/Fe = 7) system at 1550 °C [1]. Note that the form of carbon changes from graphite to silicon carbide at approximately 0.3 mole fraction of silicon.
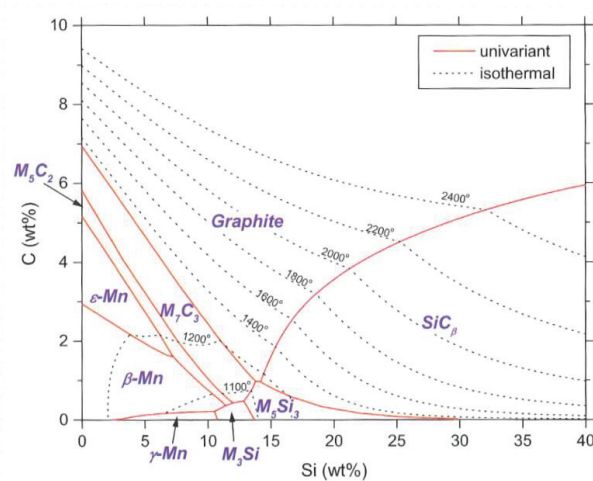
Figure 2.6: Calculated carbon solubility in Mn-Si-Fe-C$_{Sat.}$ (Mn/Fe = 7) alloys between 1100 and 2400 °C [1]. Addition of iron into the Mn-Si-C$_{Sat.}$ system reduces the carbon saturation level but not to a great extent.

The comparison of carbon solubility in Mn-Si-C and Mn-Si-Fe-C (Mn/Fe =7) systems indicates that iron reduces the carbon saturation level but not to a great extent. Concerning the SiMn production temperatures, which are between 1550 and 1650 °C, the silicon content at equilibrium in **Figure 2.6** is approximately 17 wt% in the metal. Increasing the temperature increases the solubility of carbon in the metal.

13

The calculated and measured carbon solubility with Mn/Fe ratio of 8.0 and 5.1 at different temperatures is shown in **Figure 2.7** [1, 38]. The comparison between the two different Mn/Fe ratio indicates that the carbon solubility increases with higher Mn/Fe ratio. However, the difference is not noticeable within the condition shown in **Figure 2.7**. Increasing the temperature at constant silicon content seems to be more influential.
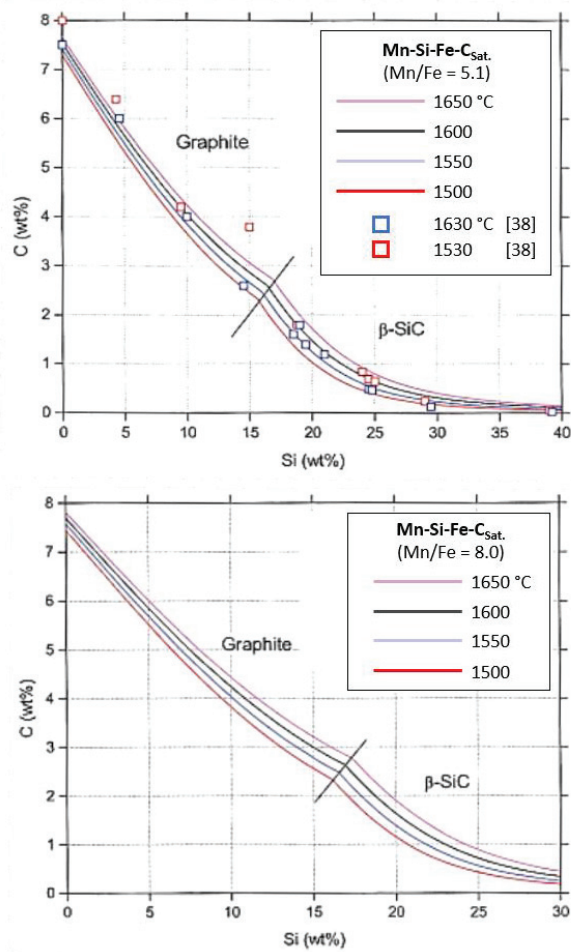
Figure 2.7: Calculated and measured carbon solubility in Mn-Si-Fe-C$_{Sat.}$ alloys between 1500 and 1650 °C [1]: Mn/Fe = 5.1 (top) [38] and Mn/Fe = 8.0 (bottom). Difference of the carbon solubility between the two different Mn/Fe ratios is insignificant. Instead, the influence of temperature at constant silicon content is more noticeable.

Based on the phase relations and carbon solubility, the calculated activities of manganese, silicon and carbon in 1400 and 1600 °C are described in **Figure 2.8**. The activities of the metal components determine the distribution of manganese and silicon between slag and metal phases.
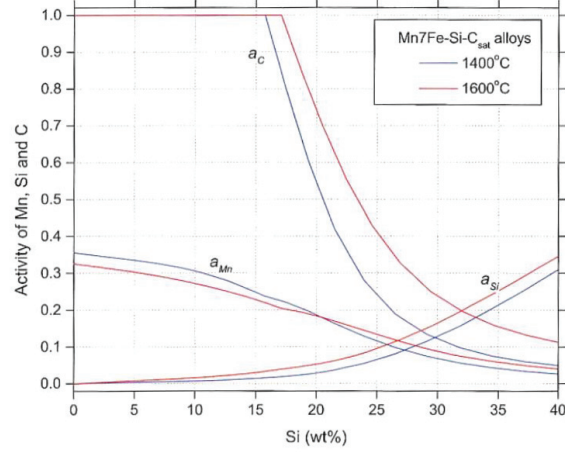
Figure 2.8: Calculated activities of manganese, silicon and carbon in Mn-Si-Fe-C$_{Sat.}$ (Mn/Fe = 7) alloys at 1400 and 1600 °C [1]. Decreasing activity of carbon with increasing silicon reflects the carbon stability.

A recent study has also expressed the activities of manganese and silicon by acquiring thermodynamic data from FactSage 7.0 [44, 45]. Pure liquid metal state (FactPS) with carbon saturation was assumed. Numerous data points with different temperatures (between 1200 and 1700 °C) and compositions were generated to calculate the activities of manganese and silicon metal. The saturation levels of carbon were considered to avoid silicon carbide stabilization at higher silicon content, where the calculations are valid for silicon concentrations up to 20 wt% and at temperatures between 1500 and 1650 °C. **Equations (2.1)** and **(2.2)** describes the mathematical formula of the activities of manganese and silicon metal. **Equation (2.3)** shows the carbon saturation level:

$$a_{Mn} = C_{Mn} \times \exp(0.0005382T - 37.41C_{Mn} - 2.966C_{Si} - 0.6835C_{Fe} + 39.52C_{Mn}^2 - 1.453C_{Si}^2 \\ - 0.5561C_{Fe}^2 + 27.48C_{Mn}C_{Si} + 38.69C_{Mn}C_{Fe} + 0.214C_{Si}C_{Fe})$$

(2.1)

$$a_{Si} = C_{Si} \times \exp\bigl(0.002464T + 10.3C_{Mn} - 1.081C_{Si} + 27.52C_{Fe} - 15.49C_{Mn}^2 - 3.713C_{Si}^2 - \\ 34.66C_{Fe}^2 + 1.324C_{Mn}C_{Si} - 47.01C_{Mn}C_{Fe} - 9.127C_{Si}C_{Fe}\bigr)$$

(2.2)

$$C_{Sat.} = (1 + 0.00071505T) \times (0.075287C_{Mn} - 0.30008C_{Si} + 0.05181C_{Fe} - 0.17998C_{Si}^2 \\ + 4.1373C_{Si}^3)$$

(2.3)

where T is the temperature deviation from 1500 °C, C$_i$ is the mass fraction of metal component *i* and C$_{Sat.}$ is the carbon saturation level [wt%].

The activities of manganese and silicon compared with FactSage 7.0 and **Equations (2.1)** and **(2.2)** are shown in **Figure 2.9**, and the same comparison of carbon saturation level is described in **Figure 2.10**. The comparisons show that the values calculated from the equations and FactSage 7.0 are in good agreement.
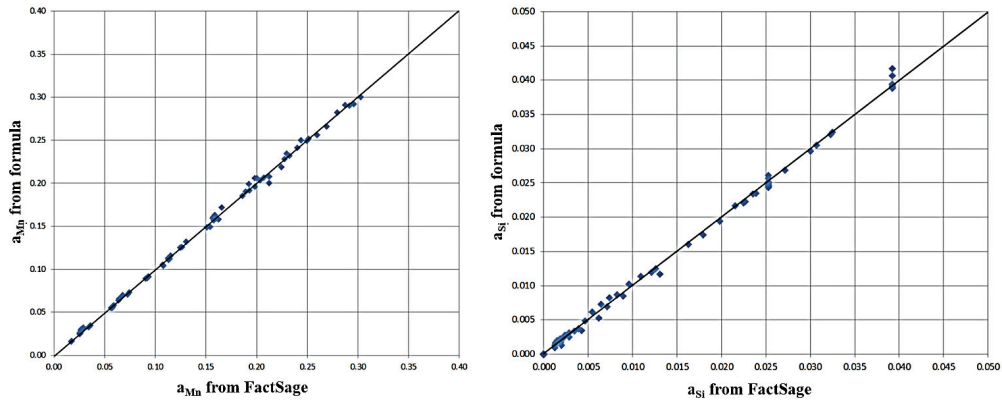
Figure 2.9: Comparison between the activities of manganese and silicon calculated by Equations (2.1) and (2.2) [44] and by FactSage 7.0 [45]. Activity values calculated from the equations were in good agreement with FactSage 7.0.
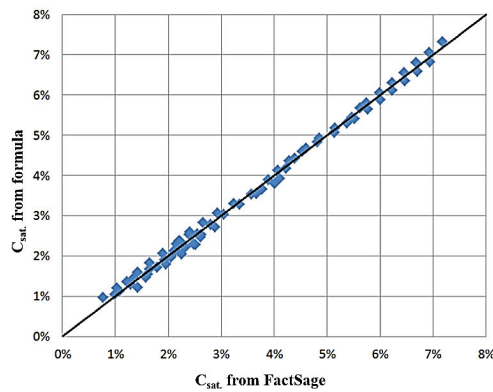
Figure 2.10: Comparison between the carbon saturation level calculated by Equation (2.3) [44] and FactSage 7.0 [45]. Calculated carbon saturation levels from Equation (2.3) showed good agreement with FactSage 7.0.

2.1.3 The SiMn slag systems

The main components in the SiMn slag systems are MnO, SiO_2, CaO, MgO and Al_2O_3. FeO is assumed to be reduced to metallic iron during the pre-reduction stage. Since both MnO and SiO_2 are the key slag components that directly relates to manganese and silicon metal production, the MnO-SiO_2 binary system can be initially discussed to reflect the SiMn slag systems. The MnO-SiO_2 binary phase diagram is described in **Figure 2.11**, where the approximate MnO/SiO_2 ratio in FeMn and SiMn slags are highlighted areas in red and blue, respectively.

16
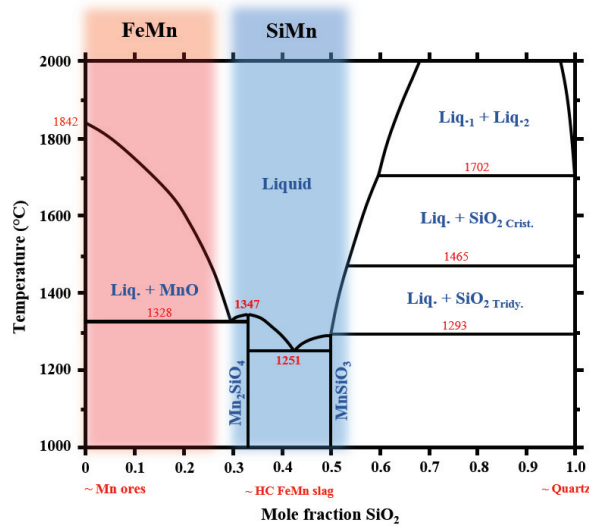
Figure 2.11: Calculated phase diagram for the MnO-SiO$_2$ binary system (re-illustrated) [1]. Note that the approximate MnO/SiO$_2$ ratios for FeMn and SiMn slags are highlighted areas with red and blue, respectively. Raw materials (~ Mn ores, ~ HC FeMn slag and ~ Quartz) reflected in the MnO-SiO$_2$ system are also presented.

In the case of FeMn slags according to the MnO-SiO$_2$ system, the melting of pre-reduced manganese ores will start above around 1330 °C if the effects of other ore components are neglected. Above the melting temperatures, the system indicates that solid MnO will always be present in the slag until the composition reaches the liquidus line due to increasing temperature and MnO reduction. The activity of MnO can assumed to be 1 in this case where solid MnO is presented in the slag. Above the liquidus line, the activity of MnO will be lower than 1.

For SiMn slags, the generation of liquid slag starts at lower temperatures than the FeMn case. However, the highlighted for SiMn in the MnO-SiO$_2$ system does not necessarily reflects this case. Unless the raw materials are only HC FeMn slag, the two manganese silicate compounds (Mn$_2$SiO$_4$ and MnSiO$_3$) cannot represent manganese ores and quartz separately. The melting behavior and kinetics of raw materials in SiMn charges are currently not well studied, and investigating the slag formation of different charge compositions are necessary. Assuming complete liquid SiMn slag above approximately 1350 °C, the activity of MnO is lower than 1 where no solid MnO is present. The calculated and measured activity of MnO in the MnO-SiO$_2$ system at three different temperatures are described in **Figure 2.12** [46].

17
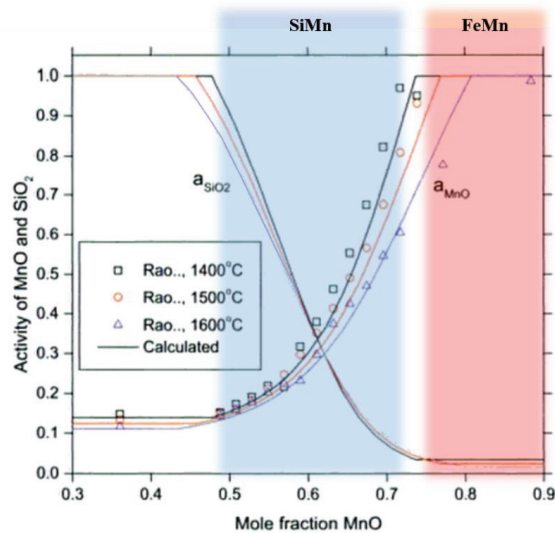
Figure 2.12: Calculated and measured activities of MnO and SiO₂ in the binary MnO-SiO₂ system (re-illustrated) [1, 46]. Highlighted areas in red and blue also describe the approximate MnO/SiO₂ ratios for the FeMn and SiMn slags, respectively according to Figure 2.11.

Similar to **Figure 2.11**, the highlighted areas in red and blue each represent the FeMn and SiMn primary slag, respectively. The activity of MnO is 1 at higher MnO mole fraction, which indicates that the FeMn slag still contains solid MnO and has not reached the liquidus line. The activity of MnO decreases rapidly when the FeMn slag is completely liquid with increasing amount of SiO₂. In SiMn slags, the activity of MnO can be assumed to be relatively low compared to FeMn slags if complete melting of raw materials has occurred. According to the binary MnO-SiO₂ system, the activity of MnO is already near 0.2 when the mole fraction of MnO is between 0.5 and 0.6. The difference in the activity of MnO between FeMn and SiMn slags implies that the reduction behavior can be different in the two types of slags. The corresponding activity of SiO₂ (a_{SiO2}) in the SiMn case is around 0.5 and 0.7. However, typical SiMn slags does not only contain MnO and SiO₂. Considerable amount of CaO, MgO and Al₂O₃ should also be considered and the activities of MnO and SiO₂ will be influenced by these slag components. Note that MnO, SiO₂ and CaO are the major slag component in typical SiMn slags.

The phase relations of the MnO-SiO₂-CaO system and the corresponding calculated activities of MnO and SiO₂ at 1500 °C are shown in **Figure 2.13**. Both activities decrease close to zero at the lower MnO and SiO₂ side where precipitation of solid phases, such as (Mn, Ca)O and Ca₂SiO₄, begins. The temperature will be important in this case to determine the activities of MnO and SiO₂. At a constant MnO/SiO₂ ratio, increasing amount of CaO indicates that the activity of MnO will increase while it will be the opposite for the activity of SiO₂. This implies that the amount of CaO in SiMn slags should be considered regarding the reduction of MnO and SiO₂. Higher amount of CaO is favorable for MnO while it is the opposite for SiO₂ reduction if the activity influences the reduction.
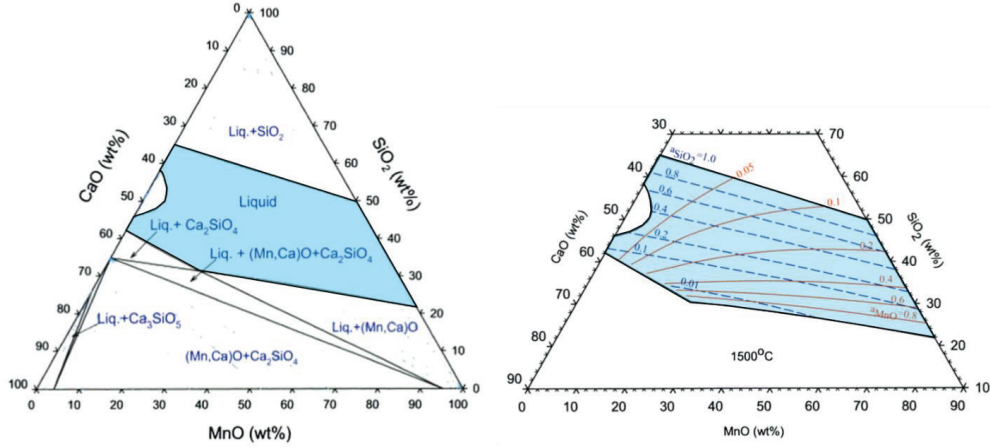
Figure 2.13: Calculated phase relations (left) and activities of MnO and SiO$_2$ (right) at 1500 °C in the MnO-SiO$_2$-CaO system [1]. Increasing amount of CaO increases the activity of MnO while decreases the activity of SiO$_2$.

The activities of MnO and SiO$_2$ in the MnO-SiO$_2$-CaO-MgO-Al$_2$O$_3$ system were recently studied [44]. Similar with from the activities of manganese and silicon metal from the previous section, the activities of MnO and SiO$_2$ were mathematically derived with solution database (FToxid) from FactSage 7.0 [45]. Numerous data points with different temperatures (between 1200 and 1700 °C) and compositions were generated to calculate the activities of MnO and SiO$_2$. **Equations (2.4)** and **(2.5)** describes the mathematical formula of the activities of MnO and SiO$_2$:

$$a_{MnO} = C_{MnO} \times \exp(0.0007576T - 123.7C_{MnO} + 30.14C_{SiO_2} + 47.84C_{MgO} + 49.54C_{CaO}$$
$$- 47.96C_{Al_2O_3} + 122.8C_{MnO}^2 - 67.78C_{SiO_2}^2 - 46.32C_{MgO}^2 - 47.68C_{CaO}^2 + 22.51C_{Al_2O_3}^2$$
$$+ 78.35C_{MnO}C_{CaO} + 77.56C_{MnO}C_{MgO} + 176.6C_{MnO}C_{Al_2O_3} + 101.2C_{MnO}C_{SiO_2}$$
$$- 71.52C_{SiO_2}C_{CaO} - 70.58C_{SiO_2}C_{MgO} + 27.35C_{SiO_2}C_{Al_2O_3} + 46C_{SiO_2}^3 - 92.97C_{CaO}C_{MgO}$$
$$+ 2.44C_{CaO}^3)$$

$$(2.4)$$

$$a_{SiO_2} = C_{SiO_2} \times \exp(-0.0003408T + 113.8C_{MnO} - 22.79C_{SiO_2} - 51.63C_{MgO} - 52.44C_{CaO}$$
$$+ 36.3C_{Al_2O_3} - 119.3C_{MnO}^2 + 42.56C_{SiO_2}^2 + 32.25C_{MgO}^2 + 30.12C_{CaO}^2 - 26.26C_{Al_2O_3}^2$$
$$- 82.725C_{MnO}C_{CaO} - 82.9C_{MnO}C_{MgO} - 155.2C_{MnO}C_{Al_2O_3} - 86.98C_{MnO}C_{SiO_2}$$
$$+ 86.21C_{SiO_2}C_{CaO} + 86.19C_{SiO_2}C_{MgO} - 23.06C_{SiO_2}C_{Al_2O_3} - 31.26C_{SiO_2}^3$$
$$+ 69.45C_{CaO}C_{MgO} + 11.29C_{CaO}^3)$$

$$(2.5)$$

where T is the temperature deviation from 1500 °C and Cj is the mass fraction of slag component j.

The comparison of the activities between the derived formulas and FactSage 7.0 are described in **Figure 2.14**, where it shows good agreement of **Equations (2.4)** and **(2.5)** to the thermodynamic data from FactSage 7.0. Note that the activities of MnO and SiO$_2$ were between 0 and 0.3 in this thesis work, and should be within the area where these equations can be used.
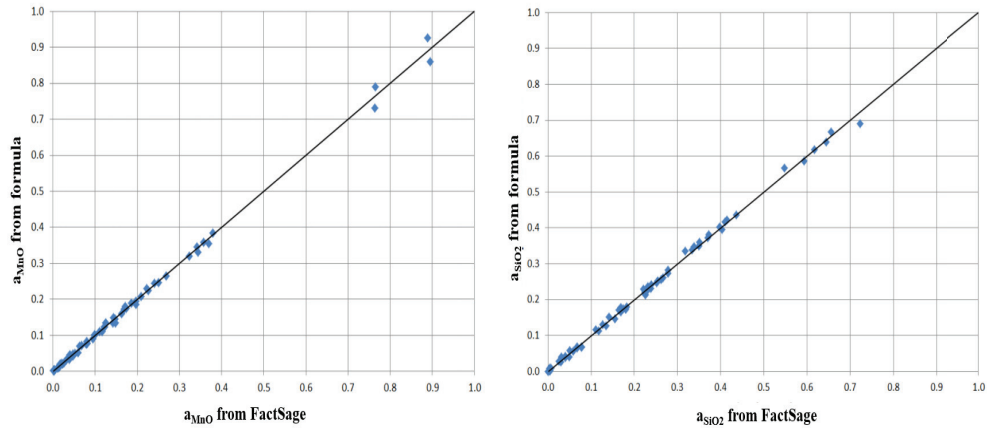
Figure 2.14: Comparison between the activities of MnO and SiO₂ calculated by Equations (2.4) and (2.5) [44] and by FactSage 7.0 [45]. Activity values calculated from the equations were in good agreement with FactSage 7.0.

2.1.4 Melting behavior of raw materials

The melting behavior of raw materials to form liquid slag should be initially considered since the reduction of MnO and SiO₂ is likely to occur in liquid state. The related phase diagrams of SiMn slags should be initially discussed as they reflect the melting behavior of raw materials.

The calculated MnO-SiO₂-CaO system between 1300 and 2000 °C is described in **Figure 2.15**. The isothermal temperatures give implications of which phases will be present during the reduction of MnO and SiO₂. For example, if an arbitrary initial slag composition at lower temperatures is approximately 40% MnO - 40% SiO₂ - 20% CaO, the maximum reduction of MnO can extend to the lower MnO side (SiO₂-CaO binary line) without precipitation of solid phases from temperatures between 1500 and 1650 °C. However, SiO₂ reduction is likely to be limited to the isothermal lines. For example, a slag composition of low MnO will precipitate solid α-Ca₂SiO₄ phase below approximately 42 wt% SiO₂ unless the temperature is higher than 1650 °C. Increasing the temperature at this condition is not likely to make significant difference.
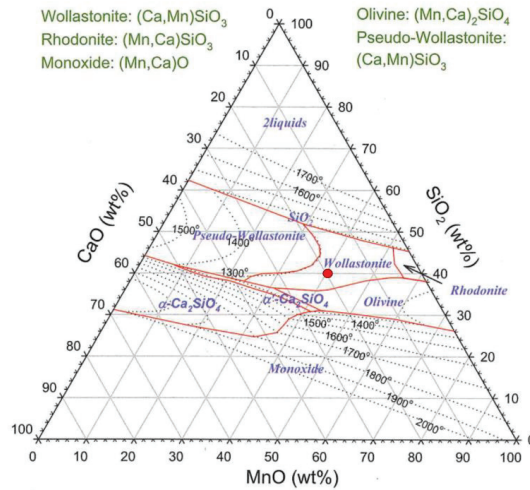
Figure 2.15: Calculated phase and liquidus relations of the MnO-SiO$_2$-CaO system [1] with an arbitrary initial composition (Red dot: 40 wt% MnO – 40 wt% SiO$_2$ – 20 wt% CaO).

The calculated MnO-SiO$_2$-Al$_2$O$_3$ system between 1200 and 2000 °C is also shown in **Figure 2.16**. Unlike the MnO-SiO$_2$-CaO system, the isothermal liquidus lines in the MnO-SiO$_2$-Al$_2$O$_3$ system implies that the extent of MnO and SiO$_2$ reductions are more limited. For example, at constant SiO$_2$/Al$_2$O$_3$ ratio, precipitation of solid phases is more occurring compared to the MnO-SiO$_2$-CaO system between 1500 and 1650 °C. Increasing amount of solid phases does not seems favorable for both MnO and SiO$_2$ reduction if the viscosity of the slag affects the reduction rates. Nevertheless, such case is not the typical slag for SiMn process and further explanation will be omitted. Instead, a typical SiMn slag will usually contain five slag components, MnO, SiO$_2$, CaO, MgO, and Al$_2$O$_3$, where the majorities are MnO, SiO$_2$ and CaO.
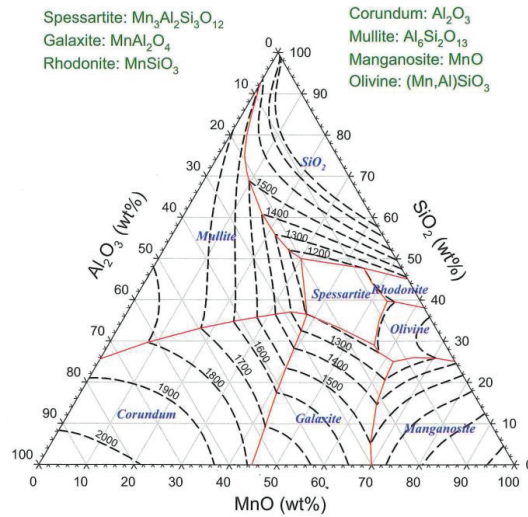
Figure 2.16: Calculated phase and liquidus relations of the MnO-SiO$_2$-Al$_2$O$_3$ system [1]. More precipitation of solid phases is likely to occur during MnO and SiO$_2$ reduction compared with MnO-SiO$_2$-CaO system between 1500 and 1650 °C.

A calculated phase relation of the MnO-SiO$_2$-CaO-MgO-Al$_2$O$_3$ system between 1100 and 2000 °C is described in **Figure 2.17**. The phase relations and the isothermal lines will depend on the ratio of the oxides (CaO/MgO, Al$_2$O$_3$/SiO$_2$ and etc.). However, it will be similar to the MnO-SiO$_2$-CaO system in general as long as the major slag components are MnO, SiO$_2$ and CaO.

The examples of typical FeMn and SiMn initial slag compositions are also described in **Figure 2.17**, where the slag system contains 60% MnO – 28% SiO$_2$ – 12% CaO and 50% MnO – 38% SiO$_2$ – 12% CaO, respectively. The initial composition of FeMn slag indicates that solid monoxides, mostly MnO, consist the slag even up to elevated temperatures between 1500 and 1600 °C. Complete melting of FeMn raw materials can be expected around these temperatures. However, the initial composition of SiMn slag shows that complete liquid slag can be thermodynamically expected at lower temperatures around 1300 °C. It is not known whether the raw materials in the SiMn charge will dissolve into liquid slag around this temperature and it is a matter of dissolving kinetics. Thus, the melting behaviors of raw materials must be observed prior to investigate the reduction of MnO and SiO$_2$ in the SiMn process.
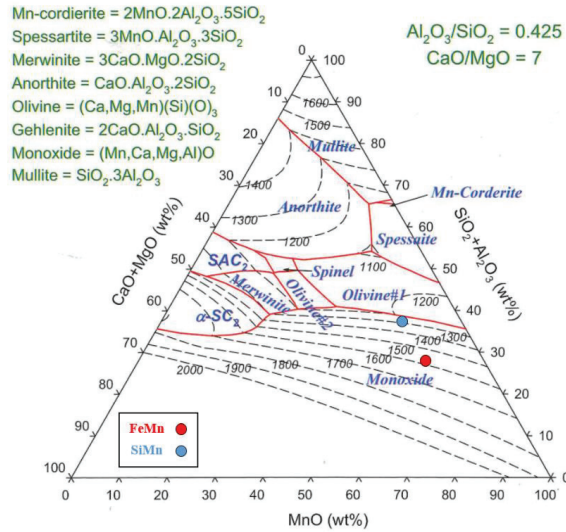
Figure 2.17: Calculated phase and liquidus relations for the MnO-SiO$_2$-CaO-MgO-Al$_2$O$_3$ (Al$_2$O$_3$/SiO$_2$ = 0.425, CaO/MgO = 7) system [1] with initial FeMn and SiMn slag compositions (FeMn: 60% MnO – 28% SiO$_2$ – 12% CaO / SiMn: 50% MnO – 38% SiO$_2$ – 12% CaO). Solid MnO is expected for the initial FeMn slag until elevated temperature, while the initial SiMn slag will be all liquid phase.

Previous studies had observed the melting behavior of several manganese sources. Gaal et al. observed the melting behavior of Assmang ore, Comilog ore and HC FeMn slag in a sessile drop furnace where the particles were placed on graphite substrates [47]. The manganese ores were pre-reduced with CO gas and quenched with argon gas prior to the main experiments. The particles were heated to 1830 °C in CO/Ar atmospheric pressure while the shape of the particles was photographed every second. **Figure 2.18** describes the changing shape of two pre-reduced Assmang ore particles between 1280 and 1660 °C, and **Table 2.1** shows the average melting range of the manganese sources. Note that the ores were heated and reduced simultaneously from the graphite substrate, and the melting temperature range was when the melting of particles starts and finishes from the observation.
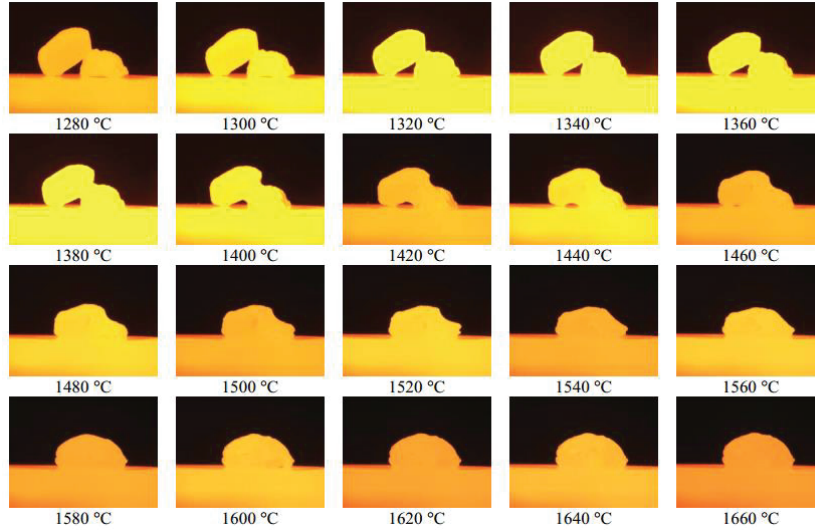
Figure 2.18: Images of the two pre-reduced Assmang ore particles on a graphite substrate being heated (5 °C/min) between 1280 and 1660 °C in CO atmospheric pressure [47]. Changing of the initial shape indicates melting between the two Assmang ore particles.

Table 2.1: Observed melting ranges of pre-reduced Assmang/Comilog ore and HC FeMn slag [47]. Melting range of HC FeMn slag was approximately 200 °C lower than the two manganese ores.

Mn source	Melting range [°C]	Note
Assmang ore (Pre-reduced)	1430 − 1570	CO atmosphere
Comilog ore (Pre-reduced)	1450 − 1490	
HC FeMn slag	1175 − 1250	Ar atmosphere

The melting behavior of the pre-reduced Assmang and Comilog ore indicates that the incipient slag from the two manganese ores will be generated at approximately 1440 °C. However, the temperature for complete melting during reduction is different as Assmang ore was about 80 °C higher than Comilog ore. The melting range for HC FeMn slag was observed to be in relatively lower temperatures between 1175 and 1250 °C. Gaal et al. concluded that the different mineralogy of the manganese sources caused the different melting behavior, and CO atmosphere promotes faster melting. The lower melting range of HC FeMn slag implies that mineralogy will have significant impact towards melting because HC FeMn slag is already in a form of manganese silicates, $(Mn, Ca)_2SiO_4$ and $(Mn, Ca)SiO_3$, where the composition of the HC FeMn slag will vary depending on the FeMn furnace operation history. The relatively small difference between Assmang and Comilog ore also seems to be from the different mineralogy and composition, where the formation of manganese silicates during gaseous reduction with CO gas and with the graphite substrate can be the reason. As expected from the phase diagrams **Figures 2.15** and **2.16**, the Comilog ore which is a more acidic (higher Al_2O_3 in **Table 1.2**) is completely melted at a lower temperature than the more basic (higher CaO **Table 1.2**) Assmang ore. A previous study also observed this similar relation between the melting and the amount of acidic/basic oxides in manganese sources [12]. However, the studies only showed

24

the individual melting of manganese ores, which can be related to raw materials melting in FeMn processes. The melting behavior of manganese ores should also be considered with the presence of quartz for SiMn production. Since considerable amount of quartz or quartzite will be used in the charge mixture in the SiMn process, different melting behaviors can be expected.

Ringdalen et al. also investigated the melting behavior of different manganese sources using a sessile drop furnace under similar experimental conditions [48]. **Figure 2.19** shows the images of a pre-reduced Assmang ore particle heated up to near 1500 °C in CO atmospheric pressure on a graphite substrate. The average melting range of Assmang ore, Gabonese ore, CVRD ore and CVRD sinter is summarized in **Table 2.2**.

(a) 20°C   **(b)** 1404°C   **(c)** 1499°C
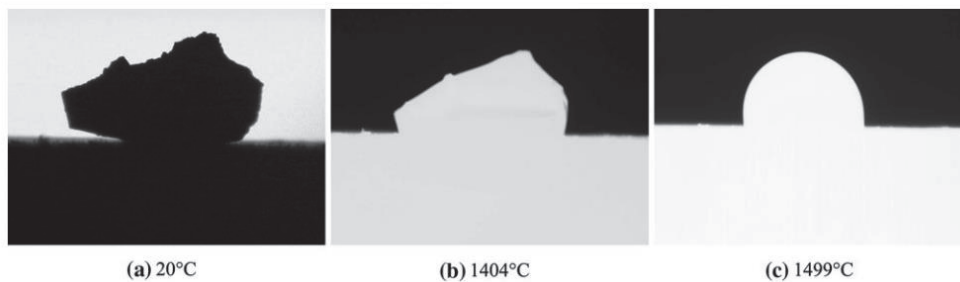
Figure 2.19: Images of a pre-reduced Assmang ore particle on a graphite substrate being heated (5 °C/min) between 20 and 1500 °C: (a) Cold sample, (b) initial melting and (c) completely molten [48].

Table 2.2: Estimated average melting ranges of manganese sources [48]. Typical melting range of manganese ores was approximately between 1450 and 1500 °C.

Mn source	Melting range [°C]	Note
Assmang ore (Pre-reduced)	1446 (±70) − 1513 (±57)	
Gabonese ore (Pre-reduced)	1485 (±11) − 1538 (±9)	CO atmosphere
CVRD ore (Pre-reduced)	1461 (±13) − 1494 (±23)	
CVRD sinter (Pre-reduced)	1395 (±85) − 1489 (±32)	

Compared with **Table 2.1**, the melting ranges of Assmang ore are similar. The other manganese ores also showed similar melting ranges, and the typical melting seems to start around 1450 °C and finish around 1500 °C. CVRD sinter seems to melt earlier than manganese ores but the error range is too high to conclude.

Ringdalen et al. also conducted quantitative x-ray diffraction (XRD) analyses of Gabonese and CVRD ores after heating at 1200 °C for 4 hours in CO gas (pre-reduction), which are described in **Table 2.3**. The melting temperature of pure MnO is higher than 1800 °C [1, 49, 50], and formation of other phases besides MnO during pre-reduction was assumed to give the melting temperatures observed in their work.

Table 2.3: Quantitative XRD analyses of Gabonese and CVRD ores after pre-reduction [48]. Manganese in the ore was mainly formed as monoxide (MnO) and silicates (Mn_2SiO_4) after pre-reduction with CO gas at 1200 °C.

Mn ore	Mineral	Formula *	Amount [wt%]
Gabonese	Manganosite	(**Mn**, Fe)O	56.3
	Tephorite	(**Mn**, Mg, Fe)$_2SiO_4$	24.3
	Spinel	(**Mn**, Mg, Fe)(Al, Fe^{3+})$_2O_4$	8.6
	α-Iron	Fe	1.4
	Unidentified	- Not Available -	9.4
CVRD	Tephorite	(**Mn**, Mg, Fe)$_2SiO_4$	36.4
	Manganosite	(**Mn**, Fe)O	34.8
	Galaxite	(**Mn**, Mg, Fe)Al_2O_4	18.9
	Olivine	(Mg, Fe)$_2SiO_4$	6.4
	α-Iron	Fe	3.3

* In bold: Major component (cation) of the solid solution

The XRD analyses of the pre-reduced Gabonese and CVRD ores indicated that manganese was mostly formed as monoxide (MnO) and silicates (Mn_2SiO_4) after pre-reduction at 1200 °C. Ringdalen et al. observed that the phase composition of Gabonese and CVRD ores changed significantly upon heating with CO gas. This implies that manganese sources with higher SiO_2 content could give different melting properties. A typical example is the comparison between manganese ores and HC FeMn slag, where the latter have higher SiO_2 content. The melting temperature of HC FeMn slag is approximately 200 °C lower than typical manganese ores.

Since quartz, as SiO_2, is a considerable amount during the melting of manganese ores in the SiMn process, it is important to investigate the melting behavior of raw materials, especially manganese ores, will behave as observed as in the previous studies. The melting of raw materials in the SiMn can be reflected by the simple MnO-SiO_2 binary phase diagram shown in **Figure 2.11**.

According to the MnO-SiO_2 system, pre-reduced manganese ores will start melting above around 1330 °C if the effect of other ore components is not considered. The area highlighted in red in **Figure 2.11** can represent the melting of manganese ores. Assuming that manganese ores start to melt at approximately 1450 °C as highlighted in previous studies [47, 48], the complete melting temperature can be estimated. Since the melting of manganese ores occurs under condition of continuous heating with coke in CO atmosphere at the top part of the coke-bed, the composition change towards the liquidus line is likely to be diagonal, where the temperature and the fraction of SiO_2 increases. Not only the temperature increases but also the reduction degree of MnO. The liquidus line will also be influenced by other pre-reduced ore components, but the approximate temperature of complete melting can estimated to be between 1500 and 1600 °C depending on the heating rate and the kinetics of MnO reduction. The reported melting ranges of different manganese ores from the previous studies are in this range. However, the area highlighted in red in **Figure 2.11** represents the melting case of the FeMn process, where the charge materials are mostly manganese ores and sinters.

For SiMn process, the charge will consist more amount of SiO_2 from adding quartz and HC FeMn slag. Assuming pure SiO_2, the melting temperature of quartz is approximately 1713 °C [1, 50, 51]. If considered individually, manganese ores and quartz will melt separately at temperatures around 1450 and 1700 °C, respectively. In other words, quartz will be dissolved in the liquid slag phase of the manganese ores.

The area highlighted in blue in **Figure 2.11** is the approximate ratio of MnO and SiO_2 for SiMn charges but does not necessarily represents the actual SiMn case. As discussed in the previous section, the two compounds are manganese silicates, Mn_2SiO_4 and $MnSiO_3$, with relatively lower melting temperatures below 1350 °C. According to previous studies [47, 48], HC FeMn slag can be represented by the blue area in **Figure 2.11** due to its lower melting temperatures. This implies that when HC FeMn slag is used as raw material for SiMn charges, the formation of SiMn slag will start at relatively lower temperature below 1350 °C. Thermodynamically, a liquid slag can be expected for HC FeMn slag above 1350 °C.

Without HC FeMn slag in the SiMn charge, it is not clear whether the melting behavior of raw materials should behave differently. Manganese ores and quartz are represented in **Figure 2.11** (both ends) and both has relatively high melting temperatures. This implies that the complete liquid SiMn slag can occur at different temperatures depending on the composition of charge materials.

2.1.5 Manganese and silicon distribution

The distribution of manganese and silicon in the SiMn slag and metal is important as it determines the composition of the product as well as the manganese yield. As the SiMn slag is a waste product, high distribution of manganese in the slag phase will be considered as loss of manganese which accompanies economic consequences. Thus, minimizing manganese in the slag phase as MnO is one of the important goal in production.

At complete equilibrium, the relation of manganese in slag and metal phases can be described by **Equation (2.6)**. Note that **Reaction (1.10)** is shown again in the following for convenience:

$$MnO_{(l)} + C = Mn_{(l)} + CO_{(g)} \tag{1.10}$$

$$K_{MnO} = \frac{a_{Mn} \cdot p_{CO}}{a_{MnO} \cdot a_C} \tag{2.6}$$

where K_{MnO} is the equilibrium constant of **Reaction (1.10)**, a_{Mn} is the activity of Mn in the metal phase, a_{MnO} is the activity of MnO in the slag phase, p_{CO} [atm] is the partial pressure of CO gas and a_C is the activity of carbon in the metal phase or as solid carbon.

The equilibrium relation of silicon between the slag and metal phases according to **Reaction (1.11)** (also shown again in the following for convenience) is also described by **Equation (2.7)**:

$$SiO_{2\,(l)} + 2C = Si_{(l)} + 2CO_{(g)} \tag{1.11}$$
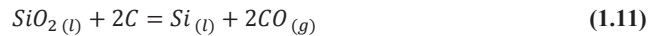
$$K_{SiO_2} = \frac{a_{Si} \cdot p_{CO}^2}{a_{SiO_2} \cdot a_C^2} \tag{2.7}$$

where K_{SiO2} is the equilibrium constant of **Reaction (1.11)**, a_{Si} is the activity of Si in the metal phase and a_{SiO2} is the activity of SiO_2 in the slag phase.

The top part of the coke-bed zone is where the reduction occurs with coke particles and CO gas as it was discussed in the previous chapter. The partial pressure of CO gas and the activity of carbon can be considered as $p_{Total} = p_{CO} \approx 1\ atm$ and $a_C = 1$. The equilibrium expression between slag and metal can then be simplified into **Equations (2.8)** and **(2.9)**:

$$a_{Mn} = K_{MnO} \cdot a_{MnO} \tag{2.8}$$

$$a_{Si} = K_{SiO_2} \cdot a_{SiO_2} \tag{2.9}$$

This indicates that the equilibrium concentration of manganese and silicon in metal mainly depends on the temperature and the slag composition influencing the activity of MnO and SiO_2.

While the transfer of manganese and silicon from slag to metal may be described by **Reactions (1.10)** and **(1.11)**, other studies proposed a possible detailed reduction route for SiO_2. These studies describe that silicon transfer from slag to metal involves the formation and reduction of silicon monoxide (SiO) gas [52-55], which are shown in **Reactions (2.10)** and **(2.11)**:

$$SiO_2 + CO_{(g)} = SiO_{(g)} + CO_{2\ (g)} \tag{2.10}$$

$$SiO_{(g)} + C = Si + CO_{(g)} \tag{2.11}$$
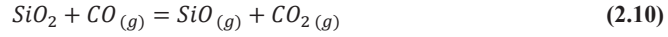
The SiO partial pressure generated by **Reaction (2.10)** will determine the driving force and kinetics of **Reaction (2.11)**. This is dependent on the CO_2 pressure at the slag and gas interface. It implies that the reaction of CO_2 gas with carbon has a possible impact on the kinetics of SiO_2 reduction.

However, the transfer of silicon from slag to metal via SiO gas formation and consumption is not likely to occur significantly in the SiMn process. While several complicated reduction mechanisms are proposed in the silicon process [56], circulation of SiO gas in the SiMn process is assumed to be insignificant. **Reaction (2.12)** [53] shows the formation of SiO gas from reaction with slag and metal, where the equilibrium constant can be described in **Equation (2.13)**:

$$SiO_{2\ (l)} + Si_{(l)} = 2SiO_{(g)} \qquad \Delta G_{1600\ °C} = +77.1\ kJ \tag{2.12}$$
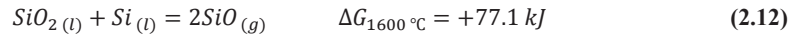
$$K_{SiO} \approx 7.1 \times 10^{-3} = \frac{p_{SiO}^2}{a_{SiO_2} \cdot a_{Si}} \tag{2.13}$$

where K_{SiO} is the equilibrium constant of **Reaction (2.12)** and p_{SiO} [atm] is the partial pressure of SiO gas.

Assuming the activity of silicon of approximately 0.02 from **Figure 2.8** (approximately 18 wt% Silicon) and the activity of SiO_2 of 0.25 from **Figure 2.13** (approximately 40 wt% SiO_2), the partial pressure of SiO gas at 1600 °C can be calculated as shown in **Equation (2.14)**:

$$p_{SiO} = \sqrt{K_{SiO} \cdot a_{SiO_2} \cdot a_{Si}} = \sqrt{7.1 \times 10^{-3} \cdot 0.25 \cdot 0.02} \approx 6.0 \times 10^{-3}\ [atm] \tag{2.14}$$

The partial pressure of SiO gas is a relatively insignificant amount compared to the dominating CO gas. Thus, the transfer of silicon from slag to metal is more likely to occur through **Reaction (1.11)** than via SiO gas formation.

The distribution of silicon also needs to be considered when carbon is stable as silicon carbide at higher silicon content in the metal. The Mn-Si-Fe-C$_{Sat.}$ system in **Figure 2.7** indicates that carbon will change from graphite to silicon carbide at approximately 18 wt% silicon when the temperature is 1650 °C. This implies that the reduction of SiO$_2$ does not occur according to **Reaction (1.11)**, where carbon as graphite is the reductant, but with silicon carbide. The reduction of SiO$_2$ with silicon carbide is described in **Reaction (2.15)** and **Equation (2.16)**:

$$SiO_{2\ (l)} + 2SiC_{(s)} = 3Si_{(l)} + 2CO_{(g)} \tag{2.15}$$
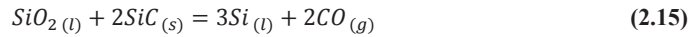
$$K_{SiC} = \frac{a_{Si}^3 \cdot p_{CO}^2}{a_{SiO_2} \cdot a_{SiC}^2} \tag{2.16}$$

where K$_{SiC}$ is the equilibrium constant of **Reaction (2.15)** and a$_{SiC}$ is the activity of silicon carbide.

Then, also assuming CO atmospheric pressure and solid silicon carbide ($a_{SiC} \approx 1$), the equilibrium expression can be simplified by **Equation (2.17)**:

$$a_{Si} = \sqrt[3]{K_{SiC} \cdot a_{SiO_2}} \tag{2.17}$$

This also indicates that the distribution of silicon in the metal phase will depend on the temperature and the composition of the slag influencing the activity of SiO$_2$, but with different magnitude compared to **Reaction (1.11)**. For convenience, the main metal producing reactions in this section are recapitulated in **Table 2.4**.

Table 2.4: Main metal producing reactions in the SiMn process: MnO and SiO$_2$ reduction. SiO$_2$ reduction occurs with either graphite or silicon carbide as carbon depending on the stability form of carbon related to the silicon metal concentration in the system.

Reduction	
MnO	SiO$_2$
MnO $_{(l)}$ + C = Mn $_{(l)}$ + CO $_{(g)}$	**SiO$_2$ $_{(l)}$ + 2C = Si $_{(l)}$ + 2CO $_{(g)}$** (Carbon as graphite) **SiO$_2$ $_{(l)}$ + 2SiC = 3Si $_{(l)}$ + 2CO $_{(g)}$** (Carbon as silicon carbide)

Notes
• Excess amount of carbon: a$_C$ ≈ 1 • CO atmospheric pressure: p$_{Total}$ = p$_{CO}$ + p$_{SiO}$ + p$_{Mn}$ [1] ≈ p$_{CO}$

Since two forms of carbon will be coexisting with the slag and metal phases, both reactions, **Reactions (1.11)** and **(2.15)**, should be considered to calculate the distribution of silicon according to the two equilibrium expressions, **Equations (2.9)** and **(2.17)**. The calculated silicon distribution with different activities of SiO$_2$, slag/metal compositions and temperatures are described in **Figure 2.20**. Note that the amphoteric effect of Al$_2$O$_3$ occurs at point A in **Figure 2.20 (b)**, where the change between "acid" and "basic" slags takes place at about 54 wt% SiO$_2$ in this particular case.
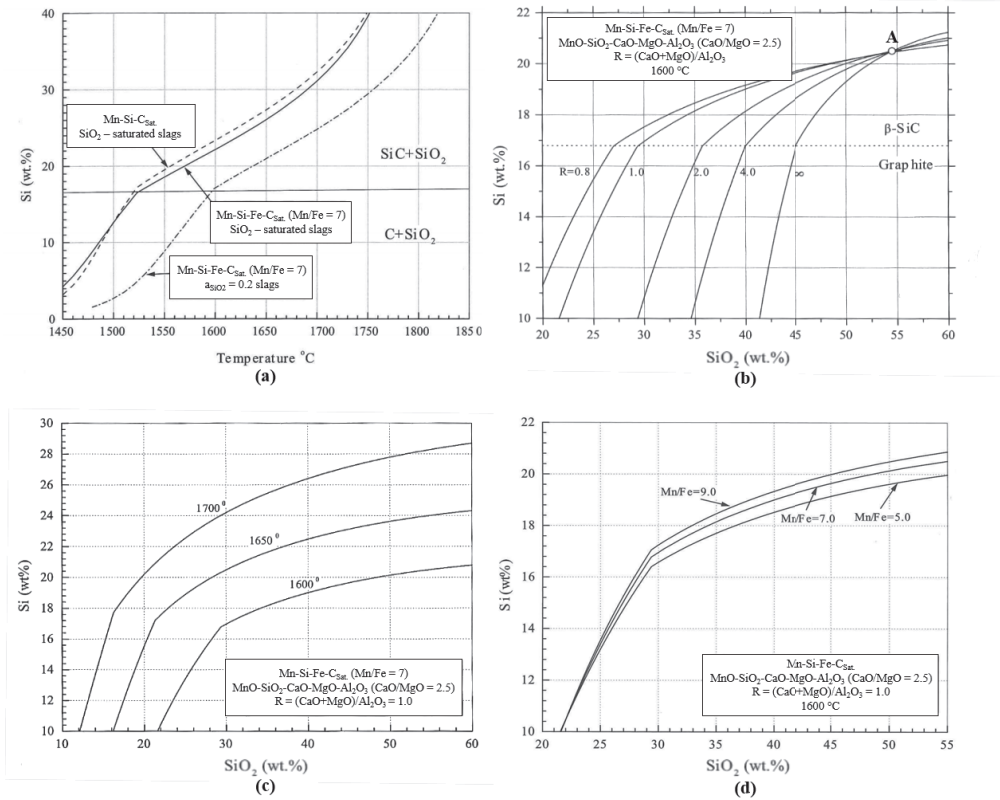
Figure 2.20: (a) Calculated silicon content at different activity of SiO_2, (b) slag compositions, (c) temperatures and (d) Mn/Fe ratio [1]. Note that the amphoteric effect of Al_2O_3 occurs at point A in Figure 2.20 (b), where the change between "acid" and "basic" slags take place in this particular case.

The sharp points in the graphs (between 16-18 wt% silicon) are clearly shown which indicate that the distribution of silicon is considered with both **Equations (2.9)** and **(2.17)**. **Figure 2.20 (a)** shows that the silicon content in the metal phase is higher with slags saturated with SiO_2. This implies that the dissolution of quartz in slag can play an important role in silicon distribution, where the melting behavior of raw materials must be observed prior to reduction. The silicon distribution with different "$(CaO+MgO)/Al_2O_3$" ratio at 1600 °C in **Figure 2.20 (b)** implies that the equilibrium silicon content in the metal can differ significantly depending on the slag composition. Thermodynamically, it describes that increasing amount of CaO or MgO is unfavorable for higher silicon content in the metal phase (not considering kinetics). The temperature also plays an important role for the silicon distribution between slag and metal. The silicon content in the metal increases with increasing temperatures, which is shown in both **Figures 2.20 (a)** and **(c)**. However, the iron content in the metal phase does not seems to give significant influence. The different iron amount in the metal phase is shown in both **Figures 2.20 (a)** and **(d)**, where the difference of the silicon content in the metal phase is low. When graphite is stable as carbon the difference of the silicon content is even lower.

30

The measurements of the SiMn metal and slag distribution were also well studied in previous studies. Ding and Olsen investigated the equilibrium distribution of slag and metal in CO atmospheric pressure [43, 57-60]. Prepared master alloys and slags were charged into graphite crucibles and heated up to temperatures between 1600 and 1700 °C and kept for 5 hours followed by rapid quenching. Assuming equilibrium between slag and metal, the composition of slag and the distribution of manganese and silicon were measured. **Figure 2.21 (a)** shows the distribution of silicon in slag and metal (Mn-Si-$C_{Sat.}$) with different slag compositions at 1600 °C. **Figure 2.21 (b)** describes the slag (MnO and SiO_2) and metal (Si) composition at different temperatures.
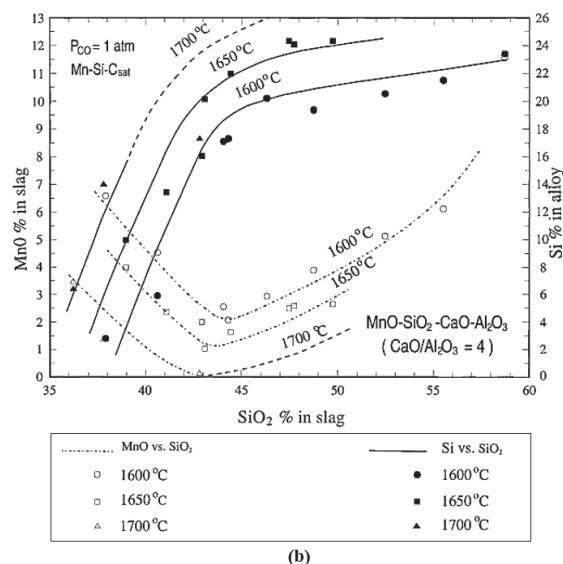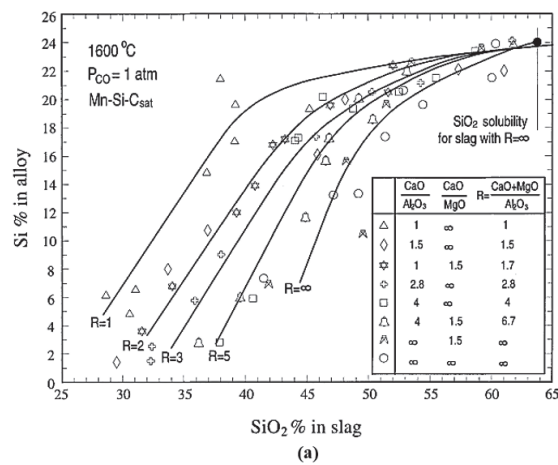
Figure 2.21: (a) Distribution of slag and metal with different slag compositions and (b) temperatures [43]. (CaO+MgO)/Al_2O_3 ratio and temperature have significant impact on the distribution equilibria.

31

Ding and Olsen observed that the temperature and the (CaO+MgO)/Al_2O_3 ratio influence the composition of slag and metal significantly. Increasing temperatures resulted in lower MnO and SiO_2 in the slag phase and lower (CaO+MgO)/Al_2O_3 ratio was favorable for silicon distributed in the metal phase. The ratio of CaO/MgO in the slag phase did not had significant influence. Note that measurements at 1700 °C were not successful due to slag loss from extreme wetting of slag. They explained that very strong wetting between the slag and graphite forced the slag to climb out of the crucible.

The equilibrium slag compositions of the MnO-SiO_2-CaO-Al_2O_3 (CaO/Al_2O_3 = 4) and MnO-SiO_2-CaO-MgO-Al_2O_3 systems are also described in **Figure 2.22** [43]. The measurement from the quaternary MnO-SiO_2-CaO-Al_2O_3 system indicates that the minimum equilibrium of MnO occurs when the SiO_2 concentration is approximately 45 wt% at 1600 °C. The comparison of the ternary MnO-SiO_2-CaO system was also similar with the first case, and this implies that the amount of CaO determines the equilibrium SiO_2 content. However, the measurements in the MnO-SiO_2-CaO-MgO-Al_2O_3 system showed that the amount of Al_2O_3 is also influential, where the equilibrium SiO_2 contents were determined by the (CaO+MgO)/Al_2O_3 ratio. It was not clear why the comparison between the ternary and quaternary slag systems regarding Al_2O_3 were similar, but clearly showed which slag composition can be expected with the (CaO+MgO)/Al_2O_3 ratio when equilibrium is established. In addition, the measured equilibrium slag compositions indicate that manganese as MnO in SiMn slags will be less than 5 wt% at temperatures higher than 1600 °C. This can be compared to FeMn slags where the MnO content is approximately 40 wt% at temperatures around 1500 °C, which implies that a high amount of MnO is likely to be reduced between 1500 and 1600 °C. It must however, be worthy to note that the slag chemistry is also different in the two cases as the SiMn process is much more acid.
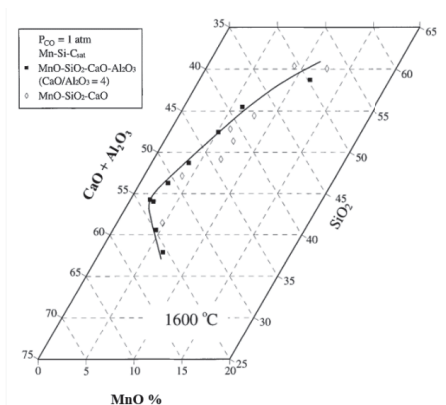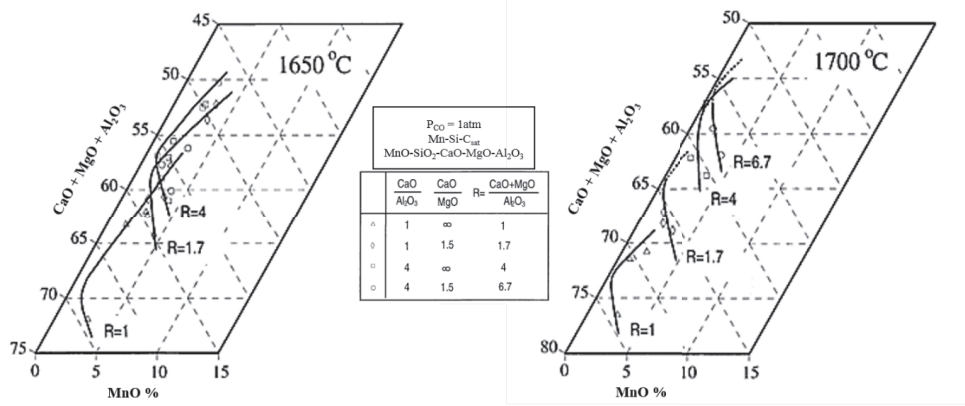
Figure 2.22: Equilibrium slag compositions: (a) MnO-SiO$_2$-CaO-Al$_2$O$_3$ (CaO/Al$_2$O$_3$ =4) system at 1600 °C and (b) MnO-SiO$_2$-CaO-MgO-Al$_2$O$_3$, R = (CaO+MgO/Al$_2$O$_3$) system at 1650 and 1700 °C [43]. Equilibrium minimum of MnO and SiO$_2$ can be determined by the (CaO+MgO)/Al$_2$O$_3$ ratio and temperature.

33

2.2 Reaction kinetics

The slag and metal at thermodynamic equilibrium only describes the final composition at fixed temperatures and does not give information of how fast the reduction occurs towards the equilibrium state. The primary and final slag and metal compositions are known and calculated, but the reduction rates and paths of MnO and SiO_2 are also required to determine the metal producing performance. Thus, the kinetics of MnO and SiO_2 reduction will determine the rate at which manganese and silicon are distributed from the initial state towards equilibrium.

While the thermodynamics of manganese ferroalloy production were studied extensively in the last three decades, kinetic information is rather scarce. In this section, previous studies of manganese kinetics are discussed. The focus of this section is on the rate model of MnO reduction, influence of slag viscosity and the influence of iron and sulfur.

2.2.1 Kinetic model of MnO reduction

The reduction rate of MnO in FeMn slags was previously studied by Ostrovski et al. and was described by **Equations (2.18)** and **(2.19)** [1, 61]:

$$r_{MnO} = k_{MnO} \cdot A \cdot (a_{MnO} - a_{MnO, \ Eq.}) \tag{2.18}$$

$$k_{MnO} = k_{o, \ MnO} \cdot e^{(-\frac{E_{MnO}}{RT})} \tag{2.19}$$

where r_{MnO} [g/min] is the rate of MnO reduction, k_{MnO} [g/min·cm^2] is the rate constant of MnO reduction A [cm^2] is the reaction area, a_{MnO} is the activity of MnO, $a_{MnO, \ Eq.}$ is the activity of MnO at equilibrium, $k_{O, MnO}$ [g/min·cm^2] is the pre-exponential constant of MnO reduction , E_{MnO} [kJ/mol] is the activation energy of MnO reduction, R [J/K·mol] is the gas constant and T [K] is the temperature. Note that **Equation (2.19)** is the Arrhenius equation.

This rate model indicates that the rate of MnO reduction is influenced by three main variables: The slag properties affecting the rate constant, the interface area between the slag and carbon reductant and the driving force, which is the difference between the real MnO content and the MnO content at equilibrium conditions.

At equilibrium, the relation between MnO in the slag phase and manganese in the metal phase has to be satisfied, which was previously described in **Section 2.2.5** as **Equation (2.8)**. Thus, the reduction rate can be described as **Equation (2.20)**:

$$r_{MnO} = k_{MnO} \cdot A \cdot (a_{MnO} - \frac{a_{Mn}}{K_{MnO}}) \tag{2.20}$$

where a_{Mn} is the activity of Mn in the metal phase and K_{MnO} is the equilibrium constant of **Reaction (1.10)**.

Previous studies observed that stirring of the slag during carbothermic reduction had no significant effect on the reduction rate and the MnO content of the slag phase [21, 62]. This implies that the resistance of the mass transfer is not significant. Instead, the reduction rate was assumed to be controlled by the chemical reaction, **Reaction (1.10)**.

Ostrovski et al. also calculated the effect of temperature, slag chemistry and coke size to observe how the three main variables affect the reduction rate of MnO [62]. The calculated results of the three effects are shown in **Figures 2.23 (a), (b)** and **(c)**.

(a)

(b)

(c)
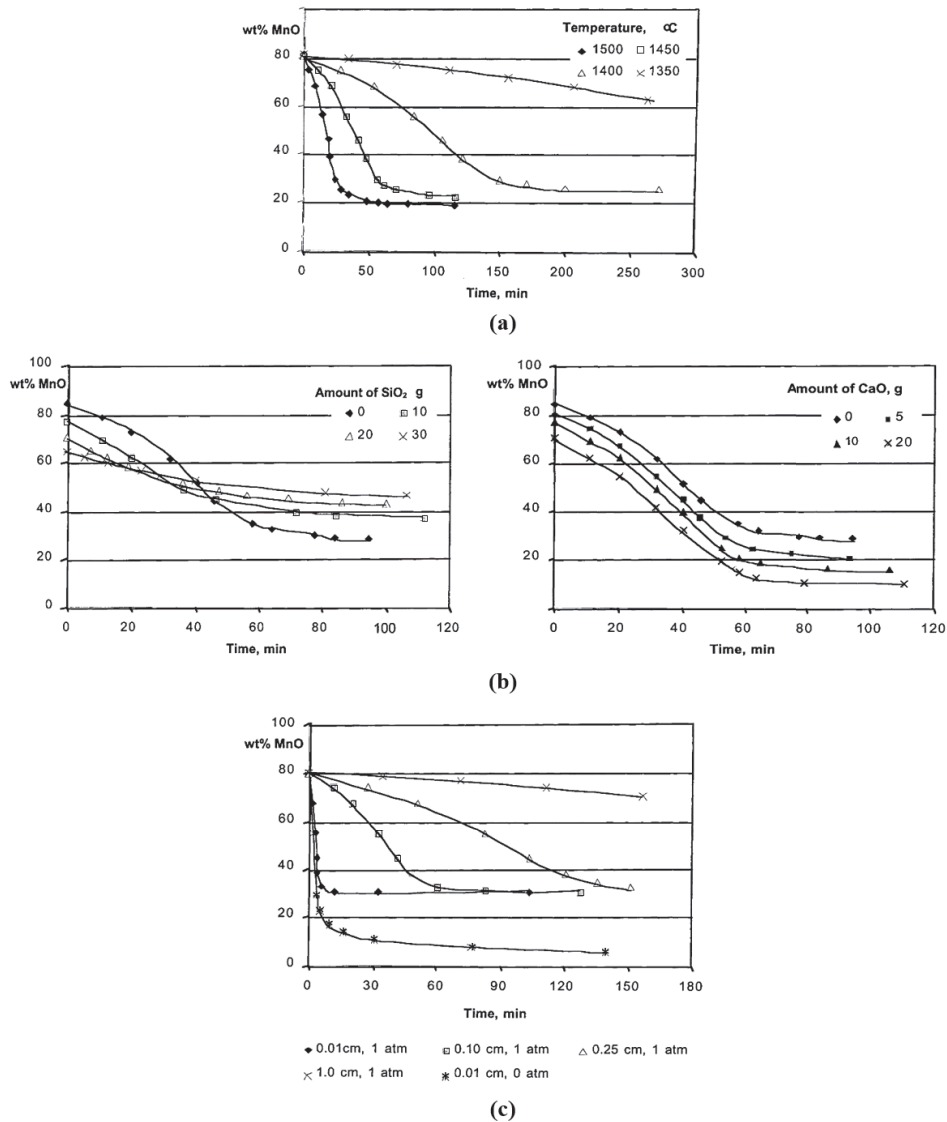
Figure 2.23: Calculated results of Equation (2.16). Reduction rate of MnO as a function of (a) temperature, (b) amount of SiO$_2$ and CaO at 1450 °C and (c) coke size at 1400 °C [61]. Reduction rate increased with higher temperatures, higher CaO/SiO$_2$ ratio and lower particle size of carbon reductant. Note that the symbols are from calculated results.

Increasing the temperature showed an increasing rate and extent of MnO reduction. The comparison between reduction at 1350 and 1500 °C indicates that the reduction rate increases drastically with increasing temperatures. The time difference towards equilibrium is also significantly comparable. This implies that reduction of MnO in manganese silicate slags can be highly sensitive to temperature. The effect of temperature on the rate constant and the driving force were thought to be the main contributions. According to the Arrhenius equation, **Equation (2.19)**, the rate constant increases with increasing temperatures. The driving force is increased due to the increasing equilibrium constant, which lowers the equilibrium part of MnO in the slag phase or the metal phase. Note that the kinetic parameters (activation energy and rate constants) from previous studies were used in the calculations [21, 63].

The effect of slag chemistry was estimated with SiO_2 and CaO addition. Increasing SiO_2 addition had retarded the reduction rate of MnO. According to the model, SiO_2 addition affected the reduction rate of MnO by decreasing the driving force. Increasing amount of SiO_2 decreased the activity of MnO and hence lowered the driving force of MnO reduction. Note that the activity relation between MnO and SiO_2 was previously discussed in the previous chapter, **Figure 2.12**. In contrast, the addition of CaO increased the reduction rate of MnO, where the driving force had increased due to the increased activity of MnO from the effect of CaO addition. However, the effect of CaO addition was not significantly high because the addition of CaO dilutes the slag with respect to MnO. Thus, Ostrovski et al. concluded that an increase in slag basicity increases the driving force by decreasing the equilibrium MnO concentration, and therefore, increase the reduction rate and extent of MnO reduction.

The effect of coke size showed obvious results. The reduction rate of MnO increased with decreasing coke diameter, where the reaction interface between slag and coke had increased. Calculated results showed that the slag can approach equilibrium faster by using smaller coke particles.

These calculated results can be useful to predict how the reduction rate of MnO in SiMn slags changes with various experimental conditions. Since SiMn slags are essentially similar with FeMn slags, the same rate expression for MnO reduction can be assumed. However, one should be aware that the reduction rate of MnO by using this rate model can show different behaviors in the SiMn process. For example, while a unit activity of MnO is expected in FeMn slags due to the presence of solid MnO, the driving force is considered to be relatively lower in SiMn slags because of the higher concentration of SiO_2. The contribution of the driving force in SiMn slags will be relatively lower than in FeMn slags, and thus, possibly performs a different reduction behavior and rate.

2.2.2 Kinetic model of SiO_2 dissolution in slag

Maroufi et al. studied the dissolution rate of SiO_2 in SiMn slags [64, 65]. From an excavation of a SiMn furnace by SINTEF/NTNU, they observed unreacted quartz particles near to the coke-bed zone and assumed that the dissolution of SiO_2 was the rate-determining step. The dissolution rate and solubility of quartz in SiMn slags were measured by dipping a rotating quartz rod into SiMn slags under an inert atmosphere between 1400 and 1550 °C. The dissolution rate of SiO_2 in SiMn slag was expressed as **Equation (2.21)**:

$$r_{SiO_2, \ (diss.)} = k \cdot \rho_{Slag} \cdot (C_s - C_b) \tag{2.21}$$

where $r_{SiO2, (diss.)}$ [g/cm$^2 \cdot$ s] is the dissolution rate of SiO_2, k [cm/s] is the mass transfer coefficient calculated from the experimental data, ρ_{Slag} [g/cm^3] is the slag density and C_s and C_b [wt%] are the concentration of SiO_2 at SiO_2-slag interface and in bulk slag, respectively.

The results of the measured dissolution rate of SiO_2 in SiMn slag with different rotation speed are described in **Figure 2.24**. Maroufi et al. observed that the dissolution rate of SiO_2 depends on the rotation speed of the SiO_2 rod, and thus concluded that the dissolution rate of SiO_2 is controlled by the mass transfer in the molten slag. In addition, adding CaO and MnO into the slag had increased the dissolution rate of SiO_2, while addition of SiO_2 and Al_2O_3 showed the opposite results. The silicate network modifying and reinforcing properties of acidic and basic oxides seem to correlate to their studies (further explained in the following section), where the network modifying CaO addition was favorable for faster dissolution rates.
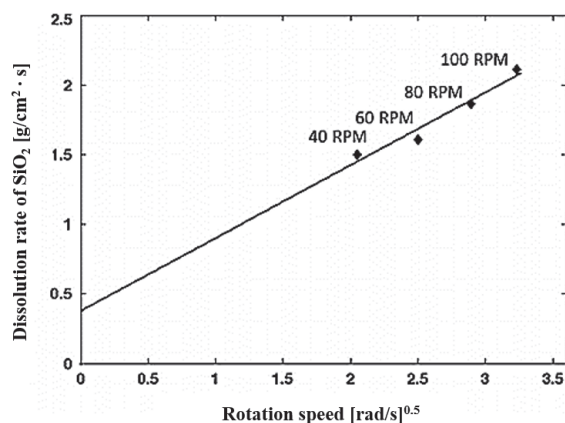
Figure 2.24: Dependence of dissolution rate of SiO_2 in SiMn slag on square root of rotation speed [64, 65]. Dependence of the dissolution rates on the rotation speed of the SiO_2 rod indicates that the dissolution rate is controlled by mass transfer in the molten slag.

However, the possibility of the chemical reaction, **Reaction (1.11)**, being the rate-determining step should also be considered. It was not clear whether the unreacted quartz particles from the excavation was due to bad furnace performance [21] or from other unexplained reasons. Since limited information is known during the operation of a furnace, the assumption of dissolution of SiO_2 being the rate-determining step may not be the case. Also, the temperatures of SiMn slags is previously reported to be approximately 1650 °C [1, 19, 22, 41], but the slag temperature in the SiO_2 dissolution experiments were about 100 °C lower.

2.2.3 Slag viscosity

Viscosity is an important property of slag which has a great impact on the flow pattern in the furnace and possibly the kinetics of slag-carbon reactions. Although the chemical reaction of MnO reduction was considered as the main assumption in the previous section, the viscosity of the slag should also be investigated. In this case, the mass transfer of MnO and SiO_2 reduction should be considered and the comparison of basicity, which can be correlated to slag viscosity, might be important.

The general definition of basicity is the ratio between the overall amount of basic and acidic oxides. An illustration of basic, intermediate and acidic oxides is described in **Figure 2.25** and the definition of slag basicity is shown in **Equation (2.22)**.
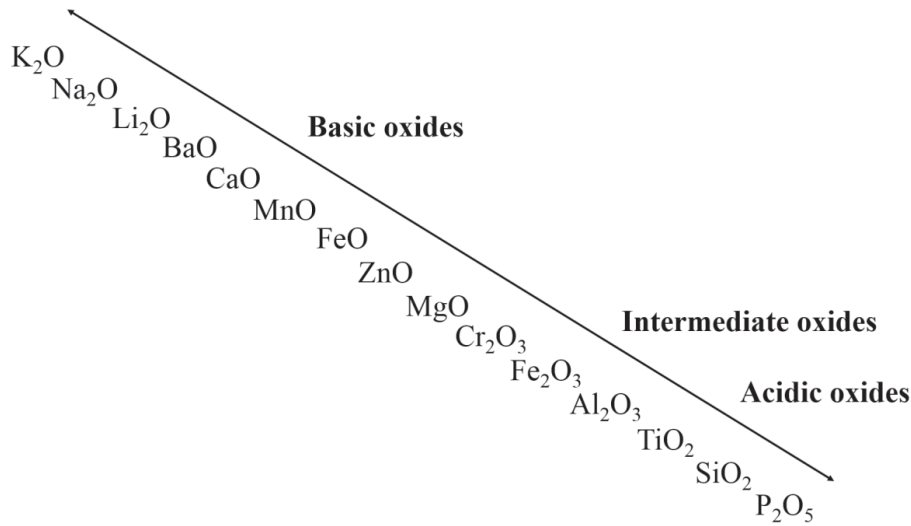
Figure 2.25: Illustration of basic, intermediate and acidic oxides. Intermediate oxides can behave as basic or acidic oxides depending on the total basicity [66].

$$Basicity = \frac{\sum Basic\ oxides}{\sum Acidic\ oxides} \tag{2.22}$$

The definition of basicity changes depending on the slag system dealt with, but the common expression for manganese ferroalloy production can be described by the following equation, **Equation (2.23)**:

$$Basicity_{(FeMn)} = \frac{CaO + MgO}{Al_2O_3 + SiO_2} \tag{2.23}$$

Since the major slag components in manganese ferroalloy slags are MnO, SiO$_2$, CaO, MgO and Al$_2$O$_3$, the basicity defined in **Equation (2.23)** is mostly used to describe the relative amount of oxides in FeMn slags where MnO is not included due to its changing amount from reduction. It was previously shown that this basicity gives better correlation with industrial data and slag properties than the often used concept "lime basicity", (CaO+MgO)/SiO$_2$ [1, 67].

For SiMn slags, the basicity defined in **Equation (2.24)** is often more important than the basicity defined in **Equation (2.23)**, since the reduction of MnO and SiO$_2$ occurs simultaneously during the process. This basicity is rather informally known as the "R-ratio". The R-ratio was briefly shown in the previous section, where it showed the relationship with the equilibrium slag and metal compositions. There are no references regarding the relationship between the R-ratio and kinetic information, and it would be interesting to observe if the reduction rate in SiMn slags correlates to the R-ratio.

$$Basicity_{(SiMn)} = R = \frac{CaO + MgO}{Al_2O_3} \tag{2.24}$$

38

The slag viscosity can be correlated to the basicity where the ratio can indicate if the viscosity of the slag is relatively high or low. The viscosity is a function of the total slag components and not just the components from the basicity expressions. The production of SiMn alloy occurs in manganese silicate slags and the viscosity can be related to the degree of polymerization of silicate melts. The degree of polymerization of silicate slags is affected by the basic and acidic type of oxides added, where the network of silicate structures is modified or reinforced [68-72]. Consequently, the polymerization changes the slag viscosity. **Figure 2.26** shows an example of the relationship between slag viscosity and polymerization of silicate structures.
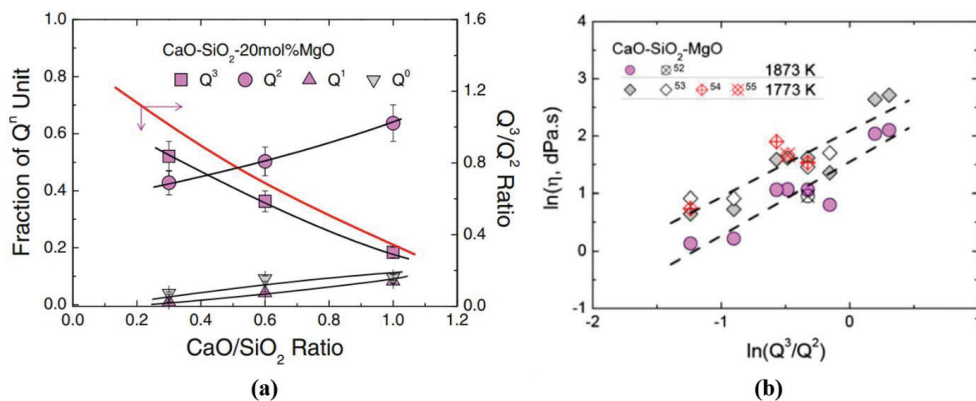
Figure 2.26: (a) Measured relationship between silicate structural units (Q^3: Sheet, Q^2: Chain, Q^1: Dimmer and Q^0: Monomer) with CaO/SiO_2 ratio at 1600 °C and with (b) viscosity at 1500 and 1600 °C in the CaO-SiO_2-MgO system [73]. Increasing CaO/SiO_2 ratio decreases the Q^3/Q^2 ratio and consequently the slag viscosity.

There are numerous studies showing the relation of silicate structures and the slag viscosity [73-76]. Addition of fluxes, such as CaO and CaF_2, in slag modifies the network of silicate structures. This relation was observed through Raman spectra measurements where the complicated "Q^3: Sheet" structures of silicates were subsequently depolymerized into "Q^2: Chain", "Q^1: Dimmer" and "Q^0: Monomer" structures with increasing amount of fluxes. Consequently, the slag viscosity decreases with increasing amount of CaO and MgO and with increasing temperatures. An example for the viscosity in the MnO-SiO_2-CaO system at 1500 °C from previous studies is described in **Figure 2.27**. It also indicates that increased content of SiO_2 reinforces the silicate network and thus increasing the slag viscosity. Network modifying CaO will show the opposite behavior.
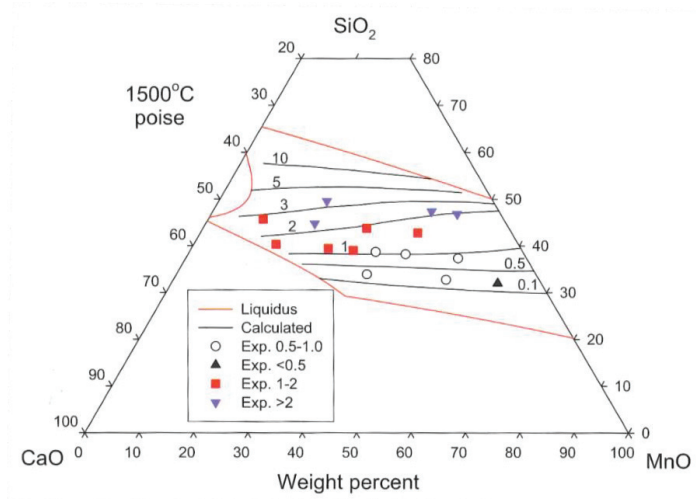
Figure 2.27: Calculated iso-viscosity [poise] curves for the MnO-SiO$_2$-CaO system at 1500 °C [1] and measured experimental data at the same temperature [77]. At constant MnO, the relationship between the CaO/SiO$_2$ ratio with slag viscosity is clearly shown: Slag viscosity decreases with increasing CaO/SiO$_2$ ratio.

2.2.4 Influence of iron and sulfur

The influence of iron on the reduction rate of MnO in slag was previously studied [62, 78, 79], as well as the effect of sulfur was observed [62, 80]. **Table 2.5** describes the analyses from SiMn slag reduced with coke and charcoal at 1600 °C [24]. Whether the carbon reductant was coke or charcoal, the concentration of MnO in the slag phase after 30 minutes were around 9 wt% for all cases. This implies that the type of carbon reductant had less correlation with the reduction of MnO, but other factors were more influencing. It was proposed that iron and sulfur were included in the initial slag phase, which seemed to contribute to the reduction.

Table 2.5: SiMn slag analyses at 1600 °C with different holding time (reorganized) [24]. Concentration of MnO in slag was similar after 30 minutes regardless of the carbon reductant type (MnO content in slag after 30 minutes are in bold).

| Reductant | Time [min] | Slag analysis [wt%] | | | | | | | Note |
		MnO	SiO_2	CaO	MgO	Al_2O_3	FeO	R*	
Charcoal 30	0	26.1	45.1	11.3	6.0	10.2	0.8	1.69	
	15	15.7	49.5	13.8	7.5	12.7	0.5	1.68	
	30	**10.5**	50.2	15.5	8.4	14.5	0.4	1.65	
Charcoal 60	0	21.2	46.5	12.6	6.7	11.6	1.1	1.66	
	15	11.2	49.7	15.5	8.5	14.5	0.5	1.65	
	30	**8.4**	50.1	16.4	8.9	15.3	0.5	1.65	T = 1600 °C
	45	7.5	49.4	17.0	9.3	16.0	0.5	1.65	
	60	7.9	47.0	16.6	9.9	17.1	1.3	1.55	Slag contained:
Coke 30	0	16.1	48.3	13.8	7.5	12.9	1.1	1.65	0.44 wt% S
	15	11.2	50.5	15.0	8.2	14.1	0.5	1.65	3.6 wt% Fe
	30	**9.0**	50.4	15.9	8.7	15.0	0.5	1.64	
Coke 60	0	22.2	47.0	12.4	6.6	11.0	0.4	1.72	
	15	14.2	48.8	14.6	7.9	13.6	0.6	1.65	
	30	**9.6**	50.6	15.9	8.7	14.6	0.3	1.68	
	60	9.4	46.7	17.2	9.5	16.5	0.5	1.62	

* R = $(CaO+MgO)/Al_2O_3$

Tranell et al. previously observed the effect of iron and gas composition in SiMn slag for reduction [79]. **Figure 2.28** shows the concentration of MnO in slag at 1600 °C as a function of time with and without the presence of iron in CO and Ar atmospheres. The results indicate that the reduction rate is faster with iron present in the slag phase regardless of the atmosphere. The difference seems to be from the increased driving force of MnO reduction in **Equation (2.20)**. The effect of iron lowers the activity of manganese and hence, the driving force is increased. From the comparison of gas composition however, the reduction of MnO was faster with CO gas. The results were against expectations because the driving force of MnO reduction should had increased by Ar gas, similar from the effect of iron.
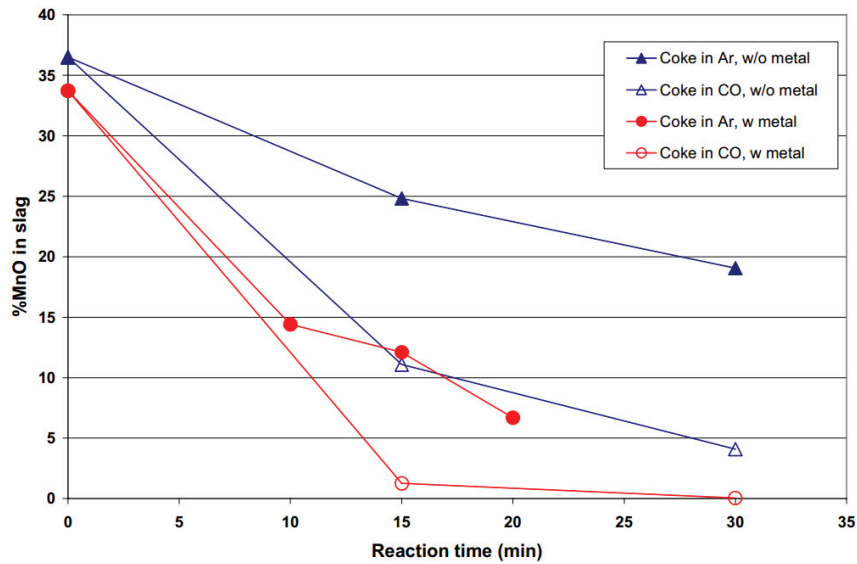
Figure 2.28: Concentration of MnO in slag as a function of time at 1600 °C with (w) or without (w/o) iron [79]. Faster reduction of with (w) iron was thought to be from the increased driving force.

Lower concentration of MnO in slag without the presence of iron were also observed in their study [79]. The measured slag compositions are shown in **Table 2.6**. The comparison between with and without iron can be observe with both "Exp. 9"/"Exp. 26" and "Exp. 18"/"Exp. 30". It indicates that the MnO concentration in the slag phase is lower with the presence of iron, but the difference is rather low below 5 wt% MnO. Both cases showed that the concentration of MnO in slag was low after 30 minutes at 1600 °C. It was also questionable if the presence of iron had actually made a difference because some of the total slag analyses were lower than 95 wt%.

Table 2.6: SiMn slag analyses at 1600 °C with various experimental conditions (reorganized) [79]. Similar degree of MnO reduction was also observed in slags without iron (comparison can be seen in bold).

Exp. No.	Metal (Fe)	Substrate	Gas	Time [min]	MnO	SiO$_2$	CaO	MgO	Al$_2$O$_3$	FeO	Total	Note
1			-	-	36.5	21.2	15.1	4.9	13.5	0.1	91.3	Init. slag
2				15	24.8	31.3	17.8	6.1	17.1	0.1	97.2	
3			Ar	15	19.5	25.4	19.0	6.3	17.1	0.2	87.5	
4				30	28.9	29.2	16.9	5.9	15.8	0.1	96.9	
5		Coke		30	9.2	31.7	21.5	6.9	21.6	0.1	91.0	
6				15	24.0	35.9	16.2	5.2	15.3	0.5	97.1	
7				15	11.1	43.1	19.0	6.2	17.3	0.1	96.8	
8			CO	15	14.6	34.8	18.0	6.1	15.9	0.3	89.7	
9				**30**	**4.1**	44.9	20.5	6.3	18.5	0.1	94.4	
10	No			30	7.4	37.2	19.9	6.5	17.2	0.4	88.8	-
11				15	28.0	29.2	17.4	5.5	16.0	0	96.1	
12				15	20.8	26.8	19.6	6.5	17.3	0.3	91.2	
13			Ar	30	24.5	31.0	18.3	5.8	16.9	0.1	96.6	
14				30	19.4	33.8	19.7	6.4	18.5	0.1	97.8	
15		Charcoal		30	12.9	29.2	21.4	7.1	19.2	0.1	89.9	
16				15	1.0	35.7	27.4	6.4	24.8	0	95.3	
17			CO	15	14.7	28.3	20.9	7.0	17.6	0.2	88.8	
18				**30**	**0.4**	35.8	27.2	6.4	24.2	0	94.1	
19				30	3.0	30.3	25.0	7.5	21.5	0.2	87.5	
20			-	-	38.4	24.3	15.5	3.5	13.4	1.4	96.5	Init. slag
21				0	33.7	24.7	16.5	4.5	15.2	0.2	94.8	
22				10	14.4	31.9	21.3	5.9	21.5	0.2	95.2	
23			Ar	15	12.1	34.2	22.6	6.0	19.8	0.2	95.0	
24		Coke		20	6.7	32.1	23.9	6.4	26.2	0.1	95.3	
	Yes			30			- Slag phase not observed -					-
25			CO	15	8.2	44.1	21.4	5.6	17.6	0.2	97.1	
26				**30**	**1.1**	43.5	24.9	5.8	20.2	0.2	95.7	
27			Ar	15	1.3	34.8	28.4	6.3	24.1	0	94.9	
28		Charcoal		30	0.1	31.9	28.8	5.4	24.4	0.1	90.6	
29			CO	15	0.2	32.0	32.3	4.0	26.1	0	94.7	
30				**30**	**0.1**	34.2	27.4	5.5	23.1	0.1	90.4	

Skjervheim et al. observed that small addition of sulfur considerably increased the reduction rate of MnO [62, 80]. 0.2 wt% sulfur was added into a three-component slag (MnO-SiO$_2$-CaO) at 1500 °C. The comparison between without and with 0.2 wt% sulfur is shown in **Figure 2.29**. It describes that sulfur affects the reduction rate considerably in manganese ferroalloy slags.
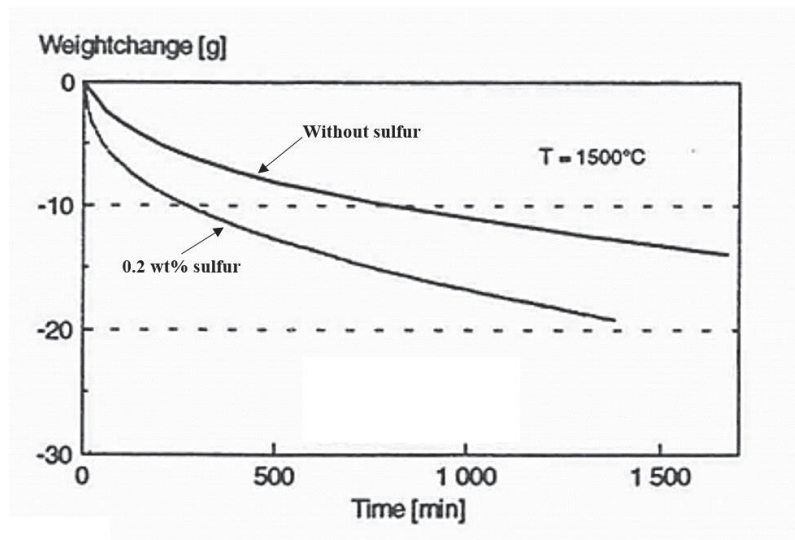
Figure 2.29: Weight change of manganese slag versus time at 1500 °C: Effect of 0.2 wt% sulfur addition [62]. Reduction rate of MnO increased significantly when sulfur was presented in the slag phase.

On the contrary, Kuangdi et al. reported opposite results where the addition of sulfur decreased the reduction rate of MnO [81]. The sulfur variation was 0.027, 0.048 and 0.079 wt% in the slag, where the components were MnO, SiO_2, CaO, MgO and FeO. The comparison of MnO reduction with different amount of sulfur at 1550 °C is shown in **Figure 2.30**. They concluded that sulfur decreased the reaction interface between slag and dissolved carbon in the metal phase and thus, the reduction rate of MnO decreased with increasing amount of sulfur. However, their results may be in contrast with known phenomena because sulfur is well known to be a surface-active specie for most metals [82]. In addition, compared to the previous case, where 0.2 wt% of sulfur had enhanced the reduction rate of MnO reduction, the sulfur amount was considerably lower. The initial amount of MnO was all different in the three case, and the sulfur amount may not had been sufficient to determine the influence on reduction.
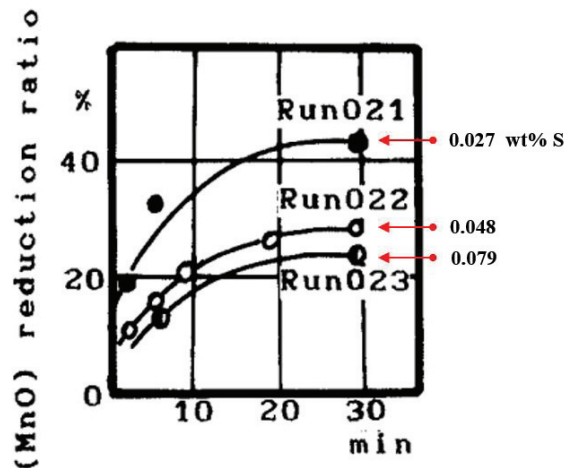
Figure 2.30: Reduction ratio of MnO in slag with sulfur content of 0.027, 0.048 and 0.079 wt% at 1550 °C [81]. Reduction rate had decreased with increasing amount of sulfur. However, the initial amount of MnO were different in the three cases, and the amount of sulfur does not seems sufficient to discuss the influence of sulfur.

2.3 Summary of theoretical background

For convenience, the summary with the author's interpretation of the thermodynamic and kinetic observation of previous studies is recapitulated in the following bulleted points:

- Thermodynamics
    - The reduction behavior between FeMn and SiMn charges can be different: The binary $MnO-SiO_2$ system (**Figure 2.11**) indicates that solid MnO will be presented in FeMn slags until liquidus temperatures (1500 − 1600 °C), while complete liquid slag is expected in SiMn slags at relatively lower temperatures around 1350 °C.

    - The melting of raw materials in SiMn charges to generate slag is not well studied: Thermodynamically, complete liquid slag is expected at above 1350 °C, but the melting temperatures of manganese ores and quartz are relatively higher than 1350 °C. Addition of HC FeMn slag is likely to contribute to the slag formation around 1350 °C due to its low melting temperature (~ 1250 °C). However, it is not clear whether the slag formation temperatures will be similar when HC FeMn slag is not included in SiMn charges.

- Kinetics
    - The chemical reaction of MnO with carbon is assumed to be the rate-determining step: This was previously studied where a rate model was derived from FeMn slags. As SiMn slags are essentially similar with FeMn slags, the same rate model can be used to determine the kinetic parameters of MnO reduction.

45

o The rate-determining step for SiO_2 reduction is not clear: The dissolution of quartz as SiO_2 was observed from previous studies. However, the melting phenomena of raw materials in SiMn charges requires more observation to confirm if the dissolution of SiO_2 into slag is rate-determining.

o The possible influence of slag viscosity on the reduction rate of MnO and SiO_2 should be considered: If the assumption of chemical reaction being the rate-determining step is not valid, the mass transfer of MnO and SiO_2 reduction should be considered, and the comparison of basicity, which can be correlated to slag viscosity, might be important.

o The effect of iron and sulfur in SiMn slags should be further investigated: The effect of iron seems valid from previous studies, but the effect of sulfur is not evidently proven.

2.4 Objective and research topics

Since the reaction mechanisms and kinetics from melting of raw materials to SiMn metal production are not well determined, the reduction of MnO and SiO_2 in the coke-bed zone will be the main focus of this study. Ascertaining the kinetic information from the melting behavior of raw materials to the reaction rates of MnO and SiO_2 reduction is focused in this work.

The main objective of this work is to determine the reaction rates of MnO and SiO_2 reduction and extract kinetic information, which may be critical in the SiMn process. To achieve this goal, the study begins with determining the melting behavior of raw materials in SiMn charges at relatively low temperatures. As the reduction of MnO and SiO_2 will take place from liquid slag, the formation of incipient slag phase from melting of raw materials is important. Raw materials with different properties, such as melting temperatures, in the SiMn charge are not well studied, and the reduction rate of MnO and SiO_2 can be different depending on the presence of solid manganese ore and quartz in the liquid slag phase.

After determining the melting behavior of raw materials in SiMn charges, the reduction rate of MnO and SiO_2 will be determined from experimental measurements, where the main variables will be the temperature and the charge composition. From the experimental results, rate models for MnO and SiO_2 reduction are considered to express the changing amount of MnO and SiO_2 during reduction at high temperatures. The reduction rates of MnO and SiO_2 should be considered based on the rate-determining step. Whether if the dissolution of manganese ore and quartz into slag or the chemical reaction of MnO and SiO_2 with carbon is the case, kinetic models are required to investigate which factors influence the metal producing rates.

According to the objective of this study, the following bulleted points describe the four subsequent research topics which will aid to ascertain the questions related to this work.

- Research topics -

- Research topic #1: The melting behavior of raw materials
  The formation of liquid slag from melting of raw materials in SiMn charges is not clear. Comparison of various SiMn charge compositions is required to determine the rate-determining steps of MnO and SiO_2 reduction. It is not clear whether the chemical reaction of MnO and SiO_2 reduction, the diffusion of MnO and SiO2 in the liquid slag or the dissolution of charge materials is the rate-determining step in the SiMn process. In this thesis, the dissolution of raw materials will be studied.

- Research topic #2: The reduction behavior of SiMn charges
  Relating to the previous topic, the reduction of SiMn charges can be different from the FeMn case. The presence of the dissolving solid manganese phase during reduction is a slag characteristic in the FeMn case, which influences the reduction rate of MnO. It is not clear whether dissolving solid manganese ore and quartz will be presented in SiMn slags and the reduction rate could be different.

- Research topic #3: Kinetic estimations
  After experimentally determining the reduction behavior of SiMn charges, extraction of further kinetic information requires numeric data, which can be compared with different experimental conditions. Establishing the adequate rate models, which can describe the reduction rates of MnO and SiO_2 in various SiMn slags, will allow important kinetic information in the SiMn process.

- Research topic #4: Confirmation through synthetic materials
  Lastly, the confirmation of kinetic information, which were obtained by using industrial materials, is necessary through experiments with synthetic materials. The kinetic information obtained from using industrial materials are not conclusive and other possible interpretation can be considered. Thus, the assumed kinetic information should be confirmed through a control experimental condition by using synthetic materials.

Under the co-supervision of the author, there has been two master's projects as well as an internship project that has been working with the same issues during the thesis work. The highlights of these projects are also presented in the results, and will be hence used in the discussion part.

Chapter 3: Experimental Apparatus, Procedures and Model Description

As stated earlier, the objectives of this work were to determine the melting behavior of raw materials and the reduction rates of MnO and SiO_2 from various SiMn charge compositions. This chapter describes the preparation of raw materials and SiMn charges, thermogravimetric analysis (TGA) furnace, considerations of kinetic calculation and analysis methods according to the research topics.

3.1 Preparation of raw materials and SiMn charges

The chemical compositions of the industrial raw materials are described in **Table 3.1**. The raw materials were analyzed by SINTEF MOLAB AS. The main part of experiments was carried out with Assmang ore where the melting and reduction behavior were observed. HC FeMn slag was also used in these experiments as it is used as raw material for the SiMn process in Norwegian manganese ferroalloy industries [1, 19].

Table 3.1: Chemical composition of industrial raw materials. Assmang ore and HC FeMn slag were used as manganese-bearing raw materials (dry basis).

Material	MnO	MnO$_2$	SiO$_2$	Fe$_2$O$_3$	CaO	MgO	Al$_2$O$_3$	S	C	CO$_2$	Total [wt%]
Assmang	32.69	33.22	5.77	15.06	6.26	1.1	0.26	0.16	0.27	3.52	98.31
Quartz	0.14	-	93.85	-	0.09	0.05	1.19	-	-	-	95.32
HCS*	35.23	-	25.45	-	18.45	7.53	12.3	0.46	0.46	-	100.06
Coke	0.04	-	5.6	0.86	0.42	0.22	2.79	0.4	87.68	-	98.01

* HCS: High Carbon FeMn Slag

SiMn charges based on synthetic materials were also studied in this work. The characteristics of the synthetic materials are described in **Table 3.2**. The use of synthetic materials along with industrial materials was to confirm the important aspects in reduction which were observed with industrial SiMn slags experiments. The influence of these aspects from the industrial slag experiments were isolated and observed in a controlled slag system by using synthetic slags.

Table 3.2: Characteristics of synthetic materials.

Material	Form	Size [mm]	Purity [%]	Source
MnO		~ 0.25	99.0	SIGMA-ALDRICH
SiO$_2$	Fine powder	~ 0.002	99.5	
CaO		< 0.01	99.95	Alfa Aesar
FeS		-	99.98	
Fe	Irregular pieces	3.18 − 6.35	99.99	

Three different ore sizes of the industrial raw materials were selected which is shown in **Table 3.3**. The different ore sizes were prepared by crushing the raw materials in a steel mortar and sieving through sieve sizes between 0.6 and 20 mm. The different particle sizes were used to observe the effect of size on the reduction rate and melting behavior of raw materials. The comparison between 0.6 − 1.6 and 4.0 − 6.3 mm

was to investigate how the size of raw materials affects the reduction rate, and the comparison between $4.0 - 6.3$ and $15 - 20$ mm was to observe the melting behavior of raw materials.

Table 3.3: Raw material sizes with experiment purposes and temperature range. Different sizes of raw materials were considered to observe the effect of particle size on the reduction behavior and melting of raw materials.

Particle size [mm]	Experiments	Temperature range [°C]
$0.6 - 1.6$	Reduction	$1500 - 1650$
$4.0 - 6.3$	Reduction / Melting	$1200 - 1650$
$15 - 20$	Melting	$1200 - 1400$
Compare	• $0.6 - 1.6$ vs. $4.0 - 6.3$ mm: Influence of raw materials size on reduction rate • $4.0 - 6.3$ vs. $15 - 20$ mm: Melting behavior between raw materials	

Graphite crucibles, which were manufactured from TANSO AB, were used to contain the raw materials. The dimensions of the graphite crucibles are described in **Figure 3.1**. The crucible is 36 mm outer diameter, 30 mm inner diameter, 70 mm height and 61 mm deep.
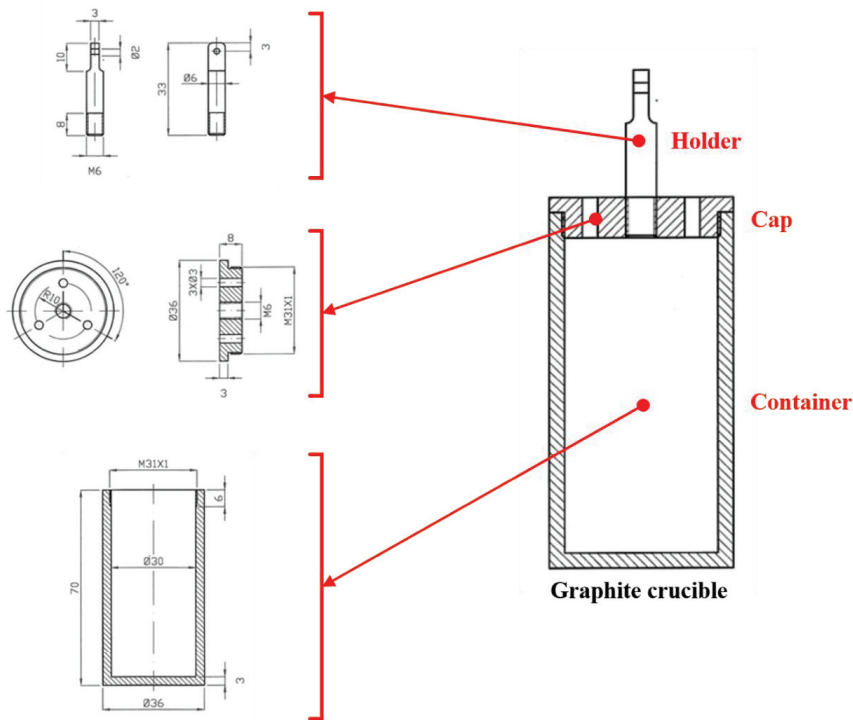
Figure 3.1: Blueprint of the dimensions (mm) of the graphite crucible used in experiments: Crucible container, cap and holder.

Based on the raw materials and particle sizes, the SiMn charges are described in **Tables 3.4, 3.5, 3.6** and **3.7**. The charges were considered based on the research topics described in the first chapter.

The SiMn charges in **Table 3.4** were used to observe the melting behavior of raw materials between temperatures 1200 and 1650 °C. As the melting behavior of SiMn raw materials is not well studied, charges "M1" and "M2" were initially considered to observe the melting of raw materials with and without HC FeMn slag. In addition, charge "M3" was used to examine the melting behavior of charge "M2" with increased particle sizes without coke. Note that charge "M3" was not an example of SiMn charge composition, but to observe the interaction between manganese ore and quartz particles.

Table 3.4: SiMn charges according to research topic #1: The melting behavior or raw materials. Charges "M1" and "M2" were initially observed between 1200 and 1650 °C, and further experiments were done with charge "M3" between 1200 and 1400 °C.

Exp. No.	Assmang	Quartz	HCS	Coke	Total [g]	Size [mm]	Note
M1	10	10	10	5	35		With HCS
M2	12	12	-	5	29	4.0 − 6.3	Without HCS
M3	15	15	-	-	30	15 − 20	Increased size of M2 Without coke

The charge compositions in **Table 3.5** were prepared to observe the different reduction behavior between FeMn and SiMn charges with two different particle sizes. The comparison was to observe if the different driving forces of MnO in FeMn and SiMn slags have different reduction behaviors, as it was previously discussed in **Section 2.3.1**. Charge "R1" represented a FeMn charge, where manganese ore is the main charge material, as reference. Charges "R2" and "R3" were used as SiMn charges to compare with the reference FeMn charge, "R1". Two different particle sizes, 0.6 − 1.6 and 4.0 − 6.3 mm, were compared for each charge type to investigate the influence of particle sizes. The charges in **Table 3.5** were all heated up to 1600 °C.

Table 3.5: SiMn charges according to research topic #2: The reduction behavior of raw materials. FeMn and SiMn charges were heated up to 1600 °C to compare the reduction behavior from the mass changes.

Exp. No.	Assmang	Quartz	HCS	Coke	Total [g]	Size [mm]	Notes
R1.a	23	-	-		30	0.6 − 1.6	Reference charge FeMn
R1.b						4.0 − 6.3	
R2.a	23	10	-	7	40	0.6 − 1.6	Without HCS SiMn
R2.b						4.0 − 6.3	
R3.a	13	7	13		40	0.6 − 1.6	With HCS SiMn
R3.a						4.0 − 6.3	

Table 3.6 shows the SiMn charges which were considered to extract kinetic information. The amount of each raw material was carefully measured to aim at approximately 5 wt% MnO and 40 wt% SiO_2 in the slag phase and 18wt% silicon in the metal phase, which is close to the thermodynamic equilibrium of slag and metal at 1600 °C. The detailed calculations of mass balance of the charge types are further shown in **Appendix A**. The experiments were conducted by using two different heating rates, 4.5 and 9 °C/min, between 1500 and 1650 °C, where several temperatures were considered. Note that the raw materials were charged into the crucible as layers to prevent undissolved quartz particles, where the details are explained in **Section 4.2.3**.

Table 3.6: SiMn charges according to research topic #3: Kinetic estimations. Note that two different heating rates (4.5 and 9 °C/min) were applied. Experiments at temperatures between 1500 and 1650 °C were conducted, where the temperature difference between measurements was 10 °C (1500, 1510, …, 1640 and 1650 °C).

Exp. No.	Assmang	Quartz	HCS	Coke	Total [g]	Size [mm]	Mn Source
As	7	1.94	-	2.2	11.14		Assmang
As/HCS	4	1.69	4	2.5	12.19	0.6 − 1.6	Assmang + HCS
HCS	-	1.46	10	3	14.46		HCS

As an additional experiment, charge "As" with different amount of sulfur was also considered, which is described in **Table 3.7**. This was conducted after kinetic estimations of the experiments of **Table 3.6**, where the amount of sulfur was assumed to affect the reduction rate significantly. All charges were heated up to 1650 °C and comparisons were made.

Table 3.7: Charge "As" with different amount of FeS (as sulfur). Charges had the same amount of raw materials of charge "As" in Table 3.6. Amount of sulfur (as FeS) was only different in the charges. All charges were heated up to 1650 °C.

Exp. No.	Assmang	Quartz	Coke	FeS	Total [g]	Int. Sulfur [wt%]
As-0.3				0.03	11.17	0.3
As-0.35				0.04	11.18	0.35
As-0.4	7	1.94	2.2	0.05	11.19	0.4
As-0.5				0.07	11.21	0.5
As-1.0				0.17	11.31	1.0

Lastly, SiMn charges based on synthetic materials, which are shown in **Table 3.8**, were considered to confirm the important aspects observed in the first three research topics. Besides the amount of sulfur, all slag and metal components were fixed, and the reduction kinetics were studied. In addition, a synthetic slag without CaO was considered as a reference slag to investigate the effect of viscosity for reduction aspects. Note that the results and findings from the first three research topic experiments were applied in the final experiment with synthetic slags.

Table 3.8: Synthetic SiMn charges according to research topic #4: Confirmation through synthetic materials. Amount of slag and metal components were controlled where only the amount of sulfur differed between charges "Syn. 0" and "Syn. 0.9". Note that charges "Syn. Ref.", "Syn. 0.15", "Syn. 0.45" and "Syn. 0.75" were heated up to only 1650 °C, whereas the rest were measured between 1500 and 1650 °C with the temperature difference of 25 °C (1500, 1525, …, 1625 and 1650 °C).

Exp. No.	MnO	SiO_2	CaO	FeS	Fe	Coke	Total [g]	Amount of sulfur [wt%]	Notes
Syn. Ref.	3	1.9	-	-	0.092	2	6.99	-	Ref. charge No CaO
Syn. 0				-	0.092		7.99	-	
Syn. 0.15				0.024	0.077		8.00	0.15	
Syn. 0.3				0.048	0.062		8.01	0.3	
Syn. 0.45	3	1.9	1	0.072	0.046	2	8.02	0.45	Amount of Fe fixed
Syn. 0.6				0.097	0.031		8.03	0.6	
Syn. 0.75				0.121	0.015		8.04	0.75	
Syn. 0.9				0.146	-		8.05	0.9	

To summarize the experimental work from the four research topics, **Table 3.9** describes the number of total experiments in subsequent order. There were total 128 experiments in this study: 16 from research topic #1, 6 from research topic #2, 74 from research topic #3 and 32 from research topic #4.

Table 3.9 (1/4): Summary of the total 128 experiments in this thesis work. Abbreviations of the industrial materials are Assmang ore (As), quartz (Q), HC FeMn slag (HCS) and coke (C). Note that experiments in research topic #3 were repeated by using two different heating rates.

Exp. No.	Materials	Size [mm]	Max temperature [°C]	Heating rate [°C/min]	Notes
M1	As + Q + HCS + C		1250		
			1400		
			1530		
			1640		
M2	As + Q + C	4.0 − 6.3	1215	4.5	Research topic #1
			1325		
			1400		
			1500		
			1560		16
			1610		experiments
M3	As + Q (Melting only)	15 − 20	1200	9	
			1250		
			1275		
			1300		
			1350		
			1400		
R1.a	As + C	0.6 − 1.6			Research topic #2
R1.b		4.0 − 6.3			
R2.a	As + Q + C	0.6 − 1.6	1600	4.5	
R2.b		4.0 − 6.3			
R3.a	As + Q + HCS + C	0.6 − 1.6			6
R3.b		4.0 − 6.3			experiments
As	As + Q + C	0.6 − 1.6	1500	4.5	Research topic #3
			1510		
			1520		
			1530		
			1540		
			1550		
			1560		
			1570		
			1580		
			1590		74
			1600		experiments
			1610		
			1620		
			1630		
			1640		
			1650		

Table 3.9 (2/4): Summary of the total experiments in this thesis work (Continue).

Exp. No.	Materials	Size [mm]	Max temperature [°C]	Heating rate [°C/min]	Notes
As/HCS	As + Q + HCS + C		1500		
			1510		
			1520		
			1530		
			1540		
			1550		
			1560		
			1570		
			1580		
			1590		
			1600		
			1610		
			1620		
			1630		
			1640		
			1650	4.5	
HCS	Q + HCS + C	0.6 – 1.6	1500		Research topic #3
			1510		
			1520		
			1530		
			1540		74 experiments
			1550		
			1560		
			1570		
			1580		
			1590		
			1600		
			1610		
			1620		
			1630		
			1640		
			1650		
As	As + Q + C		1500		
			1525		
			1550		
			1575	9	
			1600		
			1625		
			1650		

Table 3.9 (3/4): Summary of the total experiments in this thesis work (Continue).

Exp. No.	Materials	Size [mm]	Max temperature [°C]	Heating rate [°C/min]	Notes
As/HCS	As + Q + HCS + C		1500		
			1525		
			1550		
			1575		
			1600		
			1625		
			1650		
HCS	Q + HCS + C	0.6 – 1.6	1500	9	Research topic #3
			1525		
			1550		
			1575		74 experiments
			1600		
			1625		
			1650		
As-0.3	As + Q + C + FeS		1650		
As-0.35					
As-0.4					
As-0.5					
As-1.0					
Syn. Ref	MnO + SiO2 + C + Fe	Powder /Irregular	1650	9	Research topic #4
Syn. 0			1500		
			1525		
			1550		
			1575		
			1600		
			1625		
			1650		
Syn. 0.15	$MnO + SiO_2 + CaO + C + FeS + Fe$		1650		32 experiments
			1500		
			1525		
			1550		
Syn. 0.3			1575		
			1600		
			1625		
			1650		
Syn. 0.45			1650		

Table 3.9 (4/4): Summary of the total experiments in this thesis work (Continue).

Exp. No.	Materials	Size [mm]	Max temperature [°C]	Heating rate [°C/min]	Notes
Syn. 0.6			1500		
			1525		
			1550		
			1575		
			1600		
			1625		Research topic #4
			1650		
Syn. 0.75	$MnO + SiO_2 + CaO + C + FeS + Fe$	Powder /Irregular	1650	9	
			1500		32 experiments
			1525		
			1550		
Syn. 0.9			1575		
			1600		
			1625		
			1650		

3.2 Thermogravimetic analysis (TGA) and temperature schedule

The experiments were conducted in a graphite tube furnace with an installed mass balance. The furnace is more commonly known as the "TF1" in The Department of Materials Science and Engineering (DMSE) [83], Norwegian University of Science and Technology (NTNU), which is a thermogravimetric analysis (TGA) furnace. The furnace was custom made and had been previously used to study FeMn and SiMn slag systems in various experimental conditions [21, 34, 35, 43]. The schematic cross-section of the furnace is described in **Figure 3.2**.
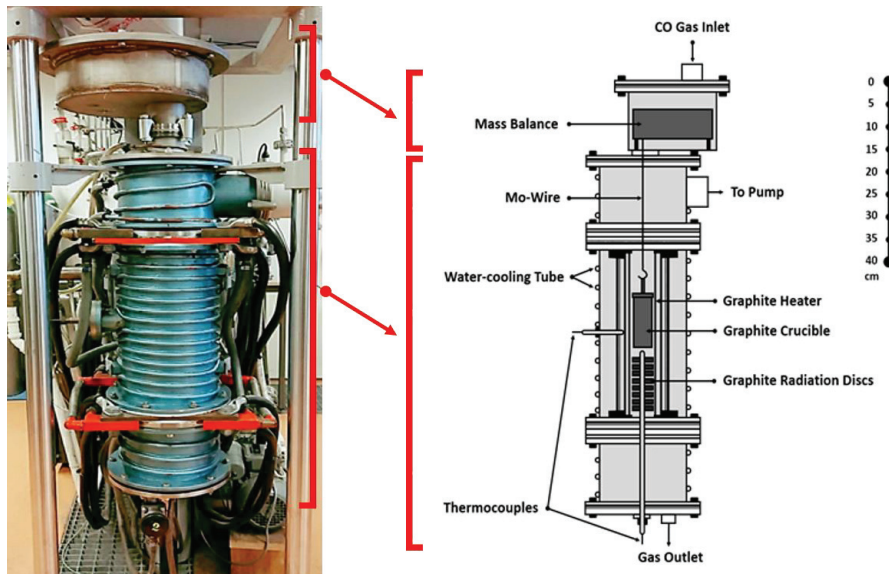
Figure 3.2: "TF1" furnace (left) and cross-section schematic (right). Note that the dimension for the graphite crucible in the figure is given in Figure 3.1.

A mass balance (METTLER-TOLEDO AS, Model: WXS204S) is installed at the top part of the furnace, and a molybdenum (Mo)-wire was used to suspend the graphite crucible inside the furnace chamber. The mass of the crucible was measured every 5 seconds during the experimental condition from the controlling computer software.

Due to the temperature gradient of the heating element in the furnace, two types of thermocouples were used to the measure the temperatures. **Table 3.10** described the two thermocouples used in this study. A B-type thermocouple was placed 1 cm beneath the graphite crucible. The length of the molybdenum wire was adjusted so that the position of the bottom part of the crucible was exposed to the highest temperature measured. Additionally, a S-type thermocouple was placed 1 cm next to the graphite crucible to measure the temperature of the heating element, which is the thermocouple controlling the heating of the furnace. Since the raw materials were mostly positioned at the bottom part of the crucible, the B-type thermocouple was used to measure the temperature in this study.

Table 3.10: Temperature range and uncertainties of thermocouples used in this study: Type-B and type-S.

Thermocouple type	Temperature range [K]	Uncertainty [K]	Position	Notes
B	573 − 2073	0.5	1 cm below crucible	Main temperature indicator
S	223 − 1973	0.3 (< 1273 K) 1 (> 1273 K)	1 cm rear to crucible	-

Prior to the experiments, several measurements of the temperature profile inside the furnace were conducted. **Figure 3.3** shows the temperature gradient of the furnace with thermocouple (B-type) position. According to the temperature measurements, the crucible (bottom part) and thermocouple were positioned at the area where the highest temperatures were measured. The height of charge materials was below 2 cm (for experiments in **Tables 3.6**, **3.7** and **3.8**) where the temperature in the charge materials will be within 0 to 10 °C from the measured value.
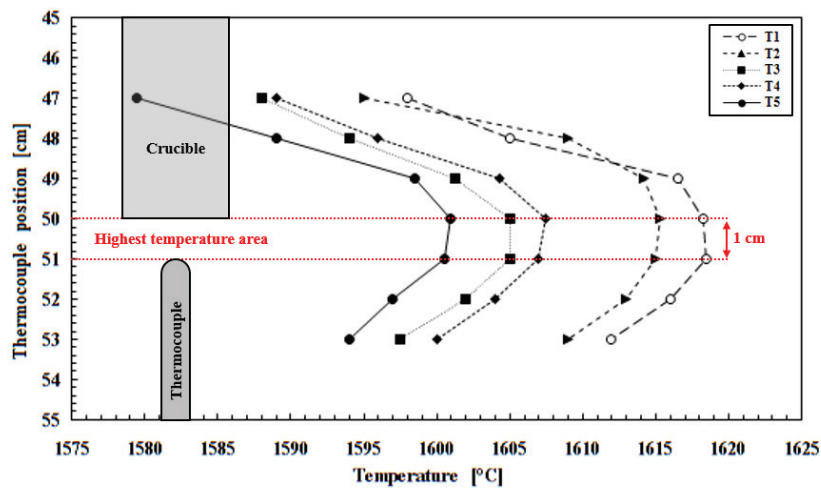
Figure 3.3: Several temperature measurements (T1 – T5) inside the furnace. Positions of crucible (bottom part) and thermocouple are indicated.

The temperature schedules of the experiments according to each research topic are described in **Figure 3.4** and organized in **Table 3.11**. Initially, the furnace was rapidly heated (25 °C/min) up to 1200 °C and held for 30 minutes. This was to ensure complete pre-reduction: Complete vaporization of moisture and all higher manganese and iron oxides are reduced in solid-state with carbon monoxide (CO) gas to MnO and metallic iron (Fe), respectively. The calculated pre-reduced slag components for charges in **Tables 3.5** and **3.6** are shown in **Table 3.12**. Detail calculations can be seen in **Appendix A**. Note that the pre-reduction condition was common for all experiments except for synthetic charges as synthetic materials do not require pre-reduction. The temperature schedule for synthetic charge was similar with the other experiments where the difference was the holding time of pre-reduction (shortened from 30 to 5 minutes).

The melting of raw materials was initially observed with smaller particles (4.0 – 6.3 mm) between 1200 and 1650 °C. Then, larger particles (15 – 20 mm) were further observed between 1200 and 1400 °C. For the reduction behavior of raw materials, FeMn and SiMn charges with two different particle sizes were heated up to 1600 °C. The temperature schedule for kinetic estimations was similar but focused between 1500 and 1650 °C. To simulate the industrial furnace operation, the crucibles were heated up to temperatures between 1500 and 1650 °C but stopped at different temperatures. This was to study the reduction degrees of MnO and SiO$_2$ in SiMn slags at different temperatures. In addition, two different heating rates, 4.5 and 9 °C/min, were applied to observe the influence of the heating rate during reduction.
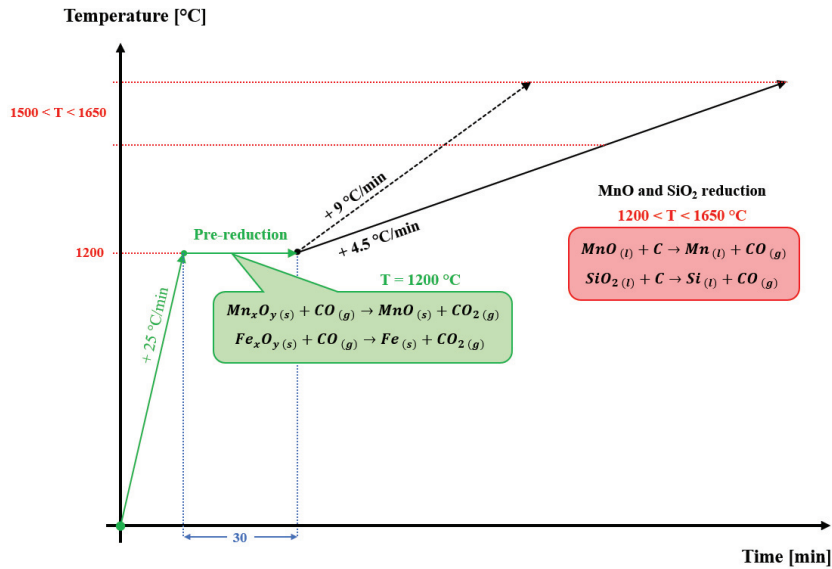
Figure 3.4: Illustration of the temperature schedule for experiments. All samples were held at 1200 °C for 30 minutes to ensure complete pre-reduction. Further heating was done according to Table 3.9. Note that the 30 minutes hold was shortened to 5 minutes for synthetic charges (Research topic #4), where pre-reduction was not required.

Table 3.11: Temperature range and heating rates of experiments after pre-reduction condition at 1200 °C according to each research topic.

Exp. No.	Measured temperatures [°C]	Heating rate [°C/min]	Notes
M1			
M2	$1200 - 1650$	9	Research topic #1
M3	$1200 - 1400$		
R1 − R3	1650	4.5	Research topic #2
As			
As/HCS	$1500 - 1650$	4.5 / 9	Research topic #3
HCS			
As-0.3 − As-1.0	1650	9	
Syn. Ref. & Syn. 0 − 0.9	$1500 - 1650$	9	Research topic #4

59

Table 3.12: Calculated slag composition of industrial FeMn and SiMn charges after pre-reduction condition at 1200 °C.

Exp. No.	MnO	SiO$_2$	CaO	MgO	Al$_2$O$_3$	Total [wt%]	(C+M)/A	Notes
R1	81.7	7.9	8.6	1.5	0.4		-	Reference charge FeMn
R2	51.4	41.6	5.4	1.0	0.7		9.1	
R3	42.2	37.3	10.9	3.8	5.8	100	2.5	
As	59.4	32.7	6.2	1.1	0.6		12.2	SiMn
As/HCS	44.5	34.0	11.5	4.0	6.1		2.5	
HCS	31.8	35.1	15.9	6.5	10.7		2.1	

High purity CO (99.99 %) and Ar (99.999 %) gases supplied by AGA AB were used in the experiments. To prevent carbon deposition at lower temperatures according to the Boudouard reaction [17], Ar gas at the rate of 0.5 l/min was initially used until the temperature was approximately 500 °C. Then, at higher temperatures CO gas of 0.5 l/min was applied into the furnace. It was considered that CO gas should be the main atmosphere to simulate the industrial furnace condition.

3.3 Analysis

Three main types of analysis methods were used to characterize the melting and reduction results of experiments from the four research topics. The summary of the methods in each research topic is described in **Table 3.13**.

Table 3.13: Summary of analysis methods for the four research topics. Mass data were obtained from the TGA experiments, and slag/metal compositions were analyzed from the electron probe micro-analyzer (EPMA). Cross-section images were made by cutting the epoxy-mounted crucibles vertically.

Research topic	Analysis methods			Notes
#1	-	Cross-section images	EPMA	Melting of raw materials
#2	Mass data	Cross-section images	EPMA	Reduction behavior
#3	Mass data	-	EPMA	Kinetic estimations
#4	Mass data	-	EPMA	Confirmation of kinetic info

First, the main information from the TGA experiments is the mass change as a function of time and temperature. The initial mass of the crucible was reset to 0 g as the reference mass. Any mass changes during the experimental conditions will indicate the information of reduction degrees and rates. Since the mass data is crucial information for kinetic estimations and observing the reduction behavior of FeMn and SiMn charges, it was used to calculate the rates of MnO and SiO$_2$ reduction.

Second, the cross-section images of the crucibles were used to observe the melting behavior of SiMn charges. An illustration of a vertically cut crucible sample showing its cross-section is shown in **Figure 3.5**. This was mainly considered for research topic #1 where the focus was to observe the incipient slag generation, and the cross-section image between FeMn and SiMn charges at 1600 °C was compared in research topic #2. After heating of raw materials in the furnace and subsequent cooling, epoxy was poured into the graphite crucibles, which was cut vertically after complete solidification. The boundaries between different materials were observed at different temperatures.
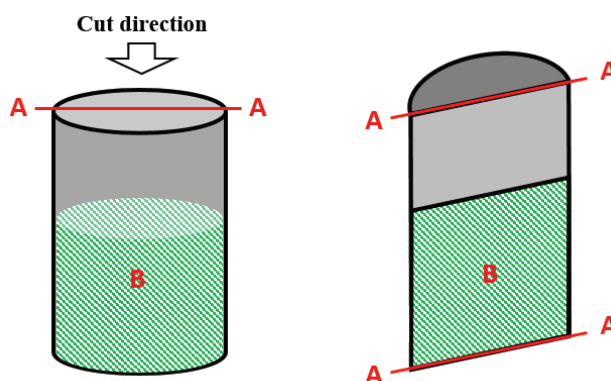
Figure 3.5: Illustration of the vertically cut crucible: Before (left) and after (right) cutting. Line A is the alignment and B is the epoxy-mounted charge materials after heating.

Third, the electron probe micro-analyzer (EPMA) was used to obtain micro-analyses. The Jeol JXA-8500F was used for the analyses, which is equipped with five wavelength dispersive X-ray spectrometers (WDS) and an energy dispersive X-ray spectrometer (EDS). The chemical compositions of slag and metal in a small area are obtainable with a high degree of accuracy from the EPMA's high probe current and small probe diameter. The slag and metal samples from the TGA experiments were initially mounted with epoxy and the surfaces were polished and coated with carbon prior to electron analyses to prevent charge build-up.

Since the same charges were heated up to different temperatures, the reduction degrees of MnO and SiO_2 can be measured either by analyzing the slag or the metal phase. The binary Fe-Mn and Mn-Si metal systems were previously discussed in **Section 2.1.2**. Unlike the Fe-Mn system where solid solution is expected, the Si-Mn system shows several intermetallic compounds after solidification. The several intermetallic compounds imply that the overall amount of manganese and silicon in the metal phase is not easy to measure. However, the degree of MnO and SiO_2 reduction can be estimated by analyzing the slag phase, which is assumed to be uniform. This assumption was verified by the EPMA analyses. The average slag compositions were obtained by analyzing several slag points. Then, the amount of manganese and silicon in the metal phase were calculated based on the average slag analyses afterwards.

Besides the back scattered electron (BSE) images and analysis of phase compositions, element mapping was also available for the EPMA. The element mapping provides the spatial distribution of elements of a sample, where the maps of different elements over the same area can help to determine which phases are present.

61

3.4 Kinetic calculations

The rate model of MnO reduction from **Equation (2.20)** was used to calculate and estimate the kinetic parameters in this work. This rate model of MnO reduction was derived from using FeMn slags. However, since SiMn slags are essentially similar with FeMn slags, it was assumed that the same rate expression can be used for SiMn slags in this study. According to **Equation (2.20)**, kinetic parameters which can be measured and calculated from are the rate, reaction interface area and the driving force (Note that **Equation (2.20)** is shown again for convenience).

$$r_{MnO} = k_{MnO} \cdot A \cdot (a_{MnO} - \frac{a_{Mn}}{K_{MnO}}) \tag{2.20}$$

The rate of MnO reduction was measured from the recorded data of TGA experiments and EPMA analyses, where higher mass change indicates higher MnO reduction and lower MnO content in the slag analysis. Since the heating of SiMn charges was stopped at different temperatures and followed by subsequent cooling, the amount of MnO in slag at different time and temperatures was determined from the EPMA analyses, and the corresponding time and temperature were extracted from the recorded TGA data.

The reaction area at the slag-coke interface was calculated based on the amount of manganese and silicon metal produced. It was assumed that the density of the coke material was 1 g/cm³ and the particles were spherical. Then, the number of coke particles were calculated according to the following relation between volume and density, **Equation (3.1)**:

$$N^o = \frac{3m_o}{4\pi r_o^3 \rho} \tag{3.1}$$

where N^o is the number of particles, m_o [g] is the initial total mass of coke particles, r_o [cm] is the initial radius of a coke particle and ρ [g/cm³] is the density of the coke material used.

It was proposed that the reduction occurs at the coke-slag interface where the coke particles are embedding in the slag matrix. An illustration of the coke-slag interface reaction is described in **Figure 3.6**.
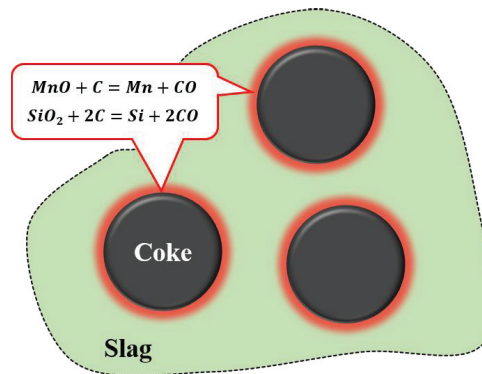
Figure 3.6: Illustration of the chemical reaction between coke and slag interface. Coke particles are embedded in the slag phase and the reduction of MnO and SiO₂ occurs at the highlighted (red) part.

The amount of carbon consumed according the **Reactions (1.10)** and **(1.11)** of each sample was calculated and consequently the consumed volume of the coke was estimated. From the changed volume of coke, the changed radius of coke can be calculated. This was used to calculate the reaction area between slag and coke particles, which is shown in **Equation (3.2)**:

$$A = 4\pi r^2 \times N^o \tag{3.2}$$

where A [cm²] is the reaction area between slag and coke and r [cm] is the changed radius of a coke particle at temperature, T [°C].

To calculate the driving force, the activity formulas of metal and slag from **Equations (2.1)** and **(2.4)** were used along with the equilibrium constants from FactSage 7.0 [45]. After measurements and calculations of the reduction rate, reaction area and driving force, the rate constant of MnO reduction was estimated and discussed. The rate constant was expressed as the Arrhenius equation in this study, and the kinetic parameters, such as the activation energy and pre-exponential constant, were obtained by describing the Arrhenius plots.

For SiO_2 reduction, a similar rate model with MnO reduction was used to calculate and estimate the kinetic parameters in this work. It was also assumed that the chemical reaction of SiO_2 with carbon, **Reaction (1.11)** was the rate-determining step in SiMn slags. This was assumed after the experiments in Research topic #1 was done, which will be more explained in the next chapter. The presumed rate expression for SiO_2 reduction is described in **Equation (3.3)**:

$$r_{SiO_2} = k_{SiO_2} \cdot A \cdot (a_{SiO_2} - a_{SiO_2,\ Eq.}) \tag{3.3}$$

where r_{SiO2} [g/min] is the rate of SiO_2 reduction, k_{SiO2} [g/min·cm²] is the rate constant of SiO_2 reduction, a_{SiO2} is the activity of SiO_2 and $a_{SiO2,\ Eq.}$ is the activity of SiO_2 at equilibrium.

At equilibrium, the relation between SiO_2 in the slag phase and silicon in the metal phase also has to be satisfied, which was previously described in **Equation (2.9)**. Thus, the reduction rate can be described by the following **Equation (3.4)**:

$$r_{SiO_2} = k_{SiO_2} \cdot A \cdot (a_{SiO_2} - \frac{a_{Si}}{K_{SiO_2}}) \tag{3.4}$$

where a_{Si} is the activity of Si in the metal phase and K_{SiO2} is the equilibrium constant of **Reaction (1.11)**.

The reduction rate, reaction area and the driving force of SiO_2 reduction were also calculated in the same methods with MnO reduction, where the kinetic parameters were obtained from the Arrhenius plots. Note that the reduction of SiO_2 by carbon as graphite, **Reaction (1.11)**, was the main focus and reduction by silicon carbide was not studied in this thesis work. For convenience, the presumed kinetic models of MnO and SiO_2 reduction considered in this study are recapitulated in **Table 3.14**.

Table 3.14: Rate models of MnO and SiO_2 reduction considered in this study. Chemical reaction of both MnO and SiO_2 reduction was assumed as the rate-determining step, where the reactions occur at the slag-coke interface.

Rate Models	
MnO + C = Mn + CO Reaction (1.10)	SiO_2 + 2C = Si + 2CO Reaction (1.11)
$$r_{MnO} = k_{MnO} \cdot A \cdot (a_{MnO} - \frac{a_{Mn}}{K_{MnO}})$$	$$r_{SiO_2} = k_{SiO_2} \cdot A \cdot (a_{SiO_2} - \frac{a_{Si}}{K_{SiO_2}})$$

Assumptions	• Rate-determining step: Chemical reaction • Reactions occur at slag-coke interface

3.5 Parallel studies

As a part of this work, two master's students [84, 85] and an internship project [86] performed similar experiments with SiMn charges based on Comilog ore and synthetic materials. This expanded the application of the results to different SiMn slags besides Assmang ore. Note that the same materials besides the manganese ore and limestone were used in the parallel studies. The chemical compositions of Comilog ore and limestone are shown in **Table 3.15**.

Table 3.15: Chemical composition of Comilog ore and limestone [84, 85].

Material	MnO	MnO_2	SiO_2	Fe_2O_3	CaO	MgO	Al_2O_3	S	C	CO_2	H_2O	Total [wt%]
Comilog ore	3.0	72.4	4.6	6.7	0.1	0.1	5.6	-	-	0.1	5.0	97.6
Limestone	-	-	0.9	-	52.2	1.0	0.3	-	-	45.7	-	100.1

Holtan investigated the melting and reduction behavior of raw materials based on Comilog ores parallel to Research topic #1 and #2 in this study [84, 87]. The charge composition is described in **Table 3.16**. Graphite crucibles, which contained particles of Comilog ore, quartz and limestone, were heated up to temperatures between 1250 and 1600 °C. Assuming the reduction rates of MnO and SiO_2 are influence by the slag viscosity and the driving force, limestone was considered to compare the difference between charges without and with limestone.

Table 3.16: Charge composition based on Comilog ore: Holtan's work [87]. Reduction behavior between FeMn charge ("H1") and SiMn charge ("H2" and "H3") was compared.

Exp. No.	Comilog ore	Quartz	Limestone	Coke	Total [g]	Notes
H1	23	-	-	7	30	Reference charge FeMn
H2	23	6	-	7	36	Without limestone SiMn
H3	18	7	5	6	36	With limestone SiMn

Later, Larssen continued Holtan's work, where the reduction behavior and kinetic estimations of SiMn charge base on Comilog ore were studied (parallel to Research topic #2 and #3 in this work) [85, 88]. Similar charge compositions were used to calculate the reduction rates of MnO and SiO$_2$ where the amount of each raw material were measured to aim at 5 wt% MnO and 40 wt% SiO$_2$ in the slag phase and 18 wt% Si in the metal phase at 1600 °C, which is approximately close the thermodynamic equilibrium at 1600 °C. Limestone was also used to observe the influence of slag viscosity and the changed driving force on the reduction rates of MnO and SiO$_2$. The charge compositions of Larssen's work is shown in **Table 3.17**.

Table 3.17: Charge composition based on Comilog ore: Larssen's work [85]. It was assumed that the reduction rate is influenced by the slag viscosity, where addition of limestone and HC FeMn slag to the charge was considered.

Exp. No.	Comilog ore	Quartz	Limestone	HCS*	Coke	Total [g]	Notes
L1	6	1.4	-	-	2	9.4	Without limestone
L2	5	1.8	1.6	-	1.9	10.3	With limestone
L3	4	1.6	-	4	2.3	11.9	With HCS

*HCS: HC FeMn slag

Along with Comilog ore based SiMn charges, Kawamoto used synthetic slag to study the reduction aspects in MnO and SiO$_2$ reduction [86]. The synthetic slags were similar to the slags based on industrial materials of this work. The amount of the major slag components (MnO, SiO$_2$, CaO, MgO and Al$_2$O$_3$) were same to the charge "As/HCS" in this study, and comparisons were made. It was assumed that sulfur as impurity element affects the reduction rates, and different amount of sulfur in the synthetic charges were considered.

The results of these parallel studies were mainly used for discussing the melting and reduction behavior of SiMn charges. This work presents some of their results in order to expand the phenomena observed in this study. Further details of the parallel works can be found in the individual reports of Holtan, Larssen and Kawamoto [84-88].

Chapter 4: Results

The experimental results of the four subsequent research topics and the parallel studies are described in this chapter.

The results from the melting behavior of charge materials (research topic #1) are described mainly by cross-section images. The images were obtained by cutting the crucibles molded with epoxy. The cross-sections at various temperatures were sketched where the relation of pre-reduced Assmang ore, quartz and HC FeMn slag particles were depicted. Micro-analyses of the charge samples were also obtained which showed the slag compositions and elemental mappings.

The reduction behavior of SiMn charges (research topic #2) was mainly described by the mass changes from the TGA experiments. The mass changes of SiMn charges were compared with FeMn charges as a function of time and temperature, where the comparisons were made from charge types and particle sizes.

The results from kinetic estimation (research topic #3) mainly describe the rate and kinetic parameters from the experiments. The rate parameters, which include rates, reaction areas and driving forces of MnO and SiO_2 reduction, were initially calculated to estimate the rate constants according to the rate models used in this work. From the estimated rate constants, the corresponding Arrhenius plots were constructed and the kinetic parameters, activation energy and pre-exponential constants, were calculated where comparison between different SiMn charges was made. Then, the calculated rate constants were compared with slag properties to observe which properties influenced the reduction rate of MnO and SiO_2.

Experiments with synthetic charges (research topic #4) are also shown to confirm the kinetic parameters observed in the first three research topics. Similar to research topic #3, the kinetic parameters were estimated from a controlled slag system where the effect of slag viscosity and sulfur was studied.

Lastly, the results from the parallel studies are described where SiMn charges based on Comilog ore and synthetic materials were used. The results of the parallel studies also show the melting behavior of charge materials, reduction behavior of SiMn charges and kinetic estimations.

4.1 The melting behavior of raw materials (Research topic #1)

The results of the melting behavior between raw materials were obtained by heating up charges containing Assmang ore, quartz, HC FeMn slag and coke according to **Tables 3.4** and **3.9**. Initially, smaller particle sizes ($4.0 - 6.3$ mm) were used to compare the melting behavior of raw materials with and without HC FeMn slag between 1200 and 1650 °C. In addition, larger particle sizes ($15 - 20$ mm) of Assmang ore and quartz were heated between 1200 and 1400 °C to observe the further interaction between the two materials. The cross-section images with their sketches at measured temperatures were depicted, and the observed phases were analyzed through EPMA analyses.

4.1.1 Cross-section images

The cross-section images with their sketches at different temperatures between 1200 and 1650 °C of charges "M1" (Assmang ore + quartz + HC FeMn slag + coke) and "M2" (Assmang ore + quartz + coke) are shown in **Figures 4.1** and **4.2**, respectively. The particle sizes of the charge materials were between 4.0 $- 6.3$ mm. Note that HC FeMn slag particles were only used in charge "M1".
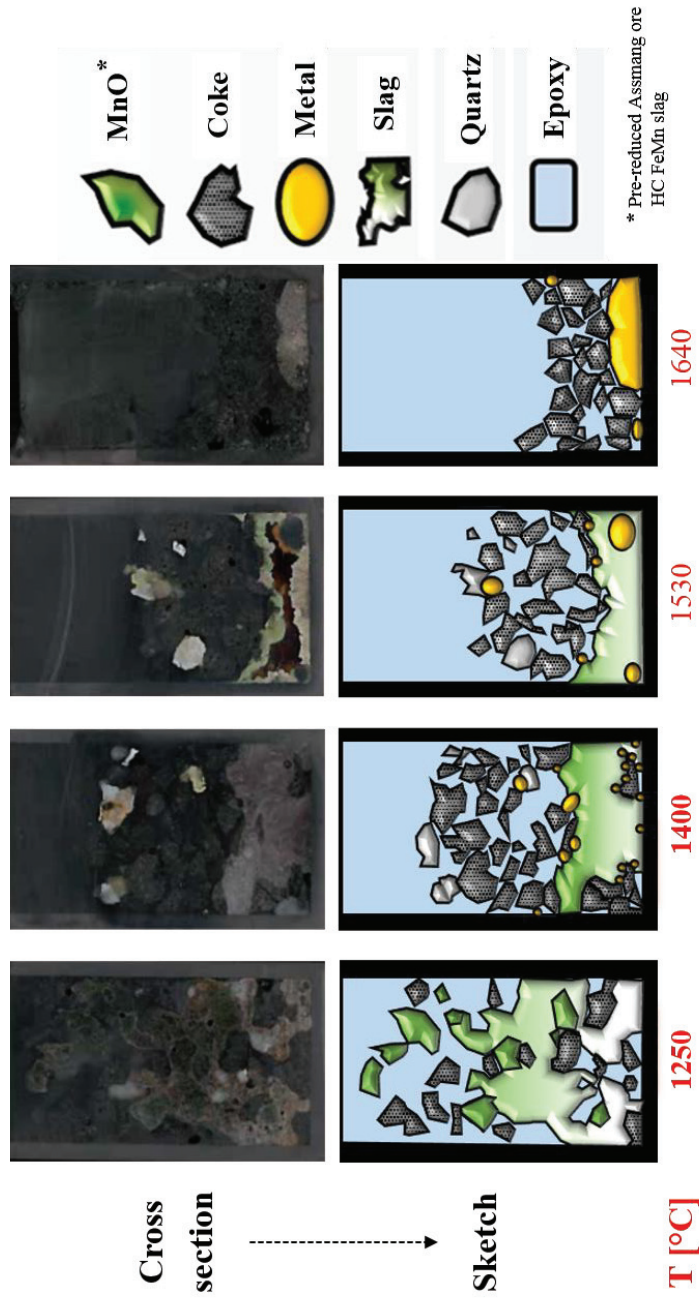
Figure 4.1: Cross-section images and sketches of charge "M1" at 1250, 1400, 1530 and 1640 °C. Charge "M1" initially contained Assmang ore, quartz, HC FeMn slag and coke particles (4.0 – 6.3 mm). Melting of raw materials was already observed at 1250 °C, and the slag phase was observed at 1400 °C. Note that pre-reduced Assmang ore and HC FeMn slag particles were described as MnO due to the unclear difference between the two particles at 1250 °C. In addition, the slag phase was not observed at the cross-section image at 1640 °C but present at different orientation.

67
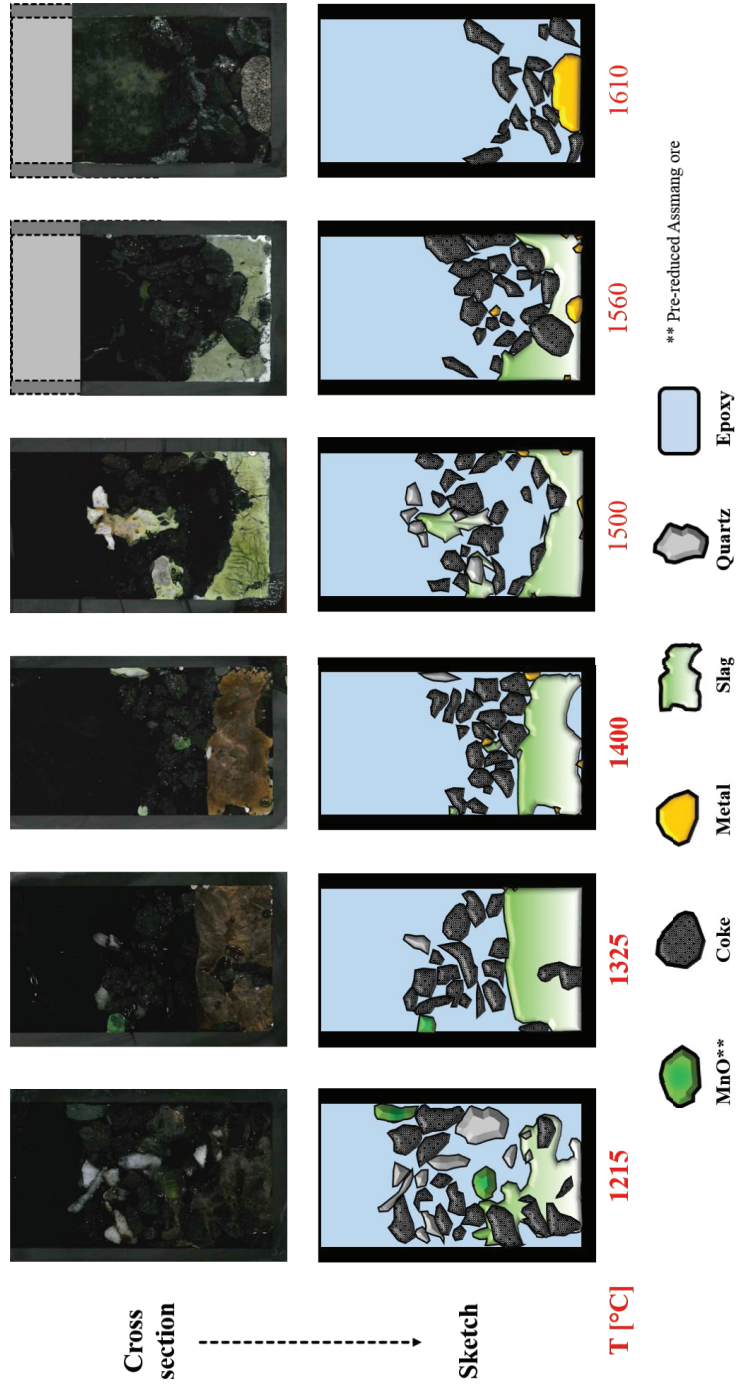
Figure 4.2: Cross-section images and sketches of charge "M2" at 1215, 1325, 1400, 1500, 1560 and 1610 °C. Charge "M2" initially contained Assmang ore, quartz and coke particles (4.0 – 6.3 mm) where HC FeMn slag was excluded. Melting of raw materials was also already observed at 1215 °C, and the slag phase was observed at 1325 °C. Note that pre-reduced Assmang ore was described as MnO. In addition, the slag phase was not observed at the cross-section image at 1610 °C but present at different orientation.

The melting behavior of the SiMn charge materials was clearly observed from the cross-section images at different temperatures between 1215 and 1400 °C. The formation of incipient slag phase was both observed in charges "M1" and "M2" regardless of the use of HC FeMn slag. The low melting temperature of HC FeMn slag, which was around 1250 °C, was assumed to contribute to slag formation at relatively lower temperatures as highlighted in the MnO-SiO$_2$ binary system in **Figure 2.11**. This was observed with charge "M1", where the observed melting range of pre-reduced Assmang ore, quartz and HC FeMn slag was between 1250 and 1400 °C. However, the similar result of slag formation at relatively low temperatures was also observed with charge "M2", where HC FeMn slag was not included. Both Assmang ore and quartz particles were dissolved where the observed melting range was between 1215 and 1325 °C. The comparison from charges "M1" and "M2" indicates that melting of Assmang ore and quartz also occurs at relatively low temperature and HC FeMn slag is not critical for contributing slag formation.

The prime example of melting between Assmang ore and quartz was observed with charge "M3" (Assmang ore + quartz), where Assmang ore and quartz with increased particle sizes (15 − 20 mm) were used. The observed melting range of charge "M3" was between 1275 and 1300 °C, where the cross-sections with their sketches are described **Figure 4.3**.
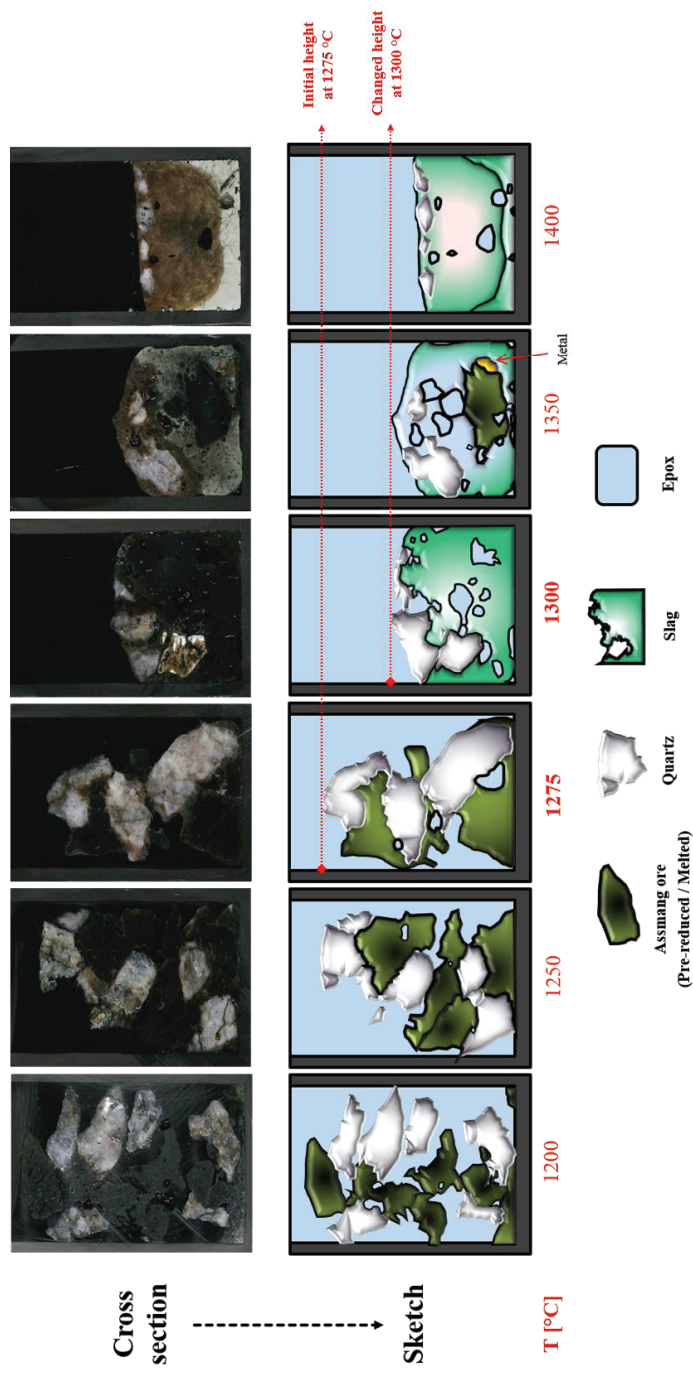
Figure 4.3: Cross-section images and sketches of charge "M3" at 1200, 1250, 1275, 1300, 1350 and 1400 °C. Charge "M3" initially contained only Assmang ore and quartz particles (15 − 20 mm) where coke was not included. Generation of the incipient slag phase was observed at approximately 1275 °C and considerable melting had occurred between 1275 and 1300 °C due to the decreased height of charge materials. Note that the time difference between 1275 and 1300 °C was less than 3 minutes.

70

The comparison of the two cross-sections at 1275 and 1300 °C implies that the melting of Assmang ore and quartz had occurred rapidly based on two reasons. First, the height of the charge materials had decreased approximately half. Both solid Assmang ore and quartz particles were packed where the initial height of the charge materials was similar to the crucible height. The decreased height of the charge materials between 1275 and 1300 °C clearly indicates that melting had occurred from Assmang ore and quartz particles. Second, the time difference between 1275 and 1300 °C was less than 3 minutes, where the heating rate was 9 °C/min. Comparing the fact that the individual melting temperatures of Assmang ore and quartz were around 1500 and 1700 °C, respectively, the results showed that formation of slag from the two materials had occurred relatively fast between 1275 and 1300 °C.

The melting of Assmang ore and quartz was also not hindered by the size of raw material within the experimental condition of this work. The sizes between charges "M1" and "M2" (4.0 – 6.3 mm) with "M3" (15 – 20 mm) were different by a factor of approximately 3.5, but the observed melting ranges of the charges were between 1215 and 1400 °C regardless of size. This also implies that the interaction between manganese sources and quartz to form slag in SiMn charges is strong.

Therefore, the melting of SiMn charge materials and formation of slag occur at temperatures lower than 1400 °C regardless of charge type. This indicates that quartz, which has the highest melting temperature, does not stay undissolved if manganese sources are presented. The few undissolved quartz particles, which were observed at the top part of the crucible or slag phase in **Figures 4.1**, **4.2** and **4.3**, were not in contact with Assmang ore or HC FeMn slag, and the temperature is assumed to be lower than the bottom part of the crucible due to the temperature gradient in the crucible.

Besides the results from the melting of charge materials, the metal phases were mainly observed in cross-section samples at temperatures higher than 1500 °C from charges "M1" and "M2". It seems that the reduction of MnO and SiO_2 significantly occurs above 1500 °C and the liquid slag is less reducing at lower temperatures. This implies that the reduction of MnO and SiO_2 is likely to occur from liquid slag in SiMn process for sizes less than 20 mm, but also possible for larger particle sizes.

4.1.2 EPMA analyses

The formation of slag at temperatures lower than 1400 °C can also be confirmed from the micro-analyses. The EPMA results, which showed the BSE images and phase compositions, of charges "M1" (Assmang ore + quartz + HC FeMn slag + coke), "M2" (Assmang ore + quartz + coke) and "M3" (Assmang ore + quartz) indicated formation of slag phase. The white spherical phases, which were mostly MnO, were dissolving pre-reduced Assmang ore, and the matrix was the slag phase from the melting of charge materials as observed in **Figures 4.1**, **4.2** and **4.3**.

The BSE images of charge "M1" at 1250, 1400 and 1530 °C are shown in **Figure 4.4**, where the images were taken from the slag phases observed from **Figure 4.l**. Three different phases were observed from the slag phase at 1250 °C, while the slag at higher temperatures showed only slag structures which were finely and uniformly distributed. The corresponding chemical analyses of the slag phases in **Figure 4.4** are described in **Table 4.1**. Each position shows the average slag composition from three analyses. The detailed analyses can be seen in **Appendix B**. The results indicated that the main composition in phase "A" was MnO, while the main components in phases "B", "C", "D", "E" and "F" were both MnO and SiO_2. Note that phases "D", "E" and "F" were de-focus (30 μm) measured due to the fine structures.
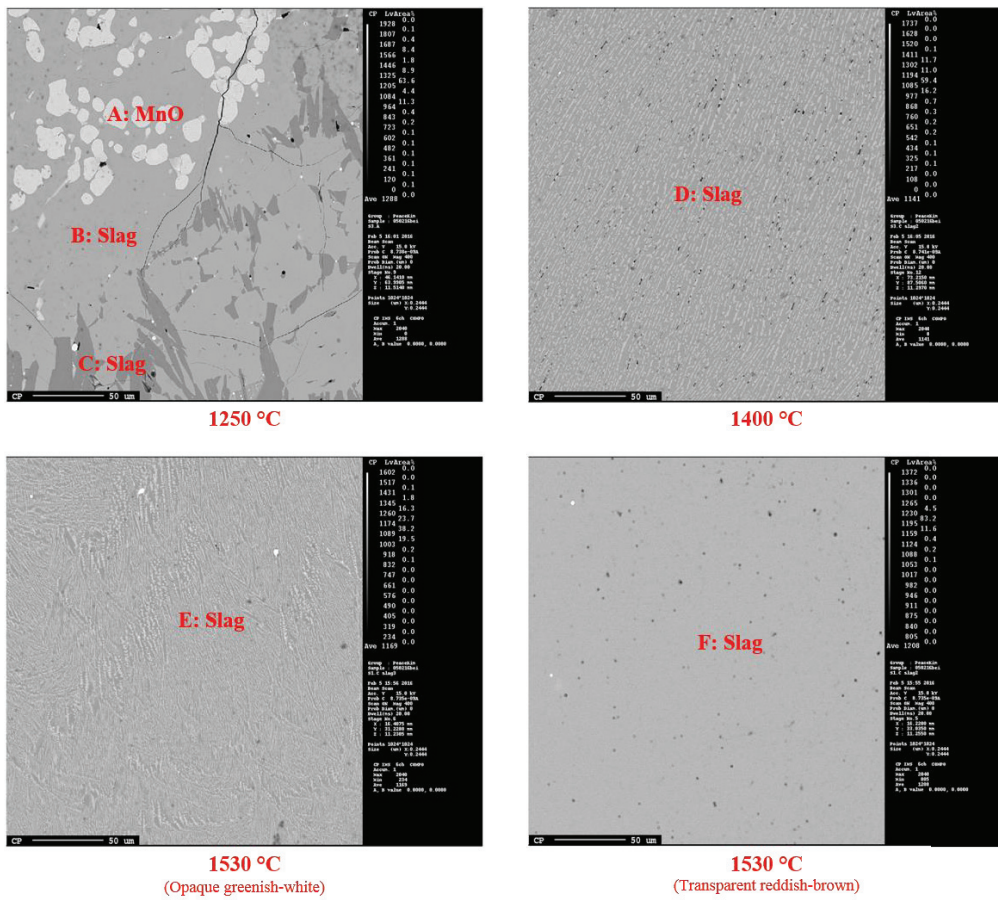
Figure 4.4: BSE images of the slag phases in charge "M1" at 1250, 1400 and 1530 °C. Spherical MnO phases "A" were only observed at 1250 °C. Slag at 1400 and 1530 °C showed a fine ("D" and "E") and uniform ("F") structure, which was initially observed from the cross-section images from Figure 4.1.

Table 4.1: Analysis of the slag compositions between phases "A" and "F" between 1250 and 1530 °C from Figure 4.4. White spherical phases were mainly MnO, while both MnO, SiO$_2$ and the rest of the oxides were in the slag matrix.

Position	MnO	SiO$_2$	CaO	MgO	Al$_2$O$_3$	Total [wt%]	Notes	Identified as	Temperature [°C]
A	96.3	0.3	2.2	0.2	0.5	99.5	White spherical	MnO	
B	61.8	31.9	2.6	1.0	0	97.3	Light grey		1250
C	43.3	48.7	8.0	0.8	0.2	101.0	Dark grey		
D	50.2	39.3	8.9	0.5	1.0	99.9		Slag	1400
E	49.8	42.8	7.8	1.1	1.2	102.7	De-focused*		
F	49.4	42.6	7.9	1.2	1.2	102.3			1530

* 30 µm de-focus measured

The spherical MnO phases indicate the dissolving Assmang ore in the SiMn slag phase. The similar structures were also observed in FeMn slags of previous work [21]. The dissolving MnO phases were previously reflected from the binary MnO-SiO$_2$ system, **Figure 2.11**, where solid MnO was expected in the FeMn slag until the liquidus temperatures. The solid MnO was also observed in the SiMn charge "M1" due to the use of Assmang ore but were not observed at temperatures higher than 1250 °C. According to the MnO-SiO$_2$ system, only liquid slag phase will be present at higher temperatures. The absence of dissolving MnO spheres at temperatures higher than 1250 °C indicates that Assmang ore and HC FeMn slag particles were completely dissolved with quartz, and only liquid slag phase was presented. This was also verified by the similar analyses of slag "D", "E" and "F", where the SiO$_2$ content is around 40 wt%.

The BSE images of charge "M2" at 1215, 1325, 1400 and 1500 °C are shown in **Figure 4.5**. The images were also taken from the slag phases observed in **Figure 4.2**. The same spherical MnO phases are not shown in the BSE images of charge "M2" due to the focus on the slag phase but were assumed to be presented near the dissolving pre-reduced Assmang ore particles. Similar slag structures with charge "M1" were observed in charge "M2" where it mainly consisted two phases (dark and light grey). The corresponding slag composition of the phases in **Figure 4.5** are shown in **Table 4.2**, where the average slag compositions were also measured from several analyses. Detailed analyses can also be seen in **Appendix B**.
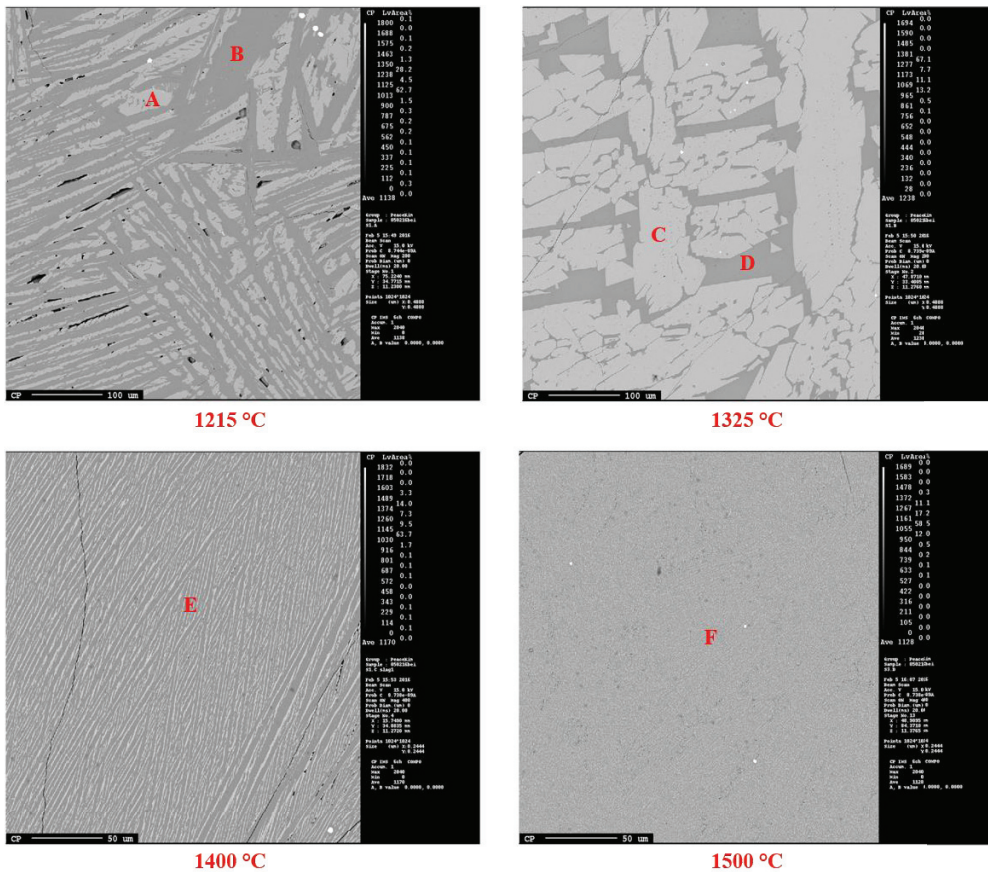
Figure 4.5: BSE images of the slag phases in charge "M2" at 1215, 1325, 1400 and 1500 °C. Spherical MnO phases were not observed in charge "M2" due to the focus of the slag phase, but the overall slag structures were similar with charge "M1".

Table 4.2: Analysis of the slag compositions between phases "A" and "F" from Figure 4.5. Slag phases were mostly composed of MnO and SiO_2, where the MnO/SiO_2 ratio was higher in the light grey phases.

Position	MnO	SiO_2	CaO	MgO	Al_2O_3	Total [wt%]	Notes	Identified as	Temperature [°C]
A	60.0	32.1	3.3	0.8	0.1	96.3	Light grey		
									1215
B	38.8	49.4	11.8	0.4	0.9	101.3	Dark grey		
C	59.5	32.2	2.4	1.8	0.1	96.0	Light grey		
								Slag	1325
D	43.6	49.3	7.0	1.6	0.3	101.8	Dark grey		
E	53.4	41.4	3.8	0.7	0.8	100.1			1400
							De-focused*		
F	48.3	44.6	8.8	1.0	2.1	104.8			1500

* 30 μm de-focus measured

The slag structures and the analyses of phases of charge "M2" at 1215 °C implies that melting of Assmang ore and quartz had occurred to form the observed slag phases. The slag structures, which showed light and dark grey phases also reflect the two manganese silicate compounds, $MnSiO_3$ and Mn_2SiO_4, in the $MnO-SiO_2$ system. The MnO/SiO_2 ratios in the light and dark grey phases were approximately 2 and 1, respectively. This shows close relation with the two manganese silicate compounds, where the MnO/SiO_2 ratios of Mn_2SiO_4 ($2MnO \cdot SiO_2$) and $MnSiO_3$ ($MnO \cdot SiO_2$) are 2 and 1, respectively. This indicates that the liquid slag phase had solidified according to the $MnO-SiO_2$ system, where the liquid slag phase was originally generated from the melting of Assmang ore and quartz particles (without HC FeMn slag).

The melting of Assmang ore and quartz was also observed from the BSE images of charge "M3" at 1200, 1250, 1275, 1300, 1350 and 1400 °C, which are described in **Figures 4.6** and **4.7**. To include the dissolving MnO and quartz phases, the images were taken in the slag phase which was near to the solid Assmang ore and quartz particles. The corresponding average slag composition of the phases in **Figures 4.6** and **4.7** are described in **Tables 4.3** and **4.4**, respectively. The detailed analyses are also shown in **Appendix B**. The results indicated that the dark phases were mainly composed of SiO_2. Similar to the slag composition results in charges "M1" and "M2", the light and dark grey phases composed mostly MnO and SiO_2, where the MnO/SiO_2 ratio was higher in the light grey phases. The white spherical phases mainly consisted MnO, which was also a similar result from charge "M1". In addition, metallic iron phases were detected in the slag phase at 1275 °C, which indicates reduction of iron oxides during the pre-reduction.

1200 °C
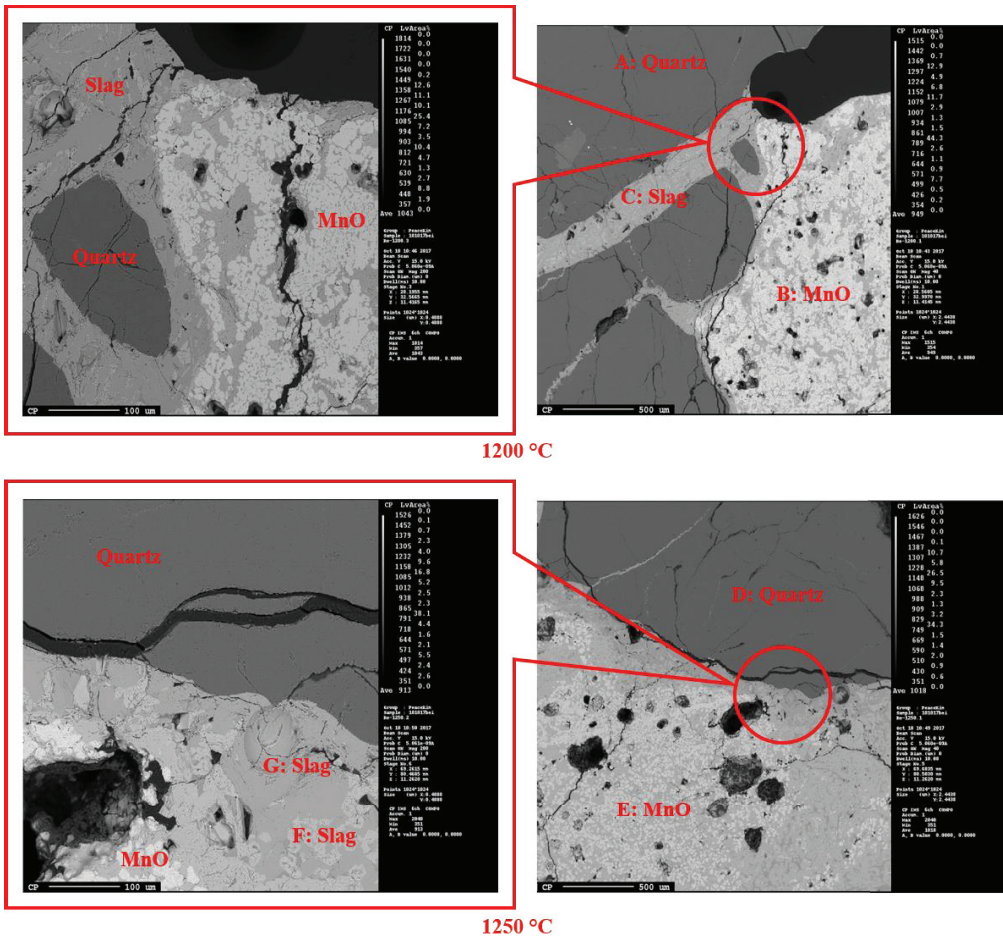
1250 °C

Figure 4.6: BSE images of the slag phases in charge "M3" at 1200 and 1250 °C. Three main phases were observed: Quartz ("A" and "D"), dissolving MnO ("B" and "E") and slag ("C", "F" and "G"). Presence of slag phases indicates that melting of Assmang ore and quartz particles had occurred at the observed temperatures.

Table 4.3: Analysis of the slag compositions between phases "A" and "G" from Figure 4.6. Dark phases ("A" and "D") were identified as quartz, and the other phases showed similar results with charges "M1" and "M2".

Position	MnO	SiO$_2$	CaO	MgO	Al$_2$O$_3$	Total [wt%]	Notes	Identified as	Temperature [°C]
A	0	99.1	0	0	0	99.1	Dark	Quartz	
B	98.4	0.6	0.2	0.4	0	99.6	White spherical	MnO	1200
C	50.4	38.9	7.6	0.9	1.4	99.2	Grey	Slag	
D	0	99.6	0.1	0	0	99.7	Dark	Quartz	
E	98.9	0.8	0.1	0.2	0.1	100.1	White spherical	MnO	1250
F	62.3	34.5	1.5	1.4	0.2	99.9	Light grey	Slag	
G	46.3	49.8	1.5	1.7	0.3	99.6	Dark grey		
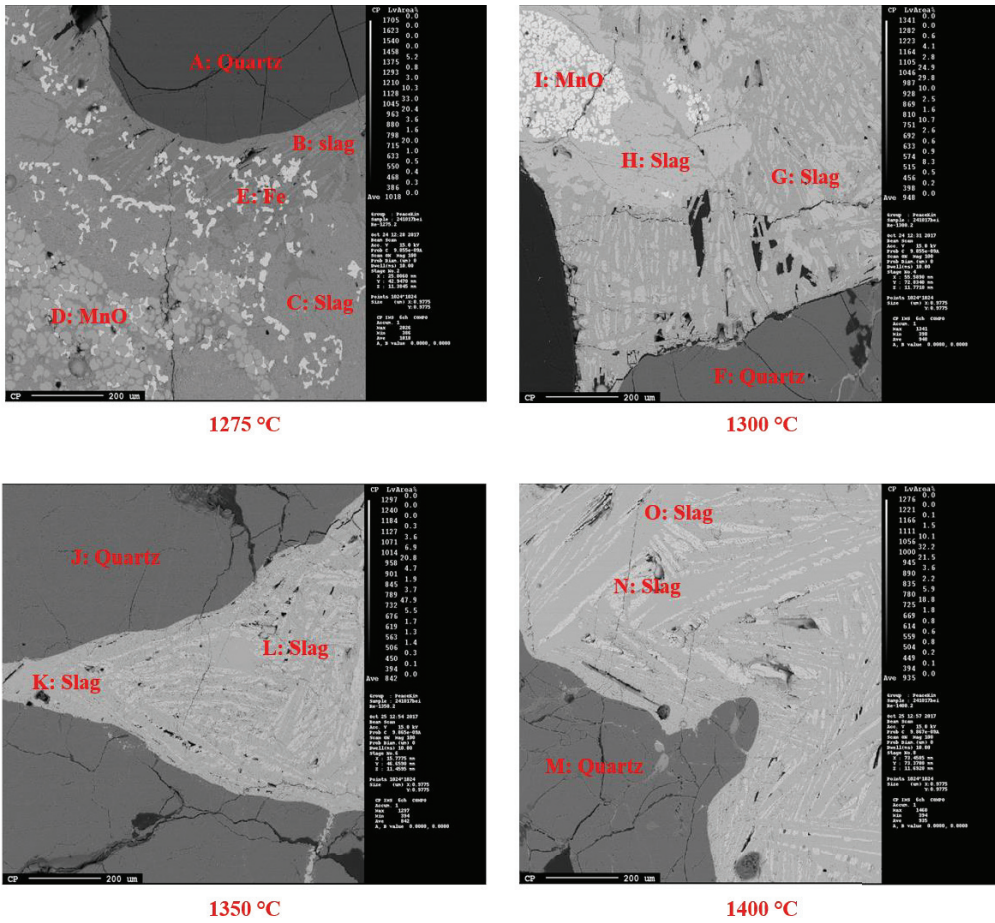
Figure 4.7: BSE images of the slag phases in charge "M3" at 1275, 1300, 1350 and 1400 °C. Spherical MnO phases ("D" and "I") were only observed until 1300 °C and were not found at higher temperatures. Metallic iron phases ("E") were also observed at 1275 °C, which were assumed to be from the pre-reduction.

Table 4.4: Analysis of the slag compositions between phases "A" and "O" from Figure 4.7. Slag analysis showed similar results with Table 4.3. Additional phase "E" at 1275 °C was identified as metallic iron.

Position	MnO	SiO$_2$	CaO	MgO	Al$_2$O$_3$	Total [wt%]	Notes	Identified as	Temperature [°C]
A	0	99.1	0	0	0	99.1	Dark	Quartz	
B	46.0	50.9	2.4	0.5	0.2	100	Dark grey	Slag	
C	61.6	36.6	1.5	0.3	0.1	100.1	Light grey		1275
D	98.8	0.6	0.2	0.4	0	100	White spherical	MnO	
E*			Fe			100	White	Metallic iron	
F	0.1	99.9	0	0	0	100	Dark	Quartz	
G	43.7	50.5	4.4	1.2	0.2	100	Dark grey	Slag	1300
H	61.1	35.6	1.8	1.4	0.1	100	Light grey		
I	97.1	0.1	0	2.7	0.1	100	White spherical	MnO	
J	0	100.2	0.1	0	0	100.3	Dark	Quartz	
K	45.7	50.3	1.2	1.9	0.1	99.2	Dark grey	Slag	1350
L	61.1	36.1	1.3	1.1	0	99.6	Light grey		
M	0.1	100.6	0	0	0	100.7	Dark	Quartz	
N	62.6	34.5	1.8	1.2	0	100.1	Light grey	Slag	1400
O	48.2	45.8	4.2	1.0	0.8	100	Dark grey		

* Metal phase: Fe

The white spherical MnO phases, which were observed from charge "M1" at 1250 °C in **Figure 4.4**, were also observed in samples between 1200 and 1300 °C of charge "M3". The relative amount of these phases decreased with increasing temperatures and was not observed in samples at 1350 and 1400 °C. This implies that the formation of SiMn slag also complies to the MnO-SiO$_2$ system when HC FeMn slag is not used. Assmang ore and quartz particles were dissolved to form liquid SiMn slag, where the dissolution of both materials was thought not to be significantly hindered due to the slag formation at lower temperatures.

The identified slag phases of charge "M3" also indicate slag formation from melting of Assmang ore and quartz particles. Similar with the slag structure results in charges "M1" and "M2", the light and dark grey slag phases in charge "M3" also reflect the two manganese silicate compounds, MnSiO$_3$ and Mn$_2$SiO$_4$, in the MnO-SiO$_2$ system. The MnO/SiO$_2$ ratios of the two slag phases clearly indicate that the liquid slag phase was solidified into the two manganese silicate compounds, where the liquid slag was formed from the melting of Assmang ore and quartz particles in charge "M3".

In addition, the elemental mappings also showed corresponding results with the BSE images and slag analyses. The elemental mapping results according to **Figures 4.6** and **4.7** are shown in **Figures 4.8**, **4.9** and **4.10**. The results indicated that silicon was more concentrated on the quartz phases, and the spherical MnO phases showed relatively higher concentration of manganese. The concentration of manganese and silicon on the slag phases were relatively medium compared to the quartz and MnO phases.
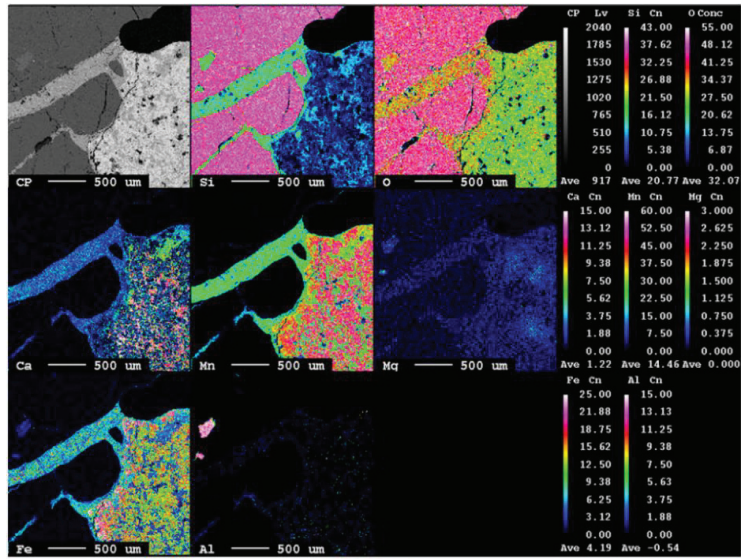
1200 °C
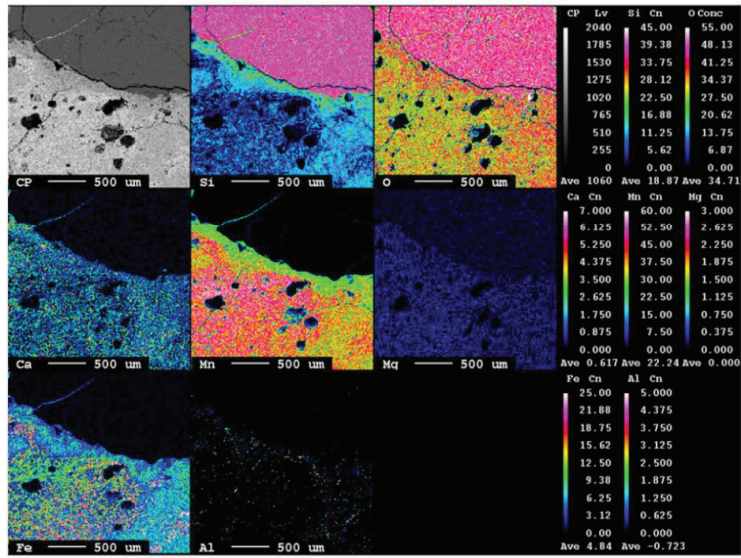
1250 °C

Figure 4.8: Elemental mapping for charge "M3" at 1200 and 1250 °C. Analyses showed corresponding results with other analyses. Manganese and silicon concentrations were relatively higher in the MnO and quartz phases, respectively. Also, the manganese and silicon distinction were clear between the quartz, slag and MnO phases, where the gradient of both elements was not observed.
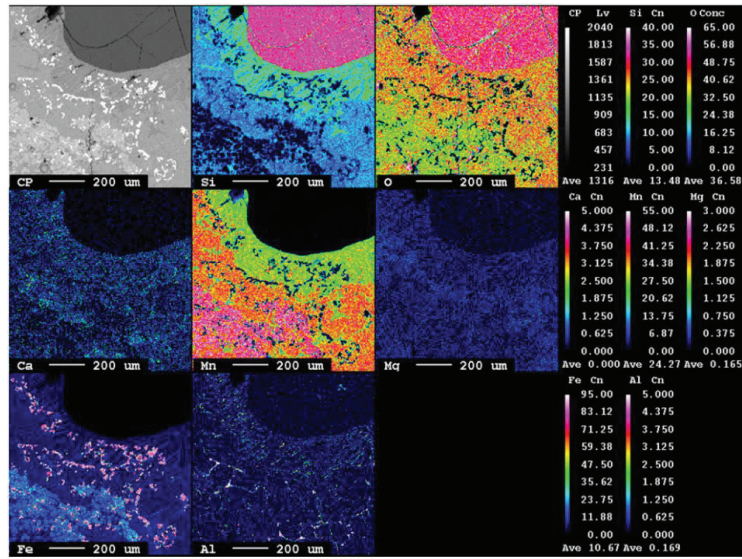
1275 °C
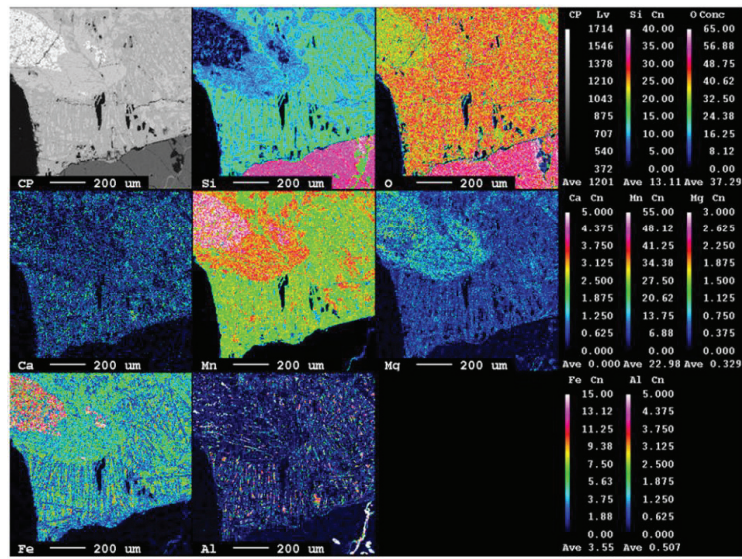
1300 °C

Figure 4.9: Elemental mapping for charge "M3" at 1275 and 1300 °C. Analyses showed corresponding results with other analyses. Clear distinction between the phases were observed from the manganese and silicon concentrations. Two slag phases (~ Mn_2SiO_4 and ~ $MnSiO_3$) were also clearly observed from the results.
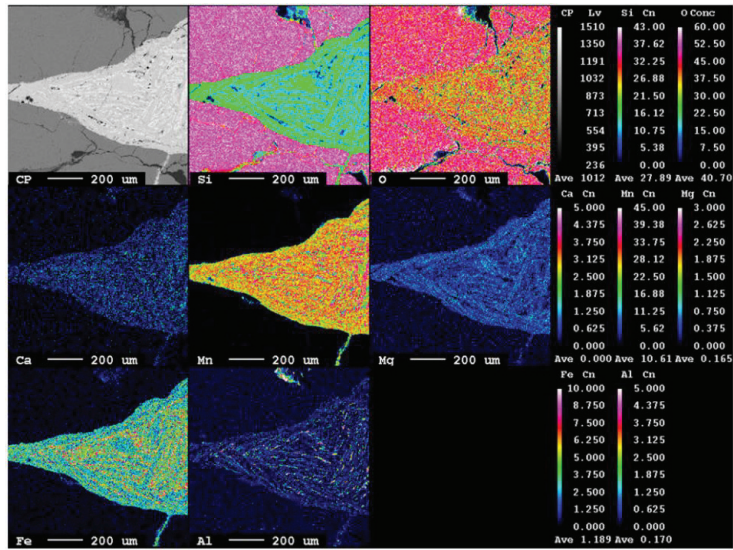
1350 °C
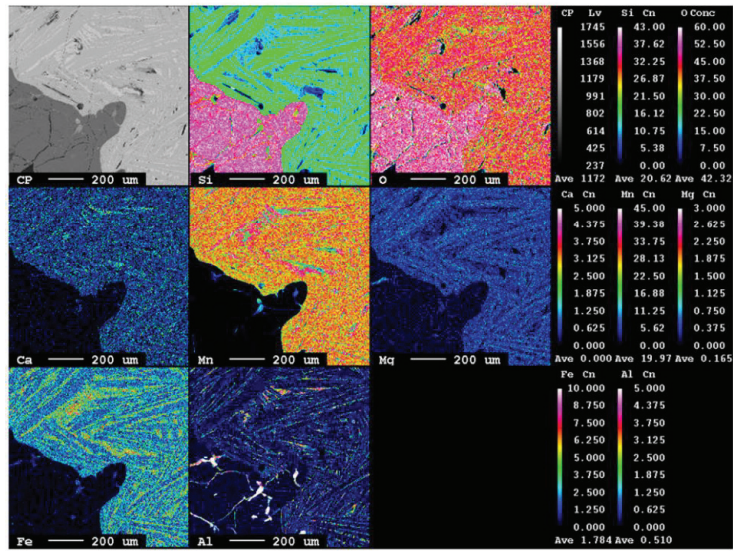
1400 °C

Figure 4.10: Elemental mapping for charge "M3" at 1350 and 1400 °C. Analyses showed corresponding results with other analyses. MnO phase was not observed at 1350 and 1400 °C, which indicates complete dissolution of pre-reduced Assmang ore particles.

The comparison between 1200 and 1300 °C shows that the distance between MnO spheres and SiO$_2$ as quartz increases with increasing temperature. **Figure 4.11** shows the observed minimum and maximum distance between MnO and SiO$_2$ at temperatures between 1200 and 1300 °C. Note that MnO spheres were not observed at 1350 and 1400 °C. The distance between MnO and SiO$_2$ at 1200 °C was around 40 to 200 μm. At higher temperatures, the distance increases rapidly, where the observed distance was between 550 and 1550 μm at 1300 °C. It indicates that the diffusion rate of MnO and SiO$_2$ in the slag is high at these temperatures.
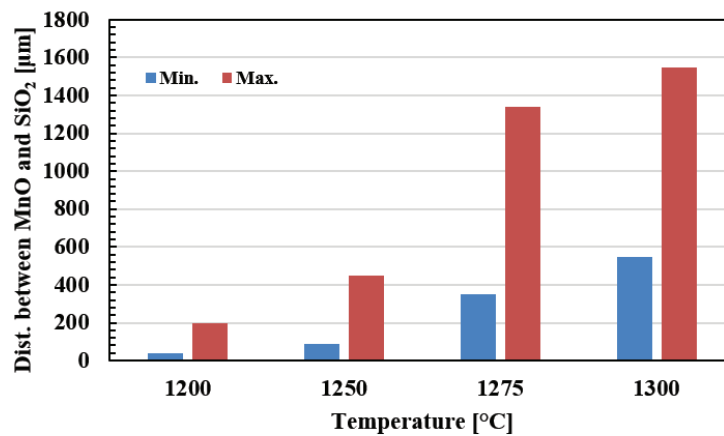
Figure 4.11: Distance between MnO spheres and SiO$_2$ as quartz in charge "M3" between 1200 and 1300 °C. Rapidly increasing distance with increasing temperature indicates that the diffusion rate of MnO and SiO$_2$ in the slag is high at low temperatures. Note that MnO spheres were not observed at 1350 and 1400 °C.

The highlights from the melting behavior of charge materials observed in the experiments are summarized at **Table 4.5**. The results showed that melting of raw materials in SiMn charges occurs at relatively lower temperature between 1200 and 1400 °C, where the incipient slag phase formation was completed below approximately 1400 °C. The generation of slag had also occurred at these temperatures regardless of the use of HC FeMn slag and particle sizes in the charge. This implies that the formation of SiMn slag complies to the MnO-SiO$_2$ system where the individual melting temperatures of manganese sources and quartz are not critically concerned.

Table 4.5: Highlighted results from the melting behavior of charge materials (Research topic #1). Melting of charge materials had occurred at relatively lower temperature between 1200 and 1400 °C. Results between the charges were similar regardless of the use of HC FeMn slag. Two different particle sizes of this work did not show significant difference in the slag forming temperature range.

Charge	Melting observed [°C]	Particle sizes [mm]	Notes
M1	1250 − 1400		With HC FeMn slag (Assmang ore + Quartz + HCS + Coke)
M2	1215 − 1325	4.0 − 6.3	Without HC FeMn slag (Assmang ore + Quartz + Coke)
M3	1275 − 1300	15 − 20	Without HC FeMn slag and coke (Assmang ore + Quartz)

4.2 The reduction behavior of SiMn charges (Research topic #2)

The results from the first part of the reduction experiments mainly illustrate the mass changes of FeMn and SiMn charges as a function of time and temperature. The charges were heated up to 1600 °C, and the comparison of mass change between FeMn and SiMn charges were obtained by TGA experiments according to **Tables 3.5** and **3.9**. The recorded temperature schedule of the experiments is described in **Figure 4.12**.
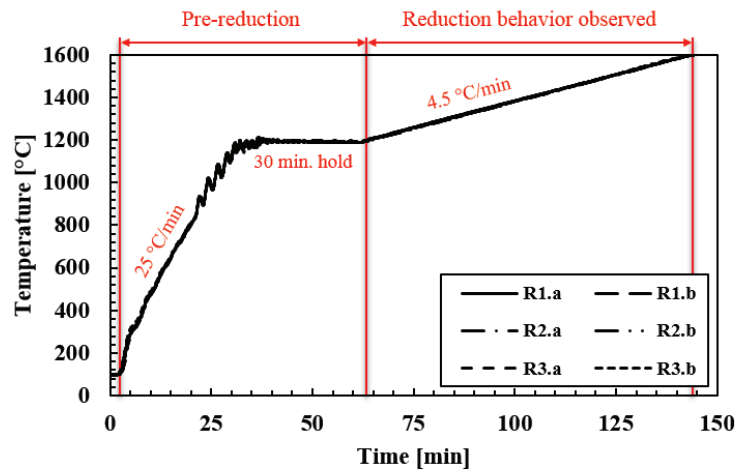
Figure 4.12: Temperature schedule of experiments from research topic #2. All six experiments were conducted in the same condition (records overlapped), and the reduction behavior of FeMn and SiMn charges were observed between 1200 and 1600 °C.

Two different particles sizes, 0.6 − 1.6 and 4.0 − 6.3 mm, were used in the charges, and the effect of particle size for reduction rate was described by comparing the TGA results. The mass changes of the charges are shown between 1200 and 1600 °C, where the results from the pre-reduction were omitted. In addition, cross-section images with their sketches at 1600 °C were illustrated and the corresponding slag compositions were obtained by EPMA analyses. Note that FeMn charge was used as a reference for comparison with SiMn charges, and the pre-reduction results can be seen in **Appendix C**.

4.2.1 Mass change comparison

The reduction behavior of SiMn charges, which was described by the mass changes, were compared with FeMn charges. The comparison between FeMn charge, "R1" (Assmang ore + coke), and SiMn charges, "R2" (Assmang ore + quartz + coke) and "R3" (Assmang ore + quartz + HC FeMn slag + coke), were observed at temperatures between 1200 and 1600 °C, where the results are described in **Figures 4.13** and **4.14**.
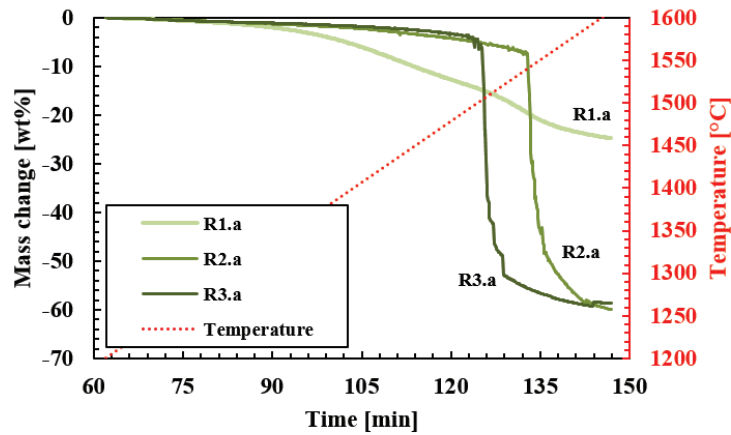
Figure 4.13: Comparison of the reduction behavior in FeMn and SiMn charges (a: 0.6 − 1.6 mm) between 1200 and 1600 °C. Mass change of FeMn charge ("R1.a") was progressive, while two different stages were observed for SiMn charges ("R2.a" and "R3.a").
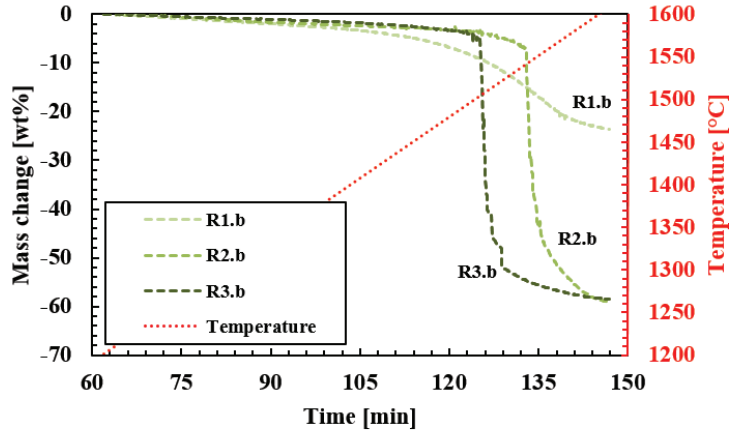
Figure 4.14: Comparison of the reduction behavior in FeMn and SiMn charges (b: 4.0 − 6.3 mm) between 1200 and 1600 °C. As similar with the results in Figure 4.15, the mass change of FeMn charge ("R1.b") was progressive, while two different stages were observed for SiMn charges ("R2.b" and "R3.b").

The comparison showed that the reduction behavior between FeMn and SiMn charges was different under the experimental conditions investigated. While the mass change of the FeMn charge, "R1", was progressive, the mass changes of SiMn charges were mainly divided into two stages. At relatively lower temperatures between 1200 and 1500 °C, the mass changes of both SiMn charges, "R2" and "R3", were relatively insignificant. However, rapid and abrupt mass changes were observed at higher temperature above 1500 °C, where the final mass changes were lower than -50 wt%. This different reduction behavior between FeMn and SiMn charges was observed regardless of the particle sizes.

The different reduction behaviors between FeMn and SiMn charges were previously discussed based on the driving force of MnO reduction, which was discussed in **Section 2.1.3**. Applying the results from the melting behavior of FeMn and SiMn charge materials (research topic #1), the activity of MnO between the FeMn and SiMn slags is expected to be different. At a constant temperature between 1200 and 1600 °C, the activity of MnO in FeMn slags is 1 unless complete dissolution of MnO has occurred, whether the activity of MnO in SiMn slags is relatively lower due to the completion of liquid slag phase. Assuming that the driving force contributes to the reduction rate of MnO reduction, the comparison between FeMn and SiMn slags can be estimated by **Equations (4.1)** and **(4.2)**. Note that the activities of MnO in primary SiMn slags from charges "R2" and "R3" are approximately 0.2, where the temperatures between 1200 and 1500 °C does not make significant difference. The activity of metal is also assumed to be close to 0 ($a_{MnO} \gg a_{Mn}/K_{MnO}$).

$$Driving\ force\ _{(FeMn)} = \left(a_{MnO} - \frac{a_{Mn}}{K_{(MnO)}}\right) \approx a_{MnO} = 1 \tag{4.1}$$

$$Driving\ force\ _{(SiMn)} = \left(a_{MnO} - \frac{a_{Mn}}{K_{(MnO)}}\right) \approx a_{MnO} \approx 0.2 \tag{4.2}$$

The estimation shows that the contribution of the driving force for MnO reduction in FeMn slags is higher than in SiMn slags by a factor of 5. This implies that the reduction rate of MnO is expected to be different between FeMn and SiMn slags. Accordingly, this was observed from the comparison of mass change between FeMn ("R1") and SiMn ("R2" and "R3") charges. Until approximately 1500 °C, the mass changes from FeMn charges were relatively faster than SiMn charges, which indicates higher reduction of MnO.

The comparison of the two different particle sizes between FeMn and SiMn charges are also shown in **Figures 4.15**, **4.16** and **4.17**. The results showed that the particle sizes had different effects between FeMn and SiMn charges. For FeMn charges, the mass change was faster with particle sizes of 0.6 − 1.6 than 4.0 − 6.3 mm. This was observed from the mass change between 1350 and 1600 °C (or 102 and 147 min.), where the mass change of charge "R1.a" was faster than "R1.b" at constant time or temperature.
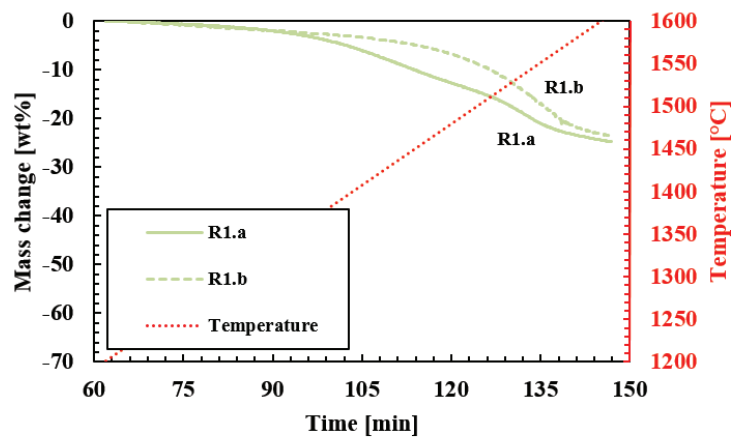
Figure 4.15: Effect of particle sizes on the reduction rate in FeMn charges: Charge "R1.a" (0.6 − 1.6 mm) and "R1.b" (4.0 − 6.3 mm). At constant time, the mass change was relatively faster with smaller particles between 1350 and 1600 °C.

However, the comparison from SiMn charges showed a different result, where the effect of particle sizes from FeMn charges was not observed. Instead, the results showed that the mass changes during the experimental condition were similar regardless of the particle sizes. This was both observed in charges "R2" and "R3", where the difference of mass changes from 0.6 − 1.6 and 4.0 − 6.3 mm particle sizes was relatively insignificant compared to the effect observed in the FeMn charges.
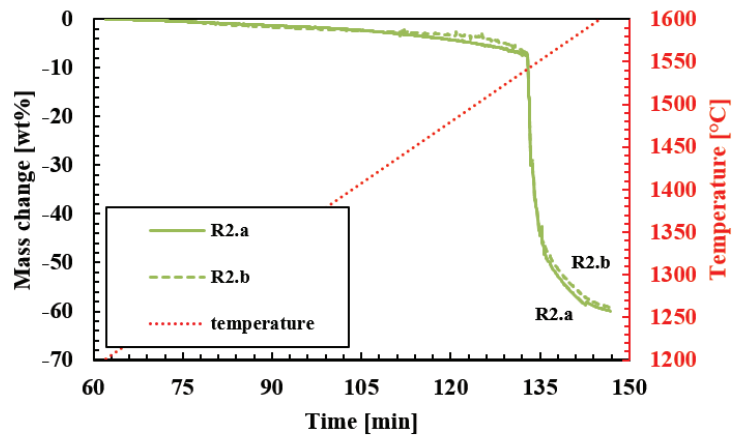
Figure 4.16: Comparison of particle sizes of 0.6 − 1.6 and 4.0 − 6.3 mm in SiMn charges ("R2.a" and "R2.b") between 1200 and 1600 °C. Mass change difference between the two different particle sizes was insignificant.
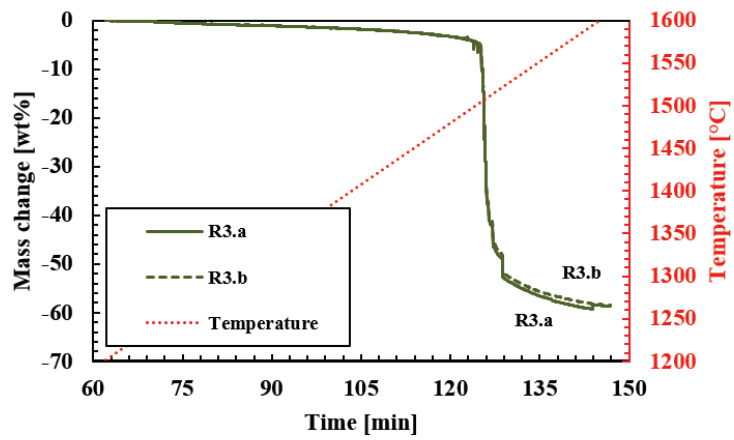
Figure 4.17: Comparison of particle sizes of 0.6 − 1.6 and 4.0 − 6.3 mm in SiMn charges ("R3.a" and "R3.b") between 1200 and 1600 °C. Mass change difference between the two different particle sizes was insignificant.

The effect of particle sizes was not observed in SiMn charges due to the melting behavior of SiMn charge materials. It was previously discussed that solid MnO phase will be present in the FeMn slag phase until liquidus temperatures. The size difference of Assmang ore will affect the reduction rate due to the dissolution rate which can affect the amount of generated slag phase. As the slag will contain a high amount of solid particles, thus having a high viscosity, the slag droplets will keep the size of the original Assmang ore particles. Accordingly, the FeMn charge with smaller particle sizes showed faster mass changes, which was observed from **Figure 4.15**. However, the different melting behavior of SiMn charges seems to have nullified the effect of particle sizes. It was observed and discussed in the previous section that the melting of SiMn charge materials and formation of slag occur relatively fast and at lower temperatures regardless of the charge type. Thus, if the formation of slag is complete before the significant reduction of MnO and SiO_2, the effect of particle sizes on the reduction rate will not be valid. This is correspondingly observed from SiMn charges in **Figures 4.16** and **4.17**, where the mass change difference between the charges with two different particle sizes was similar during the experimental condition.

4.2.2 Cross-section images and EPMA analyses

The slag phases of FeMn ("R1": Assmang ore + coke) and SiMn ("R2": Assmang ore + quartz + coke) and "R3": Assmang ore + quartz + HC FeMn slag + coke) charges, which were heated up to 1600 °C, were also analyzed through EPMA analysis to determine the reduction degrees of MnO and SiO_2. The cross-section images of FeMn and SiMn charges at 1600 °C with sketches are described in **Figure 4.18**, where the corresponding slag compositions of the charges are shown in **Table 4.6**. The detailed slag analyses can be seen in **Appendix B**. Note that part of **Table 3.11** (charges "R1", "R2" and "R3") is also shown again for convenience to compare with **Table 4.6**.
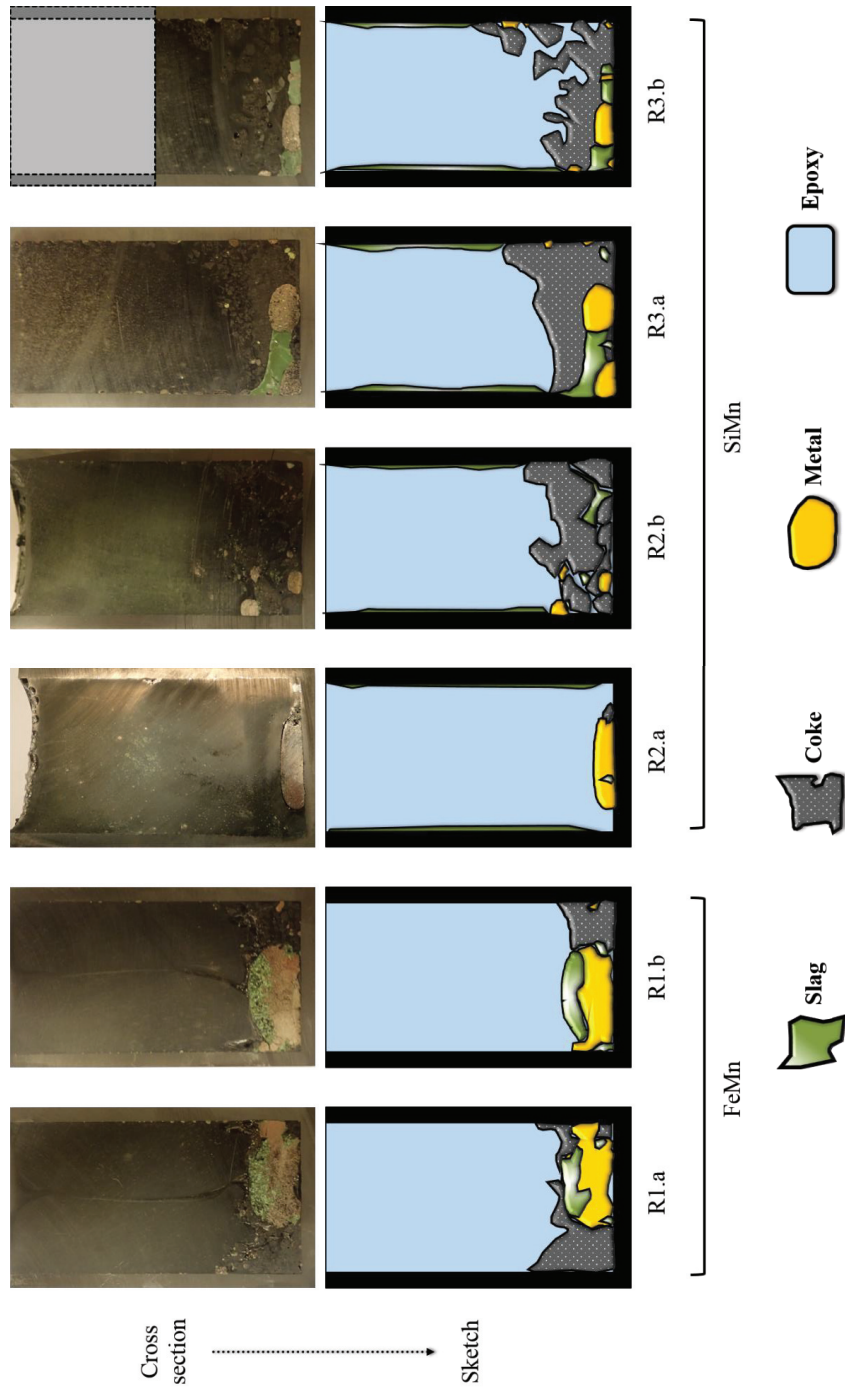
Figure 4.18: Cross-section images with sketches of FeMn ("R1") and SiMn ("R2" and "R3") charges at 1600 °C (a: 0.6 – 1.6 mm, b: 4.0 – 6.3 mm). Observed metal phases clearly indicate that the reduction of MnO and SiO_2 had occurred between 1200 and 1600 °C. Note that the crucible walls in SiMn charges were covered with thin layers of slag.

Table 3.11: Calculated primary slag composition of industrial FeMn and SiMn charges after pre-reduction at 1200 °C: Charges "R1", "R2" and "R3" from research topic #2. Note that part of Table 3.11 is shown again for convenience to compare with Table 4.6.

Exp. No.	MnO	SiO$_2$	CaO	MgO	Al$_2$O$_3$	Total [wt%]	(C+M)/A*	Notes
R1	81.7	7.9	8.6	1.5	0.4		-	Reference charge FeMn
R2	51.4	41.6	5.4	1.0	0.7	100	9.1	SiMn
R3	42.2	37.3	10.9	3.8	5.8		2.5	

*(C+M)/A: (CaO+MgO)/Al$_2$O$_3$ ratio for SiMn charges

Table 4.6: Slag compositions of FeMn and SiMn charges at 1600 °C from EPMA analyses. Comparison from the calculated primary slag composition (Table 3.11) showed that considerable reduction of MnO and SiO$_2$ had occurred between 1200 and 1600 °C. However, the reduction degrees and behavior of SiMn charges were varying due to the severe slag loss during the experiments.

Charge No.	MnO	SiO$_2$	CaO	MgO	Al$_2$O$_3$	Total [wt%]	(C+M)/A	Sizes [mm]	Notes
R1.a	16.3	40.6	35.8	5.9	1.5	100.1	-	0.6 – 1.6	Reference charge FeMn
R1.b	20.8	40.5	33.7	3.7	1.4	100.1		4.0 – 6.3	
R2.a		- Slag not observed -				-	-	0.6 – 1.6	SiMn (Severe slag loss)
R2.b	3.9	57.2	30.5	4.5	3.9	100	9.0	4.0 – 6.3	
R3.a	9.6	49.4	23.7	5.5	11.9	100.1	2.5	0.6 – 1.6	
R3.b	6.8	48.8	26.0	6.3	12.1	100	2.7	4.0 – 6.3	

The observed metal phases of FeMn ("R1") and SiMn ("R2" and "R3") charges at 1600 °C clearly indicate that the reduction of MnO and SiO$_2$ had occurred between 1200 and 1600 °C. This was also observed from the comparison of the calculated primary slag at 1200 °C (**Table 3.11**) and the slag analyses at 1600 °C (**Table 4.6**). The MnO content in the FeMn charges at 1600 °C decreased considerably from the calculated primary slag at 1200 °C, which clearly indicates MnO reduction between 1200 and 1600 °C. The reduction also seems to have occurred in the SiMn charges, where the decrease of MnO at 1600 °C from the calculated primary SiMn slag at 1200 °C was observed. The (C+M)/A ratios also showed consistency between the calculated and measured slag compositions at 1200 and 1600 °C, respectively, which can imply that all the charge materials were dissolved into the slag phase.

However, the two stage mass changes and the reduction degrees were rather uncertain to determine the reduction behavior of SiMn charges. The sharp discontinuous mass changes at approximately 1500 °C in the SiMn charges imply that the crucibles were interfered either from the furnace or from slag loss. The total mass change at 1600 °C was around -60 wt% which also implies severe interference to the crucibles or the mass balance. It was observed that a portion of slag and coke particles had escaped the SiMn charge crucibles during the rapid mass changes above 1500 °C. Traces of slag phase and coke particles, as in **Figure 4.19**, were observed at the crucible's exterior after opening the furnace chamber. This explains why the cross-section crucible walls of SiMn charges were covered with thin layer of slag phase.
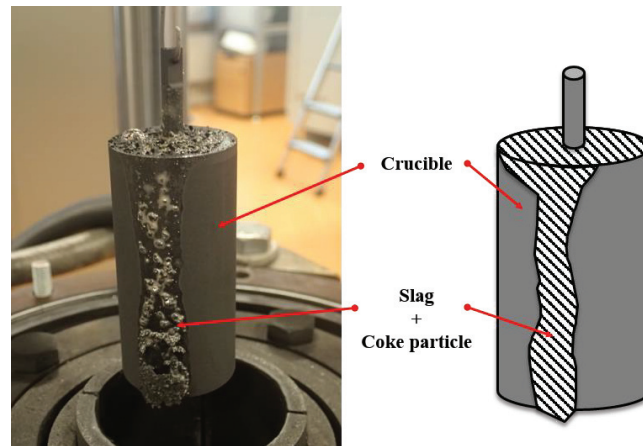
Figure 4.19: Charge "R2.a" after the TGA experiment at 1600 °C. Part of the crucible's exterior was covered with slag and coke particles, which indicated slag and coke loss during the experimental condition. This explains the thin slag layers on the crucible's inner walls of SiMn charge cross-sections. Other SiMn charges also showed the similar slag loss results.

4.2.3 Improvements and resolutions for next experiments

Two possible reasons were considered for the slag losses from SiMn charges. First, assuming that the reduction of MnO and SiO_2 occurs rapidly above 1500 °C, the massive generation of CO gas from the reduction of MnO and SiO_2 could have cause the slag loss. The produced CO gas from reduction can be captured in the slag phase to cause massive amount of piling up slag bubbles and eventually slag escaping the crucible from the top part. As the reduction occurs, the slag will be more viscous for captured CO gas to escape. Second, extreme wetting of slag could had occurred at temperatures above 1500 °C. Previously discussed in **Figure 2.21**, Ding and Olsen had reported slag losses from crucibles due to extreme wetting of slag at 1700 °C [43]. The extreme wetting of SiMn slags in this study seemed to have occurred above 1500 °C if this is the case.

To prevent the problems observed from the first two research topics, improvements were made for further experiments in research topic #3. Three main SiMn charge aspects, which are described in **Table 4.7**, were considered to solve the problems.

93

Table 4.7: Three main problematic phenomena observed from experiments of research topics #1 and #2. Reasons and resolutions of each problems are described.

Phenomena observed	Reason(s)	Resolution	Notes
Undissolved quartz particles	Not contact with Mn-sources	Layered packing	Figures 4.1 & 4.2
Slag loss	Uncertain: Slag foaming or high wetting	Decrease amount by 1/3	Figure 4.18
Rapid mass changes above 1500 °C	Possible high reduction rates	Focus between 1500 and 1650 °C	Section 4.2.1

First, layered packing of raw materials was considered for further experiments. The undissolved quartz particles at higher temperatures, which were observed from **Figures 4.1** and **4.2**, were assumed from not being in contact with Assmang ore or HC FeMn slag particles. The importance of the contact between Assmang ore and quartz to generate liquid slag phase was discussed previously in **Section 4.1**. To ensure contact between the two materials, the raw materials were packed as layers, which is described in **Figure 4.20**. Each layer was considered to behave as a raw material, where the material with the lowest melting temperature was packed on the top. The complete formation of slag will occur at relatively lower temperatures before significant reduction of MnO and SiO$_2$ according to the observations in this study.
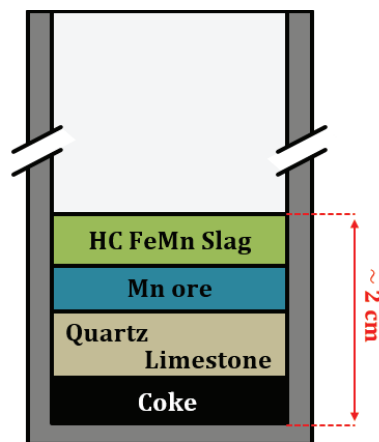
Layer packing

Figure 4.20: Illustration of layered packing of raw materials for SiMn charges in research topic #3. Raw material with the lowest melting temperature was considered to be the top layer for complete dissolution of charge materials (except coke). Complete liquid slag will occur before reduction occurs. Note that the height of the charge materials was approximately 2 cm.

Second, the total amount of charge materials was decreased to approximately 10 g, which is about 1/3 from previous experiments. Whether the slag loss was from slag foaming or extreme wetting, its occurrence was assumed to be a part of the slag characteristics and cannot be totally prevented without interfering the charge composition. The amount of charge materials in further experiments was decreased to approximately 10 g to minimize the slag loss from the crucible.

Lastly, further experiments were focused between 1500 and 1650 °C. The mass changes of SiMn charges below 1500 °C were relatively low, which indicates that the reduction of MnO and SiO_2 is not significantly occurring. It was not clear how SiMn slags behaved above 1500 °C but large portion of metal phases were observed from the cross-section images from **Figures 4.1**, **4.2** and **4.18**. It was assumed that the reduction of MnO and SiO_2 was significantly occurring between 1500 and 1650 °C.

The highlighted results of the reduction behavior in FeMn and SiMn charges from the TGA experiments is recapitulated in **Table 4.8**. The results showed that the reduction behavior and the effect of particle sizes can be different depending on the charge type. While the mass change was progressive in FeMn charges, two steps were observed in SiMn charges. The effect of particle sizes was only observed in FeMn charges while it had no effect on SiMn charges.

Table 4.8: Highlights from the reduction behavior of FeMn and SiMn charges experiments (Research topic #2). Reduction behavior and the effect of particle sizes differed on the charge type.

Charge type	Reduction behavior	Effect of particle sizes	Notes
FeMn	Progressive mass change	Yes (Faster reduction with smaller particles)	Charge "R1"
SiMn	Two steps mass change	No (Similar reduction regardless of particle sizes)	Charges "R2" and "R3"

4.3 Kinetic estimations (Research topic #3)

New experiments were performed with improved experimental methods (**Table 4.7**), and the kinetic information were obtained from different SiMn charges, which are illustrated in this section. Three different SiMn charges were heated where the focus was between 1500 and 1650 °C according to **Tables 3.6** and **3.9**. The charge composition of the three charges were "As" (Assmang ore + quartz + coke), "As/HCS" (Assmang ore + quartz + HC FeMn slag + coke) and "HCS" (quartz + HC FeMn slag + coke), where the nomenclatures represent the manganese sources in the charges. The recorded temperature schedules of the experiments are shown in **Figure 4.21**. Two separate heating rates (4.5 and 9 °C/min) were applied in the experiments to verify that the equations used were not dependent on the method.

As previously described in **Section 3.1**, the amount of raw materials in each SiMn charge of this experiment was measured to aim at 5 wt% MnO and 40 wt% SiO_2 in slag phase and 18 wt% silicon in the metal phase, which is close to the thermodynamic equilibrium at 1600 °C. All raw material particle sizes were 0.6 − 1.6 mm.
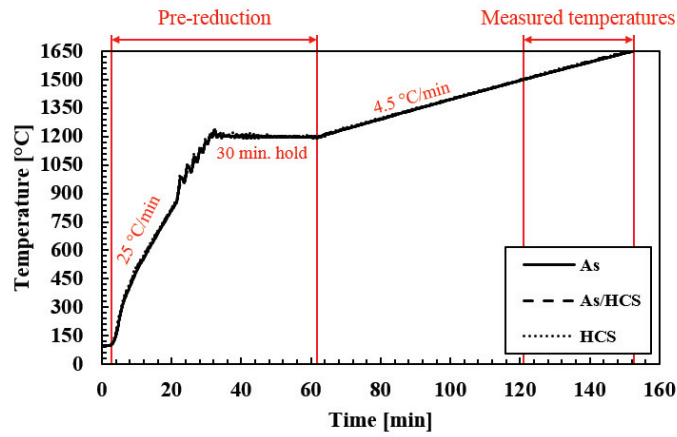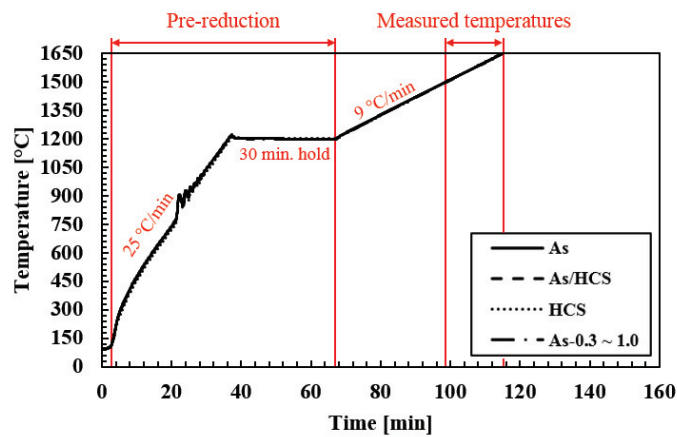
Figure 4.21: Recorded temperature schedules of experiments from research topic #3: Heating rate of (a) 4.5 °C/min and (b) 9 °C/min. The experiments were conducted in the same condition (overlapped), where the focus was between 1500 and 1650 °C. Note that additional experiments with charge "As" with different amount of sulfur (0.3 – 1.0 wt%) were also conducted after the experiments of the three different SiMn charges.

4.3.1 Mass change comparison

The mass change comparison between the different SiMn charges, "As" (Assmang ore + quartz + coke), "As/HCS" (Assmang ore + quartz + HC FeMn slag + coke) and "HCS" (quartz + HC FeMn slag + coke), are described in **Figure 4.22**. Individual mass records of the charges can be seen in **Appendix C**. Note that problems regarding undissolved quartz particles and slag loss from crucibles were not observed in experiments of research topic #3.
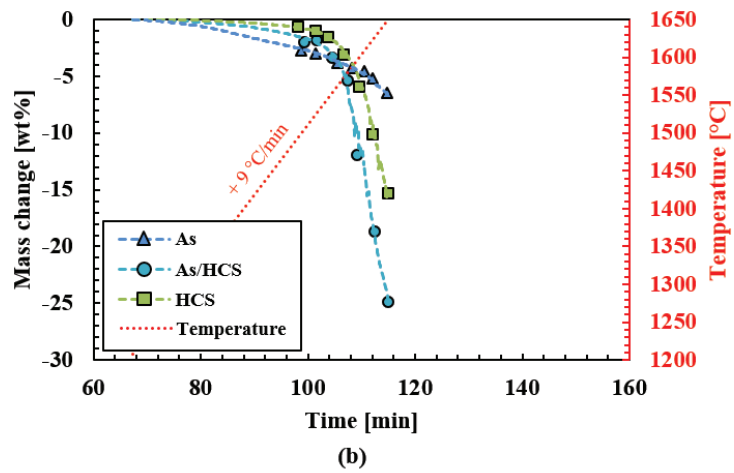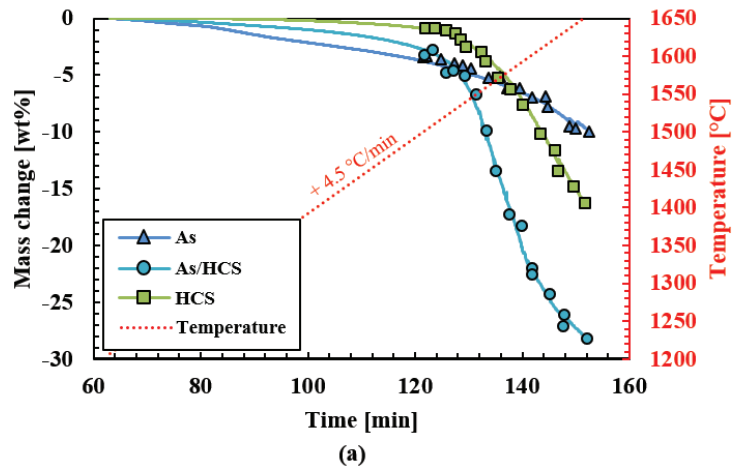
Figure 4.22: Mass change comparison of different SiMn charges between 1200 and 1650 °C: Applied heating of (a) 4.5 °C/min and (b) 9 °C/min. Lines are the average mass change while symbols are the measured mass from each experiment. Reduction was relatively slow below 1500 °C but had accelerated at higher temperatures. Also, the reduction in charges "As/HCS" and "HCS" were relatively faster than charge "As".

The mass comparison showed two interesting results regarding the reduction behavior of the three SiMn charges between 1200 and 1650 °C. First, the two stage mass changes were clearly observed from the three SiMn charges, "As", "As/HCS", and "HCS". The relatively lower mass changes below 1500 °C indicate that the reduction of MnO and SiO_2 is relatively low. The contribution of the driving force of MnO reduction seems to explain the difference. Part of **Table 3.11** (charges "As", "As/HCS" and "HCS") is also shown again for convenience to explain the different reduction degrees of the three SiMn charges below 1500 °C.

Table 3.11: Calculated primary slag composition of the three SiMn charges after pre-reduction at 1200 °C: Charges "As", "As/HCS" and "HCS" from research topic #3. Note that part of Table 3.11 is shown again for convenience to compare the different reduction degrees below 1500 °C.

Exp. No.	MnO	SiO_2	CaO	MgO	Al_2O_3	Total [wt%]	(C+M)/A*	Notes
As	59.4	32.7	6.2	1.1	0.6		12.2	
As/HCS	44.5	34.0	11.5	4.0	6.1	100	2.5	SiMn
HCS	31.8	35.1	15.9	6.5	10.7		2.1	

* (C+M)/A: (CaO + MgO)/Al_2O_3 ratio

According to the calculated primary slag compositions from **Table 3.11**, the activity of MnO was the highest in the following order: charge "As", "As/HCS" and "HCS". Accordingly, the magnitude of the driving force will be in the same order as the reduction rate and thus, the contribution from the driving force for reduction was reflected on the different mass changes below 1500 °C.

Second, the mass changes were different among the three different SiMn charges between 1500 and 1650 °C. The results shown that SiMn charges containing HC FeMn slag as charge material, charges "As/HCS" and "HCS", reduce faster than without HC FeMn slag, charge "As". The apparent effect of the different reduction degrees seems to be from the use of HC FeMn slag, but the mass changes do not necessary give more kinetic information. In addition, the (C+M)/A ratios, which can be related to the slag viscosity, do not seem to explain the different reduction rates of the three SiMn charges above 1500 °C. Note that this ratio was the same from the primary slag to the slag at maximum temperature. There was a factor of 6 difference in the (C+M)/A ratio between charge "As" and charges "As/HCS" and "HCS", where the slag of higher (C+M)/A ratio was assumed to be more favorable for reduction if the slag viscosity affects the reduction rates. Opposite results were observed in the mass change comparison, which implied that the influence of slag viscosity for reduction rate was low.

This reduction behavior from the three SiMn charges were observed in both heating rates, 4.5 and 9°C/min. To compare the mass changes from both heating rates, the mass changes as a function of only temperature were also described in **Figure 4.23**. The mass changes from the heating rate of 4.5 °C/min were faster than from the heating rate of 9 °C/min at constant temperature as one would expect with a longer time at each temperature, but the difference was less than 50 °C.
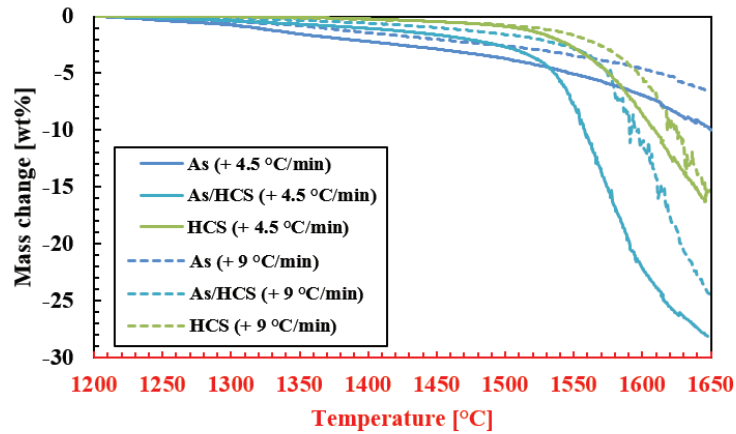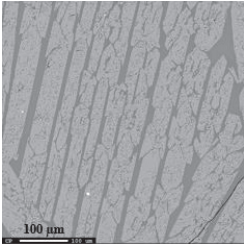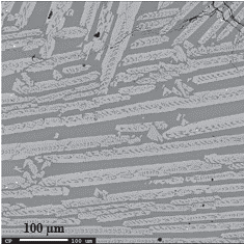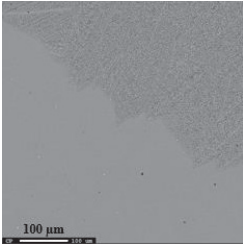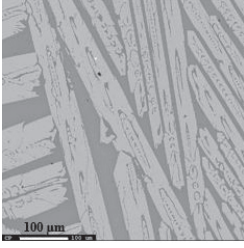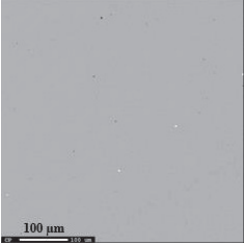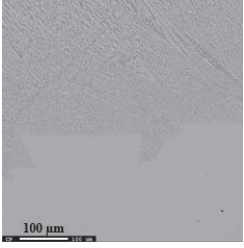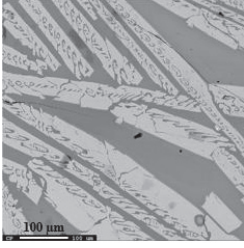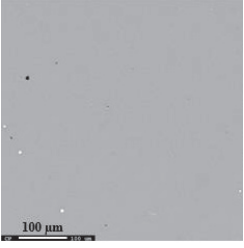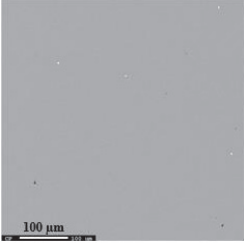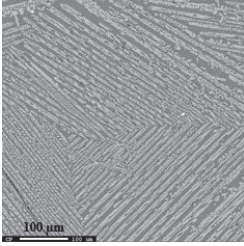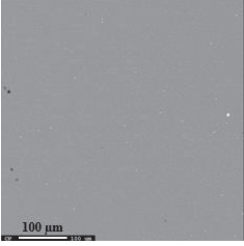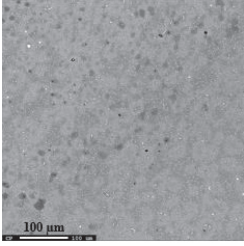
Figure 4.23: Comparison of mass change as a function of only temperature for both heating rates. At constant temperature, the mass changes from the slower heating rate (4.5 °C/min) was faster than from the higher heating rate (9 °C/min), but the difference was not large in general.

4.3.2 EPMA analyses
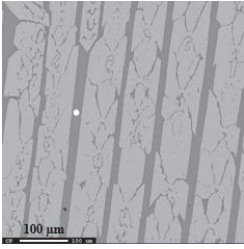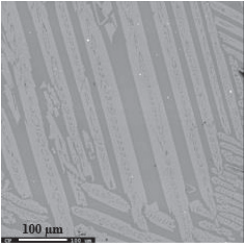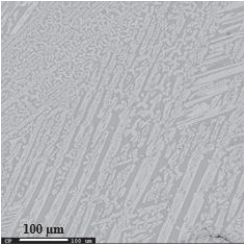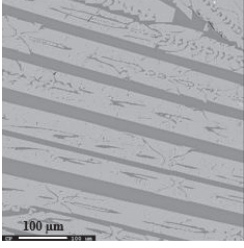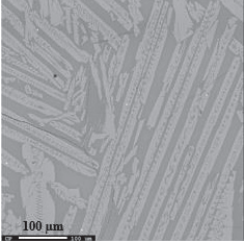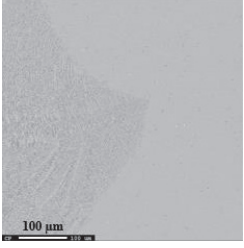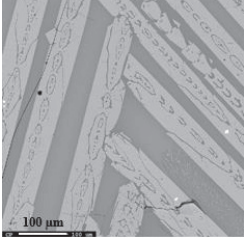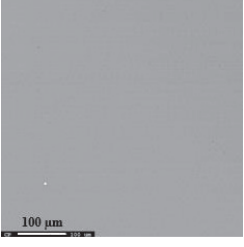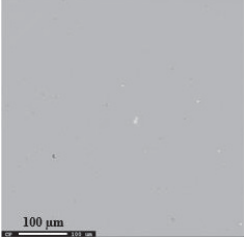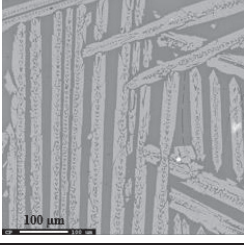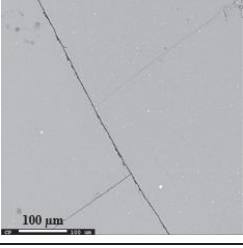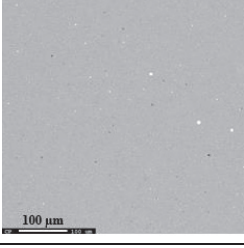
The slag structures from the EPMA analyses also described the different reduction rates of the three SiMn charges, "As" (Assmang ore + quartz + coke), "As/HCS" (Assmang ore + quartz + HC FeMn slag + coke) and "HCS" (quartz + HC FeMn slag + coke), between 1500 and 1650 °C. The BSE images of the slag phase from the three different charges at 1500, 1550, 1600 and 1650 °C are shown in **Tables 4.9** and **4.10**. Note that all slag images between 1500 and 1650 °C (heating rate 4.5 °C/min) are shown in **Appendix D**. The results showed that the initial slag structures at 1500 °C composed of two phases, which were also observed in previous experiments (Research topic #1). While the slag structures in charge "As" did not showed significant difference with increasing temperature, the slag structures in charges "As/HCS" and "HCS" became fine and eventually uniform. This was observed in slag phases from both heating rates.

99

Table 4.9: Slag structures of the three different SiMn charges at 1500, 1550, 1600 and 1650 °C (heating rate: 4.5 °C/min). No significant changes in charge "As" were observed, while the slag structures in charges "As/HCS" and "HCS" became uniform at higher temperatures.

Heating rate [°C/min]		4.5		
Charge		As	As/HCS	HCS
Temperature [°C]	1500			
	1550			
	1600			
	1650			

Table 4.10: Slag structures of the three different SiMn charges at 1500, 1550, 1600 and 1650 °C (heating rate: 9 °C/min). No significant changes in charge "As" were observed, while the slag structures in charges "As/HCS" and "HCS" became uniform at higher temperatures.

Heating rate [°C/min]		9		
Charge		As	As/HCS	HCS
Temperature [°C]	1500			
	1550			
	1600			
	1650			

The comparison of the slag structures of the three SiMn charges reflects the reduction of MnO and SiO_2 between 1200 and 1650 °C. The two light and dark grey slag phases observed at 1500 °C of the three charges resemble the slag phases which were observed at lower temperatures between 1200 and 1400 °C from experiments of research topic #1. These slag phases also represent the two manganese silicate compounds, Mn_2SiO_4 and $MnSiO_3$, from the MnO-SiO_2 system. It implies that the reaction in SiMn slags were rather inactive between 1200 and 1500 °C, where the reduction of MnO and SiO_2 was relatively insignificant. This correlates to the observed mass change comparison in **Figure 4.22**, where the reduction of MnO and SiO_2 below 1500 °C was relatively low. At temperatures between 1500 and 1650 °C, the changing slag structures of charges "As/HCS" and "HCS" indicate MnO and SiO_2 reduction, which can be observed with comparing the slag structures of charge "As". This also correlated to the observed mass changes between 1500 and 1650 °C, where the reduction was still relatively low in charge "As" even until 1650 °C. Thus, the slag structure results indicate that the liquid SiMn slag is completed at lower temperatures, but the significant reduction of MnO and SiO_2 occurs at higher temperatures.

The corresponding slag compositions of the three SiMn charges from EPMA analyses also are shown in **Tables 4.11** and **4.13**. As it was previously discussed in **Section 2.1.2**, the SiMn metal compositions are difficult to analyze due to its many intermetallic compounds. Instead, the metal compositions were calculated using assumptions: The amount of unreducible oxides (CaO, MgO and Al_2O_3) in each slag are constant. The calculation details are further explained in **Appendix E**. Note that the calculated slag and metal compositions in absolute amount (g) are also shown together in **Tables 4.12** and **4.14** due to the calculation of metal compositions.

The results in **Table 4.11** showed different reduction degrees of MnO in the three SiMn charges between 1500 and 1650 °C. The MnO content in charge "As" drops from approximately 51 to 46 wt%, which indicated a low degree of MnO reduction. On the other hand, a considerable amount of MnO reduction was observed in charges "As/HCS" and "HCS". The decrease of MnO was approximately 41 to 5 wt% and 32 to 7 wt% in charges "As/HCS" and "HCS", respectively. The slag compositions in **Table 4.13** also showed similar results, where the reduction of MnO was considerable in changes "As/HCS" and "HCS". Both MnO and SiO_2 reduction were more visible in **Tables 4.12** and **4.14** where the changing amount are shown as absolute amount (g).

Since the initial amount of MnO and SiO_2 were different among the three SiMn charges, the reduction degrees of MnO and SiO_2 were also shown in a scale between 0 and 1 by using the following **Equations (4.3)** and **(4.4)**, where **Figure 4.24** describes the comparison between the three SiMn charges from **Table 4.12**. Note that the numeric ratios are the molar weight of slag (MnO and SiO_2) and metal (manganese and silicon). The initial MnO of charges "As", "As/HCS" and "HCS" were 4.2, 3.8 and 3.7 g, respectively. The initial SiO_2 charges "As", "As/HCS" and "HCS" were 2.3, 2.9 and 4.0 g, respectively. The initial amounts were from the calculated primary slag composition at 1200 °C.

$$Reduction\ Degree_{(MnO)} = \frac{Produced\ Mn\ [g]}{Initial\ MnO\ [g]} \times \frac{70.97\ [g\ MnO/mol]}{54.94\ [g\ Mn/mol]} \qquad (4.3)$$

$$Reduction\ Degree_{(SiO_2)} = \frac{Produced\ Si\ [g]}{Initial\ SiO_2\ [g]} \times \frac{60.08\ [g\ SiO_2/mol]}{28.09\ [g\ Si/mol]} \qquad (4.4)$$

Table 4.11: Slag and metal compositions of the three different SiMn charges between 1500 and 1650 °C (heating rate: 4.5 °C/min) from the EPMA measurements. Significant MnO reduction was observed in charges "As/HCS" and "HCS".

Charge	Temperature [°C]	Slag (EPMA) [wt%]						Metal (Calculated) [wt%]			
		MnO	SiO$_2$	CaO	MgO	Al$_2$O$_3$	(C+M)/A	Mn	Si	Fe	C
As	1500	50.6	39.1	7.6	1.2	0.5	17.2	54.6	4.3	35.9	5.2
	1510	49.3	40.5	7.7	1.3	0.7	13.7	55.9	2.0	35.9	6.2
	1520	51.3	37.9	7.2	1.3	0.5	16.0	54.4	7.4	34.0	4.2
	1530	50.5	38.8	7.7	1.2	0.5	16.4	55.2	5.8	34.3	4.6
	1540	51.4	37.4	8.4	0.7	0.7	13.3	55.0	8.8	32.6	3.5
	1550	50.1	38.7	8.3	0.8	0.7	12.7	56.4	7.4	32.2	4.1
	1560	50.8	37.9	7.5	1.4	0.5	16.3	55.8	8.7	31.7	3.8
	1570	49.0	39.7	7.7	1.3	0.5	16.6	57.6	6.7	31.3	4.5
	1580	49.4	39.0	8.6	0.7	0.8	11.7	57.5	8.1	30.6	3.9
	1590	50.1	38.2	8.9	0.8	0.7	13.4	57.1	9.4	30.1	3.4
	1600	49.1	38.7	8.9	0.7	0.9	11.1	58.3	9.7	28.6	3.5
	1610	48.4	38.8	9.1	0.7	0.8	12.5	59.1	10.4	27.3	3.2
	1620	48.7	37.7	9.4	0.7	0.9	11.0	59.2	12.3	25.8	2.7
	1630	46.1	40.5	8.0	1.4	0.8	11.6	60.8	9.9	25.6	3.6
	1640	45.7	40.1	9.3	1.4	0.8	13.3	61.1	11.3	24.3	3.3
	1650	48.1	37.3	7.5	1.3	0.7	12.0	59.6	13.5	24.2	2.8
As/HCS	1500	40.5	35.1	12.3	3.8	5.2	3.1	50.0	10.7	36.5	2.9
	1510	39.8	35.4	12.2	3.5	5.8	2.7	52.7	10.6	33.8	3.0
	1520	39.1	36.6	12.0	3.9	5.6	2.9	54.5	5.2	35.6	4.7
	1530	39.1	35.7	12.1	3.7	4.9	3.3	54.6	10.5	31.8	3.1
	1540	38.3	36.8	12.2	3.9	5.0	3.2	56.8	6.4	32.4	4.4
	1550	34.1	39.0	13.2	3.7	6.3	2.7	64.8	6.5	24.1	4.6
	1560	29.5	40.4	14.4	4.0	6.7	2.7	68.4	8.9	18.7	3.9
	1570	24.0	41.8	16.2	4.3	8.0	2.6	70.2	11.1	15.3	3.4
	1580	19.7	44.1	18.3	5.2	8.8	2.7	72.0	10.3	14.1	3.7
	1590	17.2	44.2	19.2	5.2	9.2	2.7	71.8	11.6	13.2	3.4
	1600	12.7	43.8	21.6	6.2	10.4	2.7	71.3	13.9	12.0	2.9
	1610	12.3	45.4	21.2	6.0	10.7	2.6	72.2	12.4	12.1	3.2
	1620	10.9	44.6	22.5	6.4	11.5	2.5	71.6	13.7	11.7	3.0
	1630	6.8	45.5	24.2	6.7	12.4	2.5	71.8	14.1	11.1	2.9
	1640	6.8	44.0	24.9	7.2	12.8	2.5	71.0	15.2	11.0	2.8
	1650	4.9	43.9	26.5	7.1	13.8	2.4	70.9	15.7	10.7	2.8
HCS	1500	31.7	34.5	15.4	4.9	9.4	2.2	27.3	30.1	36.2	6.4
	1510	31.7	34.2	15.8	5.0	9.7	2.2	29.7	32.4	27.2	10.7
	1520	31.5	34.1	15.9	5.1	9.7	2.2	35.5	32.1	22.2	10.2
	1530	30.8	33.8	15.8	5.2	10.0	2.1	43.8	31.5	15.0	9.6
	1540	31.7	34.4	15.8	5.5	9.2	2.3	28.6	30.7	33.2	7.6
	1550	30.6	35.8	16.1	5.6	9.5	2.3	58.6	0.1	34.5	6.9
	1560	30.0	35.7	16.3	5.8	9.7	2.3	63.9	8.8	23.5	3.9
	1570	27.6	35.6	16.9	5.8	10.0	2.3	68.5	18.9	10.1	2.5
	1580	24.1	38.8	17.3	5.5	11.3	2.0	82.1	3.4	8.2	6.3
	1590	23.7	38.4	17.5	5.8	11.4	2.1	80.5	7.0	7.6	5.0
	1600	21.2	38.8	18.5	6.2	11.5	2.2	79.9	10.4	5.9	3.9
	1610	17.1	40.1	19.4	6.3	12.9	2.0	80.8	10.8	4.6	3.8
	1620	14.3	40.8	21.3	6.8	13.3	2.1	80.8	11.6	4.0	3.7
	1630	11.6	41.5	22.9	7.1	13.9	2.2	80.8	12.1	3.6	3.6
	1640	9.2	40.2	23.6	7.8	15.3	2.0	77.7	16.4	3.2	2.9
	1650	7.1	40.2	25.5	7.8	15.9	2.1	77.3	17.0	3.0	2.8

Table 4.12: Calculated slag and metal in absolute amount (g) of the three different SiMn charges between 1500 and 1650 °C (Heating rate: 4.5 °C/min). Both reduction of MnO and SiO$_2$ was more visible than Table 4.10. Reduction of MnO was high in charges "As/HCS" and "HCS".

Charge	Temperature [°C]	Slag (Calculated) [g]						Metal (Calculated) [g]				
		MnO	SiO$_2$	CaO	MgO	Al$_2$O$_3$	Total	Mn	Si	Fe	C	Total
As	1500	2.8	2.1				5.4	1.12	0.09		0.11	2.06
	1510	2.7	2.2				5.5	1.15	0.04		0.13	2.06
	1520	2.7	2.0				5.2	1.18	0.16		0.09	2.17
	1530	2.7	2.1				5.3	1.19	0.13		0.10	2.16
	1540	2.6	1.9				5.0	1.25	0.20		0.08	2.27
	1550	2.5	2.0				5.0	1.30	0.17		0.09	2.30
	1560	2.5	1.9				5.0	1.31	0.20		0.09	2.34
	1570	2.4	2.0	0.44	0.08	0.04	5.0	1.36	0.16	0.74	0.11	2.37
	1580	2.4	1.9				4.9	1.39	0.20		0.09	2.42
	1590	2.4	1.8				4.8	1.40	0.23		0.08	2.46
	1600	2.3	1.8				4.6	1.50	0.25		0.09	2.58
	1610	2.1	1.7				4.4	1.60	0.28		0.09	2.71
	1620	2.0	1.6				4.1	1.70	0.35		0.08	2.87
	1630	1.9	1.7				4.2	1.76	0.29		0.10	2.89
	1640	1.8	1.6				4.0	1.86	0.34		0.10	3.04
	1650	1.9	1.4				3.8	1.82	0.41		0.08	3.06
As/HCS	1500	3.0	2.6				7.5	0.58	0.12		0.03	1.16
	1510	2.9	2.6				7.4	0.66	0.13		0.04	1.25
	1520	3.0	2.8				7.6	0.65	0.06		0.06	1.19
	1530	2.9	2.6				7.3	0.73	0.14		0.04	1.33
	1540	2.8	2.7				7.4	0.74	0.08		0.06	1.31
	1550	2.3	2.7				6.8	1.14	0.11		0.08	1.75
	1560	1.8	2.5				6.1	1.54	0.20		0.09	2.26
	1570	1.3	2.2	0.98	0.34	0.52	5.4	1.94	0.31	0.42	0.09	2.76
	1580	1.0	2.2				5.1	2.16	0.31		0.11	3.00
	1590	0.8	2.1				4.8	2.30	0.37		0.11	3.20
	1600	0.5	1.9				4.2	2.52	0.49		0.10	3.53
	1610	0.5	2.0				4.3	2.52	0.43		0.11	3.49
	1620	0.5	1.8				4.1	2.59	0.49		0.11	3.61
	1630	0.3	1.8				3.9	2.73	0.54		0.11	3.81
	1640	0.3	1.6				3.7	2.74	0.59		0.11	3.85
	1650	0.2	1.6				3.6	2.80	0.62		0.11	3.95
HCS	1500	3.6	3.9				11.2	0.07	0.08		0.02	0.26
	1510	3.5	3.8				11.1	0.10	0.11		0.04	0.34
	1520	3.5	3.7				11.0	0.15	0.13		0.04	0.42
	1530	3.3	3.6				10.7	0.27	0.20		0.06	0.62
	1540	3.6	3.9				11.2	0.08	0.09		0.02	0.28
	1550	3.5	4.0				11.3	0.16	0.00		0.02	0.27
	1560	3.3	4.0				11.1	0.25	0.03		0.02	0.40
	1570	2.8	3.7	1.82	0.74	1.23	10.3	0.63	0.17	0.09	0.02	0.92
	1580	2.5	4.0				10.2	0.93	0.04		0.07	1.13
	1590	2.4	3.9				10.0	0.99	0.09		0.06	1.23
	1600	2.0	3.7				9.5	1.27	0.16		0.06	1.59
	1610	1.5	3.6				8.9	1.65	0.22		0.08	2.04
	1620	1.2	3.5				8.5	1.89	0.27		0.09	2.34
	1630	0.9	3.4				8.1	2.10	0.31		0.09	2.60
	1640	0.7	3.0				7.5	2.30	0.48		0.08	2.96
	1650	0.5	3.0				7.2	2.43	0.53		0.09	3.15

Table 4.13: Slag and metal compositions of the three different SiMn charges between 1500 and 1650 °C (heating rate: 9 °C/min). Significant MnO reduction was observed in charges "As/HCS" and "HCS".

Charge	Temperature [°C]	Slag (EPMA) [wt%]						Metal (Calculated) [wt%]			
		MnO	SiO$_2$	CaO	MgO	Al$_2$O$_3$	(C+M)/A	Mn	Si	Fe	C
As	1500	49.5	38.7	7.3	1.8	0.7	13.5	57.7	9.1	29.8	3.5
	1525	48.3	39.4	7.3	2.3	0.6	15.4	59.0	9.4	28.2	3.5
	1550	47.4	39.0	8.2	1.5	0.8	12.9	60.0	11.4	25.6	3.0
	1575	47.4	38.9	8.0	1.5	0.7	14.3	60.0	11.6	25.4	3.0
	1600	47.8	38.3	8.1	1.6	0.7	13.6	59.7	12.3	25.1	2.9
	1625	45.6	39.3	7.2	1.7	0.7	13.4	61.1	12.6	23.4	2.9
	1650	46.3	38.3	8.9	1.6	0.9	11.5	60.7	13.5	23.0	2.8
As/HCS	1500	40.2	36.9	11.4	6.1	5.3	3.3	47.6	0.2	45.8	6.3
	1525	40.8	35.6	11.5	5.6	6.4	2.7	46.9	9.0	40.9	3.3
	1550	40.4	34.8	11.5	6.4	6.2	2.9	49.6	14.3	33.9	2.2
	1575	36.2	38.1	12.1	6.9	6.3	3.0	60.9	7.4	27.4	4.3
	1600	27.0	42.6	15.1	8.6	7.6	3.1	70.2	7.5	17.8	4.6
	1625	18.6	46.3	17.9	9.9	8.6	3.3	73.0	8.5	14.2	4.4
	1650	7.9	45.7	23.2	13.0	12.2	3.0	71.5	14.3	11.2	2.9
HCS	1500	33.4	33.3	15.3	5.4	9.6	2.2	65.9	3.0	25.5	5.7
	1525	32.7	33.5	15.5	4.9	10.0	2.1	70.7	5.2	19.0	5.1
	1550	32.1	33.4	15.9	5.4	9.9	2.2	71.5	10.3	14.6	3.6
	1575	28.6	36.1	16.9	5.4	10.0	2.2	N/A *			
	1600	23.0	38.6	18.4	5.9	10.8	2.2	86.3	0.3	5.6	7.8
	1625	16.8	40.0	20.7	6.7	12.4	2.2	84.6	5.9	3.9	5.6
	1650	6.8	44.1	23.7	7.7	14.6	2.2	85.5	6.0	2.9	5.7

* Negative amount of silicon was calculated

Table 4.14: Calculated slag and metal in absolute amount (g) of the three different SiMn charges between 1500 and 1650 °C (Heating rate: 9 °C/min). Similar results with Table 4.11 were observed.

Charge	Temperature [°C]	Slag (Calculated) [g]						Metal (Calculated) [g]				
		MnO	SiO$_2$	CaO	MgO	Al$_2$O$_3$	Total	Mn	Si	Fe	C	Total
As	1200	4.19	2.31				7.1	0	0		0.03	0.77
	1500	2. 35	1.83				4.7	1.43	0.23		0.09	2.48
	1525	2.20	1.79				4.6	1.55	0.25		0.09	2.62
	1550	1.96	1.61	0.44	0.08	0.04	4.1	1.73	0.33	0.74	0.09	2.88
	1575	1.94	1.59				4.1	1.75	0.34		0.09	2.91
	1600	1.93	1.54				4.0	1.76	0.36		0.09	2.94
	1625	1.70	1.47				3.7	1.93	0.40		0.09	3.16
	1650	1.68	1.39				3.6	1.95	0.43		0.09	3.21
As/HCS	1200	3.78	2.95				8.6	0	0		0.02	0.44
	1500	3.21	2.95				8.0	0.44	~ 0		0.06	0.92
	1525	3.15	2.75				7.7	0.48	0.09		0.03	1.03
	1550	2.98	2.57	0.98	0.34	0.51	7.4	0.62	0.18	0.42	0.03	1.24
	1575	2.57	2.71				7.1	0.94	0.11		0.07	1.54
	1600	1.63	2.57				6.0	1.66	0.18		0.11	2.37
	1625	0.97	2.41				5.2	2.17	0.25		0.13	2.98
	1650	0.31	1.80				3.9	2.69	0.54		0.11	3.76
HCS	1200	4.10	3.80				11.7	0	0		~ 0	0.09
	1500	3.79	3.78				11.3	0.24	0.01		0.02	0.37
	1525	3.65	3.75				11.2	0.35	0.03		0.03	0.49
	1550	3.51	3.66	1.81	0.74	1.22	10.9	0.46	0.07	0.09	0.02	0.64
	1575	N/A*					-	N/A*			-	-
	1600	2.26	3.79				9.8	1.42	0.00		0.13	1.65
	1625	1.47	3.49				8.7	2.04	0.14		0.13	2.41
	1650	0.52	3.38				7.7	2.77	0.19		0.18	3.24

* Negative amount of SiO$_2$ was calculated
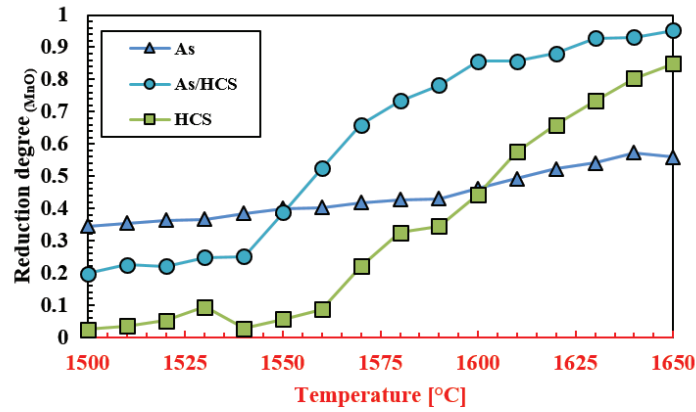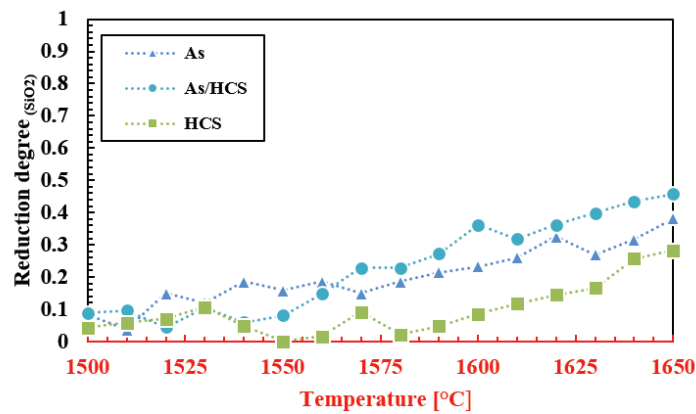
Figure 4.24: Reduction degrees of (a) MnO and (b) SiO$_2$ of the three SiMn charges in a scale of 0 and 1 between 1500 and 1650 °C from Table 4.12. Different reduction degrees of MnO at 1500 °C also reflects the contribution of the driving forces below 1500 °C. Reasons for the different reduction degrees of MnO at higher temperatures were not yet known. Reduction degrees of SiO$_2$ were similar in general between 1500 and 1650 °C.

The slag and metal compositions from **Tables 4.11**, **4.12**, **4.13** and **4.14** clearly indicate the different reduction degrees of MnO and SiO$_2$ between 1500 and 1650 °C, which shows two critical implications. First, the (C+M)/A ratio, which was discussed in **Section 2.2.3**, does not necessarily explains the different reduction degrees. The (C+M)/A ratio, which can correlate to the slag viscosity, should be favorable with charge "As" for reduction, but the higher reduction of MnO and SiO$_2$ was observed with charges "As/HCS" and "HCS". This implies that the slag viscosity has less relation with the reduction rates of MnO and SiO$_2$ in SiMn slags. Second, the amount of iron also does not seem to relate with the different reduction degrees of MnO and SiO$_2$. It was discussed in **Section 2.3.4** that higher amount of iron was likely to give higher reduction of MnO. But similar to the first case, the highest amount of iron was in charge "As" whereas the reduction of MnO and SiO$_2$ was higher in charges "As/HCS" and "HCS".

106

The reduction degrees of MnO and SiO$_2$ in **Figure 4.24** also reflect the different reduction degrees of the three SiMn charges which were discussed in the previous two sections. The higher reduction degree of MnO in charge "As" than charges "As/HCS" and "HCS" below 1500 °C, indicates the influence of the driving forces below 1500 °C. The correlating results were observed from the mass change between 1200 and 1500 °C of the three SiMn charges in **Figure 4.22**. At higher temperatures, it was not clear what could have influenced the different reduction rates of MnO reduction. Unlike MnO reduction, the reduction degrees of SiO$_2$ of the three SiMn charges were similar between 1500 and 1650 °C within the experimental conditions. It implies that the reduction of SiO$_2$ is not largely influenced by kinetic factors between 1500 and 1650 °C. Also, it shows that the reduction of MnO and SiO$_2$ occurs simultaneously.

4.3.3 Rate parameters

Further investigation was required since the reasons for the different reduction rates of MnO in the three SiMn charges, "As" (Assmang ore + quartz + coke), "As/HCS" (Assmang ore + quartz + HC FeMn slag + coke) and "HCS" (quartz + HC FeMn slag + coke), between 1500 and 1650 °C were not clear. **Equations (2.20)** and **(3.4)** were used to investigate the different reduction rates between 1500 and 1650 °C. Note that **Equations (2.20)** and **(3.4)** are shown again in this section for convenience.

$$r_{MnO} = k_{MnO} \cdot A \cdot (a_{MnO} - \frac{a_{Mn}}{K_{MnO}}) \tag{2.20}$$

$$r_{SiO_2} = k_{SiO_2} \cdot A \cdot (a_{SiO_2} - \frac{a_{Si}}{K_{SiO_2}}) \tag{3.4}$$

The reduction of MnO and SiO$_2$ occurs from liquid SiMn slag. Since liquid slag was completed before the significant reduction of MnO and SiO$_2$, the dissolution of quartz into the slag phase was considered not likely to be the rate-determining step, **Equation (2.21)**. Instead, based on previous studies [21, 62, 64], the chemical reactions of MnO and SiO$_2$ reduction was believed to determine the metal producing rates.

The following rate parameters (rate, reaction area and driving force for MnO and SiO$_2$ reduction) in bulleted points are described in **Figures 4.25**, **4.26** and **4.27**, where the numeric values are organized in **Tables 4.15**, **4.16**, **4.17** and **4.18**:

- Reduction rates of MnO and SiO$_2$ (**Figure 4.25** and **Table 4.15**): Data from the TGA results (time and temperature) and EPMA analyses (slag compositions) were used to calculate the rates.

- Reaction area (**Figure 4.26** and **Table 4.16**): Calculated from using the amount of produced metal (manganese and silicon) according to **Reactions (1.10)** and **(1.11)** and from **Equations (3.1)** and **(3.2)**.

- Driving force of MnO and SiO$_2$ reduction (**Figure 4.27** and **Tables 4.17 and 4.18**): Calculated from **Equations (1.1)**, **(1.2)**, **(1.4)** and **(1.5)**.
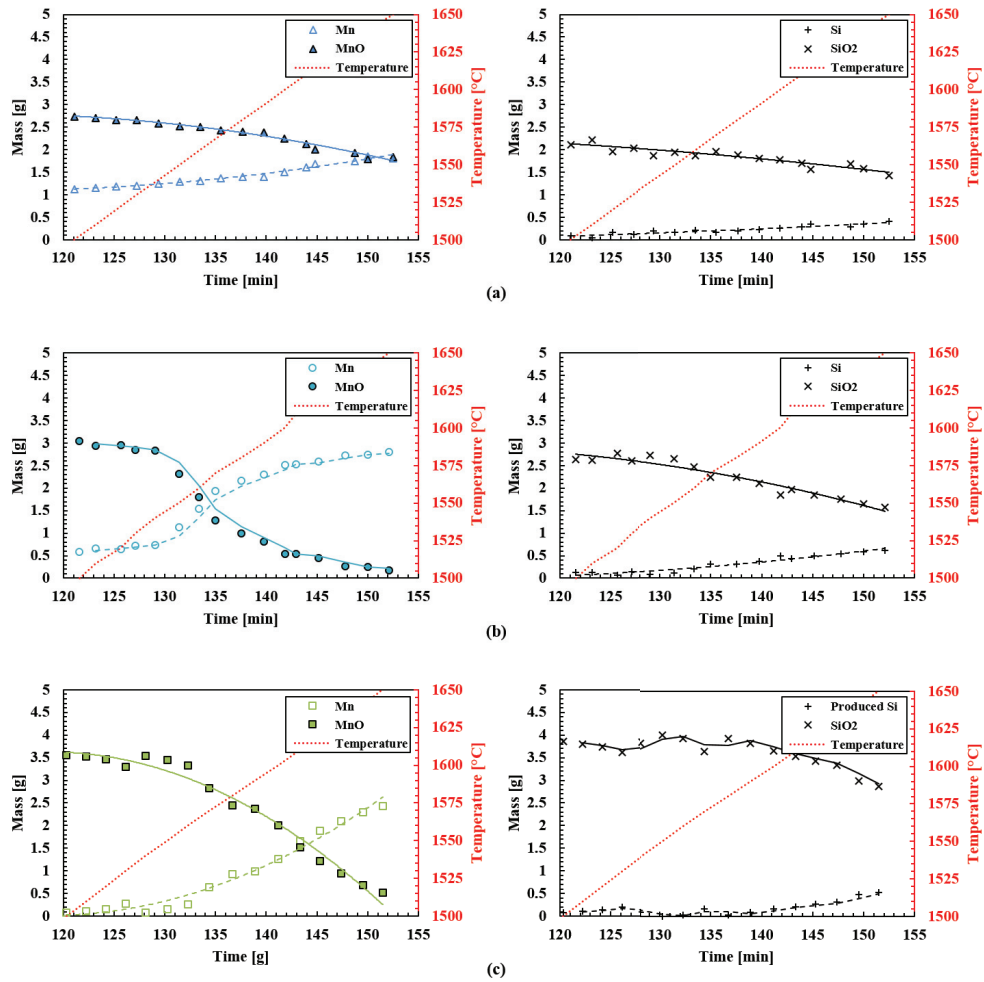
Figure 4.25: Amount of slag (MnO and SiO$_2$) and metal (manganese and silicon) as a function of time between 1500 and 1650 °C: Charge (a) "As", (b) "As/HCS" and (c) "HCS". Mass changes indicate that the reduction of MnO was relatively higher in charges "As/HCS" and "HCS". SiO$_2$ reduction was relatively low and similar with all charges.

108

Table 4.15: Calculated rates of MnO and SiO$_2$ reduction of the three SiMn charges between 1500 and 1650 °C. Unavailable (N/A) rates were due to high uncertainties.

Charge	Temperature [°C]	Reduction rates [g/min]	
		MnO	SiO$_2$
As	1500	-0.012	-0.014
	1510	-0.014	-0.015
	1520	-0.017	-0.015
	1530	-0.019	-0.016
	1540	-0.022	-0.017
	1550	-0.025	-0.018
	1560	-0.027	-0.019
	1570	-0.030	-0.020
	1580	-0.033	-0.020
	1590	-0.035	-0.021
	1600	-0.038	-0.022
	1610	-0.040	-0.023
	1620	-0.042	-0.023
	1630	-0.046	-0.025
	1640	-0.048	-0.025
	1650	-0.051	-0.026
As/HCS	1500	-0.059	-0.002
	1510	-0.072	-0.004
	1520	-0.092	-0.013
	1530	-0.103	-0.019
	1540	-0.119	-0.026
	1550	-0.137	-0.035
	1560	-0.153	-0.042
	1570	-0.166	-0.049
	1580	-0.186	-0.058
	1590	-0.204	-0.067
	1600	-0.221	-0.075
	1610		
	1620		
	1630	- N/A -	
	1640		
	1650		
HCS	1500	-0.026	
	1510	-0.036	
	1520	-0.046	- N/A -
	1530	-0.055	
	1540	-0.065	
	1550	-0.076	
	1560	-0.086	-0.003
	1570	-0.096	-0.015
	1580	-0.108	-0.028
	1590	-0.119	-0.041
	1600	-0.130	-0.054
	1610	-0.141	-0.066
	1620	-0.150	-0.077
	1630	-0.161	-0.089
	1640	-0.172	-0.101
	1650	-0.181	-0.112
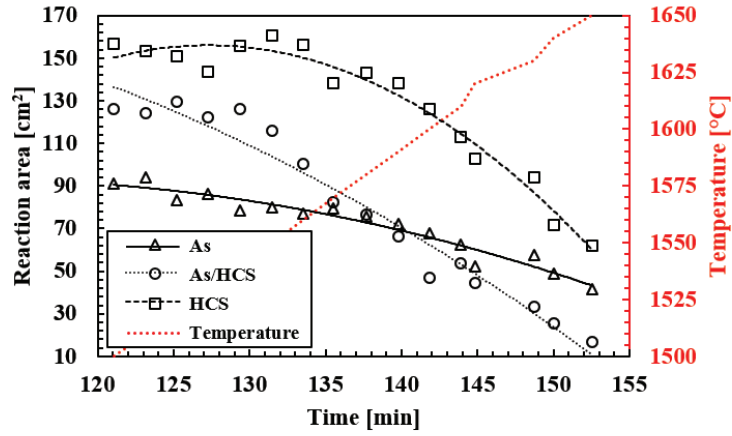
Figure 4.26: Calculated reaction areas of the three different SiMn charges between 1500 and 1650 °C. Decrease of the reaction area was high in charges "As/HCS" and "HCS", which indicated high reduction degrees of MnO and SiO_2.

Table 4.16: Calculated reaction area of the three different SiMn changes between 1500 and 1650 °C, where the values are visualized in Figure 4.26.

Time [min]	Temperature [°C]	Reaction area [cm²]		
		As	As/HCS	HCS
121.1	1500	90.9	126.2	156.6
123.2	1510	94.2	124.0	153.6
125.2	1520	83.5	129.6	150.9
127.3	1530	86.3	122.2	143.8
129.4	1540	78.5	126.1	155.8
131.5	1550	80.2	116.0	160.7
133.5	1560	76.9	100.4	156.3
135.5	1570	79.7	82.3	138.3
137.7	1580	75.7	76.6	143.0
139.8	1590	72.1	66.5	138.1
141.8	1600	67.9	47.0	125.9
143.9	1610	62.2	53.6	112.8
144.8	1620	52.2	44.5	103.0
148.7	1630	57.7	33.4	93.9
150.0	1640	48.7	25.5	71.7
152.5	1650	41.3	16.7	61.8
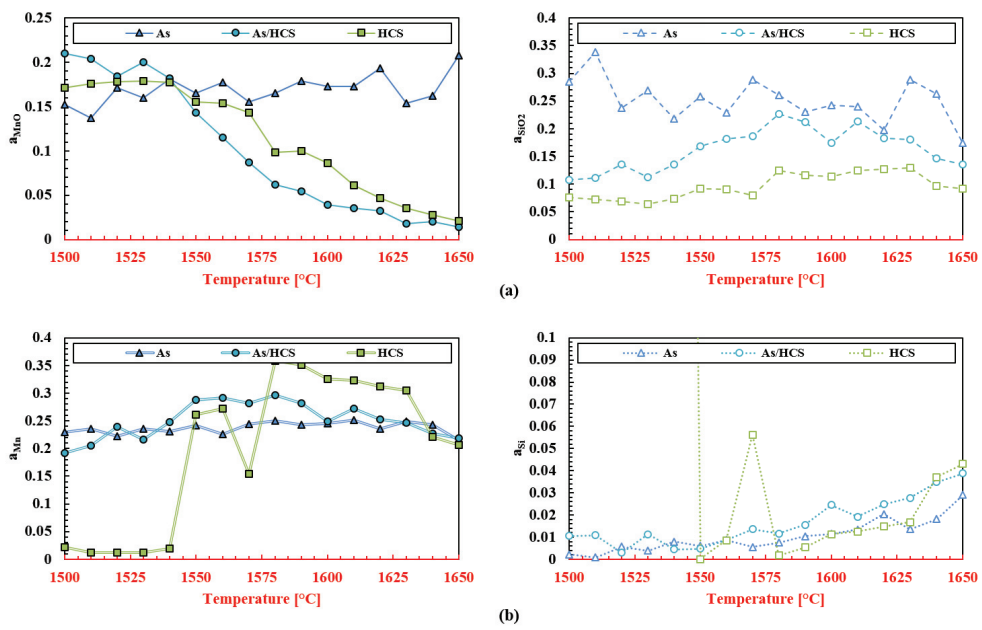
Figure 4.27: Estimated activities of (a) slag (MnO and SiO₂) and (b) metal (manganese and silicon) between 1500 and 1650 °C of the three SiMn charges. Activity of MnO was approximately 0.2 at 1500 °C regardless of the charge type. Driving forces of MnO and SiO₂ reduction are shown in Tables 4.16 and 4.17.

Table 4.17: Estimated activities (a_{MnO} and a_{Mn}) and calculated driving forces for MnO reduction between 1500 and 1650 °C of the three SiMn charges. Values of the driving force were similar to the activity of MnO: Driving force $_{(MnO)} \approx a_{MnO}$.

Temperature [°C]	a_{MnO}			a_{Mn}			K [42]	Driving force		
	As	As/HCS	HCS	As	HCS	HCS		As	HCS	HCS
1500	0.15	0.21	0.17	0.23	0.19	0.02	61.51	0.15	0.21	0.17
1510	0.14	0.20	0.18	0.24	0.21	0.01	67.72	0.13	0.20	0.18
1520	0.17	0.18	0.18	0.22	0.24	0.01	74.46	0.17	0.18	0.18
1530	0.16	0.20	0.18	0.24	0.22	0.01	81.77	0.16	0.20	0.18
1540	0.18	0.18	0.18	0.23	0.25	0.02	89.70	0.18	0.18	0.18
1550	0.17	0.14	0.16	0.24	0.29	0.26	98.27	0.16	0.14	0.15
1560	0.18	0.12	0.15	0.23	0.29	0.27	107.54	0.17	0.11	0.15
1570	0.16	0.09	0.14	0.24	0.28	0.15	117.54	0.15	0.08	0.14
1580	0.17	0.06	0.10	0.25	0.30	0.36	128.31	0.16	0.06	0.10
1590	0.18	0.05	0.10	0.24	0.28	0.35	139.90	0.18	0.05	0.10
1600	0.17	0.04	0.09	0.24	0.25	0.33	152.35	0.17	0.04	0.08
1610	0.17	0.04	0.06	0.25	0.27	0.32	165.72	0.17	0.03	0.06
1620	0.19	0.03	0.05	0.24	0.25	0.31	180.04	0.19	0.03	0.05
1630	0.15	0.02	0.04	0.25	0.25	0.30	195.37	0.15	0.02	0.03
1640	0.16	0.02	0.03	0.24	0.23	0.22	211.76	0.16	0.02	0.03
1650	0.21	0.01	0.02	0.21	0.22	0.21	229.26	0.21	0.01	0.02

Table 4.18: Estimated activities (a_{SiO2} and a_{Si}) and calculated driving forces for SiO_2 reduction between 1500 and 1650 °C of the three SiMn charges. Driving forces of charge "HCS" at lower temperatures were not able to calculate due to the low amount of silicon produced.

Temperature [°C]	a_{SiO2}			a_{Si}			K [42]	Driving force		
	As	As/HCS	HCS	As	HCS	HCS		As	HCS	HCS
1500	0.29	0.11	0.08	0.00	0.01		0.02	0.16	- N/A -	
1510	0.34	0.11	0.07	0.00	0.01		0.02	0.30		
1520	0.24	0.14	0.07	0.01	0.00	- N/A -	0.03	0.05	0.03	
1530	0.27	0.11	0.06	0.00	0.01		0.04	0.17	- N/A -	- N/A -
1540	0.22	0.14	0.07	0.01	0.00		0.05	0.06	0.04	
1550	0.26	0.17	0.09	0.01	0.00		0.07	0.17	0.09	
1560	0.23	0.18	0.09	0.01	0.01	0.01	0.08	0.13	0.08	
1570	0.29	0.19	0.08	0.01	0.01	0.06	0.11	0.24	0.06	
1580	0.26	0.23	0.12	0.01	0.01	0.00	0.14	0.21	0.14	0.11
1590	0.23	0.21	0.12	0.01	0.02	0.01	0.18	0.17	0.12	0.09
1600	0.24	0.17	0.11	0.01	0.02	0.01	0.22	0.19	0.06	0.06
1610	0.24	0.21	0.12	0.01	0.02	0.01	0.28	0.19	0.14	0.08
1620	0.20	0.18	0.13	0.02	0.02	0.01	0.35	0.14	0.11	0.08
1630	0.29	0.18	0.13	0.01	0.03	0.02	0.43	0.26	0.12	0.09
1640	0.26	0.15	0.10	0.02	0.03	0.04	0.54	0.23	0.08	0.03
1650	0.18	0.14	0.09	0.03	0.04	0.04	0.66	0.13	0.08	0.03

The following bulleted points also describe the uncertainties and results of the calculated rate parameters from the three SiMn charges between 1500 and 1650 °C.

- Rates: The reduction rates of charge "As/HCS" between 1610 and 1650 °C and charge "HCS" (SiO$_2$) between 1500 and 1550 °C were not able to estimate due to high uncertainties. Foaming or extreme wetting of slag was assumed to had occurred in charge "As/HCS" between 1610 and 1650 °C due to the thin slag phase observed in the inner crucible walls (similar to **Figure 4.18**). Slag was not lost from the crucible, but it was assumed to increase the uncertainties of MnO and SiO$_2$ reduction rates between 1610 and 1650 °C. The uncertainties in charge "HCS" between 1500 and 1550 °C were due to the small amount of silicon produced. The comparison of the amount of silicon between 1500 and 1550 °C was not meaningful.

- Reaction area: Since slag foaming or extreme wetting in charge "As/HCS" had occurred between 1610 and 1650 °C, the reaction area of slag not only covers the coke but also the graphite crucible walls. The calculated reaction area only relates to the interface between slag and coke particles and the involvement of the interface with crucible walls increases the uncertainties of the measured values between 1610 and 1650 °C.

- Driving force: Since not much silicon was produced in charge "HCS" between 1500 and 1550 °C, calculation of the driving force for SiO$_2$ reduction gave negative results. The uncertainly was high but also meaningless to discuss due to small amount of silicon produced between 1500 and 1550 °C. Also, the results from the driving force of MnO reduction showed that the values of the driving force were similar with values of the activity of MnO ($a_{MnO} \gg a_{Mn}/K_{(MnO)}$), where the expression is shown in **Equation (4.5)**.

$$Driving\ force_{(MnO\ reduction)} = a_{MnO} - \frac{a_{Mn}}{K_{(MnO)}} \approx a_{MnO} \qquad \textbf{(4.5)}$$

The comparison of the driving force for MnO reduction of the three SiMn charges between 1500 and 1650 °C showed that the rate was not highly influenced by changes in the driving force. This was observed from the comparison at 1500 °C, where the driving forces of the three SiMn charges were all approximately 0.2. According to the rate model for MnO reduction, higher driving forces should contribute to higher reduction rates. The similar driving forces of the three charges at 1500 °C cannot explain the different reduction rates at higher temperatures. Thus, the rate constants should give more explanation of the different reduction rates if the driving force is less influential. In addition, the driving forces for SiO$_2$ reduction of the three SiMn charges were rather similar within the experimental conditions.

Based on the three rate parameters, rate, reaction area and driving force of MnO and SiO$_2$ reduction, the rate constants were calculated according to the rate models, **Equations (2.20)** and **(3.4)**, between 1500 and 1650 °C. The rate constants of MnO and SiO$_2$ reduction are described in **Figure 4.28** where the calculated values are shown in **Tables 4.19** and **4.20**.
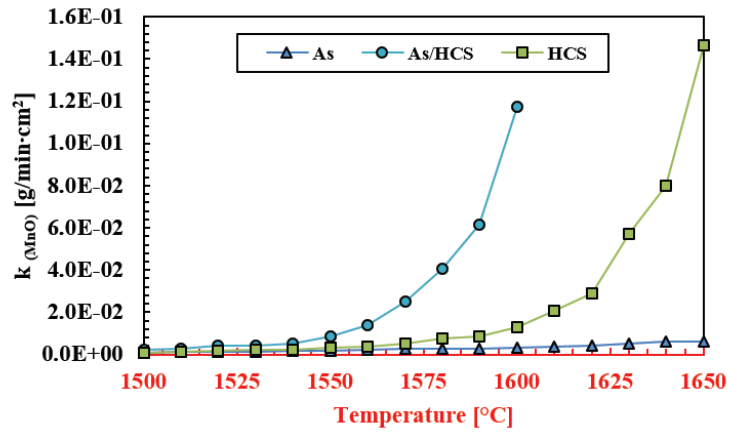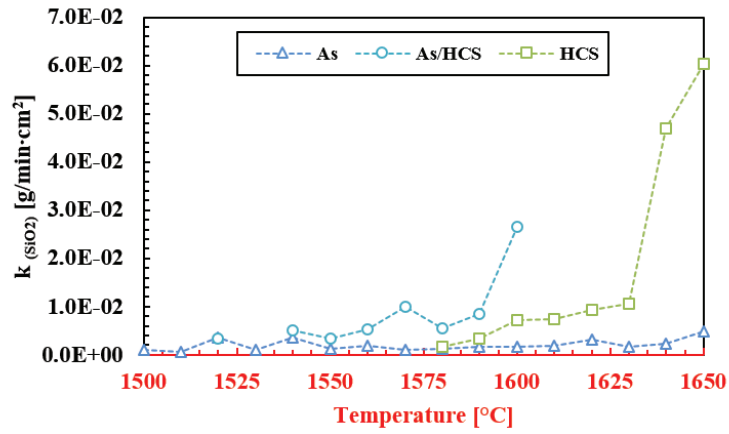
Figure 4.28: Rate constants of (a) MnO and (b) SiO_2 reduction based on the measured rate parameters between 1500 and 1650 °C. Rate constants showed significant difference between charge types. Note that the rate constants from charge "As/HCS" is only shown between 1500 and 1600 °C due to the uncertainties from the experimental measurements. Rate constants of SiO_2 reduction of charge "HCS" between 1500 and 1550 °C were also unable to describe due to small amount of produced silicon.

114

Table 4.19: Estimated rate constants of MnO reduction based on the rate parameters between 1500 and 1650 °C. Rate constants showed significant difference among SiMn charge types.

Charge	Temperature [°C]	Rate, r [g MnO/min]	Reaction area, A [cm²]	Driving force, DF	Rate constant, k [g MnO/min · cm²]	Notes
As	1500	-0.012	90.9	0.15	8.8×10^{-4}	
	1510	-0.014	94.2	0.13	1.1×10^{-3}	
	1520	-0.017	83.5	0.17	1.2×10^{-3}	
	1530	-0.019	86.3	0.16	1.4×10^{-3}	
	1540	-0.022	78.5	0.18	1.6×10^{-3}	
	1550	-0.025	80.2	0.16	2.0×10^{-3}	
	1560	-0.027	76.9	0.17	2.1×10^{-3}	
	1570	-0.030	79.7	0.15	2.5×10^{-3}	
	1580	-0.033	75.7	0.16	2.7×10^{-3}	
	1590	-0.035	72.1	0.18	2.7×10^{-3}	
	1600	-0.038	67.9	0.17	3.3×10^{-3}	
	1610	-0.040	62.2	0.17	3.8×10^{-3}	
	1620	-0.042	52.2	0.19	4.2×10^{-3}	
	1630	-0.046	57.7	0.15	5.3×10^{-3}	
	1640	-0.048	48.7	0.16	6.2×10^{-3}	
	1650	-0.051	41.3	0.21	5.9×10^{-3}	
As/HCS	1500	-0.059	126.2	0.21	2.2×10^{-3}	
	1510	-0.072	124.0	0.20	2.9×10^{-3}	
	1520	-0.092	129.6	0.18	3.9×10^{-3}	
	1530	-0.103	122.2	0.20	4.2×10^{-3}	
	1540	-0.119	126.1	0.18	5.2×10^{-3}	
	1550	-0.137	116.0	0.14	8.4×10^{-3}	
	1560	-0.153	100.4	0.11	1.4×10^{-2}	
	1570	-0.166	82.3	0.08	2.5×10^{-2}	$k = \dfrac{-r}{A \cdot DF}$
	1580	-0.186	76.6	0.06	4.1×10^{-2}	
	1590	-0.204	66.5	0.05	6.1×10^{-2}	
	1600	-0.221	47.0	0.04	1.2×10^{-1}	
	1610		53.6	0.03		
	1620		44.5	0.03		
	1630	- N/A -	33.4	0.02	- N/A -	
	1640		25.5	0.02		
	1650		16.7	0.01		
HCS	1500	-0.026	156.6	0.17	9.8×10^{-4}	
	1510	-0.036	153.6	0.18	1.3×10^{-3}	
	1520	-0.046	150.9	0.18	1.7×10^{-3}	
	1530	-0.055	143.8	0.18	2.1×10^{-3}	
	1540	-0.065	155.8	0.18	2.3×10^{-3}	
	1550	-0.076	160.7	0.15	3.2×10^{-3}	
	1560	-0.086	156.3	0.15	3.7×10^{-3}	
	1570	-0.096	138.3	0.14	5.0×10^{-3}	
	1580	-0.108	143.0	0.10	7.6×10^{-3}	
	1590	-0.119	138.1	0.10	8.6×10^{-3}	
	1600	-0.130	125.9	0.08	1.3×10^{-2}	
	1610	-0.141	112.8	0.06	2.1×10^{-2}	
	1620	-0.150	103.0	0.05	2.9×10^{-2}	
	1630	-0.161	93.9	0.03	5.7×10^{-2}	
	1640	-0.172	71.7	0.03	8.0×10^{-2}	
	1650	-0.181	61.8	0.02	1.5×10^{-1}	

Table 4.20: Estimated rate constants of SiO_2 reduction based on the rate parameters between 1500 and 1650 °C. Rate constants showed significant difference among SiMn charge types.

Charge	Temperature [°C]	Rate, r [g SiO$_2$/min]	Reaction area, A [cm^2]	Driving force, DF	Rate constant, k [g SiO$_2$/min · cm^2]	Notes
As	1500	-0.014	90.9	0.16	9.6×10^{-4}	
	1510	-0.015	94.2	0.30	5.3×10^{-4}	
	1520	-0.015	83.5	0.05	3.6×10^{-3}	
	1530	-0.016	86.3	0.17	1.1×10^{-3}	
	1540	-0.017	78.5	0.06	3.6×10^{-3}	
	1550	-0.018	80.2	0.17	1.3×10^{-3}	
	1560	-0.019	76.9	0.13	1.9×10^{-3}	
	1570	-0.02	79.7	0.24	1.1×10^{-3}	
	1580	-0.02	75.7	0.21	1.3×10^{-3}	
	1590	-0.021	72.1	0.17	1.7×10^{-3}	
	1600	-0.022	67.9	0.19	1.7×10^{-3}	
	1610	-0.023	62.2	0.19	2.0×10^{-3}	
	1620	-0.023	52.2	0.14	3.2×10^{-3}	
	1630	-0.025	57.7	0.26	1.7×10^{-3}	
	1640	-0.025	48.7	0.23	2.3×10^{-3}	
	1650	-0.026	41.3	0.13	4.8×10^{-3}	
As/HCS	1500	-0.002	126.2	- N/A -	- N/A -	
	1510	-0.004	124.0			
	1520	-0.013	129.6	0.03	3.3×10^{-3}	
	1530	-0.019	122.2	- N/A -	- N/A -	
	1540	-0.026	126.1	0.04	5.2×10^{-3}	
	1550	-0.035	116.0	0.09	3.4×10^{-3}	
	1560	-0.042	100.4	0.08	5.2×10^{-3}	
	1570	-0.049	82.3	0.06	9.9×10^{-3}	$k = \dfrac{-r}{A \cdot DF}$
	1580	-0.058	76.6	0.14	5.4×10^{-3}	
	1590	-0.067	66.5	0.12	8.4×10^{-3}	
	1600	-0.075	47.0	0.06	2.7×10^{-2}	
	1610		53.6	0.14		
	1620		44.5	0.11		
	1630	- N/A -	33.4	0.12	- N/A -	
	1640		25.5	0.08		
	1650		16.7	0.08		
HCS	1500		156.6			
	1510		153.6			
	1520		150.9			
	1530	- N/A -	143.8			
	1540		155.8	- N/A -	- N/A -	
	1550		160.7			
	1560	-0.003	156.3			
	1570	-0.015	138.3			
	1580	-0.028	143.0	0.11	1.8×10^{-3}	
	1590	-0.041	138.1	0.09	3.3×10^{-3}	
	1600	-0.054	125.9	0.06	7.2×10^{-3}	
	1610	-0.066	112.8	0.08	7.3×10^{-3}	
	1620	-0.077	103.0	0.08	9.3×10^{-3}	
	1630	-0.089	93.9	0.09	1.1×10^{-2}	
	1640	-0.101	71.7	0.03	4.7×10^{-2}	
	1650	-0.112	61.8	0.03	6.0×10^{-2}	

The results showed that the rate constants in charges "As/HCS" and "HCS" increased more rapidly than charge "As" with increasing temperatures between 1500 and 1650 °C. This implies that the reduction of MnO and SiO$_2$ becomes highly sensitive to temperature between 1500 and 1650 °C depending on the SiMn charge composition. It seems the use of HC FeMn slag as charge material affects the temperature dependencies of MnO and SiO$_2$ reduction between 1500 and 1650 °C, where this was described from the mass change comparison results in **Section 4.3.1**. This implies that the choice of charge materials can affect the metal producing performance significantly assuming good furnace performance in the SiMn process.

4.3.4 Arrhenius plots

The rate constants in the rate models, **Equations (2.20)** and **(3.4)**, were expressed as the Arrhenius equation, and the kinetic parameters were estimated from constructing the Arrhenius plots of MnO and SiO$_2$ reduction. The activation energy (or temperature dependency) and pre-exponential constants were obtained from the Arrhenius plots, which were used to recalculate the rate constants between 1500 and 1650 °C. For convenience, **Equation (2.19)** is shown again below this paragraph. **Figure 4.29** describes the Arrhenius plots of MnO and SiO$_2$ reduction and **Table 4.21** summarizes the approximate activation energies (or temperature dependencies) and pre-exponential constants of the three SiMn charges, "As" (Assmang ore + quartz + coke, "As/HCS" (Assmang ore + quartz + HC FeMn slag + coke) and "HCS" (quartz + HC FeMn slag + coke).

$$k_{MnO} = k_{o, \ MnO} \cdot e^{(-\frac{E_{MnO}}{RT})} \tag{2.19}$$
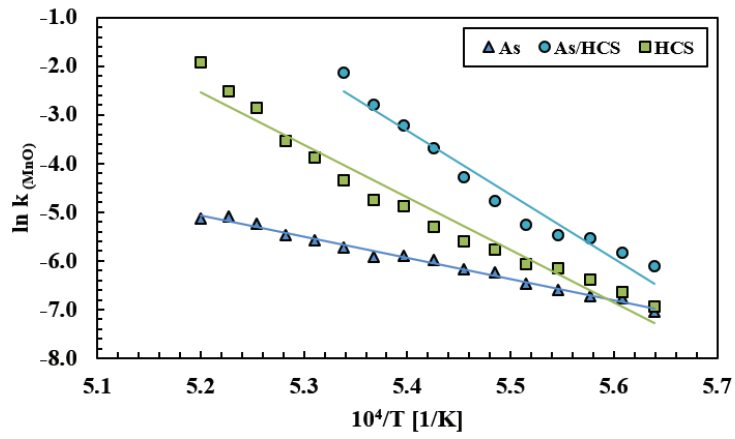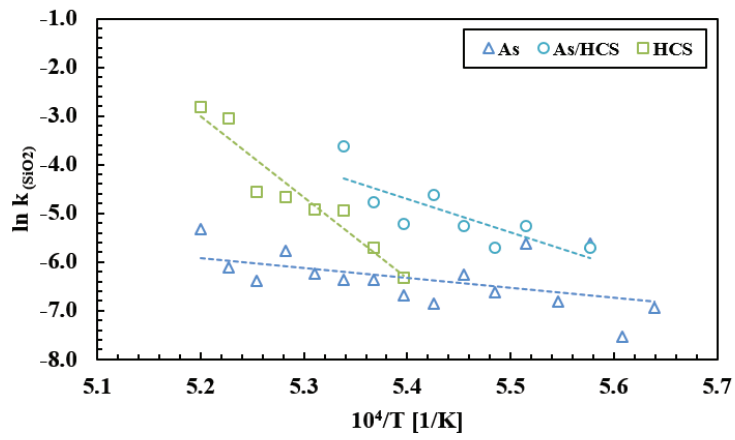
Figure 4.29: Arrhenius plots of (a) MnO and (b) SiO_2 reduction of the three SiMn charges between 1500 and 1650 °C. Temperature dependencies of charge "As/HCS" and "HCS" were higher than charge "As" for both MnO and SiO_2 reduction.

118

Table 4.21: Summary of the activation energies and pre-exponential constants of the three different charges between 1500 and 1650 °C. Kinetic parameters are the approximate value from the experiments.

Reduction	Charge	E_a [kJ/mol]	k_O [g/min · cm^2]
MnO	As	~ 250	9.66×10^3
	As/HCS	~ 920	1.62×10^{24}
	HCS	~ 780	5.87×10^{19}
SiO2	As	~ 160	3.04×10^0
	As/HCS	~ 870	5.92×10^{21}
	HCS	~ 1130	6.61×10^{28}

As expected from the previous section, **Figure 4.28**, the reduction of MnO and SiO$_2$ in charges "As/HCS" and "HCS" was more sensitive to temperature than charge "As". The higher activation energies with faster reduction rates of charges "As/HCS" and "HCS" seem contradicting according to **Equation (2.19)**, but the activation energy does not necessarily give information of the different reduction rates. The activation energy is an empirical value which indicates the temperature sensitivity of reactions, and it is the pre-exponential constant and the activation energy together that produce the reaction rates.

The rate constants calculated from the kinetic parameters were compared with the slag properties, which can possibly relate to the different reduction rates observed in three SiMn charges between 1500 and 1650 °C. The rate constants of MnO and SiO$_2$ reduction, which were recalculated from the kinetic parameters, are shown in **Figure 4.30**. Note that **Equation (2.19)** was used to calculate the rate constants.
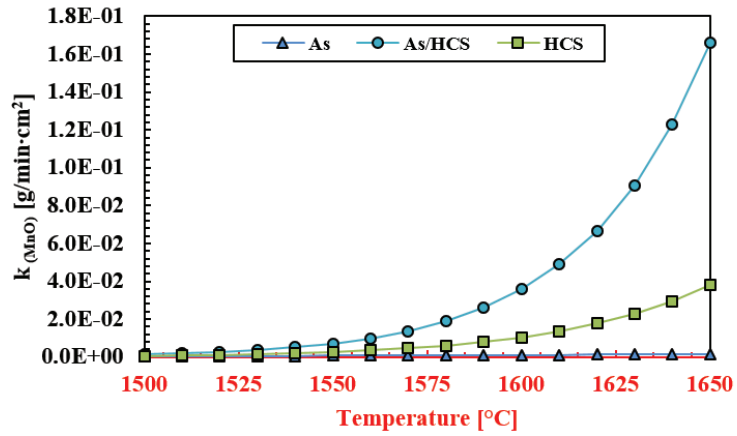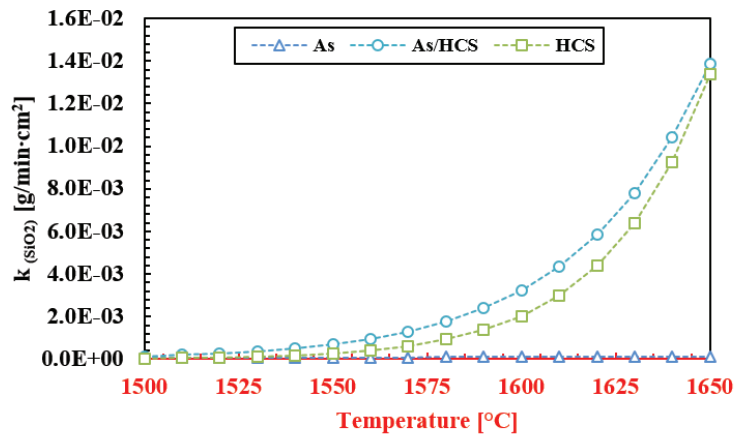
Figure 4.30: Recalculated rate constants of (a) MnO and (b) SiO_2 reduction of the three SiMn charges between 1500 and 1650 °C, where the kinetic parameters obtained from the experiments were used. Note that the rate constants for MnO reduction in charge "As/HCS" are extended to 1650 °C compared to Figure 4.28. Rate constants of SiO_2 reduction for charge "HCS" between 1500 and 1550 °C are also included.

The relation between slag viscosity and the reduction rate was previously discussed several times in **Sections 4.3.1** and **4.3.2**. It was discussed that there was not likely to be a noticeable relation between the slag viscosity and the reduction rates of MnO and SiO_2 reduction. The plotted relation between the rate constants of MnO and SiO_2 reduction and the (C+M)/A ratio between 1500 and 1650 °C is described in **Figure 4.31**. The slag viscosities, which can be related to the basicity, of the three SiMn charges between 1500 and 1650 °C are also shown in **Figure 4.32**.
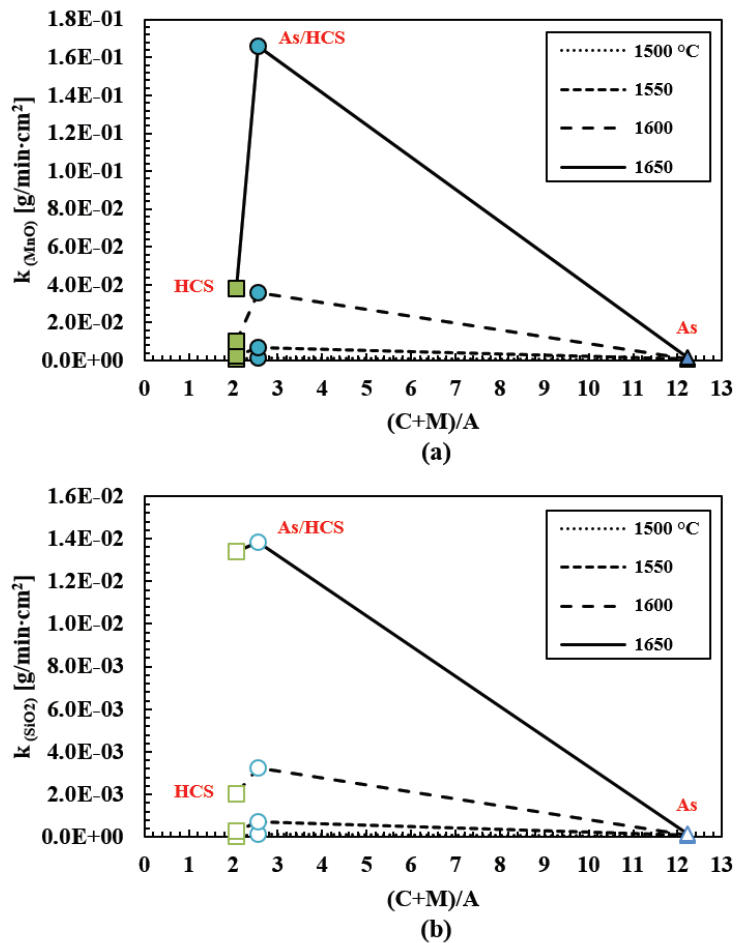
Figure 4.31: Plotted relation between the (C+M)/A ratio and the rate constants of (a) MnO and (b) SiO_2 reduction between 1500 and 1650 °C. Results indicate that there was no noticeable relation between the reduction rates and (C+M)/A ratio, which can relate to slag viscosity.
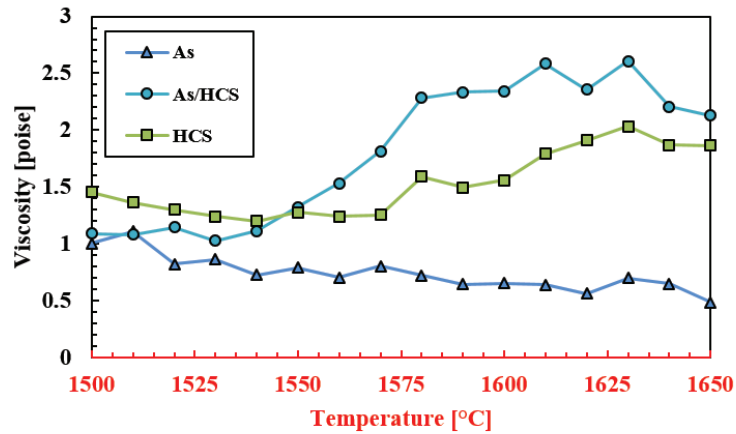
Figure 4.32: Slag viscosities of charges "As", "As/HCS" and "HCS" between 1500 and 1650 °C. Viscosities of the three SiMn slags at 1500 °C were approximately 1.3 poise. This indicates that the slag viscosity cannot explain the different reduction rates of the three SiMn charges between 1500 and 1650 °C. Note that the viscosities were calculated from FactSage 7.0 [45].

The comparison shows that the basicity of the slag cannot explain the different reduction rates observed in the three SiMn charges. The (C+M)/A ratio was the highest in charge "As", which should had been favorable for reduction if the mass transfer of MnO or manganese was the rate-determining step. However, higher rate constants were observed in charges "As/HCS" and "HCS" where the (C+M)/A ratio was considerably lower. The slag viscosity, which can be related to the basicity, also showed that it does not relate to the reduction rates. At 1500 °C, the slag viscosity of the charges showed correlating relation with the (C+M)/A ratio where the lowest viscosity was observed in charge "As" and highest in charge "HCS". However, the viscosities were similar at approximately 1.3 poise at 1500 °C. This indicates that the slag viscosity cannot explain the different reduction rates at higher temperatures. If the viscosities of the three SiMn slags were considerably different at 1500 °C and showed that the reduction rates were faster in the slag with lower viscosity, the effect of slag viscosity on the reduction rate might had been acceptable. Thus, the slag basicity and viscosity do not significantly affect the reduction rates of MnO and SiO_2 in SiMn slags. This also indicates that the reduction of MnO and SiO_2 is more likely to be controlled by the chemical reaction rather than the mass transfer in SiMn slags.

The influence of iron from **Section 2.3.4** was also considered since the slag basicity and viscosity do not relate to the reduction rates. The plotted relation between the rate constants of MnO and SiO_2 reduction and the amount of iron between 1500 and 1650 °C is described in **Figure 4.33**.
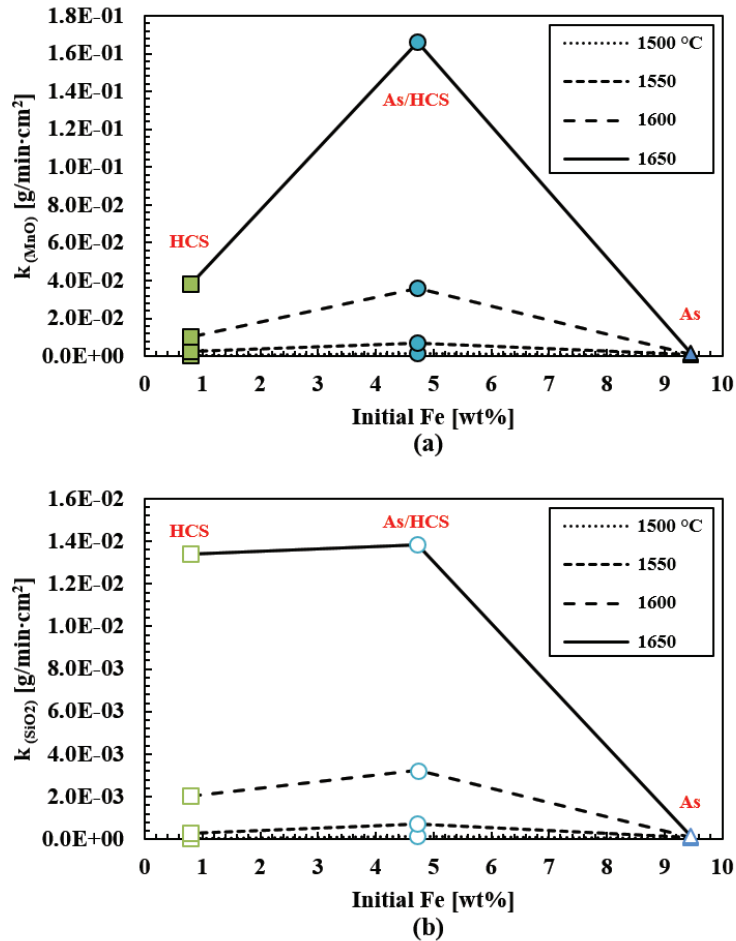
Figure 4.33: Plotted relation between the amount of iron and the rate constants of (a) MnO and (b) SiO$_2$ reduction between 1500 and 1650 °C. Results showed that the amount of iron does not relate with the different reduction rates of the three SiMn charges. Note that the amount of initial iron is the percentage of iron from the primary charge components excluding coke.

On the contrary to previous studies [62, 78, 79], the results showed that the amount of iron also does not relate to the different reduction rates of MnO and SiO$_2$. Higher amount of iron should have had led to more reduction where charge "As" was favorable for having the highest amount of iron. But the rate constants were considerably higher in charges "As/HCS" and "HCS". The comparison was more readily observed by comparing charge "As" to charge "HCS", which nearly lacked iron. It was not clear why the opposite result was observed, and the comparison can be skeptical because the effect of iron was well studied from previous works. This could imply that the influence from other kinetic factors can be more superior, where the effect of iron is less noticeable.

Along with the effect of iron, the effect of sulfur was also briefly discussed in **Section 2.3.4**. The plotted relation between the rate constants of MnO and SiO_2 reduction and the amount of sulfur between 1500 and 1650 °C is shown in **Figure 4.34**.
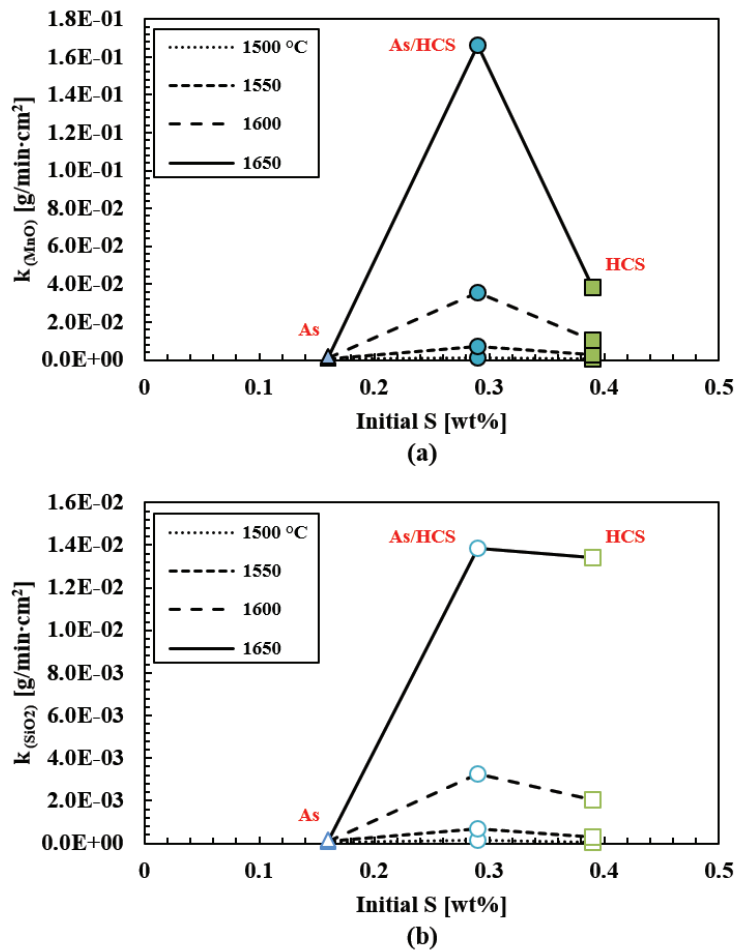
Figure 4.34: Plotted relation between the amount of sulfur and the rate constants of (a) MnO and (b) SiO_2 reduction between 1500 and 1650 °C. Results showed that the rate constants were higher with increasing amount of sulfur and temperature. But the relation was not conclusive because the highest rate constants were observed in charge "As/HCS" and not "HCS".

The results showed that the rate constants of MnO and SiO_2 reduction increased with the amount of sulfur, where the relation was more vividly observed with higher temperatures. This indicates that the amount of sulfur strongly affects the reduction rates of MnO and SiO_2 than the amount of iron, slag basicity and viscosity. As sulfur is known to behave as a strong surface-active specie for most metals [82], it implies that the reduction of MnO and SiO_2 with dissolved carbon in the metal phase might had significantly occurred. However, it was not clear whether the sulfur content gave the relatively slower reduction rates in charge "HCS" than "As/HCS". As the manganese source in charge "HCS" was only HC FeMn slag, which lacks iron, the combined effect of iron and sulfur could had occurred in charge "As/HCS". Thus, the effect of sulfur in SiMn slags was observed but not conclusive from using industrial materials with different charge compositions.

It was suspected that sulfur had a strong influence on the reduction rate. Assuming that the effect of sulfur was superior to the effect of iron in SiMn slags, an additional experiment with charge "As" was also conducted according to **Tables 3.7** and **3.9**. The amount of sulfur as iron sulfide (FeS) between 0.3 and 1.0 wt% was added into charge "As", where the other charge aspects were controlled. The mass change comparison of charge "As" with different amount of sulfur between 1500 and 1650 °C is described in **Figure 4.35**. The corresponding slag and metal compositions at 1650 °C with their respective activities are also shown in **Tables 4.22** and **4.23**.
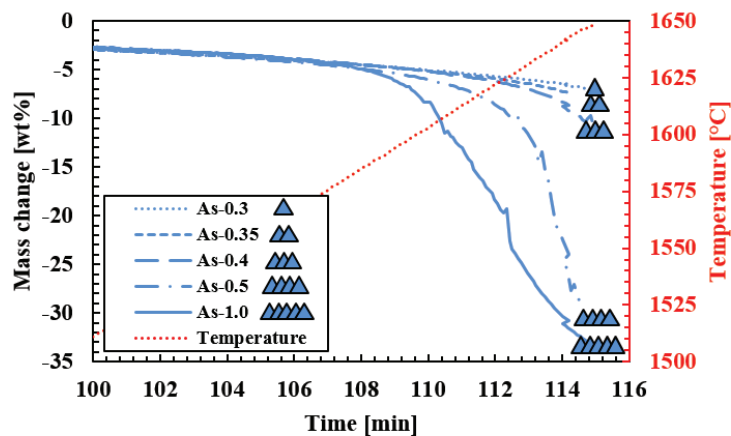
Figure 4.35: Mass change comparison of charge "As" with different amount of sulfur (0.3 and 1.0 wt%) between 1500 and 1650 °C. Mass changes of the charges were similar until approximately 1575 °C but differed considerably afterwards where increasing amount of sulfur showed faster and higher reduction.

Table 4.22: Measured slag and calculated metal compositions of charge "As" with different amount of sulfur between 0.3 and 1.0 wt% at 1650 °C. Lower concentration of MnO was observed in the slag phase with increasing amount of sulfur, where the activity of MnO showed corresponding results. Note that the metal compositions were calculated with similar methods in **Appendix E**.

Charge No.	Slag (EPMA) [wt%]							Metal (Calculated) [wt%]					
	MnO	SiO$_2$	CaO	MgO	Al$_2$O$_3$	a_{MnO}	a_{SiO2}	Mn	Si	Fe	C	$a_{Mn}/K_{(MnO)}$	$a_{Si}/K_{(SiO2)}$
As-0.3	47.6	38.6	8.3	2.8	0.8	0.18	0.22	59.7	12.0	25.2	3.1	0.0010	0.0303
As-0.35	44.5	41.4	9.5	2.6	1.0	0.15	0.31	61.8	10.2	24.4	3.6	0.0011	0.0216
As-0.4	38.3	45.6	10.0	3.1	1.4	0.11	0.45	64.7	9.9	21.6	3.8	0.0011	0.0203
As-0.5	18.7	50.8	20.9	6.3	3.4	0.06	0.44	66.4	14.4	16.5	2.8	0.0010	0.0475
As-1.0	12.2	47.4	26.2	7.3	3.6	0.05	0.24	65.6	16.3	15.6	2.6	0.0009	0.0672

Table 4.23: Calculated amount of slag and metal components in absolute amount (g) of charge "As" with different amount of sulfur between 0.3 and 1.0 wt% at 1650 °C. Results showed that when the initial sulfur content was 1 wt% in the slag near all MnO and more than half of SiO$_2$ from the primary slag at 1200 °C were reduced at 1650 °C. Note that the amount of slag and metal components of primary slag at 1200 °C is also shown in the table as reference.

Charge No.	Slag (Calculated) [g]						Metal (Calculated) [g]				
	MnO	SiO$_2$	CaO	Al$_2$O$_3$	MgO	Total	Mn	Si	Fe	C	Total
As (1200)*	4.2	2.3	0.44	0.08	0.04	7.1	-	-	~0.74	0.03	0.77
As-0.3	1.9	1.6				4.1	1.75	0.35		0.09	2.93
As-0.35	1.8	1.7				4.0	1.87	0.31		0.11	3.03
As-0.4	1.3	1.6	0.44	0.08		3.5	2.21	0.34	~0.74	0.13	3.42
As-0.5	0.3	0.9				1.8	2.98	0.65		0.13	4.49
As-1.0	0.2	0.7				1.4	3.12	0.77		0.12	4.75

The results showed that the reduction rates increased significantly with increasing amount of sulfur and temperature. The mass changes of the charges were similar until approximately 1575 °C, but differed considerably at higher temperatures, where increasing amount of sulfur showed faster and higher reduction rates. The corresponding results were also observed from the slag and metal compositions. When the sulfur content in the charge increased from 0.3 to 1.0 wt%, the MnO content decreased from 47.6 to 12.2 wt% at 1650 °C. According to the calculated amount in **Table 4.23**, near all MnO and more than half of SiO_2 from the primary slag at 1200 °C were reduced at 1650 °C when the sulfur content was increased to 1.0 wt% in the charge. Thus, the effect of sulfur on MnO and SiO_2 reduction in industrial SiMn slags was clearly observed, where increasing amount of sulfur in the charge gave higher and faster reduction with increasing temperatures.

However, it was also worthy to note that other kinetic factors could had influenced the reduction rates regarding the temperature. The temperature, which divides the two stage reductions, was approximately 1575 °C from the experiments with charge "As" with different amount of sulfur. Comparing to the experiments from charges "As/HCS" and "HCS", the dividing temperature was around 1500 °C, which is 75 °C lower. The difference of the dividing temperature implies that other kinetic factors can also play a role in the reduction rates in SiMn slags. Since industrial materials with different amount and compositions were used, the ratio of slag components in the slag phase seems to give the difference.

Based on the kinetic parameters obtained in this study, the reduction rates of MnO and SiO_2 in the three SiMn charges, "As", "As/HCS" and "HCS" were described by using the rate models, **Equations (2.20)** and **(3.4)**. **Figures 4.36** and **4.37** describe the comparison of the calculated and measured amount of MnO and SiO_2 between 1200 and 1650 °C from two different heating rates, + 4.5 and + 9 °C /min, respectively. Note that the rate models are shown again in the following paragraph for convenience, and the same kinetic parameters obtained from **Table 4.21** were applied to both heating rates.

$$r_{MnO} = k_{MnO} \cdot A \cdot (a_{MnO} - \frac{a_{Mn}}{K_{MnO}}) \qquad\qquad (2.20)$$

$$r_{SiO_2} = k_{SiO_2} \cdot A \cdot (a_{SiO_2} - \frac{a_{Si}}{K_{SiO_2}}) \qquad\qquad (3.4)$$
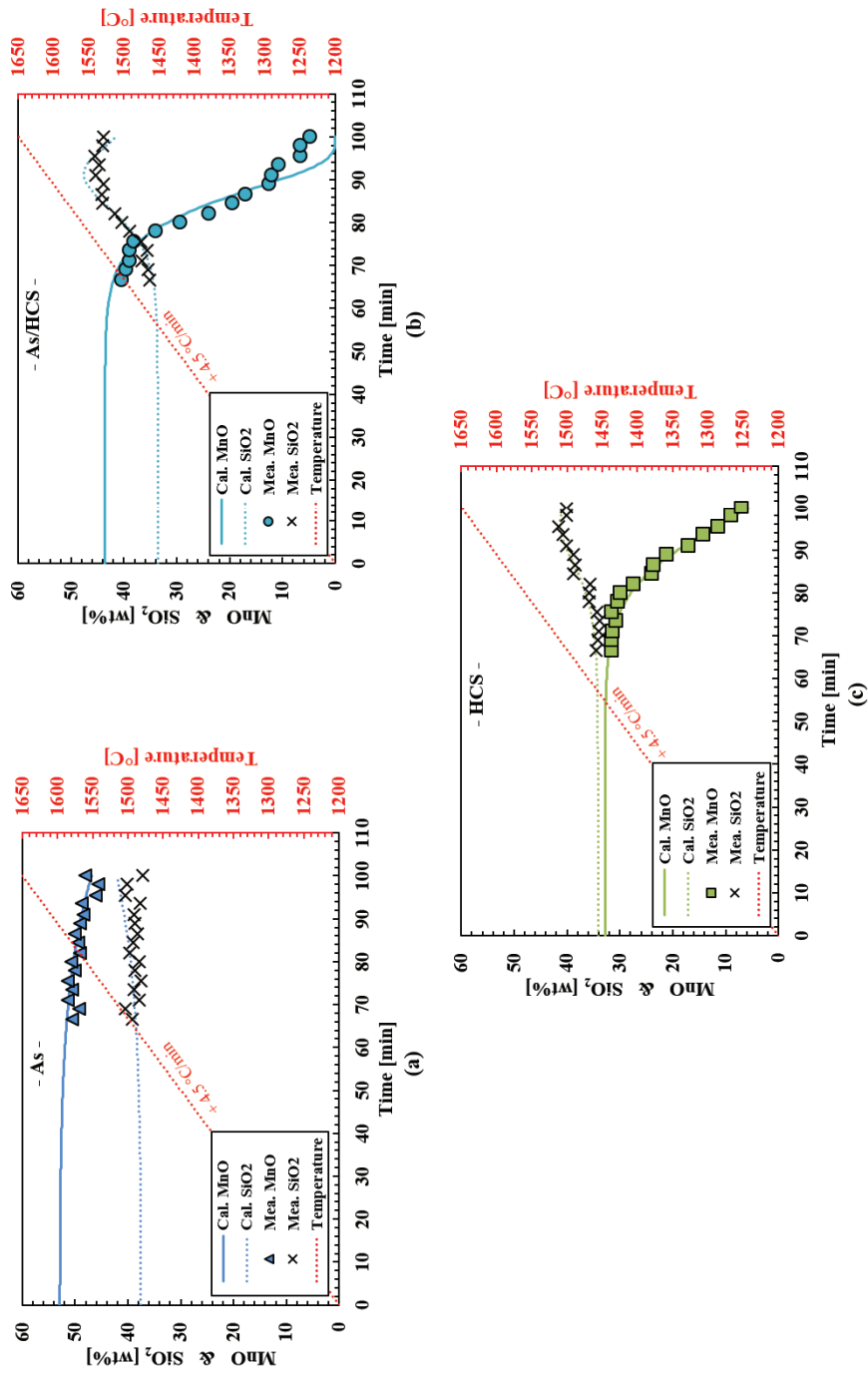
Figure 4.36: Comparison of calculated (solid and dotted lines) and measured (symbols) amount of MnO and SiO$_2$ in charges (a) "As", (b) "As/HCS" and (c) "HCS" between 1200 and 1650 °C, where the heating rate was + 4.5 °C/min. Calculated amounts, which were obtained from the rate models, corresponded to the measured amounts from the experiments. Note that the amount of MnO in charge "As/HCS" between 1600 and 1650 °C showed discrepancy due to the measurement uncertainties.
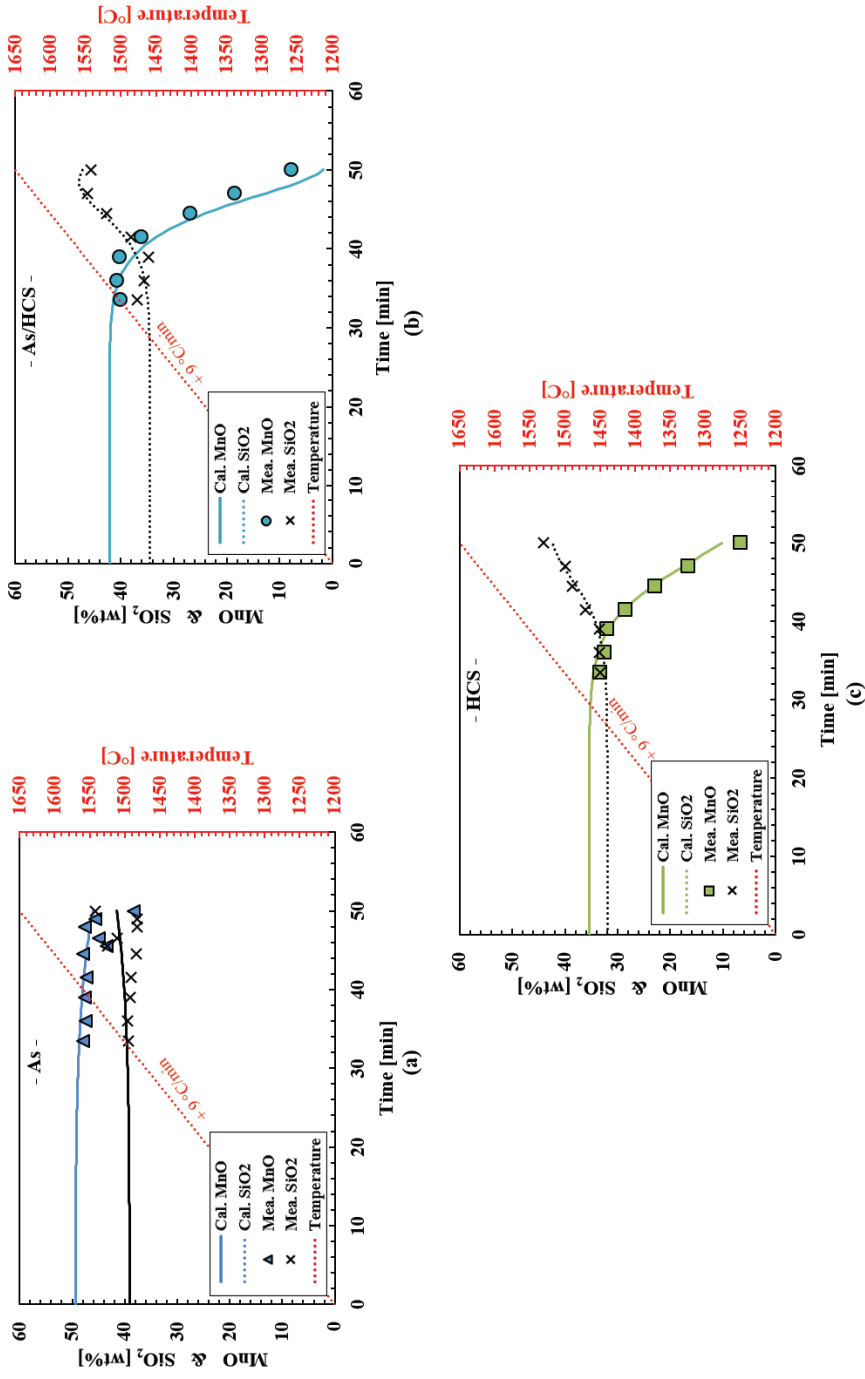
Figure 4.37: Comparison of calculated (solid and dotted lines) and measured (symbols) amount of MnO and SiO$_2$ in charges (a) "As", (b) "As/HCS" and (b) "HCS" between 1200 and 1650 °C, where the heating rate was + 9 °C/min. Calculated amounts, which were obtained from the rate models, corresponded to the measured amounts from the experiments. Note that the amount of MnO in charge "As/HCS" between 1600 and 1650 °C showed discrepancy due to the measurement uncertainties.

The comparison showed that the models were applicable to describe the changing amounts of MnO and SiO$_2$ in SiMn slags between 1200 and 1650 °C. The calculated amounts of MnO and SiO$_2$ were coordinated to the measured amounts from the experiments, whether the reduction degree was high or low. This indicates that the presumed rate models, which were considered in this work, were reliable and the relating assumptions were also adequate. The chemical reactions of MnO and SiO$_2$ reduction were the rate-determining steps in the SiMn process, where the amount of sulfur affects the reduction rates. It was also worth noting that the application of the rate models could be expand into SiMn slags because the rate model of MnO reduction was originally from FeMn process. Note that the discrepancy in charge "As/HCS" between 1610 and 1650 °C was due the uncertainties from the experiments, which was discussed in **Section 4.3.3**.

The highlighted results of **Section 4.3** are recapitulated in the following bulleted points:

- The reduction rates differed among different SiMn charges, where charges with HC FeMn slag as raw material showed relatively faster mass change.

- The activation energy (temperature dependency) of MnO and SiO$_2$ reduction was higher with charges containing HC FeMn slag as raw materials.

- The different reduction rates were not explained by slag basicity, viscosity and amount of iron, which showed less relations.

- The effect of sulfur in SiMn slags was clear, where the addition of sulfur had increased the reduction rates significantly.

- The rate models of MnO and SiO$_2$ were applicable to describe the reduction rates of MnO and SiO$_2$ in different SiMn charges regardless of the reduction degree.

4.4 Confirmation through synthetic materials (Research topic #4)

SiMn charges using synthetic materials were also conducted to confirm the kinetic information from the previous experiments in research topic #3. Since the effect of sulfur was not entirely conclusive from using industrial materials, a controlled slag system according to **Tables 3.8** and **3.9** was considered for further experiments with sulfur in SiMn slag, where the similar methods from the previous experiments in research topic #3 were used. The rate parameters were also measured to extract kinetic information from MnO and SiO$_2$ reduction in synthetic slags with different amount of sulfur. Three slag components, MnO, SiO$_2$ and CaO, composed the synthetic SiMn slag and different amount of sulfur as iron sulfide between 0 and 0.9 wt% was added into the charges. Also, the amount of iron was kept constant by adding compensative amounts to the different amount of iron sulfide. Note that the amount of slag components was also measured to aim at approximately 5 wt% MnO and 40 wt% SiO$_2$ in the slag phase and 18 wt% silicon in the metal phase, which is close to the thermodynamic equilibrium at 1600 °C. The recorded temperature schedules of the experiments are shown in **Figure 4.38**, where pre-reduction was not necessary for synthetic materials.
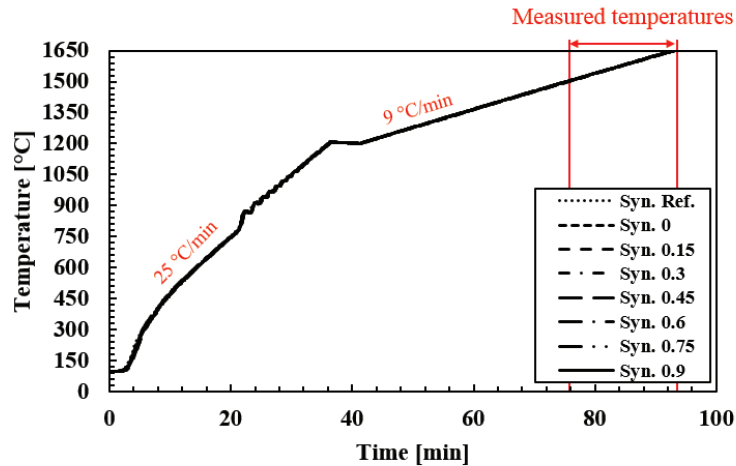
Figure 4.38: Recorded temperature schedules of experiments from research topic #4. Experiments were conducted in the same condition (overlapped), where the focus was also between 1500 and 1650 °C. Note that pre-reduction was not required for synthetic charges.

4.4.1 Mass change comparison

The mass change comparison of synthetic SiMn charges between 1200 and 1650 °C is shown in **Figure 4.39**. The individual mass change results of charges can be seen in **Appendix C**. The results showed that the reduction also occurred in two stages, where it was faster and higher with higher amount of sulfur in the charge. Until 1500 °C, the mass changes from the charges were relatively low and similar regardless of the different amount of sulfur. Above 1500 °C, the mass changes of charges with sulfur amount between 0.3 and 0.9 wt% had increased significantly, while charges with less amount of sulfur did not showed the similar mass change. The relatively larger mass change clearly indicates high reduction of MnO and SiO_2, where the effect of sulfur was observed. Among the charges with significant mass change however, increasing amount of sulfur in the charge did not show large differences. The mass changes between charges "Syn. 0.3" and "Syn. 0.9" were similar where the final mass change at 1650 °C was approximately -30 wt%. It was not clear why the reduction degrees were similar between 0.3 and 0.9 wt% sulfur but seems that a minimum amount of sulfur was necessary for enhancing the reduction rate.

In addition, the charge without CaO, "Syn. Ref.", showed the lowest mass change among the synthetic charges. Adding CaO in the charge, which was charge "Syn. 0", did not show much difference. This indicates that the effect of viscosity on the reduction rate was relatively low, which was also observed and discussed in the previous section.
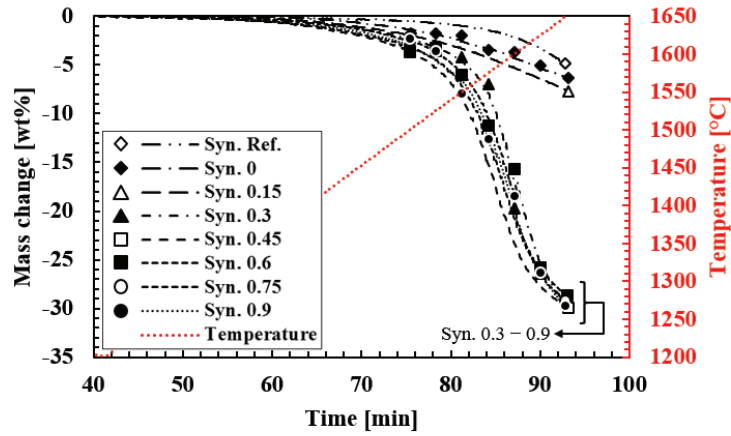
Figure 4.39: Mass change comparison of synthetic charges with different amount of sulfur between 1500 and 1650 °C, where the lines and symbols are the average and measured mass records, respectively. Mass changes significantly with sulfur content between 0.3 and 0.9 wt% at above 1500 °C, but the difference was not large. Also, addition of CaO did not showed much difference to the mass change.

4.4.2 EPMA analyses

The corresponding analyzed slag and calculated metal compositions of the synthetic charges with different amount of sulfur are shown in **Table 4.24**. Note that the metal compositions were calculated using the same assumptions which were previously discussed in **Section 4.3.2**. The calculated slag and metal composition in absolute amount (g) are also shown together in **Table 4.25** due to the calculation of metal compositions.

Table 4.24: Slag and metal compositions of synthetic SiMn charges with different amount of initial sulfur between 1500 and 1650 °C. Higher reduction of MnO was observed with charges containing sulfur between 0.3 and 0.9 wt%. MnO content was less than 5 wt% at 1650 °C. Note that slag and metal compositions at 1650 °C are in bold for convenient comparison.

Charge No.	Temperature [°C]	Slag (EPMA) [wt%]			Metal (Calculated) [wt%]				Int. Sulfur [wt%]
		MnO	SiO₂	CaO	Mn	Si	Fe	C	
Syn. Ref.	**1650**	**59.1**	**39.2**	-	**59.7**	**13.5**	**24.1**	**2.8**	0
Syn. 0	1500	42.6	37.9	17.2	81.0	1.5	10.8	6.6	0
	1525	41.4	37.6	20.7	79.3	7.5	8.7	4.6	
	1550	40.2	38.4	19.1	80.2	6.9	8.1	4.9	
	1575	40.8	37.4	21.1	78.4	9.9	7.8	3.9	
	1600	40.0	37.3	21.7	77.9	11.3	7.2	3.6	
	1625	39.0	38.5	20.9	79.4	9.1	7.2	4.3	
	1650	**39.0**	**38.5**	**20.9**	**75.8**	**15.5**	**5.7**	**2.9**	
Syn. 0.15	**1650**	**41.2**	**37.0**	**20.8**	**77.9**	**10.1**	**8.0**	**4.1**	0.15
Syn. 0.3	1500	49.3	33.5	17.0	58.3	0.0	35.1	6.7	0.3
	1525	41.8	37.7	20.1	80.3	4.4	9.7	5.7	
	1550	38.0	39.9	23.1	82.0	4.9	7.5	5.6	
	1575	40.4	36.5	22.4	76.9	12.8	7.2	3.2	
	1600	18.4	45.9	36.7	80.3	12.4	3.8	3.4	
	1625	8.0	45.4	51.5	78.1	15.7	3.3	2.9	
	1650	**3.4**	**44.9**	**58.0**	**77.3**	**16.7**	**3.1**	**2.9**	
Syn. 0.45	**1650**	**4.2**	**43.6**	**56.7**	**76.9**	**17.1**	**3.1**	**2.8**	0.45
Syn. 0.6	1500	44.6	36.0	19.3	77.6	2.9	13.5	6.0	0.6
	1525	44.2	34.9	21.8	74.8	11.7	10.2	3.3	
	1550	40.3	36.4	19.8	77.1	12.4	7.3	3.2	
	1575	31.6	39.5	25.8	78.6	13.3	5.0	3.1	
	1600	22.3	45.0	31.1	81.0	11.0	4.2	3.8	
	1625	6.6	44.5	47.4	77.7	16.3	3.3	2.8	
	1650	**0.6**	**47.0**	**53.9**	**78.1**	**15.9**	**3.1**	**2.9**	
Syn. 0.75	**1650**	**4.1**	**45.3**	**51.9**	**77.8**	**16.1**	**3.2**	**2.9**	0.75
Syn. 0.9	1500	44.6	33.5	19.2	72.1	16.0	9.4	2.5	0.9
	1525	43.8	33.7	20.2	72.7	16.2	8.6	2.5	
	1550	38.4	37.1	22.6	78.0	12.1	6.9	3.3	
	1575	34.1	39.2	23.9	79.3	11.6	5.6	3.5	
	1600	14.1	47.4	36.9	80.7	12.1	3.7	3.5	
	1625	7.7	46.0	44.6	78.7	14.9	3.3	3.0	
	1650	**4.6**	**44.4**	**48.2**	**77.6**	**16.4**	**3.2**	**2.9**	

Table 4.25: Calculated slag and metal compositions in absolute amount (g) of synthetic SiMn charges with different amount of initial sulfur between 1500 and 1650 °C. Higher reduction of both MnO and SiO_2 were observed with charges containing sulfur between 0.3 and 0.9 wt%: Near all MnO and approximately half of SiO_2 were reduced at 1650 °C. Note that slag and metal amount at 1650 °C are in bold for convenient comparison.

Charge No.	Temperature [°C]	Slag (Calculated) [g]				Metal (Calculated) [g]					Int. Sulfur [g]
		MnO	SiO$_2$	CaO	Total	Mn	Si	Fe	C	Total	
Syn. Ref.	**1650**	**2.70**	**1.79**	0	**4.49**	**0.23**	**0.05**	0.09	**0.01**	**0.38**	0
Syn. 0	1500	2.10	1.87		4.94	0.69	0.01		0.06	0.85	0
	1525	1.90	1.73		4.60	0.84	0.08		0.05	1.06	
	1550	1.81	1.73		4.51	0.92	0.08		0.06	1.14	
	1575	1.80	1.65		4.42	0.92	0.12		0.05	1.18	
	1600	1.70	1.59		4.25	1.00	0.15		0.05	1.29	
	1625	1.67	1.65		4.29	1.02	0.12		0.06	1.29	
	1650	**1.42**	**1.37**		**3.75**	**1.22**	**0.25**		**0.05**	**1.61**	
Syn. 0.15	**1650**	**1.84**	**1.65**		**4.45**	**0.90**	**0.12**		**0.05**	**1.15**	0.01
Syn. 0.3	1500	2.80	1.90		5.66	0.15	0.00		0.02	0.26	0.02
	1525	2.01	1.81		4.78	0.76	0.04		0.05	0.95	
	1550	1.69	1.77		4.43	1.01	0.06		0.07	1.23	
	1575	1.72	1.55		4.23	0.99	0.16		0.04	1.29	
	1600	0.51	1.26		2.73	1.93	0.30		0.08	2.40	
	1625	0.17	0.96		2.09	2.19	0.44		0.08	2.80	
	1650	**0.06**	**0.85**		**1.88**	**2.27**	**0.49**		**0.08**	**2.93**	
Syn. 0.45	**1650**	**0.08**	**0.83**	0.96	**1.87**	**2.26**	**0.50**	0.09	**0.08**	**2.93**	0.03
Syn. 0.6	1500	2.30	1.86		5.12	0.54	0.02		0.04	0.69	0.04
	1525	2.12	1.67		4.76	0.68	0.11		0.03	0.91	
	1550	1.73	1.56		4.26	0.98	0.16		0.04	1.27	
	1575	1.09	1.37		3.42	1.47	0.25		0.06	1.87	
	1600	0.68	1.38		3.03	1.79	0.24		0.08	2.21	
	1625	0.13	0.91		2.01	2.22	0.46		0.08	2.85	
	1650	**0.01**	**0.90**		**1.87**	**2.31**	**0.47**		**0.09**	**2.96**	
Syn. 0.75	**1650**	**0.08**	**0.90**		**1.95**	**2.26**	**0.47**		**0.08**	**2.90**	0.04
Syn. 0.9	1500	2.08	1.56		4.60	0.71	0.16		0.02	0.99	0.05
	1525	1.98	1.53		4.47	0.78	0.17		0.03	1.08	
	1550	1.60	1.54		4.10	1.08	0.17		0.05	1.39	
	1575	1.29	1.49		3.75	1.32	0.19		0.06	1.66	
	1600	0.37	1.25		2.59	2.03	0.30		0.09	2.51	
	1625	0.17	1.01		2.15	2.19	0.42		0.08	2.78	
	1650	**0.09**	**0.88**		**1.94**	**2.25**	**0.48**		**0.08**	**2.90**	

The high reduction of MnO was clearly observed with charges containing sulfur between 0.3 and 0.9 wt%. The MnO content in slag was between 45 and 50 wt% at 1500 °C but decreased to below 5 wt% at 1650 °C. During the same condition, not much change was observed from charges with lower amount of sulfur. The calculated amount (g) of MnO and SiO_2 also showed corresponding results, where it indicated near all MnO and approximately half of SiO_2 had been reduced when the sulfur content was between 0.3 and 0.9 wt%. Thus, the effect of sulfur in SiMn charges was clearly observed where sulfur increases the reduction degrees of MnO and SiO_2 at higher temperature. The similar slag and metal compositions observed for charges between 0.3 and 0.9 wt% sulfur, which was initially observed from the mass comparison, also imply that a certain minimum amount of sulfur was required for enhanced reduction rates and more amount did not gave significant difference.

4.4.3 Rate parameters

The rate parameters of MnO and SiO_2 reduction from the synthetic charges between 1500 and 1650 °C are described in this section. The reduction rates, reaction areas and driving forces of MnO and SiO_2 reduction were estimated based on the TGA results and slag/metal compositions, where the same methods from **Section 4.3.3** were considered. Note that **Equations (2.20)** and **(3.4)** are shown again in this section for convenience.

$$r_{MnO} = k_{MnO} \cdot A \cdot (a_{MnO} - \frac{a_{Mn}}{K_{MnO}}) \qquad (2.20)$$

$$r_{SiO_2} = k_{SiO_2} \cdot A \cdot (a_{SiO_2} - \frac{a_{Si}}{K_{SiO_2}}) \qquad (3.4)$$

The following rate parameters (rate, reaction area and driving force for MnO and SiO_2 reduction) in bulleted points are described in **Figures 4.40**, **4.41** and **4.42**, where the numeric values are organized in **Tables 4.26**, **4.27**, **4.28** and **4.29**:

- Reduction rates of MnO and SiO_2 (**Figure 4.40** and **Table 4.26**): Data from the TGA results (time and temperature) and EPMA analyses (slag compositions) were used to calculate the rates.

- Reaction area (**Figure 4.41** and **Table 4.27**): Calculated from using the amount of produced metal (manganese and silicon) according to **Reactions (1.10)** and **(1.11)** and from **Equations (3.1)** and **(3.2)**.

- Driving force of MnO and SiO_2 reduction (**Figure 4.42** and **Tables 4.28 and 4.29**): Calculated from **Equations (1.1)**, **(1.2)**, **(1.4)** and **(1.5)**.
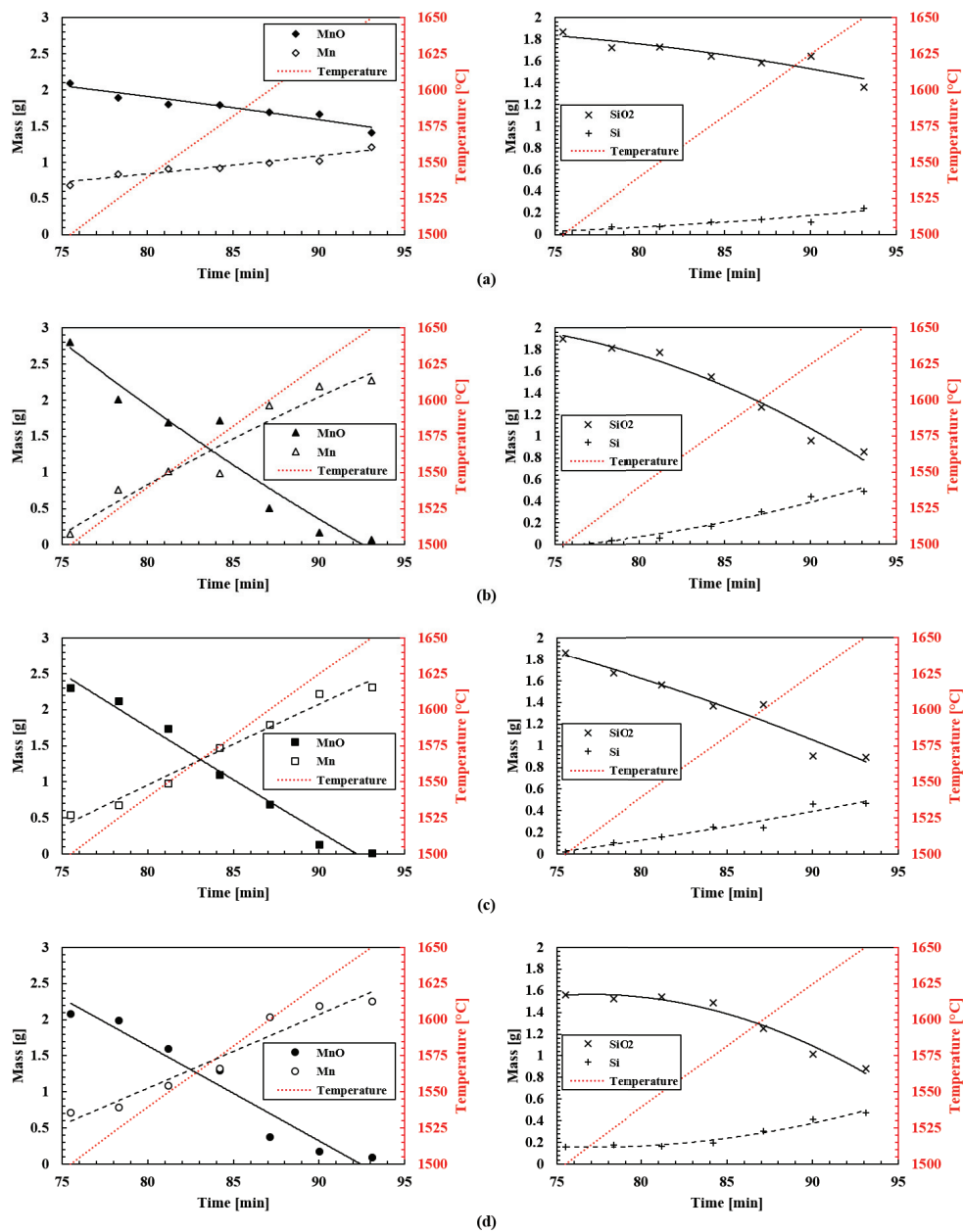
Figure 4.40: Amount of slag (MnO and SiO₂) and metal (manganese and silicon) as a function of time between 1500 and 1650 °C: (a) Charge "Syn. 0", (b) "Syn. 0.3", (c) "Syn. 0.6" and (d) "Syn. 0.9". Reduction of MnO and SiO₂ was higher when the sulfur content was between 0.3 and 0.9 wt% in the charge.

Table 4.26: Calculated rates of MnO and SiO$_2$ reduction of charges "Syn. 0", "Syn. 0.3", "Syn. 0.6" and "Syn. 0.9" between 1500 and 1650 °C. Reduction rates of MnO and SiO$_2$ were higher when the sulfur content was between 0.3 and 0.9 wt%.

Charge No.	Temperature [°C]	Reduction rates [g/min]	
		MnO	SiO$_2$
Syn. 0	1500	-0.029	-0.014
	1525	-0.030	-0.016
	1550	-0.031	-0.019
	1575	-0.032	-0.022
	1600	-0.032	-0.024
	1625	-0.033	-0.028
	1650	-0.034	-0.030
Syn. 0.3	1500	-0.249	-0.028
	1525	-0.222	-0.039
	1550	-0.189	-0.053
	1575	-0.159	-0.065
	1600	-0.128	-0.078
	1625	-0.097	-0.091
	1650	-0.068	-0.103
Syn. 0.6	1500	-0.074	-0.039
	1525	-0.104	-0.045
	1550	-0.169	-0.050
	1575	-0.191	-0.055
	1600	-0.170	-0.060
	1625	-0.119	-0.064
	1650	-0.013	-0.069
Syn. 0.9	1500	-0.034	-0.006
	1525	-0.080	-0.007
	1550	-0.171	-0.024
	1575	-0.204	-0.042
	1600	-0.174	-0.060
	1625	-0.094	-0.076
	1650	-0.026	-0.094
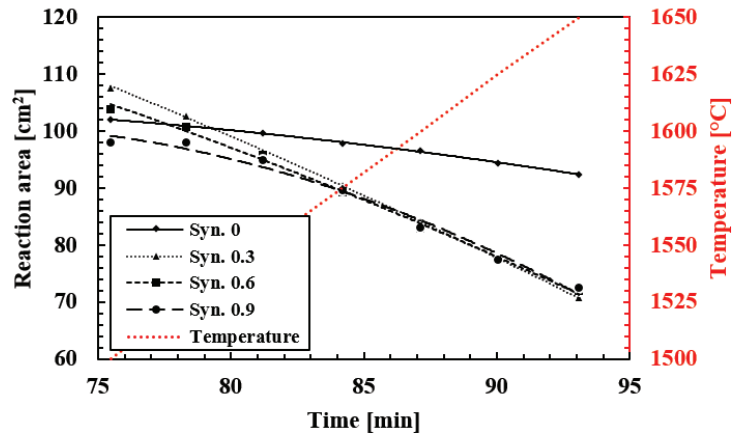
Figure 4.41: Calculated reaction area of charges "Syn. 0", "Syn. 0.3", "Syn. 0.6" and "Syn. 0.9" between 1500 and 1650 °C. Decrease of the reaction area was higher when the sulfur content was between 0.3 and 0.9 wt%, which indicates higher reduction degrees of MnO and SiO_2.

Table 4.27: Calculated reaction area of charges "Syn. 0", "Syn. 0.3", "Syn. 0.6" and "Syn. 0.9" between 1500 and 1650 °C, where the values are visualized in Figure 4.34.

Time [min]	Temperature [°C]	Reaction area [cm²]			
		Syn. 0	Syn. 0.3	Syn. 0.6	Syn. 0.9
75.5	1500	102.0	107.7	103.9	98.0
78.3	1525	100.9	102.8	100.8	97.9
81.2	1550	99.6	96.4	95.9	94.9
84.2	1575	97.9	90.5	89.3	89.6
87.1	1600	96.5	84.1	82.8	83.1
90.0	1625	94.5	77.4	77.4	77.4
93.1	1650	92.4	70.8	72.0	72.4

138
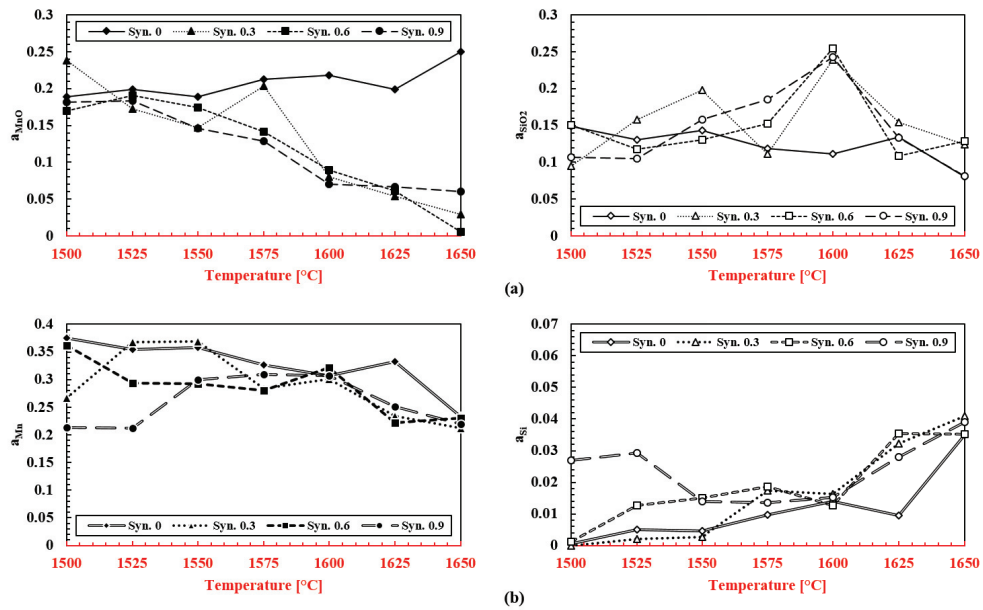
Figure 4.42: Estimated activities of (a) slag (MnO and SiO₂) and (b) metal (manganese and silicon) between 1500 and 1650 °C of charges "Syn. 0", "Syn. 0.3", "Syn. 0.6" and "Syn. 0.9". Activity of MnO was approximately 0.2 at 1500 °C but decreased to near 0 at 1650 °C when the sulfur content was between 0.3 and 0.9 wt% in the charge.

Table 4.28: Estimated activities (a_{MnO} and a_{Mn}) and calculated driving forces for MnO reduction between 1500 and 1650 °C of the synthetic SiMn charges. Values of the driving force were similar to the activity of MnO: Driving force $_{(MnO)} \approx a_{MnO}$.

Temperature [°C]	a_{MnO}				a_{Mn}				K [42]	Driving force			
	Syn. 0	Syn. 0.3	Syn. 0.6	Syn. 0.9	Syn. 0	Syn. 0.3	Syn. 0.6	Syn. 0.9		Syn. 0	Syn. 0.3	Syn. 0.6	Syn. 0.9
1500	0.19	0.24	0.17	0.18	0.38	0.27	0.36	0.21	61.51	0.18	0.23	0.16	0.18
1525	0.20	0.17	0.19	0.18	0.35	0.37	0.29	0.21	78.04	0.19	0.17	0.19	0.18
1550	0.19	0.15	0.17	0.15	0.36	0.37	0.29	0.30	98.27	0.19	0.14	0.17	0.14
1575	0.21	0.20	0.14	0.13	0.33	0.28	0.28	0.31	122.83	0.21	0.20	0.14	0.13
1600	0.22	0.08	0.09	0.07	0.31	0.30	0.32	0.31	152.35	0.22	0.08	0.09	0.07
1625	0.20	0.05	0.06	0.07	0.33	0.23	0.22	0.25	187.58	0.20	0.05	0.06	0.07
1650	0.25	0.03	0.01	0.06	0.23	0.21	0.23	0.22	229.26	0.25	0.03	~ 0	0.06

Table 4.29: Estimated activities (a_{SiO2} and a_{Si}) and calculated driving forces for SiO_2 reduction between 1500 and 1650 °C of the synthetic SiMn charges. Driving forces at lower temperatures were not able to calculate due to the low amount of silicon produced (negative values).

Temperature [°C]	a_{SiO2}				a_{Si}				K [42]	Driving force			
	Syn. 0	Syn. 0.3	Syn. 0.6	Syn. 0.9	Syn. 0	Syn. 0.3	Syn. 0.6	Syn. 0.9		Syn. 0	Syn. 0.3	Syn. 0.6	Syn. 0.9
1500	0.15	0.09	0.15	0.11	~ 0	~ 0	~ 0	0.03	0.02	0.12	0.09	0.08	
1525	0.13	0.16	0.12	0.11	~ 0	~ 0	0.01	0.03	0.03	-N/A-	0.09	-N/A-	-N/A-
1550	0.14	0.20	0.13	0.16	~ 0	~ 0	0.01	0.01	0.07	0.07	0.16		
1575	0.12	0.11	0.15	0.19	0.01	0.02	0.02	0.01	0.12	0.04	-N/A-	~ 0	0.08
1600	0.11	0.24	0.25	0.24	0.01	0.02	0.01	0.02	0.22	0.05	0.17	0.20	0.17
1625	0.13	0.15	0.11	0.13	0.01	0.03	0.04	0.03	0.39	0.11	0.07	0.02	0.06
1650	0.08	0.12	0.13	0.08	0.03	0.04	0.04	0.04	0.66	0.03	0.06	0.07	0.02

The uncertainty of measured results was mainly from the calculation of the driving force for SiO_2 reduction at lower temperatures. Since lower amount of silicon was produced at temperatures between 1500 and 1575 °C, it was difficult to observe the difference of the produced amount and the calculation of the driving force gave negative results. In addition, the results from the driving force of MnO reduction showed that the values of the driving forces were also similar to the values of the activity of MnO ($a_{MnO} \gg a_{Mn}/K_{(MnO)}$), which was previously observed from **Section 4.4.3**.

As the charges with different amount of sulfur were basically the same SiMn slag, the driving forces of MnO and SiO_2 did not explained the different reduction rates and the rate constants were compared instead. Based on the three rate parameters, rate, reaction area and driving force of MnO and SiO_2 reduction, the rate constants were calculated according to the rate models, **Equations (2.20)** and **(3.4)**, between 1500 and 1650 °C. The rate constants of MnO and SiO_2 reduction are described in **Figure 4.43** where the calculated values are shown in **Tables 4.30** and **4.31**.
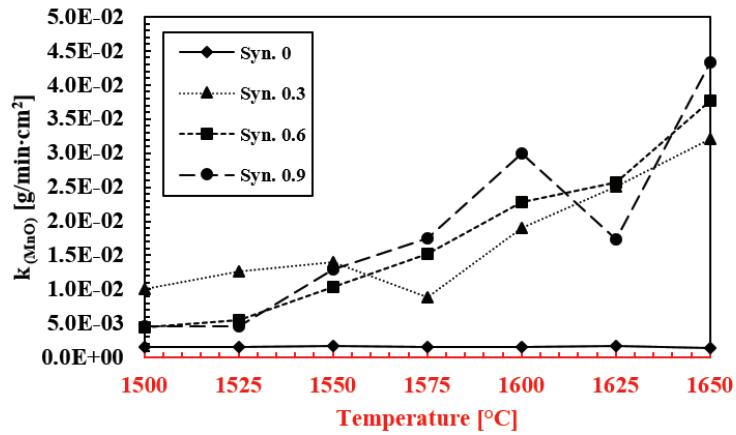
(a)
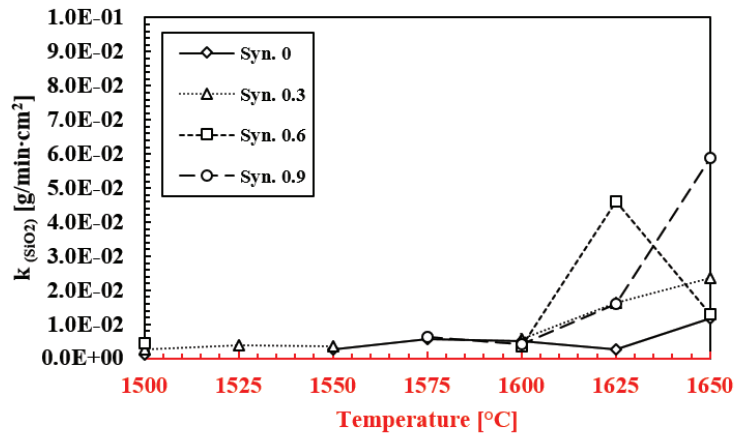
(b)

Figure 4.43: Estimated rate constants of (a) MnO and (b) SiO_2 reduction based on the calculated rate parameters between 1500 and 1650 °C. Rate constants for MnO reduction were increasing with increasing temperatures when the sulfur content was between 0.3 and 0.9 wt%. Estimation of rate constants for SiO_2 reduction were not clear but rather similar regardless of the sulfur content between 0.3 and 0.9 wt% in the charge. Note that the missing rate constants for SiO_2 reduction at lower temperatures were due to the uncertainties from the measurements.

Table 4.30: Estimated rate constants of MnO reduction based on the rate parameters between 1500 and 1650 °C of charges "Syn. 0", "Syn. 0.3", "Syn. 0.6" and "Syn. 0.9". Rate constants are visualized in Figure 4.36 (a).

Charge No.	Temperature [°C]	Rate, r [g MnO/min]	Reaction area, A [cm²]	Driving force, DF	Rate constant, k [g MnO/min · cm²]	Notes
Syn.0	1500	-0.029	102.0	0.18	1.58×10^{-3}	
	1525	-0.030	100.9	0.19	1.56×10^{-3}	
	1550	-0.031	99.6	0.19	1.64×10^{-3}	
	1575	-0.032	97.9	0.21	1.56×10^{-3}	
	1600	-0.032	96.5	0.22	1.51×10^{-3}	
	1625	-0.033	94.5	0.2	1.75×10^{-3}	
	1650	-0.034	92.4	0.25	1.47×10^{-3}	
Syn. 0.3	1500	-0.249	107.7	0.23	1.01×10^{-2}	
	1525	-0.222	102.8	0.17	1.27×10^{-2}	
	1550	-0.189	96.4	0.14	1.40×10^{-2}	
	1575	-0.159	90.5	0.20	8.78×10^{-3}	
	1600	-0.128	84.1	0.08	1.90×10^{-2}	
	1625	-0.097	77.4	0.05	2.51×10^{-2}	
	1650	-0.068	70.8	0.03	3.20×10^{-2}	$k = \dfrac{-r}{A \cdot DF}$
Syn. 0.6	1500	-0.074	103.9	0.16	4.45×10^{-3}	
	1525	-0.104	100.8	0.19	5.43×10^{-3}	
	1550	-0.169	95.9	0.17	1.04×10^{-2}	
	1575	-0.191	89.3	0.14	1.53×10^{-2}	
	1600	-0.170	82.8	0.09	2.28×10^{-2}	
	1625	-0.119	77.4	0.06	2.56×10^{-2}	
	1650	-0.013	72.0	~ 0	3.77×10^{-2}	
Syn. 0.9	1500	-0.034	98.0	0.18	1.93×10^{-3}	
	1525	-0.080	97.9	0.18	4.54×10^{-3}	
	1550	-0.171	94.9	0.14	1.29×10^{-2}	
	1575	-0.204	89.6	0.13	1.75×10^{-2}	
	1600	-0.174	83.1	0.07	2.99×10^{-2}	
	1625	-0.094	77.4	0.07	1.73×10^{-2}	
	1650	-0.026	72.4	0.06	5.99×10^{-3}	

Table 4.31: Estimated rate constants of SiO_2 reduction based on the rate parameters between 1500 and 1650 °C of charges "Syn. 0", "Syn. 0.3", "Syn. 0.6" and "Syn. 0.9". Rate constants are visualized in Figure 4.36 (b). Note that unavailable (N/A) driving forces were from insignificant amount of silicon produce.

Charge No.	Temperature [°C]	Rate, r [g SiO$_2$/min]	Reaction area, A [cm^2]	Driving force, DF	Rate constant, k [g SiO$_2$/min · cm^2]	Notes
Syn.0	1500	-0.014	102.0	0.12	1.14×10^{-3}	
	1525	-0.016	100.9	- N/A -	-	
	1550	-0.019	99.6	0.07	2.73×10^{-3}	
	1575	-0.022	97.9	0.04	5.62×10^{-3}	
	1600	-0.024	96.5	0.05	4.97×10^{-3}	
	1625	-0.028	94.5	0.11	2.69×10^{-3}	
	1650	-0.030	92.4	0.03	1.08×10^{-2}	
Syn. 0.3	1500	-0.028	107.7	0.09	2.89×10^{-3}	
	1525	-0.039	102.8	0.09	4.22×10^{-3}	
	1550	-0.053	96.4	0.16	3.44×10^{-3}	
	1575	-0.065	90.5	- N/A -	-	
	1600	-0.078	84.1	0.17	5.46×10^{-3}	
	1625	-0.091	77.4	0.07	1.68×10^{-2}	
	1650	-0.103	70.8	0.06	2.42×10^{-2}	$k = \dfrac{-r}{A \cdot DF}$
Syn. 0.6	1500	-0.039	103.9	0.08	4.69×10^{-3}	
	1525	-0.045	100.8	- N/A -	-	
	1550	-0.050	95.9			
	1575	-0.055	89.3	~ 0	3.89×10^{-1}	
	1600	-0.060	82.8	0.20	3.62×10^{-3}	
	1625	-0.064	77.4	0.02	4.13×10^{-2}	
	1650	-0.069	72.0	0.07	1.37×10^{-2}	
Syn. 0.9	1500	-0.006	98.0			
	1525	-0.007	97.9	- N/A -	-	
	1550	-0.024	94.9			
	1575	-0.042	89.6	0.08	5.86×10^{-3}	
	1600	-0.060	83.1	0.17	4.25×10^{-3}	
	1625	-0.076	77.4	0.06	1.64×10^{-2}	
	1650	-0.094	72.4	0.02	6.49×10^{-2}	

The comparison showed that the rate constants were higher with sulfur content between 0.3 and 0.9 wt% than without sulfur in the charge. This relation was clearly observed from MnO reduction where the rate constant comparison between charges with and without sulfur showed considerable difference with increasing temperatures. The same relation was not easy to observe for SiO_2 reduction, where calculations of the rate constants at lower temperature were unable due to the uncertainties from the experimental measurements. However, from the comparison of slag and metal composition in **Tables 4.24** and **4.25**, the rate constants seem to be higher with sulfur content between 0.3 and 0.9 wt% than without.

4.4.4 Arrhenius plots

The Arrhenius plots for MnO and SiO_2 reduction of the synthetic charges with different amount of sulfur were also constructed based on the rate parameters from the previous section. The same method, which were used in **Section 4.3.4,** was considered to calculate the kinetic parameters. **Figure 4.44** describes the Arrhenius plots of MnO and SiO_2 reduction of the synthetic charges between 1500 and 1650 °C, where **Table 4.32** summarizes the estimated kinetic parameters.
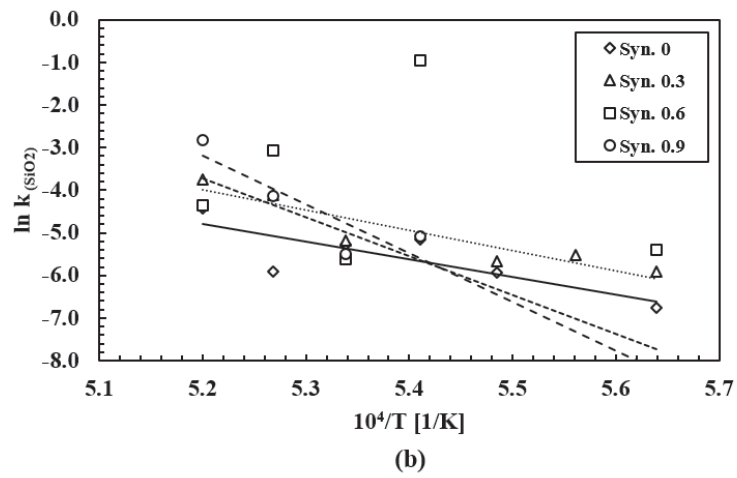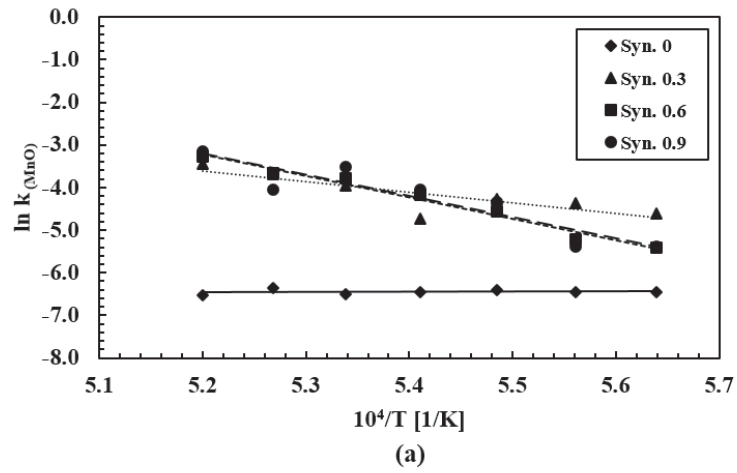
Figure 4.44: Arrhenius plots of (a) MnO and (b) SiO_2 reduction of the synthetic charges with different amount of sulfur between 1500 and 1650 °C. Temperature dependencies were higher when the sulfur content was between 0.3 and 0.9 wt% in the charge.

Table 4.32: Summary of the activation energies and pre-exponential constants of the synthetic charges with different amount of sulfur between 1500 and 1650 °C. Kinetic parameters are the approximate value from the experiments.

Reduction	Charge	E_a [kJ/mol]	k_0 [g/min · cm^2]
MnO	Syn. 0	~ 30	1.04×10^{-2}
	Syn. 0.3	~ 215	1.56×10^{4}
	Syn. 0.6	~ 415	7.99×10^{9}
	Syn. 0.9	~ 425	1.51×10^{10}
SiO$_2$	Syn. 0	~ 345	2.02×10^{7}
	Syn. 0.3	~ 390	8.12×10^{8}
	Syn. 0.6	~ 765	1.57×10^{19}
	Syn. 0.9	~ 950	3.24×10^{24}

The results showed that the reduction of MnO and SiO$_2$ becomes more sensitive to temperature when the sulfur content was between 0.3 and 0.9 wt%, which it implies that sulfur does not behaves as a catalyst in the reactions. According to current kinetic theory, catalysts increase the rate of a chemical reaction by lowering the energy barrier (activation energy), where often small amounts are required [89-92]. The increasing activation energy with increasing amount of sulfur contradicts this, and it implies that sulfur does not directly participates in the reactions of MnO and SiO$_2$ reduction.

A possible explanation for the effect of sulfur can be related to the reduction surface between slag and dissolved carbon in the metal phase. **Figure 4.45** shows the elemental mapping result of slag and metal phases of charge "Syn. 0.9" at 1650 °C. The result indicates that a layer-like phase surrounds the metal phase, which was composed of manganese sulfide (MnS) according the manganese and sulfur concentration from the elemental mapping. The melting point of manganese sulfide was previously reported to be approximately 1530 °C [19, 50], which the surrounding manganese sulfide layer seems to have been precipitated during cooling. It was not clear how sulfur behaved at high temperatures, but since sulfur is known to behave as a surface-active specie for most metal [82], it is possible that the reduction rate between slag and dissolved carbon in the metal phase was enhanced by sulfur. The competition between carbon dissolution into metal and reduction by dissolved carbon in the metal phase can be further investigatged if this was the case.
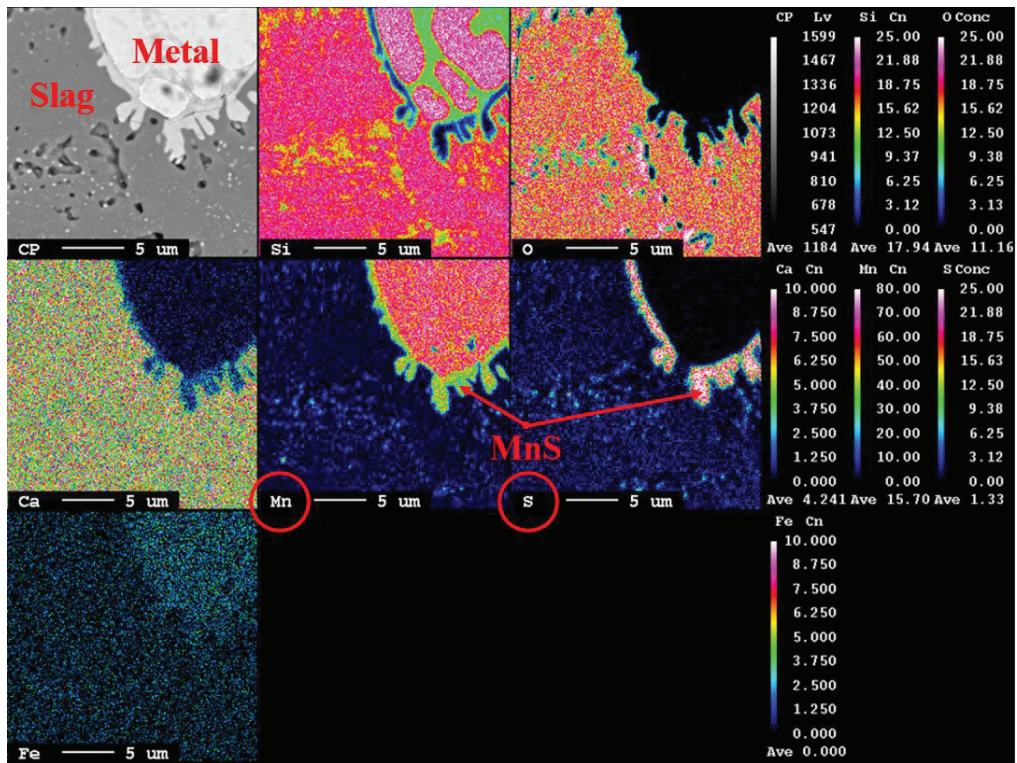
Figure 4.45: Elemental mapping of slag and metal phase of charge "Syn. 0.9" at 1650 °C. Manganese and sulfur concentration indicates that the thin layer surrounding the metal phase is manganese sulfide (MnS), which implies the effect of sulfur with MnO reduction by dissolved carbon in the metal phase. Note that charges with sulfur content between 0.3 and 0.9 wt% also showed the similar elemental mapping results.

The rate constants of MnO and SiO$_2$ reduction were also recalculated by applying the estimated kinetic parameters in **Table 4.32**, where **Figure 4.46** describes the comparison of the synthetic charges with different amount of sulfur between 1500 and 1650 °C.
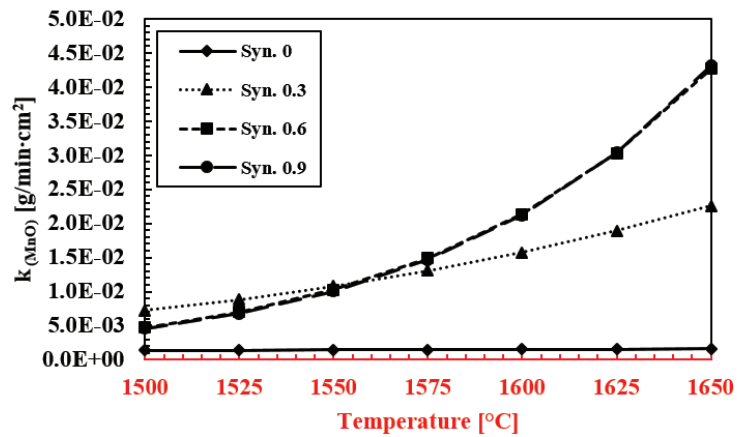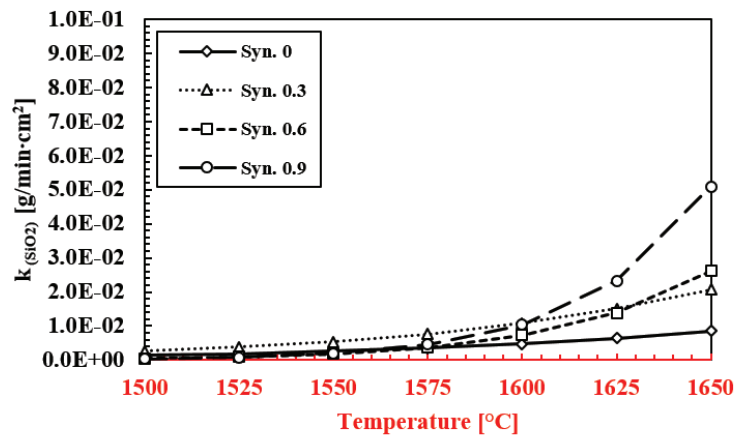
Figure 4.46: Recalculated rate constants of (a) MnO and (b) SiO$_2$ reduction of the synthetic SiMn charges between 1500 and 1650 °C, where the kinetic parameters obtained from the experiments were used. Relation between the rate constants and amount of sulfur was clearly shown.

Since the purpose of research topic #4 was to confirm the effect of sulfur, which the kinetic information was extracted from previous experiments in research topic #3, the comparison of the rate constants of MnO and SiO$_2$ reduction with different amount of sulfur between 1500 and 1650 °C is described in **Figure 4.47**.
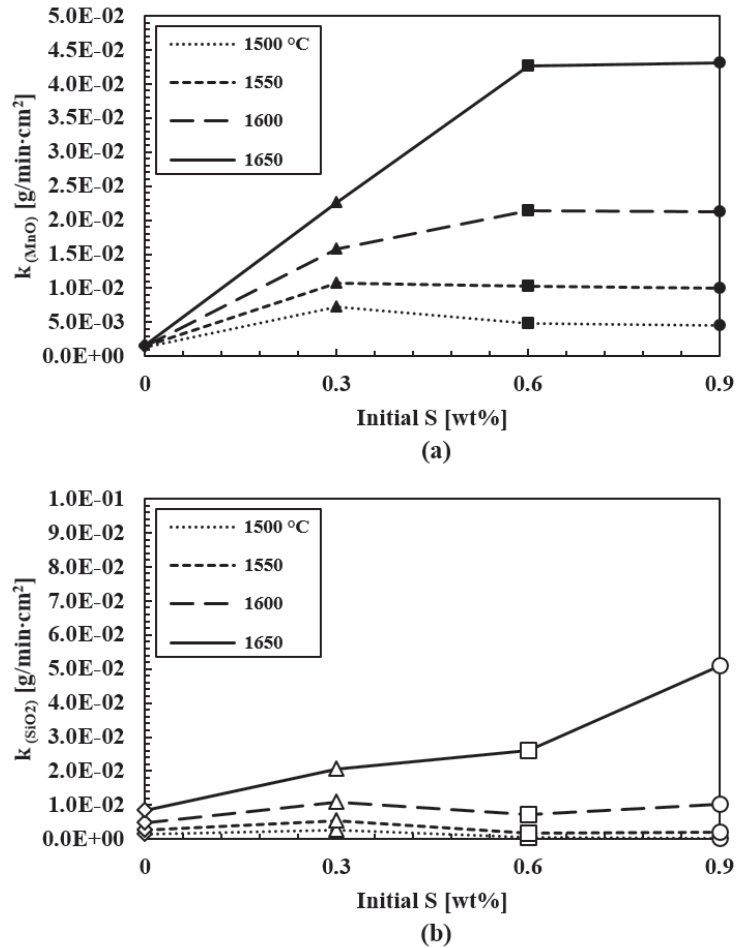
Figure 4.47: Comparison of rate constants for (a) MnO and (b) SiO$_2$ reduction with different initial amount of sulfur between 1500 and 1650 °C. Effect of sulfur was clearly observed with MnO reduction where the reduction rate was enhanced. Effect on SiO$_2$ reduction was less visible than MnO reduction, but higher amount of sulfur gave higher reduction of SiO$_2$.

The comparison result clearly indicates the effect of sulfur for MnO reduction in SiMn slags. The rate constant of MnO reduction increased with increasing amount of sulfur and temperature, where the threshold amount was 0.3 wt% sulfur. This was the similar amount of sulfur which was also discussed from experiments with industrial SiMn charges in **Section 4.3.4**. The effect of sulfur was not likely to be visible with lower amount, which explains why the previous study in **Figure 2.30** [81] showed the opposite results.

The effect of sulfur on SiO$_2$ reduction was less visible compared to MnO reduction, and the results from **Figure 4.45** also did not gave clear information where the silicon concentration was low in the manganese sulfide phase. But higher amount of silicon metal was produced with increasing amount of sulfur despite

the unclear effect of sulfur on SiO_2 reduction. It seems that more SiO_2 reduction can be expected when the reduction of MnO is relatively high from the effect of sulfur.

The comparison of the calculated and measured amount of MnO and SiO_2 was made from using the kinetic parameters and the rate models. Since a three-component slag system was considered for synthetic charges, the comparison between calculated and measured amount was described in the MnO-SiO_2-CaO slag system to construe the reduction path of MnO and SiO_2. The measured and calculated amount of MnO and SiO_2 of synthetic charges with different amount of sulfur is shown in **Figure 4.48**.
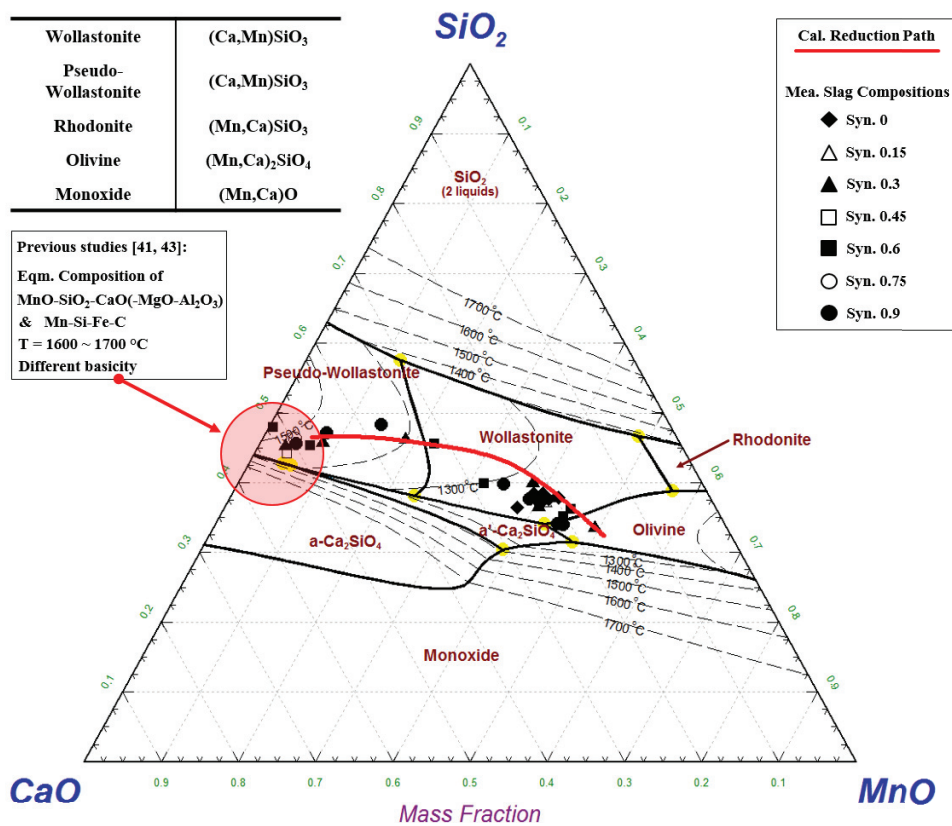
Figure 4.48: Calculated reduction path and measured slag compositions of MnO and SiO_2 reduction in the MnO-SiO_2-CaO system between 1200 and 1650 °C. Initial direction of the reduction was determined by the SiO_2/CaO ratio, and the reduction degree was determined by the amount of sulfur in the slag. In addition, the reduction path of high reduction corresponded to the previous studies of slag and metal equilibria [41, 43]. Note that FactSage 7.0 [45] was used to construct the MnO-SiO_2-CaO system between 1300 and 1700 °C.

The comparison results indicated two reduction aspects of MnO and SiO_2 in the MnO-SiO_2-CaO system. First, the rate models of MnO and SiO_2 reduction were applicable to describe the changing amount of MnO and SiO_2, which was initially observed from **Figures 4.36** and **4.37** with industrial SiMn charges. The

151

calculated and measured slag components displayed a good fit. It showed that the direction of reduction was initially determined by the SiO_2/CaO ratio, where the change of direction indicated the occurrence of considerable SiO_2 reduction. However, the reduction degrees of MnO and SiO_2 were determined by the amount of sulfur in the slag. Second, the calculated reduction path showed corresponding results to previous equilibrium studies [41, 43]. This was observed from the reduction path at high reduction (low MnO and approximately 45 wt% SiO_2) which was close to the slag and metal equilibria between 1600 and 1700 °C (red circle). The reduction paths of industrial SiMn charges, "As", "As/HCS" and "HCS", from **Section 4.3** are also described in **Appendix F**. Thus, the comparison indicates that the rate models of MnO and SiO_2 reduction are applicable for SiMn slag systems. Note that the discrepancy at the low reduction region was due to the low amount of silicon produced between 1500 and 1550 °C, which was discussed in the previous section.

The highlighted results from experiments with synthetic charges with different amount of sulfur are recapitulated in the following bulleted points:

- Higher and faster reduction of MnO and SiO_2 were observed when the sulfur content was between 0.3 and 0.9 wt% in the charge. However, increasing the amount of sulfur between 0.3 and 0.9 wt% did not showed significant difference in the reduction of MnO and SiO_2.

- Sulfur was observed not to behave as a catalyst, where the activation energy increased with increasing amount of sulfur. Instead, it was suggested that sulfur may influence the reduction rate of MnO between slag and dissolved carbon in the metal phase, but further investigation is required to clarify the mechanism of sulfur in MnO reduction.

- The reduction paths of MnO and SiO_2 reduction in the MnO-SiO_2-CaO system were available from using the rate models of MnO and SiO_2 reduction. The initial direction of the reduction was determined by the SiO_2/CaO ratio and the reduction degree determined by the sulfur content in the slag. Also, the reduction paths corresponded to the slag and metal equilibria from previous studies.

4.5 Results of parallel studies

As previous mentioned in **Section 3.5**, there were two master's students and an internship project which were closely related to this work. Their work also involved the research topics of this thesis by using Comilog-based and synthetic SiMn charges. The melting of raw materials [84] and reduction behavior [84, 85] in Comilog-based SiMn charges was initially observed. Then, the kinetic estimation from Comilog-based SiMn charges was also studied along with comparison with synthetic SiMn charges [85, 86].
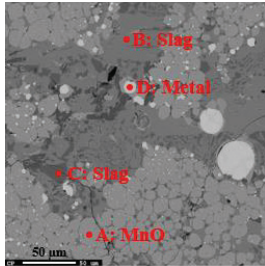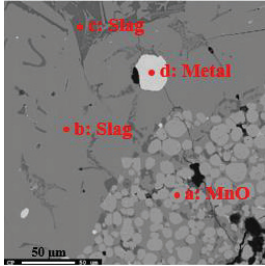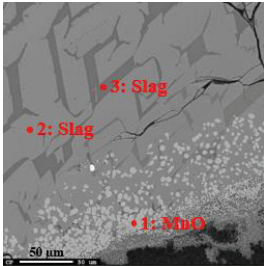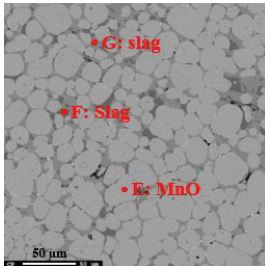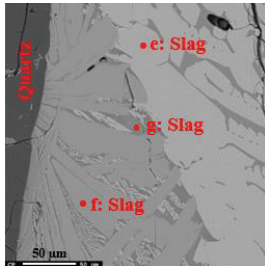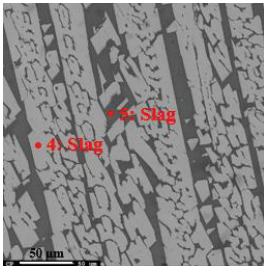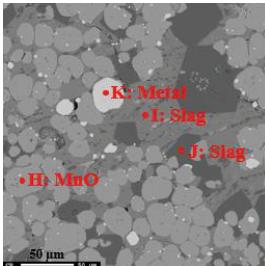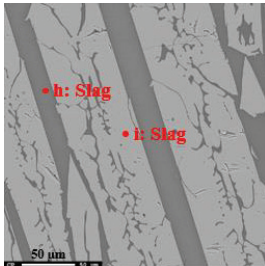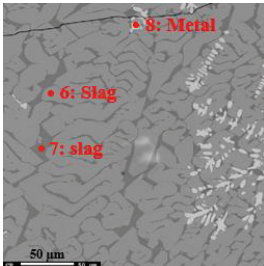
4.5.1 Melting of raw materials in Comilog-based SiMn charges

The melting behavior of Comilog-based FeMn, "H1" (Comilog ore + coke), and SiMn, "H2" (Comilog ore + quartz + coke) and "H3" (Comilog ore + quartz + limestone + coke), charges according to **Table 3.16** at 1250, 1300 and 1400 °C are described in **Table 4.33** [84]. The BSE images showed slag samples which were observed near pre-reduced Comilog ore and quartz particles. The corresponding phase analyses are also shown in **Table 4.34**. The BSE image comparison between FeMn (charge "H1") and SiMn (charges "H2" and "H3") showed different results. While MnO spheres (grey spherical phases) were observed in all temperatures in charge "H1", the same phases were not observed in charges "H2" and "H3" at 1300 and 1400 °C. These results were similar to the observation of SiMn charges based on Assmang ore in **Section**

4.1.2. The slag phases (light and dark grey) mostly consisted MnO and SiO_2 with some portion of CaO and Al_2O_3 and showed similar structures, which were observed in Assmang-based SiMn charges.

The comparison between FeMn and SiMn slag structures also showed the different melting behaviors of the two types of charges, which was previously reflected on the $MnO-SiO_2$ system in **Section 2.1.3**. Primary FeMn slag contained solid phases until liquidus temperatures, while only liquid SiMn slag was observed at relatively low temperatures. A recent study also observed the melting behavior of raw materials by comparing FeMn and SiMn charge based on Assmang and Comilog ore, where similar results with this work were observed [93].

Table 4.33: BSE images of slag phase from Comilog-based charges at 1250, 1300 and 1400 °C (reorganized) [84]. Spherical MnO phases in the FeMn charge "H1" were presented in the slag phases at all temperatures, while they were only observed at 1250 °C in SiMn charges "H2" and "H3".

Temperature [°C]	Comilog-based charges		
	H1	H2	H3
1250			
1300			
1400			
Notes	FeMn charge (Comilog)	SiMn charge (Comilog + Quartz)	(Comilog + Quartz + Limestone)

153

Table 4.34: Analyzed slag and metal compositions of charges "H1", "H2" and "H3" analyzed in Table 4.33 at 1250, 1300 and 1400 °C (reorganized) [84]. Grey spherical phases were mostly composed of MnO, and the light and grey phases were slag with mostly both MnO and SiO_2.

Charge No.	Position	MnO	SiO$_2$	CaO	Al$_2$O$_3$	Other	Total [wt%]	Notes	Identified as:	Temperature [°C]
H1	A	90.4	0.2	0	1.0	0.5	92.1	Grey spherical	MnO	
	B	63.1	29.6	1.9	0.8	0.6	96.0	Light grey	Slag	1250
	C	38.9	0.3	0	55.3	0.7	95.2	Dark grey		
	D	13.0 Fe – 86.9 Mn					99.9	Metal	FeMn	
	E	93.2	0	0	0.3	0.2	93.7	Grey spherical	MnO	
	F	65.6	28.9	0.4	0.9	0.2	96.0	Light grey	Slag	1300
	G	39.6	0.2	0	58.8	0.1	98.7	Dark grey		
	H	93.4	0.1	0.1	0.4	0.3	94.3	Grey spherical	MnO	
	I	64.4	29.1	1.2	1.2	0.3	96.2	Light grey	Slag	1400
	J	39.2	0.2	0	57.9	0.1	97.4	Dark grey		
	K	32.3 Fe – 67.7 Mn					100	Metal	FeMn	
H2	a	92.9	0.2	0	0.3	0.9	94.3	Grey spherical	MnO	
	b	49.8	45.8	0.1	1.3	0.3	97.3	Light grey	Slag	1250
	c	35.4	35.2	0.4	23.3	1.8	96.1	Dark grey		
	d	2.6 Fe – 97.3 Mn – 0.1 Si					100	Metal	FeMn	
	e	65.2	30.5	0.1	0.3	0.2	96.3	White		
	f	50.1	46.1	0.1	0.9	0.2	97.4	Light grey		1300
	g	30.9	50.0	0.6	13.3	1.8	96.6	Dark grey	Slag	
	h	65.0	30.9	0.2	0.2	0.2	96.5	Light grey		
	i	37.6	40.3	0.9	15.7	1.4	95.9	Dark grey		1400
H3	1	93.0	0.1	0.2	0.4	1.0	94.7	Grey spherical	MnO	
	2	58.9	30.8	6.4	0.2	0.5	96.8	Light grey		1250
	3	22.1	41.0	17.7	15.5	1.5	97.8	Dark grey		
	4	58.0	30.9	7.3	0.2	0.3	96.7	Light grey	Slag	1300
	5	22.3	40.3	17.6	15.6	1.4	97.2	Dark grey		
	6	53.3	31.1	12.3	0.3	0.4	97.4	Light grey		
	7	33.8	20.1	11.2	27.9	0.1	93.1	Dark grey		1400
	8	67.6 Fe – 32.4 Mn					100	Metal	FeMn	

4.5.2 Reduction behavior of Comilog-based SiMn charges

The reduction behavior of Comilog-based SiMn charges was observed from the two master's students according to **Tables 3.16** and **3.17**. Holtan used two different particle sizes (0.6 − 1.6 and 4.0 − 6.3 mm) to compare the mass change between FeMn and SiMn charges [84], where the same method from this thesis was considered. Later, Larssen repeated the observation of SiMn charges with smaller particles (0.6 − 1.6 mm) [85]. Note that the recorded temperature schedules of Holtan's and Larssen's work were similar with this work in **Figure 4.12**.

The mass change comparisons between FeMn and SiMn charges from Holtan's observation are shown in **Figures 4.49** and **4.50**. The results also showed similar mass changes of FeMn and SiMn charges to the Assmang charges from **Section 4.1.1**. The mass change of FeMn charge, "H1" (Comilog ore + coke), was progressive during the experiment, while the mass changes of SiMn charges, "H2" (Comilog ore + quartz + coke) and "H3" (Comilog ore + quartz + limestone + coke), were divided into two stages. The mass changes of SiMn charges were relatively low below 1500 °C but rapidly increased at higher temperatures. The reduction behavior of FeMn and SiMn charges were observed regardless of particle sizes.

The different reduction behavior between FeMn and SiMn charges were described previously in **Section 4.1.1** where the driving force of MnO reduction was discussed. Below 1500 °C, the driving force in FeMn slags was assumed to be higher than in SiMn slags due to the presence of solid MnO. As a result, higher reduction rate was observed with higher driving force of MnO reduction below 1500 °C.

The two-stage reduction observed in Comilog-based SiMn charges seemed uncertain due to the abrupt changes in the measured mass, which was previously observed with Assmang-based SiMn charges in **Section 4.2.2**. Holtan had also reported slag loss from the crucibles after the experiments. Note that these problems were fixed in Larssen's work where the resolutions from **Table 4.7** were used in her work.
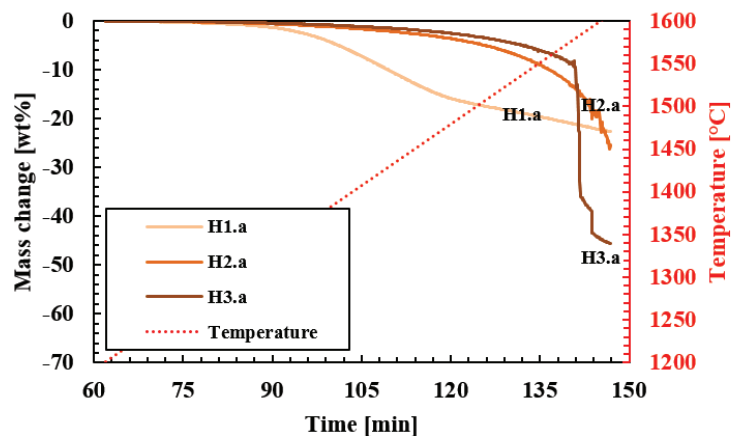
Figure 4.49: Mass change comparison of FeMn and SiMn charges (a: 0.6 − 1.6 mm) between 1200 and 1600 °C [84]. Mass change of FeMn ("H1.a") was progressive, while two different stages were observed for SiMn charges ("H2.a" and "H3.a").

155
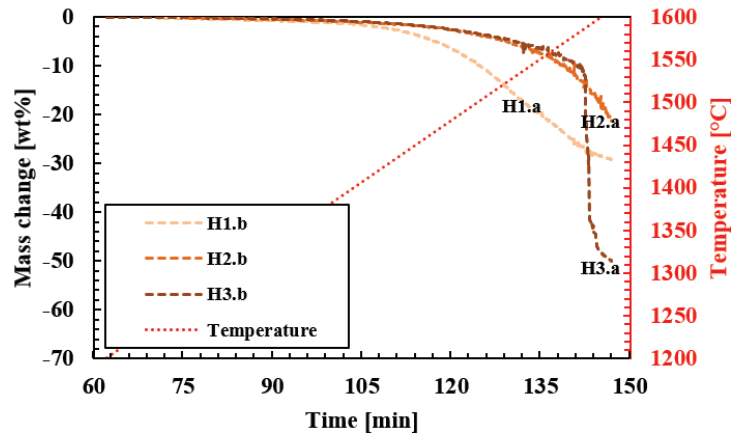
Figure 4.50: Mass change comparison of FeMn and SiMn charges (b: 4.0 − 6.3 mm) between 1200 and 1600 °C [84]. As similar with the results in Figure 4.38, the mass change of FeMn ("H1.b") was progressive, while two different stages were observed for SiMn charges ("H2.b" and "H3.b").

The effect of particle size comparisons between FeMn and SiMn charges are also described in **Figures 4.51**, **4.52** and **4.53**. The comparisons also showed similar results which were observed from Assmang-based SiMn charges in **Section 4.1.1**. Smaller particles showed faster mass change in FeMn comparison until approximately 1550 °C. As an exception, the charge with larger particle sizes was faster at higher temperature. However, the reasons were unclear. For SiMn case, the effect from the particle sizes was not observed. Regardless of the particle sizes, the mass changes of SiMn charges were similar during the experimental condition. This also reflected the melting behavior of SiMn charge materials which was discussed in **Section 4.1**. Complete formation of liquid SiMn slag had occurred at relatively low temperatures around 1400 °C before the considerable reduction of MnO and SiO_2 above 1500 °C. Thus, the effect of particle sizes could still be valid but is not critical during the reduction above 1500 °C.
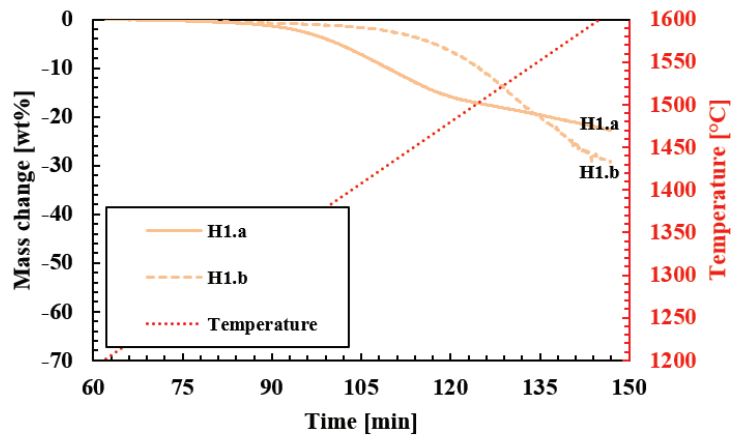
Figure 4.51: Effect of particle sizes on the reduction rate in Comilog-based FeMn charges: Charges "H1.a" (0.6 − 1.6 mm) and "H1.b" (4.0 − 6.3 mm) [84]. Smaller particle sizes showed faster mass change until approximately 1550 °C, while it was opposite at higher temperatures.
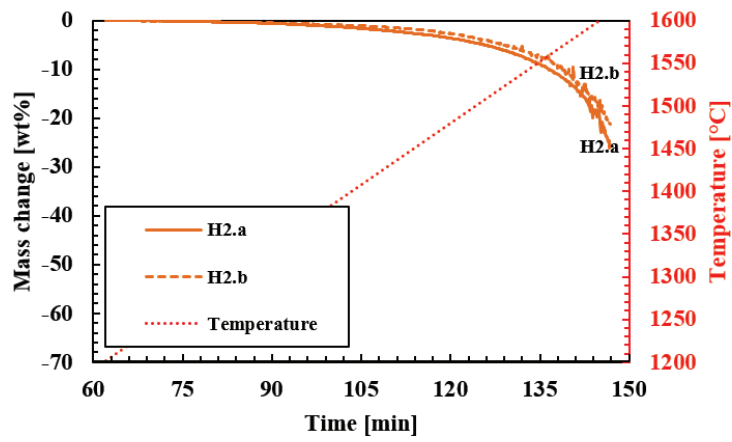
Figure 4.52: Comparison of reduction of Comilog-based SiMn Charges "H2.a" (0.6 − 1.6 mm) and "H2.b" (4.0 − 6.3 mm) between 1200 and 1600 °C [84]. Mass change difference between the two different particle sizes was insignificant.

157
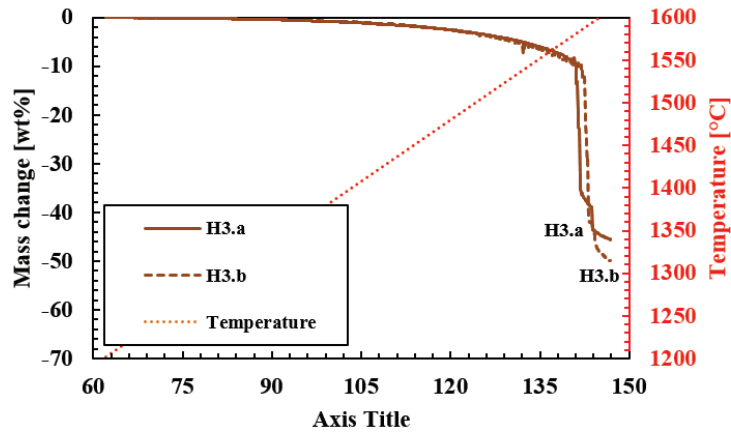
Figure 4.53: Comparison of reduction of Comilog-based SiMn Charges "H3.a" (0.6 − 1.6 mm) and "H3.b" (4.0 − 6.3 mm) between 1200 and 1600 °C [84]. Mass change difference between the two different particle sizes was insignificant.

The mass change comparison of Comilog-based SiMn charges from Larssen's work is also described in **Figure 4.54** [85]. Note that charges "H2" and "L1" contain the same type of raw materials, which were Comilog ore, quartz and coke. Charges "H3" and "L2" were also the similar SiMn charges, where the raw materials were Comilog ore, quartz, limestone and coke. The different results from Holtan were due to the slag loss problem, where the resolutions were made in Larssen's work. Since charges "L1" and "L2" indicate low reduction even until 1600 °C, it seems that extreme wetting of slag had occurred in Holtan's case rather than slag foaming. Foaming of slag accompanies CO gas production which indicates reduction of MnO and SiO_2. The raw materials in Charge "L3" were Comilog ore, quartz, HC FeMn slag and coke. Nevertheless, further examination is required to ascertain the reasons of the slag lost phenomena.

The addition of limestone into the charge did not made significant difference, where the mass changes of charges "L1" and "L2" were similar during the experimental condition. This implies that the effect of slag viscosity on reduction rate is not significant in SiMn slags, which was also discussed previously with synthetic and Assmang-based SiMn charges. Instead, replacing limestone with HC FeMn slag had increased the reduction rate significantly. Charge "L3" showed significant difference in mass change than the first two Comilog-based SiMn charges, which was also previously observed with Assmang-based charges in **Figure 4.22**. The reason for the enhanced reduction rate was believed to be due to the effect of sulfur from experiments in research topics #3 and #4. The sufficient sulfur content in HC FeMn slag as raw material seems to explain the results of charge "L3".
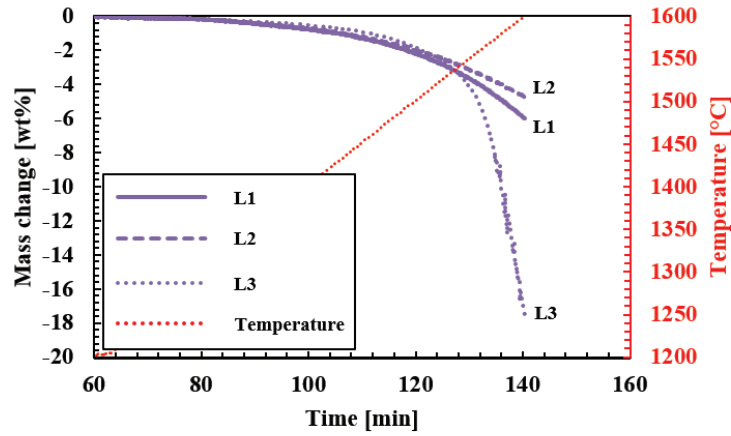
Figure 4.54: Average mass change comparison between Comilog-based SiMn charges "L1" (Comilog ore + quartz + coke), "L2" (Comilog ore + quartz + limestone + coke) and "L3" (Comilog ore + quartz + HC FeMn slag + coke) between 1200 and 1600 °C [85]. Results showed that limestone addition did not gave significant difference, while addition of HC FeMn slag had enhanced the reduction rate significantly. Effect of sulfur was confirmed from synthetic and Assmang-based SiMn charges, where the sufficient sulfur content from HC FeMn slag explains the enhanced reduction rate of charge "L3".

4.5.3 Kinetic estimation from Comilog-based SiMn charges

Larssen also continued to estimate the kinetic parameters from Comilog-based SiMn charges according to **Table 3.17** [85]. The same methods and assumptions of this thesis were considered in her estimation, where the temperature schedules for Comilog-based charges were similar from this work in **Table 4.20 (a)**. To compare the SiMn charges based on the two manganese ores, Assmang and Comilog, the rate constants of MnO reduction from **Section 4.3.4** and Larssen's work are compared together with the amount of sulfur at 1500, 1575 and 1650 °C in **Figure 4.55**.
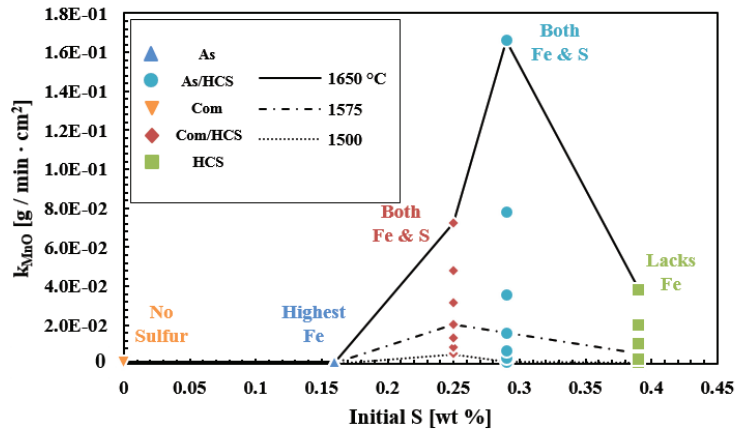
Figure 4.55: Comparison between the rate constants of MnO reduction and the amount of initial sulfur in SiMn charges based on Assmang and Comilog [85] ores at 1500, 1575 and 1650 °C. Relative characteristics regarding the amount of iron and sulfur are noted for each SiMn charge type, where the effect of sulfur is shown. Note that "Com" and "Com/HCS" are charges "L1" and "L3", respectively.

The comparison showed that the reduction rate of MnO increased with higher amount of sulfur and temperature. The possible combined effect of iron and sulfur was discussed previously in **Section 4.3.4**, and the superior effect of sulfur than iron was confirmed on **Section 4.4**. For faster reduction rate of MnO, it seems that the amount of sulfur in the total charge composition was more important than the iron amount in different manganese ores. This was observed from comparing the rate constants charge "As" and "Com" ("L1"), where both charges showed low reduction regardless of the iron content. Thus, the sulfur content from the total charge composition will affect the reduction rate more than the different iron content of manganese ores.

The comparison between the calculated and measured amount of MnO and SiO_2 in Comilog-based SiMn slags are shown in **Figure 4.56**. Note that the kinetic parameters estimated from Larssen's work [85] were used to calculate the amount of MnO and SiO_2 by using the rate models, **Equations (2.20)** and **(3.4)**. Similar to the results in **Figures 4.36** and **4.37**, the rate models were also applicable with Comilog-based SiMn slags whether the reduction degree was high or low. This indicates that the rate models are reliable to describe the reduction rates of MnO and SiO_2 in SiMn slags of different charge compositions.
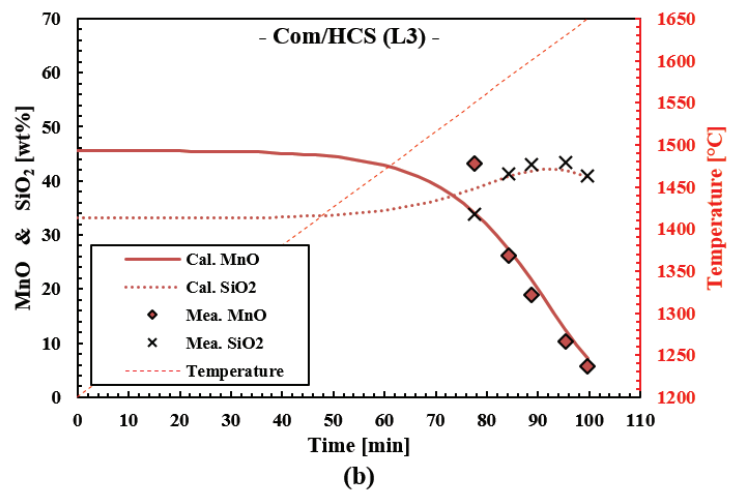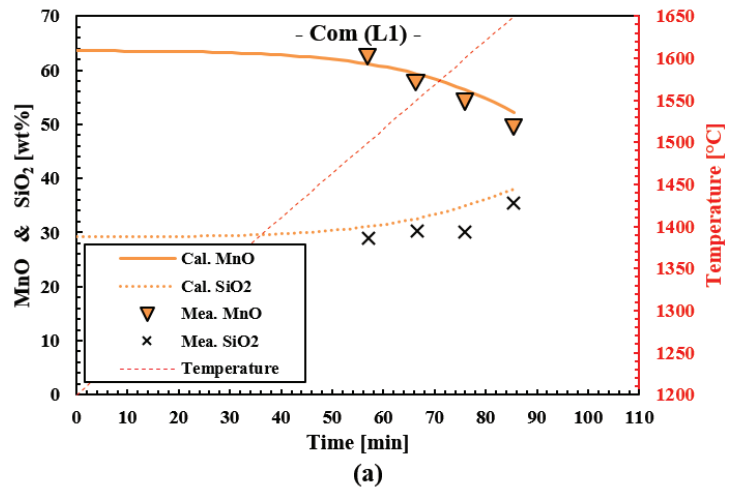
Figure 4.56: Comparison of calculated (lines) and measured (symbols) amount of MnO and SiO$_2$ in charge (a) "L1" (Com) and (b) "L3" (Com/HCS) between 1200 and 1650 °C [85]. Results showed that the rate models of MnO and SiO$_2$ reduction were also applicable with Comilog-based SiMn charges.

4.5.4 Comparison between industrial and synthetic SiMn charges

Kawamoto compared the mass change between industrial and synthetic SiMn charges using the similar methods of this work [86]. As described in **Section 3.5**, the charge "As/HCS" (Assmang ore + quartz + HC FeMn slag + coke) in this work was represented as an industrial example to be compared with a replicated synthetic SiMn charge. The synthetic replica contained the same amount of slag (MnO, SiO_2, CaO, MgO, Al_2O_3) and metal (iron) components with the pre-reduced charge "As/HCS", where the only difference was the amount of impurity elements. Assuming sulfur as impurity element affects the reduction rate, the mass change comparison of the industrial and synthetic SiMn charges between 1200 and 1650 °C is described in **Figure 4.57**, where the variation of the sulfur content in the synthetic replica was 0, 0.26 and 1.0 wt%. Note that the temperature schedule of the synthetic charge was similar to **Table 4.20 (a)**.
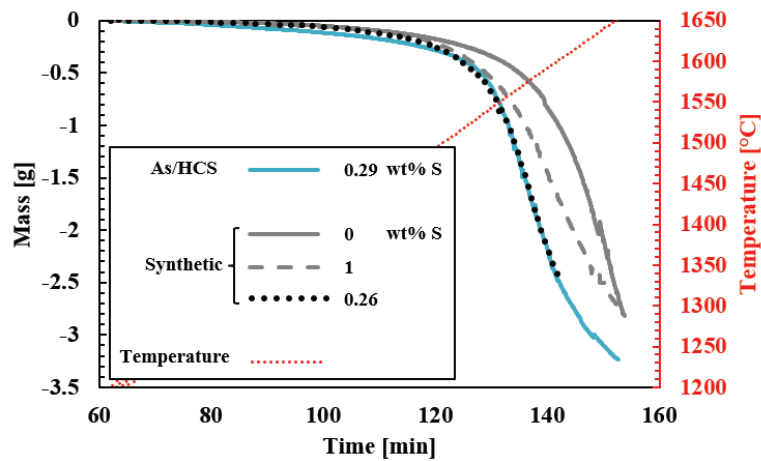
Figure 4.57: Mass change comparison of industrial ("As/HCS") and synthetic charge between 1200 and 1650 °C [86]. It was observed that the difference between the industrial and synthetic charges was the amount of sulfur: Mass change results of the two cases overlapped when the sulfur content in the synthetic charges was similar with the industrial charge.

The initial comparison between the industrial and the synthetic replica with no sulfur addition showed that the reduction in the first case was faster. After adding 1 wt% of sulfur in the synthetic replica, the result showed that the reduction rate of the synthetic replica had increased but still with a difference of mass loss. Controlling the sulfur content to 0.26 wt%, which was the similar sulfur content in the industrial case (0.29 wt% sulfur), the comparison showed overlapping mass changes between the industrial and synthetic charges. The difference between the two charges was clearly the sulfur content, which implies an optimal amount of sulfur may exist for the reduction rate in SiMn slags.

The highlighted results from the parallel studies are recapitulated in **Table 4.35**. The Comilog-based FeMn and SiMn charges showed similar results with charges based on Assmang ore in this work.

Table 4.35: Highlighted results of the parallel studies, where Comilog-based and synthetic charges were used. Results showed similar reduction phenomena which were observed with Assmang-based charges in this study.

Research topic	Result highlights
#1 Melting or raw materials	• Spherical MnO phases were observed in FeMn slag at all temperatures between 1250 and 1400 °C. • Spherical MnO phases were only observed at 1250 °C in SiMn slags, and only liquid slag at higher temperatures.
#2 Reduction behavior	• The addition of limestone did not give significant difference, while the addition of HC FeMn slag enhanced the reduction rate considerably. • The effect of particle size was observed in FeMn charge comparison but not in SiMn charges.
#3 Kinetic estimation	• The effect of sulfur content from the total charge composition was more influential than the different iron contents of manganese ores on reduction. • The effect of sulfur was superior than the effect of iron.
#4 Comparison between industrial and synthetic slags	• The mass change behaviors between industrial and synthetic charges were similar but the industrial case was faster. The difference was the amount of sulfur.

Chapter 5: Discussion

This chapter summarizes the main conclusions from the experimental work including investigation methods and possible effects on the industrial SiMn process. The first two sections discuss the results from the experimental work, which were the factors affecting the formation of slag and reduction rates. The third section discusses the rate and kinetic parameters of the rate models. The calculation and methods from the experimental measurements affecting the obtained results are discussed in detail. The next section discusses the industrial relevance of the experimental results. The melting and reduction behavior observed from this work and the observation from previous industrial excavations are compared to the relating aspects in the coke-bed zone. Lastly, the effect of sulfur is further discussed by comparing the present thesis work with recent observation in iron and steel production. Based on the observed results and comparison, a conceptual mechanistic information of the effect of sulfur in MnO reduction is proposed through comparing the kinetic parameters from Arrhenius and Eyring equations.

5.1 The formation of primary SiMn slags

The composition of the SiMn charges did not affected the formation of slag between 1200 and 1400 °C. The liquid slag phase of different charges started to form shortly after pre-reduction at 1200 °C and was completed around 1400 °C regardless of the charge composition. The individual melting temperatures of different raw materials were of less consequence to the formation of the SiMn slag phase. This was the case from low melting raw materials like HC FeMn slag to high melting manganese sources such as Assmang ore, as the difference of the liquid slag formation was not large. The formation of liquid slag at low temperatures was an unexpected result compared to previous studies, where the slag forming temperatures were assumed to be influenced by raw materials with different melting temperatures [47, 48]. The primary example was observed in charge "M3" (Assmang ore + quartz), where HC FeMn slag as raw material with low melting temperature around 1250 °C was not included. Assmang ore and quartz with relatively high melting temperatures around 1500 and 1713 °C [1, 47, 48, 50, 51], respectively, had formed a liquid slag phase at low temperatures between 1200 and 1400 °C, which implied that there was a strong interaction between manganese sources and quartz.

The particle size of raw materials between 4 and 20 mm had little influence on the formation of slag phase between 1200 and 1400 °C. The cross-section image comparison of charges "M1" (Assmang ore + quartz + HC FeMn slag + coke) and "M2" (Assmang ore + quartz + coke) with charge "M3" at 1400 °C was an example, which is described in **Figure 5.1**. The sizes between charges "M1" and "M2" (4.0 – 6.3 mm) with "M3" (15 – 20 mm) were different by a factor of approximately 3.5, but the observed melting ranges of the charges were between 1215 and 1400 °C regardless of size. This also implies that the interaction between manganese sources and quartz to form slag in SiMn charges between 1200 and 1400 °C is strong. However, the melting and slag formation of particle sizes bigger than 20 mm should also be observed if bigger sizes are considered in the process.
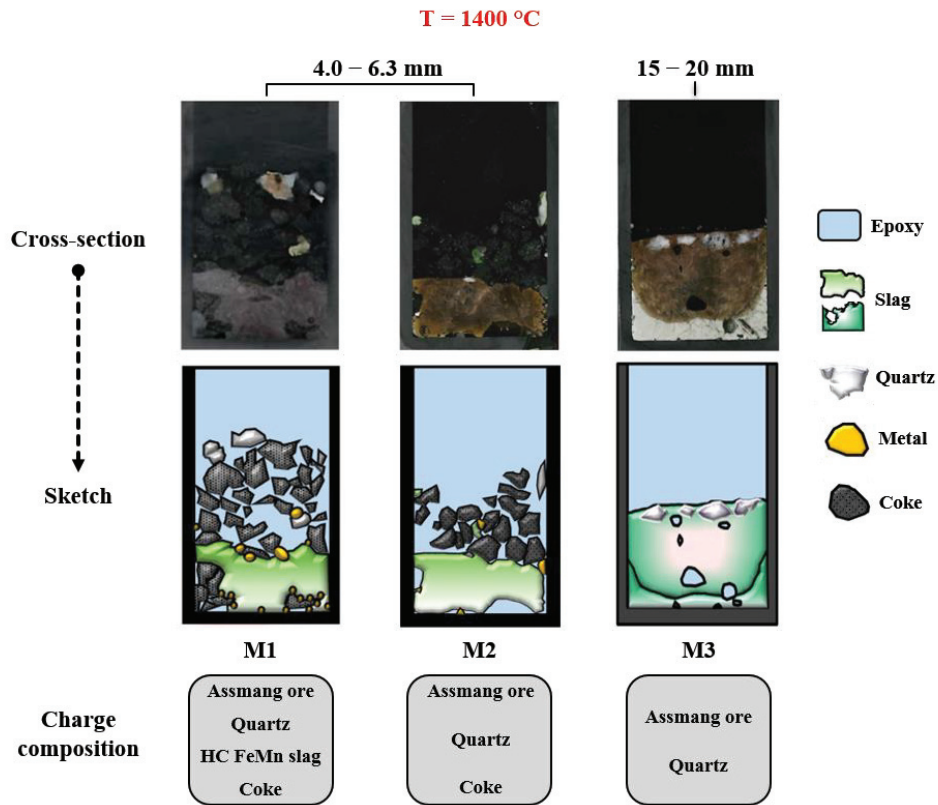
Figure 5.1: Comparison of cross-section images of charges "M1", "M2" and "M3" at 1400 °C. Regardless of the charge composition and particle sizes between 4 and 20 mm, the slag phase was formed around 1400 °C. Note that few quartz particles in charge "M3" were not fully dissolved due to low MnO/SiO_2 ratio as it will be discussed below.

It appears that the formation of liquid slag occurs between 1200 and 1400 °C by relatively fast dissolution of manganese sources and quartz in SiMn charges. The distance between MnO spheres and SiO_2 as quartz increased rapidly with increasing temperature between 1200 and 1300 °C, as observed in **Figure 4.11**. This was not in agreement with previous studies of dissolution of quartz being the rate determining-step in SiMn slags [64, 65]. Instead, it was observed from the cross-section images of charges "M2" (Assmang ore + quartz + coke) and "M3" (Assmang ore + quartz) that the contact between manganese ore and quartz was the prerequisite factor for the generation of liquid slag phase, where the present work observed relatively fast dissolution of quartz in SiMn charges based on Assmang and Comilog [84] ores.

The fast dissolution of raw materials can be explained by comparing the slag viscosities of the primary FeMn and SiMn slags. **Figure 2.17** from **Section 2.1.4** is shown again for convenience. According to the $MnO-SiO_2-CaO-MgO-Al_2O_3$ system, the equilibrium phase relation at 1400 °C between primary FeMn and SiMn slags can be compared. At 1400 °C, solid monoxide mainly as MnO will be present in the primary FeMn slag, while it will be only liquid phase in the primary SiMn slag. This implies that the fast dissolution of manganese ores and quartz in the primary SiMn slags could had been possible because the slag viscosity was low enough for diffusion.
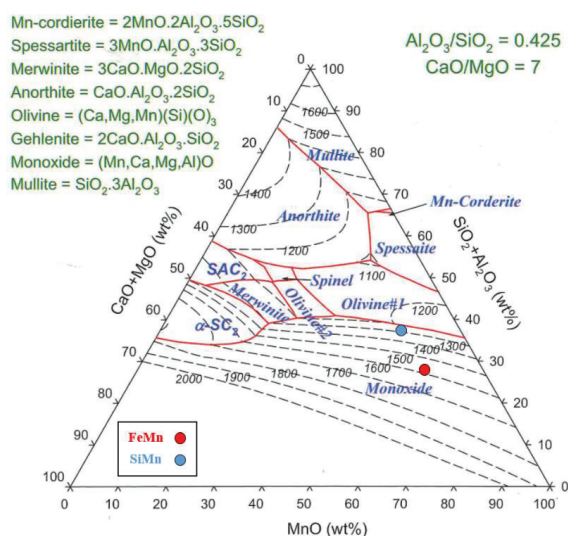
Figure 2.17: Calculated phase and liquidus relations for the $MnO-SiO_2-CaO-MgO-Al_2O_3$ (Al_2O_3/SiO_2 = 0.425, CaO/MgO = 7) system [1] with examples of primary FeMn and SiMn slag compositions (FeMn: 60% MnO – 28% SiO_2 – 12% CaO / SiMn: 50% MnO – 38% SiO_2 – 12% CaO). Solid MnO is expected for the primary FeMn slag until elevated temperature, while the primary SiMn slag will already be all liquid at low temperatures.

In order for manganese ore and quartz to dissolve into the SiMn slag phase, both MnO and SiO_2 should diffuse and react together to form the slag phase. An illustration of dissolving manganese ore and quartz in primary SiMn slag and calculated viscosities of primary FeMn and SiMn slag are shown in **Figure 5.2**. The viscosity of the primary SiMn slag in **Figure 2.17** at 1300, 1350 and 1400 °C is 2.3, 1.8 and 1.4 poise, respectively, according to the calculation by FactSage 7.0 [45]. On the other hand, the viscosity of the primary FeMn slag at 1400 °C in **Figure 2.17** is higher around 10 poise, which can be extrapolated from **Figure 5.2 (b)** at 60 wt% MnO. The relatively lower slag viscosity in the primary SiMn slags seems to be the reason for the fast dissolution of manganese ores and quartz at low temperatures. As the slag viscosity represents the resistance to the diffusivity of molecules over another, the diffusivity will be hindered by both the size and shape of the structural units of silicates, which was discussed in **Section 2.2.3** [68-77]. The viscosity of the primary SiMn slag was low enough for MnO and SiO_2 to diffuse and form the slag phase.

166
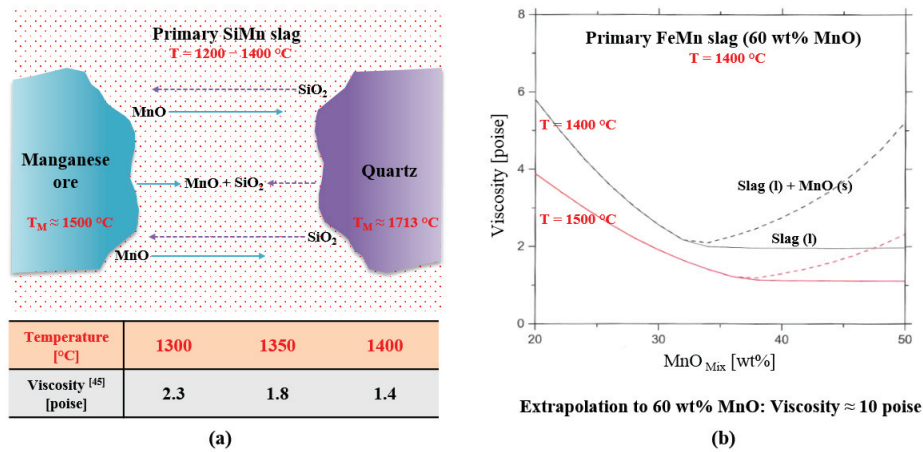
Figure 5.2: (a) Illustration of dissolving manganese ore and quartz into the primary SiMn slag between 1200 and 1400 °C, and (b) calculated primary FeMn slag viscosities at 1400 and 1500 °C between 20 and 50 wt% MnO [1]. Primary SiMn slag is already low around 2 poise at low temperatures, while it is relatively higher in primary FeMn slag. At 1400 °C, extrapolation to 60 wt% MnO gives around 10 poise for primary FeMn slag.

The ratio between manganese sources and quartz in the charge also seems to be a factor for the formation of the slag phase between 1200 and 1400 °C. The results in charge "M3" at 1400 °C from **Figures 4.3** and **4.7** also showed few undissolved quartz particles, which were located at the top part of the slag phase. For convenience, the cross-section sketch of charge "M3" at 1400 °C is shown again in **Figure 5.3**. Note that the interaction between quartz and manganese ore was focused, where quartz/ore ratio was higher than typical industrial charge.
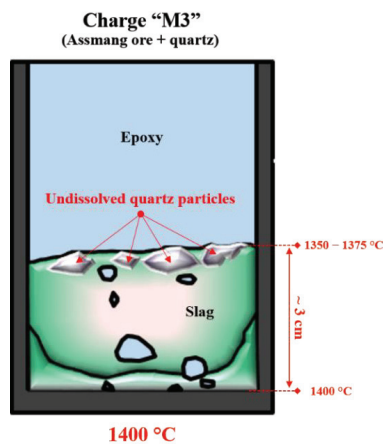
Figure 5.3: Cross-section sketch of charge "M3" at 1400 °C. Undissolved quartz particles on the top part of the slag phase imply that the MnO/SiO$_2$ ratio is lower than 1, where the amount of MnO from manganese sources was not sufficient to react with SiO$_2$ (from quartz) to form the slag phase.

167

The undissolved quartz particles can imply that the amount of MnO from manganese sources was not sufficient to react with SiO_2 (as quartz) to form the slag phase. If the formation of slag occurs by the reaction of MnO and SiO_2 as illustrated in **Figure 5.2 (a)**, the ratio of MnO/SiO_2 in the charge will be important, where complete slag can be assumed when the ratio of MnO/SiO_2 is 1. The MnO/SiO_2 ratio of charge "M3" was 0.58, which can be the reason for the undissolved quartz particles at 1400 °C. An industrial charge would typically be around 1.3 and 1.8. This can also relate to the previous studies of quartz dissolution being the rate-determining step in the SiMn process [64, 65]. It can be expected that the dissolution of quartz in the slag phase to be relatively slow if the MnO/SiO_2 ratio was lower than 1. The approximate slag compositions of charge "M3" between 1300 and 1400 °C are shown in the MnO-SiO_2-CaO system in **Figure 5.4**, where the major slag components were MnO, SiO_2 and CaO. The composition is quite close to the SiO_2 saturation limit at 1300 and 1400 °C, which can explain a slower dissolution rate.
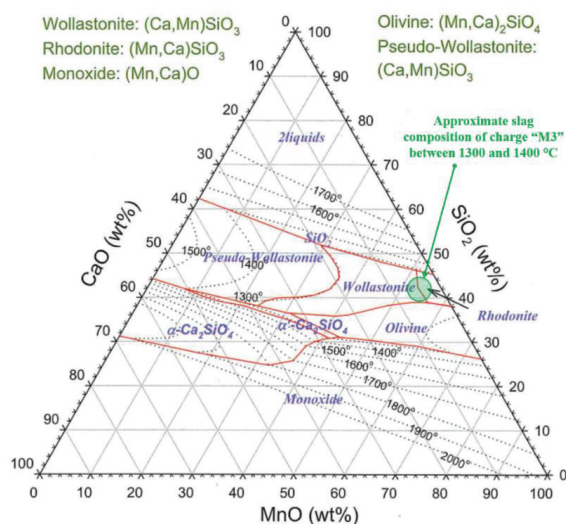
Figure 5.4: Approximate slag compositions (green circle) of charge "M3" between 1300 and 1400 °C in the MnO-SiO_2-CaO system. Charge "M3" consisted Assmang ore and quartz where the major slag components were MnO, SiO_2 and CaO.

In addition, the lower temperature of the undissolved quartz particles from the temperature gradient can be another reason for the incomplete melting. According to the temperature gradient test in **Figure 3.3**, the temperature of the quartz particles was approximately 40 °C below the thermocouple, which was around 1360 °C. However, it was observed in **Figure 4.3** that significant melting had occurred between 1275 and 1300 °C, which implies that the undissolved quartz particles seem to be from the low MnO/SiO_2 ratio rather than the temperature.

The overall melting of raw materials showed close relation to the binary MnO-SiO_2 system in **Figure 2.11**, where the EPMA analyses of the cross-sections were useful to ascertain the formation of slag in SiMn charges. In dissolving manganese ores, the solid MnO phases will be present in FeMn slags until liquidus temperature as previously observed [1, 21]. For SiMn case, only liquid phase will occur above approximately 1350 °C whether the charge contains HC FeMn slag or not. This was highlighted from the results of charge "M3" (Assmang ore + quartz), which contained raw materials of relatively high melting temperatures. The

liquid slag at 1350 and 1400 °C were solidified into the two manganese silicate compounds, Mn_2SiO_4 and $MnSiO_3$, and no spherical MnO phases were presented. The observation of these manganese silicates clearly indicated that pre-reduced Assmang ore (MnO) and quartz (SiO_2) particles had melted into liquid slag and solidified to Mn_2SiO_4 and $MnSiO_3$ according to the phase diagram showing the equilibrium phases. Thus, the slag forming temperatures of SiMn charges in this study were able to determine from the binary MnO-SiO_2 system.

5.2 The reduction of MnO and SiO$_2$ in SiMn slags

The production of manganese and silicon occurs simultaneously during the reduction of MnO and SiO_2 between 1500 and 1650 °C, as it was observed in **Figure 4.24**. The accumulated Si/Mn ratios of the produced metal in charges "As" (Assmang ore + quartz + coke), "As/HCS" (Assmang ore + quartz + HC FeMn slag + coke) and "HCS" (quartz + HC FeMn slag + coke) are shown as a function of temperature in **Figure 5.5**. Though the variation was large, the accumulated ratios were mainly between 0.1 and 0.2 at all temperatures. The average Si/Mn ratio of the three charges at 1650 °C was about 0.22.
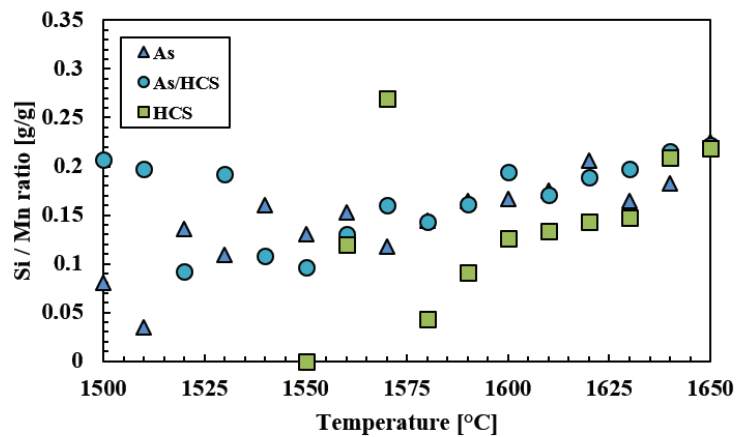
Figure 5.5: Si/Mn ratio of charges "As", "As/HCS" and "HCS" between 1500 and 1650 °C. Manganese and silicon production occurs simultaneously, where the Si/Mn ratio was mainly between 0.1 and 0.2 between 1500 and 1650 °C. At 1650 °C, the average Si/Mn ratio of the three SiMn charges was around 0.22.

The reduction rate of SiMn charges differed depending on the temperature of the process between 1200 and 1650 °C. At increasing temperature, the reduction rates were mainly divided into two stages: Low and high reduction where the dividing temperature was around 1500 °C. **Figure 4.24** is shown again to describe the reduction degrees of MnO and SiO_2 of charges "As", "As/HCS" and "HCS" between 1500 and 1650 °C in a scale of 0 and 1 from **Equations (4.3)** and **(4.4)**. Note that the reduction degrees of MnO and SiO_2 according to the thermodynamic equilibrium at 1600 °C (approximately 5 wt% MnO and 40 wt% SiO_2 in the slag phase) in each charge, which was discussed in **Section 3.1**, are also included. The comparison of the reduction degrees between the measured and thermodynamic equilibrium at 1600 °C indicates that the reduction of MnO and SiO_2 in charges "As/HCS" and "HCS" is faster than charge "As".
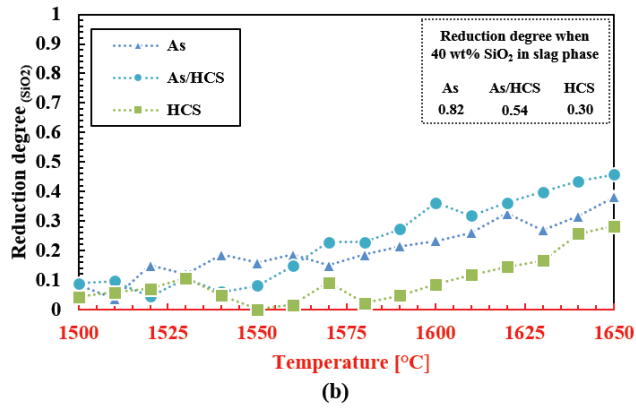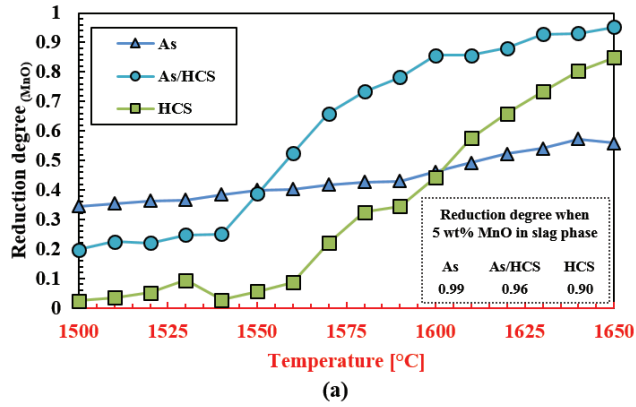
169

Figure 4.24: Reduction degrees of (a) MnO and (b) SiO_2 of the three SiMn charges in a scale of 0 and 1 between 1500 and 1650 °C. Figure is shown again to indicate the progress of MnO and SiO_2 reduction towards the thermodynamic equilibrium at 1600 °C, which is approximately 5 wt% MnO and 40 wt% SiO_2 in slag phase. Reduction of SiO_2 seems similar among the charges but comparison with the thermodynamic equilibrium at 1600 °C indicates that the reduction was faster in charges "As/HCS" and "HCS" than charge "As".

As observed from **Figure 4.24**, around 10 to 30 % MnO and 10 % SiO_2 from the total amount were reduced until 1500 °C, whereas most of the reduction had occurred between 1500 and 1650 °C. This agreed with previous studies where the reduction rate increases with increasing temperature [21, 62, 63]. The effect of temperature on the rate constant and driving force seems to be the main contribution. The rate constant increases with increasing temperature according to the Arrhenius equation, **Equation (2.19)**. The driving force also increases due to the increasing equilibrium constant, which lowers the equilibrium part of MnO in the slag phase or the metal phase. The high reduction between 1500 and 1650 °C also relates to the metal producing temperatures in the industrial operation, where the temperature of the tapped slag and metal was around 1600 °C [1, 20-24, 28, 94, 95].

The activation energy of MnO reduction in charges "As/HCS" and "HCS" in this work was considerably higher than the activation energies estimated for FeMn slags in previous studies, where it was reported to be around 360 kJ/mol between 1450 and 1550 °C [1, 21]. For convenience, part of the estimated kinetic parameters of the industrial SiMn charges "As" (Assmang ore + quartz + coke), "As/HCS" (Assmang ore + quartz + HC FeMn slag + coke) and "HCS" (quartz + HC FeMn slag + coke) between 1500 and 1650 °C from **Table 4.21** is shown again below:

Table 4.21: Summary of the activation energies and pre-exponential constants of the three different charges between 1500 and 1650 °C. Kinetic parameters are the approximate value from the experiments. Note that the MnO reduction part is shown again for convenience.

Reduction	Charge	Ea [kJ/mol]	k_O [g/min · cm²]
MnO	As	~ 250	9.66×10^3
	As/HCS	~ 920	1.62×10^{24}
	HCS	~ 780	5.87×10^{19}

The activation energy shows the temperature dependence of a reaction, and a high activation energy shows that a second stage with rapid reduction will occur during increasing temperature. The high activation energy may be due to the reason that there was foaming or wetting in the slag and thereby increasing the reduction rate giving an exceptional high activation energy.

The reduction rates of MnO and SiO_2 between 1200 and 1650 °C also differed with the charge composition, where the relative amount of MnO from manganese sources and the use of HC FeMn slag as raw material were important factors affecting the reduction rates.

It appears that the amount of MnO from manganese sources determines the reduction rate in the first stage of reduction between 1200 and 1500 °C. The first stage reduction of SiMn charges was compared to FeMn charges between 1200 and 1500 °C, where the driving force of MnO reduction was assumed to give the difference. This comparison was based on the activity difference of MnO in **Figure 2.12**. The activity of MnO will be close to 1 as long as solid MnO as dissolving manganese sources are presented in FeMn slags, while it will be considerably lower in SiMn slags around 0.2 due to the complete liquid slag formation from manganese sources with quartz. This was observed with both Assmang- and Comilog- [85] based FeMn and SiMn charges until 1500 °C. The activity of MnO among SiMn charges also explained the different reduction degrees of MnO up to 1500 °C. The primary SiMn slag with higher MnO content from manganese sources showed higher reduction in the first stage. The amount of MnO at 1500 °C was the highest in the following order: Charge "As" (Assmang ore + quartz + coke), "As/HCS" (Assmang ore + quartz + HC FeMn slag + coke) and "HCS" (quartz + HC FeMn slag + coke), where the reduction degrees of MnO were approximately 0.34, 0.19 and 0.02, respectively.

The use of HC FeMn slag as raw material in SiMn charge affects the reduction rate in the second stage of reduction between 1500 and 1650 °C. The reduction rate of SiMn charges containing HC FeMn slag as raw material was observed to be significantly faster than charges without. The type of manganese ore, such as Assmang and Comilog ores, had less impact on the reduction rates because the activity of MnO was approximately 0.2 at 1500 °C for all SiMn charges. This showed that the relation between the driving force and the reduction rate was less important in the second stage of reduction between 1500 and 1650 °C. Instead, the reduction rate between 1500 and 1650 °C was more related to the kinetics affected by the slag properties, because the use of HC FeMn slag as raw material affected the properties of slag, such as viscosity

and amount of impurity elements. Note that the discussion of the effect of slag properties on reduction rate is continued in this next section.

The particle size of raw materials between 0.6 and 1.6 mm does not affect the reduction rate of SiMn charges between 1200 and 1650 °C. This was opposite to the effect of particle sizes in FeMn slags, where the reduction rate was inversely proportional to the particle sizes [1, 21]. Instead, it was observed from the melting part of this work, where the liquid slag phase of SiMn charges was completed around 1400 °C. The reduction below 1500 °C was low and all raw materials had dissolved into the slag phase before the high reduction step. This was observed from the mass change comparison of SiMn charges with two different particle sizes, 0.6 – 1.6 and 4.0 – 6.3 mm, between 1200 and 1600 °C in **Section 4.2.1**, which the mass changes were observed to be similar. The formation of SiMn slag was completed before the significant reduction of MnO and SiO$_2$, which nullified the effect of particle sizes on reduction rate.

It was observed that the initial amount of sulfur in the primary SiMn charge affects the reduction rate significantly between 1500 and 1650 °C rather than the amount of iron or the slag viscosity affecting the mass transfer. The comparison of the rate constants of MnO and SiO$_2$ reduction with the amount of initial sulfur at 1650 °C from industrial and synthetic SiMn charges is described in **Figure 5.6**. The rate constant of MnO reduction in charges "As/HCS" (Assmang ore + quartz + HC FeMn slag + coke) and "L3" (Comilog ore + quartz + HC FeMn slag + coke) at 1650 °C was rather high compared to other charges. This was believed to be from the slag foaming or wetting which was discussed in **Section 4.2.2**. Note that this will be discussed together with the rate models in **Section 5.3**.

The threshold amount of sulfur was observed to be approximately 0.3 wt% for enhanced reduction rates. This explains why SiMn charges containing HC FeMn slag as raw material showed faster and higher reduction rates. HC FeMn slag already consisted around 0.46 wt% sulfur (**Table 3.1**) from the FeMn process, which was a sufficient amount of sulfur to enhance the reduction rates. The effect of sulfur was also observed from SiMn charges without HC FeMn slag but with addition of iron sulfide (FeS) as sulfur, which was described in **Figures 4.35**, **4.39** and **4.57**. Note that individual work on Comilog ore-based SiMn charges with sulfur can be observed in Larssen's work [86]. It also explained why the previous study of Kuangdi at el. with sulfur content between 0.027 and 0.079 wt% showed the opposite result [81]. The amount of sulfur was not sufficient to observe the effect of sulfur on the reduction rates in their study. Thus, the effect of sulfur enhancing the reduction rate was in agreement with other previous observations [62, 80].

The effect of sulfur was not further investigated experimentally, but it is worth noting that the reduction rate from the slag and dissolved carbon in the metal phase could be influenced by sulfur. As sulfur is known to be a surface-active specie to most metals [82], it is plausible that the surface tension between the slag and metal phase was decreased by sulfur. In addition, a parallel study recently investigated the reduction rates of MnO in SiMn slags, where similar experimental methods with this work were considered [96]. Synthetic SiMn slags with different amount of sulfur between 0.2 and 1.0 wt% were heated up to 1600 °C in CO atmospheric pressure, where the reduction rates of MnO between slag-coke and slag-metal interfaces were compared. The effect of sulfur was also confirmed, and it was observed that the reduction rate of slag-metal interface was much higher than the slag-coke interface, where sulfur had a greater acceleration impact on the former.
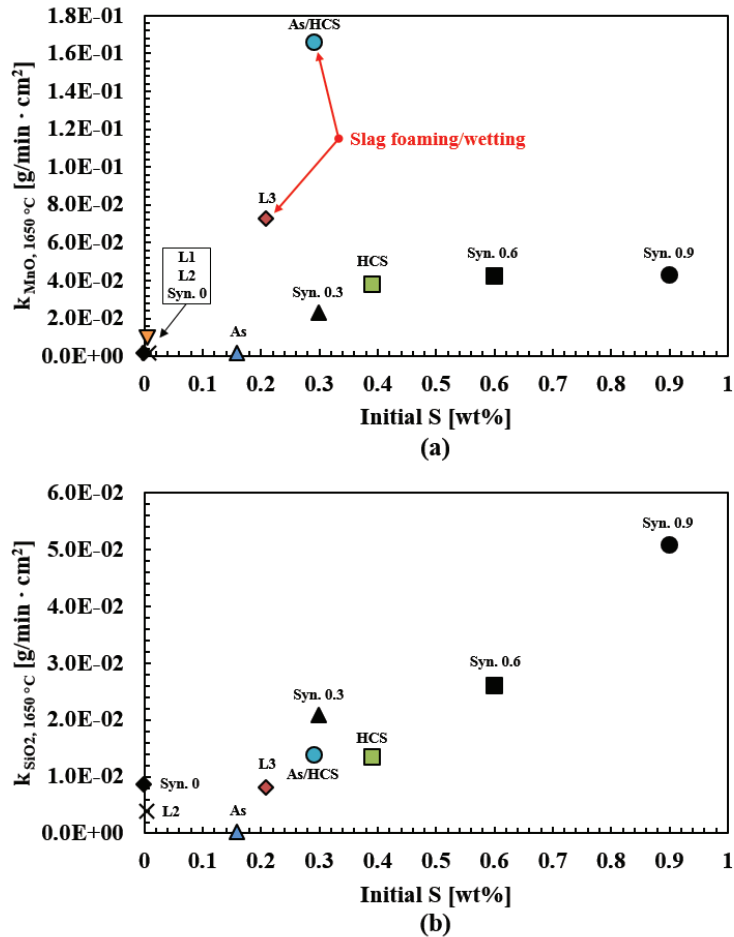
Figure 5.6: Rate constants of (a) MnO and (b) SiO$_2$ reduction at 1650 °C from various industrial and synthetic SiMn charges compared with the amount of initial sulfur. Comparison explained why charges containing HC FeMn slag as raw material showed faster and higher reduction than without. It was also observed that the threshold amount of sulfur was approximately 0.3 wt% for enhanced reduction rates. Note that the relatively high rate constants of MnO reduction in charges "As/HCS" and "L3" could had been attributed by slag foaming or wetting at higher temperatures.

Charges: "As" (Assmang ore + quartz + coke), "As/HCS" (Assmang ore + quartz + HC FeMn slag + coke), "HCS" (quartz + HC FeMn slag + coke), "L1" (Comilog ore + quartz + coke), "L2" (Comilog ore + quartz + limestone + coke), "L3" (Comilog ore + quartz + HC FeMn slag + coke) and "Syn. 0 − 0.9" (Synthetic MnO-SiO$_2$-CaO + S + coke)

It appears that the amount of iron does not significantly affects the reduction rate in the SiMn process between 1500 and 1650 °C. The comparison of the rate constants of MnO and SiO$_2$ reduction with the initial amount of iron at 1650 °C from industrial and synthetic SiMn charges is shown in **Figure 5.7**. The findings in the present work showed opposite results to previous studies, where the amount of initial metal

as iron increased the reduction rate from increasing the driving force by lowering the activity of manganese [62, 78, 79]. The driving force of MnO at 1500 °C was around 0.2 regardless of the charge composition considered in this work. This seems to explain why the amount of iron showed less relation with the different reduction rates, as the rate constants were more varying than the driving forces between 1500 and 1650 °C. The effect of iron on the reduction rate was not observable due to the effect of sulfur.
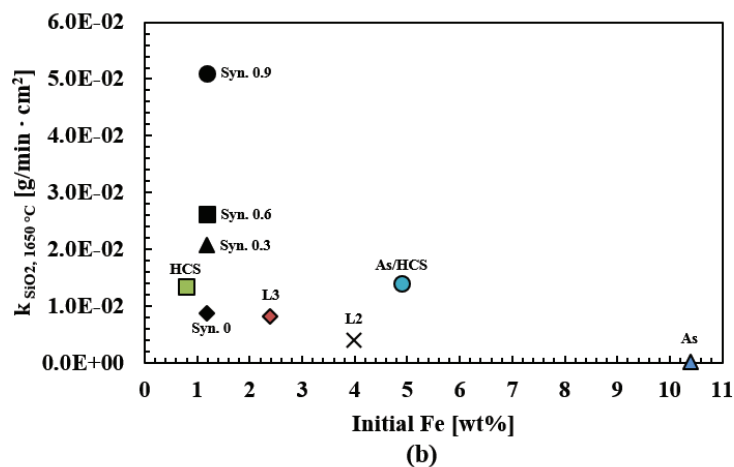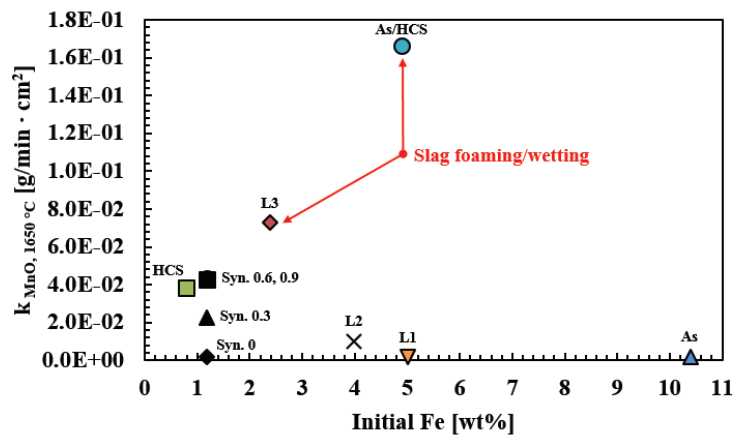
Figure 5.7: Rate constants of (a) MnO and (b) SiO$_2$ reduction at 1650 °C from various industrial and synthetic SiMn charges compared to the amount of initial iron. Reduction rate of MnO and SiO$_2$ has less relation with the amount of initial iron. This can be observed especially from the comparison of synthetic charges. Note that the relatively high rate constants of MnO reduction in charges "As/HCS" and "L3" were due to the slag foaming or wetting at higher temperatures.

Charges: "As" (Assmang ore + quartz + coke), "As/HCS" (Assmang ore + quartz + HC FeMn slag + coke), "HCS" (quartz + HC FeMn slag + coke), "L1" (Comilog ore + quartz + coke), "L2" (Comilog ore + quartz + limestone + coke), "L3" (Comilog ore + quartz + HC FeMn slag + coke) and "Syn. 0 − 0.9" (Synthetic MnO-SiO2-CaO + S + coke)

174

Under the current experimental conditions and observations, the slag viscosity had no significant effect on the reduction rate of MnO and SiO_2 reduction. This was also in disagreement with the previous studies in FeMn slags, where the slag viscosity (or as basicity) correlates to the reduction rate [1, 21, 67]. The viscosity of the industrial SiMn slags between 1500 and 1650 °C of this work is described in **Figure 5.8**. It was observed that the slag viscosities were around 1 poise at 1500 °C regardless of the charge composition. The similar viscosities at 1500 °C cannot explain the different reduction rates at higher temperature. If the reduction rate was influenced by the slag viscosity, the slag with the lowest viscosity should had been favorable. This was not observed in this study, and the $(CaO+MgO)/Al_2O_3$ ratio showed less relation. Also, adding limestone into the SiMn charge did not increase the reduction rate even until 1600 °C, as it was observed between charges "L1" (Comilog ore + quartz + coke) and "L2" (Comilog ore + quartz + limestone + coke) [85] in **Figure 4.54**.
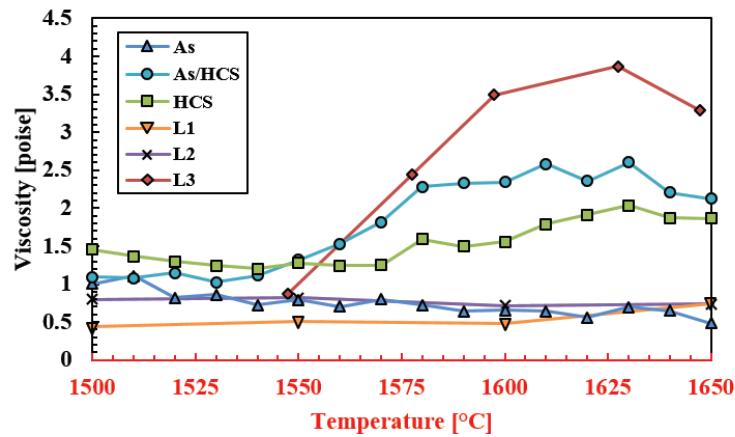
Figure 5.8: Viscosities of industrial SiMn charges based on Assmang and Comilog ore. Viscosities were around 1 poise at 1500 °C regardless of charge type. This does not explain the different reduction rates of SiMn charges at higher temperature. Note that the viscosities were calculated by FactSage 7.0 [45].

Charges: "As" (Assmang ore + quartz + coke), "As/HCS" (Assmang ore + quartz + HC FeMn slag + coke), "HCS" (quartz + HC FeMn slag + coke), "L1" (Comilog ore + quartz + coke), "L2" (Comilog ore + quartz + limestone + coke) and "L3" (Comilog ore + quartz + HC FeMn slag + coke).

5.3 Discussion of the rate models

The rate models of MnO and SiO_2 reduction are discussed in this section by evaluating the rate and kinetic parameters, calculated and estimated between 1500 and 1650 °C. For convenience, the two rate models (**Equation (2.20)** and **(3.4)**) and the Arrhenius equation (**Equation (2.19)**) are shown again below:

$$r_{MnO} = k_{MnO} \cdot A \cdot (a_{MnO} - \frac{a_{Mn} \cdot p_{CO}}{K_{MnO} \cdot a_C}) \tag{2.20}$$

$$r_{SiO_2} = k_{SiO_2} \cdot A \cdot (a_{SiO_2} - \frac{a_{Si} \cdot p_{CO}^2}{K_{SiO_2} \cdot a_C^2}) \tag{3.4}$$

$$k_{MnO\,(SiO_2)} = k_{o,\ MnO\,(SiO_2)} \cdot e^{(-\frac{E_{MnO\,(SiO_2)}}{RT})} \tag{2.19}$$

The two rate models were able to describe most of the reduction rates of MnO and SiO$_2$ between 1200 and 1650 °C. This was observed from using various industrial and synthetic SiMn charges with two different heating rates, 4.5 and 9.0 °C/min. For example, the comparison of MnO and SiO$_2$ between the measured and the rate models, where the heating rate was 4.5 °C/min, is described in **Figure 5.9**. Note that the calculated primary MnO and SiO$_2$ in each SiMn slag, which was shown in **Table 3.12**, and the deviation between the rate model and measured (Cal.-Mea.) amount of MnO between 1500 and 1650 °C are also shown in the comparison.

The analysis of raw materials seems to have affected the comparison between the rate model and measured amount of MnO and SiO$_2$. This can be observed from **Figure 5.9 (a)** of charge "As" (Assmang ore + quartz + coke) at 1200 °C, where the amount of MnO and SiO$_2$ from the rate model and primary slag composition shows approximately 5 wt% deviation. The deviation implies that primary slag composition may not be what was analyzed, where the raw material composition may had changed from particle to particle. If the primary slag composition of the SiMn charges were not reliable, the discussion of kinetic information from using the rate models would be meaningless. However, since the other two SiMn charges, "As/HCS" (Assmang ore + quartz + HC FeMn slag + coke) and "HCS" (quartz + HC FeMn slag + coke), in **Figures 5.9 (b)** and **5.9 (c)** showed fair agreement between the rate model and primary amount of MnO and SiO$_2$ at 1200 °C, it may be more reasonable that the deviation observed in charge "As" was from the varying raw material analysis.

The comparison from charges "As/HCS" and "HCS" also shows that the rate models can be applied at low temperatures between 1200 and 1500 °C. The deviation between the model and primary amount of MnO and SiO$_2$ at 1200 °C was not high, and the reduction rate of MnO and SiO$_2$ was low between 1200 and 1500 °C, which was observed from the TGA results in **Figure 4.22**. This implies that the rate models expressing the calculated amount of MnO and SiO$_2$ between 1200 and 1500 °C are valid at low temperatures, and thus the whole temperature region between 1200 and 1650 °C.
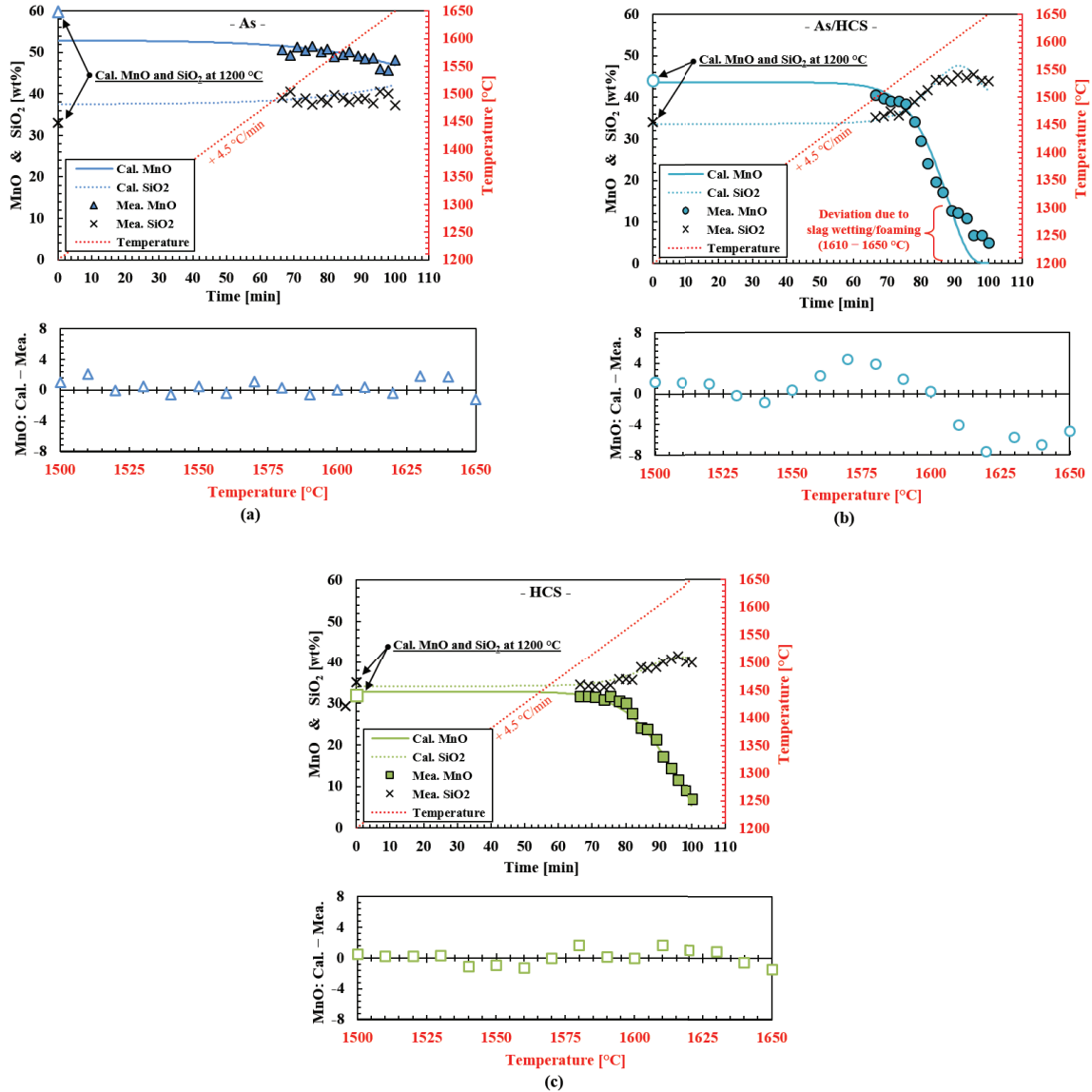
Figure 5.9: Comparison of measured (symbols) and calculated (lines) amount of MnO and SiO$_2$ between 1200 and 1650 °C from industrial SiMn charges (a) "As", (b) "As/HCS" and (c) "HCS", where the heating rate was 4.5 °C/min. Note that the primary amount of MnO and SiO$_2$ at 1200 °C, and the deviation between the rate model and measured (Cal. – Mea.) amount of MnO between 1500 and 1650 °C are also included in the comparison. Comparison shows that the rate models were mostly able to describe the reduction rates of MnO and SiO$_2$.

The comparison also showed that the two rate models used in this work were not completely optimal to describe the changing amount of MnO and SiO_2. This was observed from the deviation between the rate model and measured (Cal. – Mea.) amount of MnO in charge "As/HCS" between 1500 and 1650 °C. The possibility of slag wetting or foaming in charge "As/HCS" between 1610 and 1650 °C was previously shown in **Section 4.3.3**. This implies that the reduction of MnO and SiO_2 can occur with two different mechanisms, with or without slag wetting/foaming, at high temperature depending on the process conditions. Although the two rate models were able to describe the reduction rates of MnO and SiO_2 with different charge compositions and heating rates, the slag wetting or foaming phenomena affecting the rate models should be further investigated in future work. In addition, the deviation between the rate model and measured amount of MnO at high temperatures, where the MnO content was lower than 5 wt%, also implies possible changing reaction mechanism, such as going from a chemical rate control to diffusion control.

The influence of slag wetting or foaming on the reaction area at high temperature can be an example to considered for future work. The total reaction area due to slag wetting or foaming in charge "As/HCS" between 1610 and 1650 °C not only covers the coke particles but also the graphite crucible walls, which will eventually affect the kinetic parameters such as the activation energy. The comparison of the Arrhenius plot with different reaction areas can be made to investigate how much deviation of the activation energy can be made from the slag wetting/foaming in charge "As/HCS". **Figure 5.10** shows the Arrhenius plot of MnO reduction of charges "As/HCS" between 1500 and 1650 with two different cases: The calculated reaction area of this work (**Table 4.25**) and using a constant reaction area (125 cm^2).
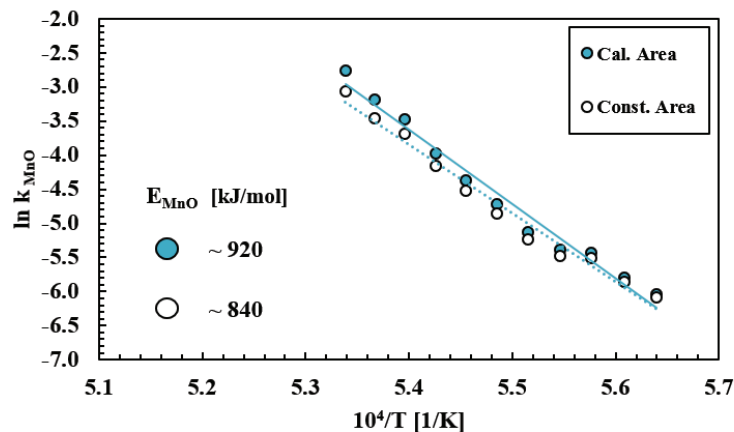
Figure 5.10: Comparison of Arrhenius plot for MnO reduction in charge "As/HCS" between 1500 and 1600 °C with two different cases of reaction area: Measured reaction area and constant initial reaction area. Deviation shows that the estimation of activation energy will be affected by the reaction area.

The comparison shows that the activation energy will vary around 80 kJ/mol from the reaction area of two cases. The deviation of rate constant also increases with increasing temperatures. This indicates that the estimation of activation energy is influenced by the reaction area, and the difference in the rate constant will be even more above 1600 °C. This may explain the deviation between calculated and measured amount of MnO in **Figure 5.9 (b)** between 1610 and 1650 °C. It also relates to the high rate constant of MnO reduction of charge "As/HCS" at 1650 °C in **Figures 5.6 (a)** and **5.7 (a)**, where the rate constant was

significantly higher than other industrial and synthetic charges. If slag wetting or foaming in charge "As/HCS" had not occurred between 1610 and 1650 °C, the rate constant of MnO reduction at 1650 °C is likely to be around 4.0×10^{-2} g/min·cm^2, which is similar with charge "Syn. 0.3" because of the similar sulfur content. Thus, an improvement of calculating the reaction area which can also encompass the slag wetting or foaming between 1610 and 1650 °C is necessary for estimating the activation energy.

In addition, the reactivity of carbon materials, such as coke and graphite, can also be further compared in the future work. It was previously observed that the reduction rate of MnO by coke materials was higher than graphite materials [97], where the reduction contribution from the graphite crucible could have been low. However, more reduction of MnO and SiO$_2$ by graphite crucible may occur if the foaming or wetting of slag is occurring at high temperatures, which the rate constants will be affected by both coke and graphite materials. The comparison of MnO and SiO$_2$ reduction in SiMn slags with different areas of coke and graphite materials can be further investigated.

5.4 Industrial relevance of experimental work

The kinetic information obtained from this thesis work can be used to discuss the reduction aspects in the coke-bed zone of industrial SiMn furnaces. The temperatures regarding melting of industrial raw materials and reduction of MnO and SiO$_2$ observed from the experiments are summarized in **Table 5.1**. It was observed that the melting of raw materials started to occur shortly after the pre-reduction at 1200 °C and the formation of liquid slag was completed around 1400 °C, regardless of SiMn charge compositions. The liquid slag has a low reduction rate until 1500 °C, but significant reduction of MnO and SiO$_2$ starts to take place at higher temperatures between 1500 and 1650 °C.

Table 5.1: Summary of temperature ranges regarding melting of raw materials and reduction of MnO and SiO$_2$ in industrial SiMn slags observed from present work. Liquid slag was completed at relatively low temperature around 1400 °C and the significant reduction of MnO and SiO$_2$ occurred above 1500 °C.

Research observation	Occurring temperature [°C]	Notes
Melting of raw materials	1200 – 1400	Research topic #1
Reduction of MnO and SiO$_2$	1500 – 1650	Research topics #2 and #3

According to previous excavation of industrial and pilot-scale FeMn and SiMn furnaces [1, 20-24, 28, 94, 95], the top part of the coke-bed zone shows relation to both observations of melting and reduction in this present work. It was observed that the melting of SiMn charge materials had occurred at the top part of the coke-bed zone where the distinction between pre-reduced charge materials and liquid slag was clear. Comparing the slag forming temperature range observed in this study, the temperature of the top part coke-bed zone can be assumed to be higher than 1200 °C.

However, previous excavation also observed that slag phase with low MnO and metal phase with considerable manganese and silicon content were present at the top part of the coke-bed zone [20, 22-24]. Most of the reduction had occurred at the top part of the coke-bed zone. In this thesis work, the temperature was higher than 1500 °C when the significant reduction of MnO and SiO$_2$ in SiMn slags had occurred. This implies that the temperature of the top part of the coke-bed zone can be higher than 1500 °C, which is sufficient for both melting of charge materials and reduction of MnO and SiO$_2$ in liquid slag.

The fact that most of MnO and SiO$_2$ reduction had occurred at the top part of the coke-bed zone can be related to the viscosity change of SiMn slag with high reduction rates, which was shown in **Figure 4.32**. It was observed that the viscosities of SiMn slags with high reduction rates, charges "As/HCS" (Assmang ore + quartz + HC FeMn slag + coke) and "HCS" (quartz + HC FeMn slag + coke), had increased due to the reduction of MnO despite with increasing temperatures. Increasing slag viscosity at the top part of the coke-bed zone is considered not to be favorable for slag to flow into the coke-bed zone. Unless this can be visually observed, it is not clear why most of the reduction occurs at the top part of the coke-bed zone [21-23, 95], but the increasing slag viscosity due to high and fast reduction rates of MnO and SiO$_2$ can be related.

Based on effect of sulfur on the reduction rate of MnO and SiO$_2$, it is plausible that the initial amount of sulfur in the charge materials, which is mainly from using HC FeMn slag as raw material, may play an important role because the effect of sulfur for enhanced reduction rates was clearly observed in this thesis work. Without using HC FeMn slag as raw material, it is also plausible to achieve high reduction from adding sulfur containing raw materials, because high reduction was also observed from charge "As" (Assmang ore + quartz + coke) with different amount of sulfur in **Figure 4.35**. In addition, the temperatures, which were observed in the experimental work, can be used as references related to the materials flow in the SiMn process. For convenience of discussing the temperature relevance between observation from this thesis work and previous excavations, an illustration of the materials flow in the SiMn process is depicted in **Figure 5.11**.

Materials flow

Initial charge * **Pre-reduction** **Melting** **Complete liq. slag** **Reduction**

Mn-sources

$Mn_xO_{y\,(s)} + CO_{\,(g)} \rightarrow MnO_{\,(s)} + CO_{2\,(g)}$
$Fe_xO_{y\,(s)} + CO_{\,(g)} \rightarrow Fe_{\,(s)} + CO_{2\,(g)}$
(Solid-state reduction)

$MnO_{\,(s)} \rightarrow MnO_{\,(l)}$

$Fe_{\,(s)} \rightarrow Fe_{\,(l)}$
(Carbon saturated)

MnO
SiO_2
CaO
MgO
Al_2O_3
(Liquid SiMn slag)

SiMn slag

$MnO_{\,(l)} + C \rightarrow Mn_{\,(l)} + CO_{\,(g)}$
$SiO_{2\,(l)} + 2C \rightarrow Si_{\,(l)} + 2CO_{\,(g)}$
(SiMn metal)

Quartz / Quartzite

$SiO_{2\,(s)}$

$SiO_{2\,(s)} \rightarrow SiO_{2\,(l)}$

Fluxes

$CaCO_{3\,(s)} \rightarrow CaO_{\,(s)} + CO_{2\,(g)}$
$CaMg(CO_3)_{2\,(s)} \rightarrow CaO \cdot MgO_{\,(s)} + 2CO_{2\,(g)}$
(Decomposition)

$CaO_{\,(s)} \rightarrow CaO_{\,(l)}$
$MgO_{\,(s)} \rightarrow MgO_{\,(l)}$

$Fe_{\,(l)}$
(Carbon saturated)

Coke

$C_{\,(s)}$

$C_{\,(s,\,diss.)}$

$C_{\,(s,\,diss.)}$

$C_{\,(s,\,diss)}$

$H_2O_{\,(l)} \rightarrow H_2O_{\,(g)}$
(Evaporation of moisture: Common)

Sulfur affects the reduction rate considerably

Temperature Ambient temperatures before furnace

T < 1200 °C ~ 1200 °C ~ 1400 °C 1500 − 1650 °C

Pre-reduction zone Coke-bed zone (top part)

* **The initial amount of sulfur is critical for high reduction: S > 0.3 wt%**

Figure 5.11: Materials flow and temperature based on the previous SiMn furnace excavations [1, 20-24, 28, 94, 95] and the present thesis work. General liquid slag is complete at approximately 1400 °C, and the significant reduction starts to occur above 1500 °C. Initial sulfur content in the charge can be an important factor to consider for SiMn process as it will significantly influence the reduction rate of MnO and SiO_2 at the top part of the coke-bed zone. Note that the solid-state reduction of manganese sources is only for expression (chemical stoichiometry incorrect).

5.5 The effect of sulfur in SiMn slags

The effect of sulfur on the reduction rates of MnO and SiO_2 in SiMn slags was clearly observed in this study. Sulfur content of more than approximately 0.3 wt% in the initial SiMn charge was necessary to enhance the reduction rates. However, it was only assumed in this work that sulfur had influenced the metal producing rate of MnO reduction by lowering the interface tension between metal (dissolved carbon) and slag. In this section, the effect of sulfur from previous and recent studies in iron and steel production is briefly discussed and compared with the thesis work to find kinetic information on the effect of sulfur during MnO reduction in SiMn slags. Accumulating the results and information, a conceptual mechanism for the effect of sulfur in MnO reduction from SiMn slags is proposed by comparing the Arrhenius and Eyring equations. Note that the limitation of the proposition is also described in the discussion.

The reduction of MnO between slag and dissolved carbon in the metal phase was assumed to be influenced by sulfur in this study. The metal phases were covered with a manganese sulfide (MnS) layer which was shown in the elemental mapping results in **Figure 4.45**. As sulfur is known to be a surface-active specie for most metals [82], the reduction rate of MnO between slag and dissolved carbon in the metal phase may had been possibly enhanced by sulfur. Sulfur decreases the metal surface tension and eventually increases more nucleation sites for CO gas formation.

Besides the parallel projects discussed so far, another parallel work also studied the reduction rates of MnO in SiMn slags [96], where similar experimental methods with this work were considered. Synthetic SiMn slags with different amount of sulfur between 0.2 and 1.0 wt% were heated up to 1600 °C in CO atmospheric pressure, where the reduction rates of MnO between slag-coke and slag-metal interfaces were compared. The effect of sulfur was also confirmed, and it was observed that the reduction rate of slag-metal interface was much higher than the slag-coke interface, where sulfur had a greater acceleration impact on the former.

The influence of sulfur in iron and steel production was observed and studied for more than 50 years, where similar effects were observed [98-102]. Recent studies observed that the sulfur amount had controlled the CO gas evolution rate between slag and metal interfaces [101, 102]. Decreased metal surface tension by sulfur had increased the nucleation rate of gas bubbles, while also simultaneously poisoning the bubble surface to decrease the bubble growth rate. The competing relation due to the effect of sulfur is described in **Figure 5.12**.
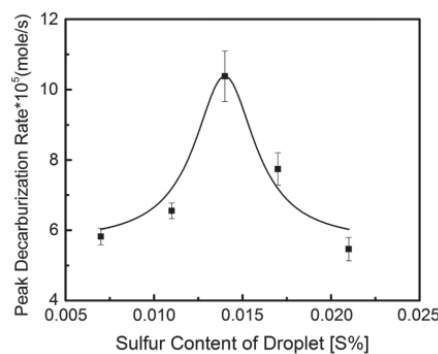
Figure 5.12: Peak decarburization rate as a function of metal sulfur content [102]. Result shows the competing relation between formation of nucleation sites and surface poisoning of CO gas from the effect of sulfur.

Comparing the effect of sulfur between MnO reduction and iron/steel production at the slag-metal interface, it is plausible that the similar phenomena of CO gas evolution from iron and steel production had also occurred with MnO reduction in SiMn slags. The high reduction rates of MnO observed from this thesis work implies high evolution rate of CO gas due to the effect of sulfur.

The high reduction rates in this study indicate that massive evolution of CO gas had occurred from the effect of sulfur. Part of **Table 4.32**, which is the summarized activation energy and pre-exponential constants from experiments with synthetic SiMn charges (research topic #4), is shown again for convenience to discuss the effect of sulfur.

Table 4.32: Summary of the activation energies and pre-exponential constants for MnO reduction of the synthetic charges with different amount of sulfur between 1500 and 1650 °C. Increasing pre-exponential constant implies increasing nucleation sites for CO gas evolution with increasing amount of sulfur. Note that part of MnO reduction in Table 4.32 is shown again for convenience.

Reduction	Charge	E_a [kJ/mol]	k_0 [g/min · cm^2]	Int. Sulfur [wt%]
MnO	Syn. 0	∼ 30	1.04×10^{-2}	0
	Syn. 0.3	∼ 215	1.56×10^{4}	0.3
	Syn. 0.6	∼ 415	7.99×10^{9}	0.6
	Syn. 0.9	∼ 425	1.51×10^{10}	0.9

According to current or classical kinetic theory [89-92], the pre-exponential constant can be thought to be the rate of MnO reduction from an ideal state, where the energy barrier (activation energy) is absent. Correspondingly, the pre-exponential constant relates to the CO gas evolution rate, which implies that nucleation sites for CO gas evolution increases with increasing amount of sulfur. The wetting characteristics of sulfur is likely to increase more valid nucleation sites for CO gas evolution.

Although the comparison between MnO reduction in SiMn slags to iron/steel production can be used to envisage the vague mechanism from the effect of sulfur, the kinetic parameters from the Arrhenius equation are not suitable to support this conception. It should carefully be aware that both the Arrhenius activation energy and pre-exponential constant are determined experimentally, where the parameters do not simply relate to the threshold energies and number of successful reactions. In other words, the Arrhenius equation derives from empirical observations and ignores any mechanistic considerations. It is a phenomenal expression of reactions, which many reactions follow.

To support and relate the CO gas evolution from the effect of sulfur for MnO reduction in SiMn slags, a theoretical approach can be considered since further kinetic information is difficult to obtain from the empirical (Arrhenius) studies. The transition state theory (TST), which was developed by H. Eyring, M. G. Evans and M. Polanyi, was successful to address the meaning of the activation energy and pre-exponential constant [103-105]. The transition state theory is further briefly explained and discussed to support the concept of CO gas evolution from the effect of sulfur. Note that this is a theoretical approach based on observation from previous and present work, and the limitation of this approach is also described in the later part of this section.

The transition state theory leads to the Eyring equation which is shown in **Equations (5.1)** and **(5.2)**, and a simple illustration of the theory is shown in **Figure 5.13**. For convenience, the comparison between the Arrhenius and Eyring equations is also described in **Table 5.2**.

$$k_{Ey.} = \left(\frac{k_B \cdot T}{h}\right) \cdot e^{\frac{R + \Delta S^{\ddagger}}{R}} \cdot e^{-\frac{Ea}{RT}} = k_* \cdot e^{-\frac{Ea}{RT}} \tag{5.1}$$

$$k_* = \left(\frac{k_B \cdot T}{h}\right) \cdot e^{\frac{R + \Delta S^{\ddagger}}{R}} \tag{5.2}$$

where $k_{Ey.}$ [1/s] is the reaction rate constant by the transition state theory, k_B [J/K] is the Boltzmann constant, T [K] is the temperature, h [J·s] is the Planck's constant, R [J/K·mol] is the gas constant, $\Delta S^{\ddagger}$ [kJ/K·mol] is the entropy of activation and Ea [kJ/mol] is the activation energy.

$$A + B \rightleftarrows X^{\ddagger} \rightarrow C + D$$
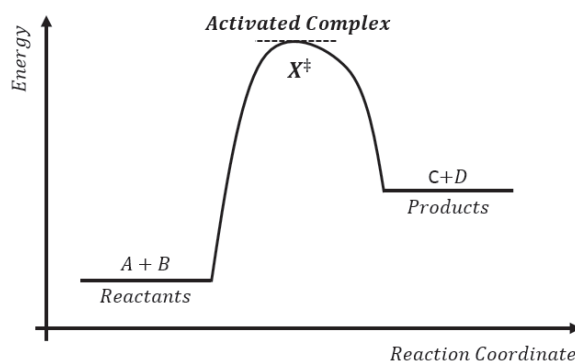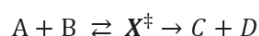
Figure 5.13: Illustration of the transition state theory. Theory assumed that the activated complexes ($X^{\ddagger}$) are in quasi-equilibrium state with the reactants with relatively high energy, which are to be always in the process of decomposing.

Table 5.2: Comparison between Arrhenius (Equation (2.19)) and Eyring equation. Limitation of kinetic information from the Arrhenius equation can be expanded and discussed by the Eyring equation. Note that two kinetic expressions are analogous where the key difference is the pre-exponential constant.

Kinetic expression	Notes
- Arrhenius - $k_{Arr.} = k_o \cdot e^{-\frac{Ea}{RT}}$	• Phenomenal expression of chemical reactions, which many reactions follow • Kinetic parameters are empirically determined, which lack physical meanings • Ignores mechanistic information of reactions
- Eyring - $k_{Ey.} = k_* \cdot e^{-\frac{Ea}{RT}}$	• Theoretical approach of chemical reactions • Based on the transition state theory (TST) • Provides clues of reaction mechanisms

The theory assumes that the activated complexes ($X^{\ddagger}$) are in quasi-equilibrium state with the reactants, where the formation details of the activated complexes are not important. The activated complexes are relatively high in energy and are assumed to always be in the process of decomposing. When the potential energy is sufficient, the activated complexes can convert into products, and the kinetic theory can be used to calculate the rate of this conversion. Calculating the entropy of activation ($\Delta S^{\ddagger}$) will provide mechanistic information of the reaction since it indicates the degree of disorder when the reactants change from their initial state to the activated complexes (or transition state).

To apply the transition state theory to the present thesis work, the Eyring plot of MnO reduction for industrial and synthetic SiMn charges in experiments from research topics #3 and #4 were constructed based on the following assumption below this paragraph. Note that the Eyring plot is the analogous expression with Arrhenius plot, which were described in **Figures 4.29 (a)** and **4.44 (a)**. The Eyring plot considered for this work is described in **Figure 5.14**, where the added term "$A/60m_{MnO}$" is the amount of MnO (m_{MnO}) and reaction area (A) from the experiments to unify the units of rate constants (g/min·cm^2).

$$\ln\left(\frac{k_{Ey.}}{T} \times \frac{A}{60m_{MnO}}\right) = \ln\left(\frac{k_B}{h}\right) + \frac{R + \Delta S^{\ddagger}}{R} - \frac{E_{MnO}}{R} \cdot \left(\frac{1}{T}\right)$$

$$\ln k_{Arr} = \ln k_o - \frac{E_{MnO}}{R} \cdot \left(\frac{1}{T}\right)$$

Figure 5.14: Illustration describing the similarity between Eyring (top equation) and Arrhenius (bottom equation) plots. Key difference is that the pre-exponential term in Eyring plot provides clues of the reaction mechanism for MnO reduction ($\Delta S^{\ddagger}$). Note that term "$A/60m_{MnO}$" is added to unify the units.

- Assumption: The measured rate constants of MnO reduction from the Arrhenius plot represent the rate of MnO reduction in SiMn slags but without physical meaning: $k_{Arr.} \approx k_{Ey.}$

The calculated entropies of activation for industrial and synthetic SiMn charges are shown in **Tables 5.3** and **5.4**, respectively. The activation energies estimated from both Arrhenius and Eyring plots are also shown for comparison.

Table 5.3: Calculated entropy of activation ($\Delta S^{\ddagger}$) of MnO reduction from industrial SiMn charges (research topic #3) between 1500 and 1650 °C. Comparison of the activation energies between Arrhenius and Eyring plots are also shown. Positive entropies of activation indicate that the activated complexes are more disordered than the reactants, which can related to the increasing CO gas evolution from the effect of sulfur. Note that the activation energies from both Arrhenius and Eyring plots were similar.

Charge No.	Entropy of activation, $\Delta S^{\ddagger}$ [kJ/K·mol MnO]	Activation energy, E_{MnO} [kJ/mol MnO]		Notes
		Arrhenius plot	Eyring plot	
As	**-0.20**	~ 250	225	Low reduction (Low sulfur: S < 0.3 wt%)
As/HCS	**0.20**	~ 920	930	High reduction (High sulfur: S > 0.3 wt%)
HCS	**0.10**	~ 780	760	

As: Assmang ore + quartz + coke
As/HCS: Assmang ore + quartz + HC FeMn slag + coke
HCS: quartz + HC FeMn slag + coke

Table 5.4: Calculated entropy of activation ($\Delta S^{\ddagger}$) of MnO reduction from synthetic SiMn charges (research topic #4) between 1500 and 1650 °C. Comparison of the activation energies between Arrhenius and Eyring plots are also shown. Competing relation between formation of nucleation sites and surface poisoning of CO gas from the effect of sulfur is reflected by the different positive values of the entropies of activation in charges "Syn. 0.3", "Syn. 0.6" and "Syn. 0.9". Note that the discrepancy of the activation energies was not clear but assumed to be from the amount of data between 1500 and 1650 °C. Only 7 experiments were between 1500 and 1650 °C with synthetic charges, while it was 16 with industrial charges.

Charge No.	Entropy of activation, $\Delta S^{\ddagger}$ [kJ/K·mol MnO]	Activation energy, E_{MnO} [kJ/mol MnO]		Notes
		Arrehnius plot	Eyring plot	
Syn. 0	**-0.29**	~ 30	57	Low reduction (without sulfur: 0 wt%)
Syn. 0.3	**0.15**	~ 215	830	High reduction (with sulfur: 0.3 − 0.9 wt%)
Syn. 0.6	**0.38**	~ 415	1240	
Syn. 0.9	**0.24**	~ 425	985	

Syn: MnO-SiO$_2$-CaO + Sulfur between 0 and 0.9 wt%

The calculated entropies of activation showed corresponding results to the conception of CO gas evolution in MnO reduction, which was envisaged based on the effect of sulfur from this thesis work and from recent iron and steel production studies. The negative entropy of activation of charge "As" indicates that the activated complexes in the transition state are less disordered than the reactants, MnO and C. However, the positive values in charges "As/HCS" and "HCS" indicate that the activated complexes at the transition state are relatively more disordered than the reactants. The positive entropies of activation suggest that the entropy increases upon achieving the transition state, which often leads to a dissociative mechanism [106]. The activated complexes are loosely bound and about to dissociate. To relate this with the evolution rate of CO gas from the effect of sulfur, it is plausible that sulfur allows the "cis effect" [107, 108] where more unstable CO ligands are formed from increased wetting between slag and metal by sulfur. A ligand is an ion or molecule that binds to a central metal atom to form a complex. The same inducement can be observed with synthetic SiMn charges, where the calculated entropies of activation showed the similar results. Positive values were calculated only with synthetic charges containing sulfur.

In addition, the different positive values of the entropy of activation suggest that both high evolution and surface poisoning of CO gas from the effect of sulfur also occurs for MnO reduction in SiMn slags. The competing relation was discussed from the recent iron and steel production studies in **Figure 5.12** [101, 102]. The lower entropy of activation in charge "HCS" than "As/HCS" implies that the nucleation sites of CO gas evolution on the metal surface can be simultaneously hindered by CO gas bubbles. This can correlate to the reduction rates observed in this study, where the reduction rate was faster with charge "As/HCS" than "HCS". The comparison of the positive entropies of activation with synthetic SiMn charges seems to show the same reason. The reduction rates of synthetic charges with sulfur content between 0.3 and 0.9 wt% were similar between 1500 and 1650 °C, but the lowest MnO content at 1650 °C was observed with charge "Syn. 0.6" in **Tables 4.24** and **4.25**. This can also correlate to the mass change results of parallel study in **Figure 4.57** [86], where the fastest reduction of the synthetic replica was observed when the sulfur content was 0.26 wt% rather than 1.0 wt%. An illustration of the effect of sulfur in MnO reduction with the conceptual mechanistic information from this discussion is described in **Figure 5.15**.

Sulfur: Allows more unstable CO ligands

2 *Super weak bonds*

$$MnO \; + \; C \; \rightleftharpoons \; Mn \cdots \cdots O \cdots \cdots C \; \longrightarrow \; Mn \; + \; CO$$

Reactants　　　　**Activated complex**　　　　**Products**

$X^{\ddagger}$
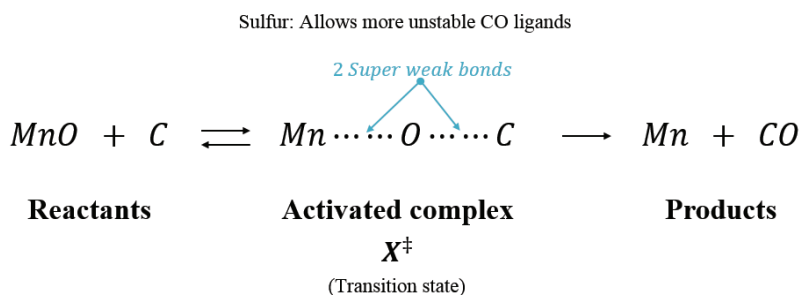
(Transition state)

Figure 5.15: Conceptual illustration of the MnO reduction in SiMn slags based on the transition state theory. Positive entropy of activation from Tables 5.3 and 5.4 suggests that the activated complex is more disordered than the reactants, which can lead to a dissociative mechanism. Sulfur seems to control the amount of unstable CO ligands.

Thus, the calculated entropy of activation by adapting the transition state theory into this work supports the mechanistic concept of the effect of sulfur in MnO reduction from SiMn slags, which was not able to assert from using kinetic information by Arrhenius equation.

However, one should carefully be aware that the discussion of the effect of sulfur is only based on the results of this work and similar observations from iron and steel studies and holds a critical limitation to accept the proposed mechanistic information of the effect of sulfur. Although the transition state theory allows conceptual mechanisms of chemical reactions, the activated complex ($X^{\ddagger}$) cannot be studied spectroscopically and one needs to make assumptions about size, shape and structure of the complex. The transition state theory can be useful to illustrate ideals of how chemical reactions occur in a molecular level and many studies had considered it [109], but without evidential existence of the activated complex, the theory is limited to conceptual description of kinetic information.

Chapter 6: Conclusions

The kinetic information in the SiMn process from the melting of raw materials to the production of metal was studied in this thesis work. It was observed that formation of SiMn slag occurs at relatively low temperature below 1400 °C but the main reduction starts to occur above 1500 °C. During the reduction of MnO and SiO$_2$ at relatively high temperatures, the amount of sulfur clearly influenced the reduction rates where the threshold amount was approximately 0.3 wt%. The last chapter summarizes the experimental methods and highlighted results from the four research topics. In addition, recommendations for further work are summarized.

6.1 The melting behavior of raw materials (Research topic #1)

The formation of slag from melting of SiMn charge materials were studied between 1200 and 1400 °C under CO atmospheric pressure. Two arbitrary SiMn charges with particle sizes between 4.0 and 6.3 mm, "M1" (Assmang ore + quartz + HC FeMn slag + coke) and "M2" (Assmang ore + quartz + coke), were initially compared to observe the effect of HC FeMn slag, which has a relatively low melting temperature around 1250 °C. The following bulleted points summarizes the conclusions of the melting behavior or raw materials:

- Regardless of using HC FeMn slag as raw material, both charges "M1" and "M2" showed similar melting temperatures, where the initial melting of raw materials were observed at around 1250 °C and completion of liquid slag at 1400 °C.

- As an additional experiment, melting of raw materials in Charge "M3" (Assmang ore + quartz) with increased particle sizes between 15 and 20 mm was also observed. The melting of Assmang ore and quartz had rapidly occurred between 1275 and 1300 °C, and the general liquid slag was completed around 1400 °C. It was observed that there was a strong interaction between manganese source and quartz, namely MnO and SiO2, where the contact between the two materials was the prerequisite factor for slag generation between 1200 and 1400 °C.

- The EPMA analyses gave corresponding results, where it was observed that the formation of SiMn slag complies to the simple MnO-SiO$_2$ binary system regardless of the charge compositions. The individual melting temperatures of raw materials were of less relation. Parallel and recent studies with Comilog ore had also shown the similar results.

6.2 The reduction behavior of SiMn charges (Research topic #2)

The reduction behavior of arbitrary SiMn charges were observed through mass change data obtained from TGA experiments between 1200 and 1600 °C in CO atmospheric pressure. As reference, a FeMn charge was also used for comparison. FeMn charge "R1" (Assmang ore + coke) and SiMn charges "R2" (Assmang ore + quartz + coke) and "R3" (Assmang ore + quartz + HC FeMn slag + coke) were each divided into two particle size groups, 0.6 − 1.6 and 4.0 − 6.3 mm, to observe the effect of particle sizes during reduction. The conclusions from the comparison of the reduction behavior are shown in the following bulleted points:

- The reduction behavior differed between charge types. The reduction of FeMn charge was progressive, while the reduction of SiMn charges was divided into two stages between 1200 and 1600 °C. SiMn charges initially showed a relatively low reduction and a subsequent rapid reduction, where the dividing temperature was approximately 1500 °C. Charges based on Comilog ore had also showed the similar results.

- The effect of particle sizes was only observed with FeMn charges, where the charge with smaller particles showed faster reduction. The reduction rates were similar with SiMn charges regardless of the particle sizes. Similar results were also observed with Comilog-based charges.

- The reduction behavior comparison between FeMn and SiMn charges below 1500 °C was reflected from the different driving forces of MnO reduction. The driving force in FeMn charge is relatively higher than SiMn charges due to the presence of solid MnO phases in slag, while it is considerably lower in SiMn slags due to the presence of only liquid slag phase.

- The different effect of particle sizes in FeMn and SiMn charges were explained from the results of previous experiments in research topic #1. The effect of particle sizes in SiMn charges are nullified due to the early slag formation at relatively low temperatures.

6.3 Kinetic estimations (Research topic #3)

The kinetic information of MnO and SiO_2 reduction with SiMn charges between 1500 and 1650 °C under CO atmospheric pressure was studied. The following rate models were used to describe the reduction rates of MnO and SiO_2, where the chemical reaction was assumed to be the rate-determining step:

$$r_{MnO} = k_{MnO} \cdot A \cdot (a_{MnO} - \frac{a_{Mn}}{K_{MnO}})$$

$$r_{SiO_2} = k_{SiO_2} \cdot A \cdot (a_{SiO_2} - \frac{a_{Si}}{K_{SiO_2}})$$

Three Assmang ore-based SiMn charges based on the manganese bearing materials were considered Charges "As" (Assmang ore + quartz + coke), "As/HCS" (Assmang ore + quartz + HC FeMn slag + coke) and "HCS" (quartz + HC FeMn slag + coke). Three Comilog ore-based SiMn charges from parallel studies were also observed: Charges "L1" (Comilog ore + quartz + coke), "L2" (Comilog ore + quartz + limestone + coke) and "L3" (Comilog ore + quartz + HC FeMn slag + coke). The following bulleted points describes the conclusions of research topic #3:

- It was observed that SiMn charges containing HC FeMn slag as raw material showed faster and higher reduction rates than charges without. Addition of limestone did not affect the reduction rates.

- The results and comparisons had indicated that the reduction rates of different SiMn charges were more influenced by the slag properties (rate constant) rather than the driving force. Comparison from the slag properties showed implications that the amount of sulfur as impurity element affects the reduction rates more than the slag viscosity and amount of iron.

- The two rate models were applicable to describe the changing amounts of MnO and SiO_2 in various SiMn slag with different reduction degrees.
- Assuming that the effect of sulfur is superior than the effect of iron, additional experiments with charge "As" with different amount of sulfur between 0.3 and 1.0 wt% were conducted. The results showed that the reduction rates increase significantly with increasing amount of sulfur.

6.4 Confirmation through synthetic materials (Research topic #4)

The effect of sulfur in MnO and SiO_2 reduction was further studied with synthetic SiMn slags between 1500 and 1650 °C in CO atmospheric pressure. Controlled synthetic slags of three components, MnO-SiO_2-CaO, with different amount of sulfur between 0 and 0.9 wt% were compared to observe the effect of sulfur in MnO and SiO_2 reduction. In addition, a synthetic slag without CaO was used as a reference to observe the effect of slag viscosity in reduction rates. The conclusions are described in the following bulleted points:

- The results from the mass change data showed that 0.3 wt% sulfur was the threshold amount for enhanced reduction rates and increasing the amount of sulfur between 0.3 and 0.9 wt% did not gave significant difference. CaO addition did not gave considerable difference on the reduction rates.

- From the kinetic estimations, it was observed that sulfur does not behaves as a catalyst in the reduction of MnO but was assumed to influence the reduction rate by increasing the wetting between slag and dissolved carbon in the metal phase.

- The reduction path in the MnO-SiO_2-CaO system between 1200 and 1650 °C was described by using the two rate models of MnO and SiO_2 reduction. The initial direction of the reduction was determined by the CaO/SiO_2 ratio, where the alteration of the direction indicates occurrence of considerable SiO_2 reduction. However, the degree of reduction was determined by the amount of sulfur in the system.

6.5 Further work

There remain some areas in the melting behavior of raw materials and reduction rate of MnO and SiO_2 in the SiMn process which can be further investigated. The following additional experiments are recommended for further ascertaining the kinetic information in the SiMn process.

- It is recommended to find other possible factors which can influence the melting of raw materials in the SiMn process. The results of the present work showed that the contact between pre-reduced manganese source and quartz was the main reason for the slag generation between 1200 and 1400 °C in CO gas. Since the melting behavior was observed with industrial materials, further investigation of gangue properties in the raw materials can be done. For example, the slag forming behavior of MnO and SiO_2 with different amount of CaO, MgO, Al_2O_3 and Fe_3C at different temperatures between 1200 and 1400 °C can be further investigated with synthetic materials.

- The slag loss from wetting or foaming of slag could be investigated more thoroughly. As described from the mass change results, slag samples were loss from the crucibles at temperatures higher than 1600 °C. It is unclear whether wetting or foaming of slag had occurred during the experiments and the reasons can be further investigated.

- The wetting or foaming or slag affecting the two rate models can also be further investigated in future studies. Although the two rate models were able to describe the changing amount of MnO and SiO_2 in different SiMn slags, reduction rates and heating rates, deviation between the model and measured had occurred due to wetting or foaming of slag between 1610 and 1650 °C. This was assumed to affect the reaction area of reduction and caused the deviation between the model and measured. Thus, an improvement of the two rate models which can also encompass the slag wetting or foaming at high temperatures is necessary.

- The effect of slag viscosity, iron and sulfur on the reduction rate of MnO and SiO_2 should be further observed in larger scale experiments. Although the amount of sulfur was more effective than the slag viscosity or the amount of iron, the results were observed in small-scale laboratory experiments. Each factors influencing the reduction rate should be investigated in larger portion and experimental methods, such as pilot-scale furnace experiments, before authoritative propositions can be made.

References

[1]   S. E. Olsen, M. Tangstad & T. Lindstad. "Production of Mangansese Ferroalloys". Tapir Academic Press, Trondheim (Norway) 2007.

[2]   International Manganese Institute (2014), www.manganese.org. Accessed Sept. 2015.

[3]   Y. Tomota, M. Strum & J. Morris Jr.. "The Relationship Between Toughness and Microstructure in Fe-high Mn Binary Alloys". Metallurgical Transactions A, 1987. 18(6).

[4]   D. K. Subramanyam, A. E. Swansiger & H. S. Avery. "Austenitic Manganese Steels in Properties and Selection: Irons, Steels and High-Performance Alloys". ASM International, 1990. 822-840.

[5]   G. F. Deev. V. V. Popovich & V. N. Palash. "Role of FeS in The Formation of Cracks in Weld Joints". Materials Science, Vol. 18 No. 3, May-Jun. 1982. 109-112.

[6]   J. R. Cain. "Influence of Sulphur, Oxygen, Copper and Manganese on the Red-Shortness of Iron". Technological Papers of The Bureau of Standards No. 261 (Department of commerce, USA), Jul. 30, 1924. 327-335.

[7]   S. I. Gubenko & A. M. Galkin. "Nature of The Red-Shortness of Steel". Metal Science & Heat Treatment, Vol. 26 Issue 10, Oct. 1984. 732-737.

[8]   O. Grong, T. A. Siewert, G. P. Martins & D. L. Olson. "A Model for The Silicomanganese Deoxidation of Steel Weld Metal". Metallurgical Transactions, Vol. 17A, Oct. 1986. 1797-1807.

[9]   R. Elliott, K. Coley, S. Mostaghel and M. Barati. "Review of Manganese Processing for Production of TRIP/TWIP Steels, Part 1: Current Practice and Processing Fundamentals". The Journal of The Minerals, Metals & Materials Society (TMS), 2018. 1-11.

[10]   ASTM International. Designation: A99-82 and A483-10. www.astm.org. Accessed Mar. 2018.

[11]   M. Tangstad, P. Calvert, H. Brun & A. G. Lindseth. "Use of Comilog Ore in FeMn Production". The 10th International Ferroalloys Congress (INFACON 10), Cape Town, Feb. 2004. 213-222.

[12]   Thomas Brynjulfsen. "Reduction of Manganese Ore Agglomerates". PhD Thesis, Dec. 2013, Department of Materials Science and Engineering, Norwegian University of Science and Technology.

[13]   K. Turkova, D. Slizovskiy and M. Tangstad. "CO Reactivity and Porosity of Manganese Materials". ISIJ International, Vol. 54, No. 6, 2014. 1204-1208.

[14]   E. G. Hoel. "Structures and Phase Relations in SiMn Alloys". PhD Thesis, 1998, Department of Metallurgy, Norwegian University of Science and Technology.

[15]   Lalita Boonpriwan. "The South China Sea Dispute: Evolution, Conflict Management and Resolution". ICIRD, 2012.

[16]   Kamrul Hossain. "The UNCLOS and the China-US Hegemoic Competition Over the South China Sea". Journal of East Asia and International Law, No. 6, Apr. 2013. 1-32.

[17]   Terkel Rosenqvist. Principles of Extractive Metallurgy". McGraw-Hill, New York, 131-132.

[18] C. Palache, H. Berman & C. Frondel. "Dana's System of Mineralogy, 7th Ed., Vol. 2". Wiley & Sons, New York 1951. 208-217.

[19] Merete Tangstad. "Metal Production in Norway". Akademika Publishing, Trondheim (Norway) 2013.

[20] S. E. Olsen and M. Tangstad. "Silicomanganese Production – Process Understanding". The 10th International Ferroalloys Congress (INFACON 10), Cape Town, Feb. 2004. 231-238.

[21] Merete Tangstad. "The High Carbon Ferromanganese Process – Coke-bed Relations". PhD Thesis, Apr. 1996, Department of Metallurgy, The Norwegian Institute of Technology (Currently NTNU).

[22] E. Ringdalen and M. Tangstad. "Study of SiMn Production in Pilot Scale Experiments – Comparison of Carajas Sinter and Assmang Ore". The 13th International Ferroalloys Congress (INFACON 13), Almaty, Jun. 2013. 195-206.

[23] P. P. Kim. "SiMn Pilot Scale Experiments: Cross-Section Plates Analyses". Internal report, Department of Materials Science and Engineering, Norwegian University of Science and Technology.

[24] B. Monsen, M. Tangstad, I. Solheim, M. Syvertsen, R. Ishak and H. Midtgaard. "Charcoal for Manganese Alloy Production". The 11th International Ferroalloys Congress (INFACON 11), New Delhi, Feb. 2007. 297-310.

[25] P. A. Eidem, M. Tangstad and J. A. Bakken. "Electrical Conditions of A Coke Bed in SiMn Production". Canadian Metallurgical Quarterly, Vol. 48, No. 4, 2009. 355-368.

[26] M. Tanstad, B. Heiland, S. E. Olsen and R. Tronstad. "SiMn Production in A 150kVA Pilot Scale Furnace". The 9th International Ferroalloys Congress (INFACON 9), Quebec City, Jun. 2001. 202-207.

[27] N. A. Barcza, A. Koursaris, J. B. See and W. A. Gericke. "The Dig-out of A 75 MVA High Carbon Ferromanganese Electric Smelting Furnace". The 37th Electric Furnace Conference, Detroit, Dec. 1979. 19-33.

[28] Merete Tangstad. "Excavation of FeMn Furnaces in 1994 and 1995". Elkem internal report. 1999.

[29] Hamideh Kaffash. "Dissolution Kinetics of Carbon in FeMn Alloys". The 15th International Ferroalloys Congress (INFACON 15), Cape Town, Feb. 2018.

[30] J. K. Wright and B. R. Baldock. "Dissolution Kinetics of Particulate Graphite Injected into Iron/Carbon Melts". Metallurgical and Materials Transactions B, Vol. 19B, 1988. 375-382.

[31] C. Wu and V. Sahajwalla. "Dissolution Rates of Coals and Graphite in Fe-C-S Melts in Direct Ironmaking: Influence of Melt Carbon and Sulfur on Carbon Dissolution". Metallurgical and Materials Transactions B, Vol. 31B, 2000. 241-253.

[32] D. Bandyopadhyay, S. D. Singh, K. K. Singh and K. N. Singh. "A Study on Dissolution Kinetics of Carbon in Liquid Iron Bath". Chemical Engineering Journal, Vol. 92 No. 2, 2003. 79-92.

[33] S. T. Cham, r. Sakurovs, H. Sun and V. Sahajwalla. "Influence of Temperature on Carbon Dissolution of Cokes in Molten Iron". ISIJ International, Vol. 46, 2006. 652-659.

[34]   Jens E. Davidsen. "Formation of Silicon Carbide in The Silicomanganese Process". Master's Thesis, Jun. 2011, Department of Materials Science and Engineering, Norwegian University of Science and Technology.

[35]   Jonas Einan. "Formation of Silicon Carbide and Graphite in The Silicomanganese Process". Master's Thesis, Jun. 2012, Department of Materials Science and Engineering, Norwegian University of Science and Technology.

[36]   E. T. Turkdogan, R. A. Hancock and S. I. Herlitz. "The Solubility of Graphite in Manganese, Cobalt and Nickle". Journal of the Iron and Steel Institute, Vol. 182, 1956. 274-277.

[37]   E. T. Turkdogan and R. A. Hancock. Transactions of the Institute of Mining and Metallurgy Vol. 67, 1957. 1958-1959.

[38]   J. Kr. Tuset and J. Sandvik. "The Solubility of Carbon in Ferrosilicomanganese at 1330-1630 ºC". SINTEF Project, No. B2268 340358. SINTEF, Trondheim (Norway), 1970.

[39]   R. Gee and T. Rosenqvist. "The Vapor Pressure of Liquid Manganese and Activities in Liquid Mn-Si and Carbon-Saturated Mn-Si Alloys". Scandinavian Journal of Metallurgy, Vol. 7, 1976. 57-62.

[40]   R. Ni, Z. Ma and S. Wei. "Thermodynamics of Mn-Fe-C and Mn-Si-C System". Steel Research, Vol. 61, 1990. 113-116.

[41]   W. Z. Ding. "Equilibrium Relations in the Production of Manganese Alloys". PhD Thesis, 1993, Department of Metallurgy, The Norwegian Institute of Technology (Currently NTNU).

[42]   K. Tang, V. Olsø and S. E. Olsen. "Manganese and Silicon Activities in Liquid Carbon-Saturated Mn-Si-C Alloys". Steel Research, Vol. 73, 2002. 77-81.

[43]   W. Ding and S. E. Olsen. "Manganese and Silicon Distribution between Slag and Metal in SiMn Production". ISIJ International, Vol. 40, No. 9, 2000. 850-856.

[44]   Håkon Aleksander Hartvedt Olsen. "A Theoretical Study on the Reaction Rates in the SiMn Production Process". Master's Thesis, Jul. 2016, Department of Materials Science and Engineering, Norwegian University of Science and Technology.

[45]   FactSage 7.0 (CRCT: Canada, GTT: Germany, www.factsage.com. Accessed Sept. 2015.

[46]   B. K. D. P. Rao and D. R. Gaskell. "The Thermodynamic Properties of Melts in The System MnO-SiO2". Metallurgical Transaction B, Vo. 12B, 1981. 311-317.

[47]   S. Gaal, D. Lou, S. Wasbø, B. Ravary and M. Tangstad. "Melting Phenomena in Ferromanganese Production". The 11th International Ferroalloys Congress (INFACON 11), New Delhi, Feb. 2007. 247-257.

[48]   E. Ringdalen, S. Gaal, M. Tangstad and O. Ostrovski. "Ore Melting and Reduction in SiMn Production". Metallurgical and Materials Transactions B, Vol. 41B, 2010. 1220-1229.

[49]   A. G. Blackman, L. R. Gahan, G. Aylward and T. Findlay. "Aylward and Findlay's SI Chemical Data (7th Ed). John Wiley & Sons Australia, Ltd., 2014. 35-92.

[50]   Ihsan Barin. "Thermochemical Data of Pure Substances (3rd Ed.)". VCH Verlagsgesellschaft mbH, 1995. ISBN: 9783527287451. 993-1079.

[51]   W. M. Haynes. "CRC Handbook of Chemistry and Physics (92nd Ed.)". CRC Press, 2011. ISBN: 1439855110.

[52]   S. Gaal, K. Berg, G. Tranell, S. E. Olsen and M. Tangstad. "An Investigation into Aspects of Liquid Phase Reduction of Manganese and Silica Containing Slag". The 7th International Conference of Molten Slags, Fluxes and Salts, Cape Town, Jan. 2004. 651-657.

[53]   R. J. Pomfret and P. Grieveson. "Kinetics of Slag-Metal Reactions". Canadian Metallurgical Quarterly, Vol. 22 No.3, 1983. 287-299

[54]   E. T. Turkdogan, P. Grieveson and J. F. Beisler. "Kinetic and Equilibrium Considerations for Silicon Reaction Between Silicate Melts and Graphite-saturated Iron Part 2: Reaction Kinetics of Silica Reduction". Transactions of the Metallurgical Society of AIME 227, 1963. 1265-1274.

[55]   M. Yastreboff, O. Ostrovski and S. Ganguly. "Effect of Gas Composition on The Carbothermic Reduction of Manganese Oxide". ISIJ International Vol. 43 No. 2, 2003. 161-165.

[56]   A. Schei, J. Kr. Tuset and H. Tveit. "Production of High Silicon Alloys" Tapir Forlag, Trondheim (Norway) 1998. ISBN: 82-519-1317-9. 21-45.

[57]   Weizhong Ding. "Equilibrium Relations in The Production of Manganese Alloys". PhD Thesis, 1993, Department of Metallurgy, The Norwegian Institute of Technology (Currently NTNU).

[58]   W. Ding and S. E. Olsen. "Reaction Equilibria in the Production of Manganese Ferroalloys". Metallurgical and Materials Transaction B, Vol. 27B, 1996. 5-17.

[59]   W. Ding and S. E. Olsen. "Reactions between Multicomponent Slags and Mn-Fe-Si-C Alloys". Scandinavian Journal of Metallurgy, Vol. 25, 1996. 232-243.

[60]   S. E. Olsen, W. Ding, O. A. Kossyreva and M. Tangstad. "Equilibrium in Production of High Carbon Ferromanganese". The 7th International Ferroalloys Congress (INFACON 7), Trondheim, Jun. 1995. 591-600.

[61]   O. Ostrovski, S. E. Olsen, M. Tangstad and M. Yastreboff. "Kinetic Modelling of MnO Reduction from Manganese Ores". Canadian Metallurgical Quarterly, Vol. 41, No. 3, 2002. 309-318.

[62]   Tore-André Skjervheim. "Kinetics and Mechanisms for Transfer of Manganese and Silicon from Molten Oxide to Liquid Manganese Metal". PhD Thesis, Oct. 1994, Department of Metallurgy, the Norwegian Institute of Technology (Currently NTNU).

[63]   O. Olsø, M. Tangstad and S. Olsen. "Reduction Kinetics of MnO-Saturated Slags". SINTEF Report, 1997, STF24 A97624.

[64]   S. Maroufi, G. Ciezki, S. Jahanshahi, S. Sun and O. Ostrovski. "Dissolution of Silica in Slag in Silicomanganese Production". The 14th International Ferroalloys Congress (INFACON 14), Ukraine, May 2015. 479-487.

[65]   S. Maroufi, G. Ciezki, S. Jahanshahi, S. Sun and O. Ostrovski. "Dissolution Rate and Diffusivity of Silica in SiMn Slag". Metallurgical and Materials Transactions B, Vol. 46B, Feb. 2015. 101-108.

[66]   Verein Deutscher Eisenhüttenleute (VDEh). "Slag Atlas, 2nd Edition". Verlag Stahleisen GmbH, D-Düsseldorf (Germany), 1995. 9-20.

[67]   S. E. Olsen. "The Slag Basicity Concept in the HC FeMn Process". The 9th International Ferroalloys Congress (INFACON 9), Quebec City, Jun. 2001. 280-285.

[68]   R. Moretti. "Polymerization, Basicity, Oxidation Stat and Their Role in Ionic Modeling of Silicate Melts". Annals of Geophysics, Vol. 48, 2005. 583-608.

[69]   R. Mozzi and B. Warren. "The Structure of Vitreous Silica". Journal of Applied Crystallography, Vol. 2, 1969. 164-172.

[70]   B. Mysen. "The Structure of Silicate Melts". Annual Review of Earth and Planetary Sciences, Vol. 11, 1983. 75-97.

[71]   B. Mysen. "Relationship Between Silicate Melt Structure and Petrologic Processes". Earth-Science Reviews, Vol. 27, 1990. 281-365

[72]   B. Mysen and P. Richet. "Silicate Glasses and Melts: Properties and Structure; Developments in Geochemistry". Elsevier, Amsterdam (Netherlands) 2005.199-230.

[73]   JH Park. "Structure-Property Relationship of CaO-MgO-SiO$_2$ Slag: Quantitative Analysis of Raman Spectra". Metallurgical and Materials Transactions B, Vol. 44B, 2013. 938-947.

[74]   KY. Ko and JH. Park. "Effect of CaF$_2$ Addition on the Viscosity and Structure of CaO-SiO$_2$-MnO Slags". ISIJ International, Vol. 53, No. 6, 2013. 958-965.'

[75]   JH Park, KY Ko and TS Kim. "Influence of CaF$_2$ on the Viscosity and Structure of Manganese Ferroalloy Smelting Slags". Metallurgical and Materials Transaction B, Vol. 46B, 2015. 741-748.

[76]   JooHyun Park. "Effect of Silicate Structure on Thermodynamic Properties of Calcium Silicate Melts: Quantitative Analysis of Raman Spectra". Metal and Materials International, Vol. 19, No. 3, 2013. 577-584.

[77]   K. Tang and M. Tanstad. "Modeling Viscosities of Ferromanganese Slag". The 11th International Ferroalloys Congress (INFACON 11), New Delhi, Feb. 2007. 344-357.

[78]   J. Safarian, L. Kolbeinsen, M. Tangstad and G. Tranell. "Kinetics and Mechanism of the Simultaneous Carbothermic Reduction of FeO and MnO from High-Carbon Ferromanganese Slag". Metallurgical and Materials Transactions B, Vol. 40B, Dec. 2009. 929-939.

[79]   G. Tranell, S. Gaal, D. Lu, M. Tangstad and J. Safarian. "Reduction Kinetics of Manganese Oxide from HC FeMn Slags". The 11th International Ferroalloys Congress (INFACON 11), New Delhi, Feb. 2007. 231-240.

[80]   T. Skjervheim and S. E. Olsen. "The Rate and Mechanism for Reduction of Manganese Oxides from Silicate Slag". The 7th International Ferroalloys Congress (INFACON 7), Trondheim, Jun. 1995. 631-640.

[81]   X. Kuangdi, J. Guochang, D. Weizhong, G. Liping, G. Shuqiang and Z. Baixiong. "The Kinetics of Reduction of MnO in Molten Slag with Carbon Saturated Liquid Iron". ISIJ International, Vol. 33, No. 1, 1993. 104-108.

[82]   S. Stølen and T. Grande. "Chemical Thermodynamics of Materials". John Wiley & Sons Ltd., (England) 2004.

[83]   Department of materials science and engineering – Laboratory equipment, https://www.ntnu.no/wiki/display/imtlab/Department+of+materials+science+and+engineering+-+Laboratory+equipment. Accessed Sept. 2015.

[84]   Joakim Holtan. "Production of Silicomanganese from Comilog Ore". Master's Thesis, Jun. 2016, Department of Materials Science and Engineering, Norwegian University of Science and Technology.

[85]   Trine A. Larssen. "Reduction of MnO and SiO_2 from Assmang and Comilog based Slags". Master's Thesis, Jun. 2017, Department of Materials Science and Engineering, Norwegian University of Science and Technology.

[86]   Ryosuke Kawamoto. "Effect of Sulphur Addition on Reduction Mechanism of Synthetic Silicomanganese Ore". Unpublished research (Report: TMT 4500 Materials Technology Specialization Project), 2016, Department of Materials Science and Engineering, Norwegian University of Science and Technology.

[87]   P. P. Kim, J. Holtan and M. Tangstad. "Reduction Behavior of Asssmang and Comilog Ore in The SiMn Process". The 10th International Conference on Molten Slags, Fluxes and Salts (MOLTEN 16), Seattle, 2016. 1285-1292.

[88]   P. P. Kim, T. A. Larssen, R. Kawamoto and M. Tangstad. "Empirical Activation Energies of MnO and SiO_2 Reduction in SiMn Slags Between 1500 and 1650 °C". Applications of Process Engineering Principles in Materials Processing, Energy and Environmental Technologies (TMS 17), San Diego, 2017. 475-483.

[89]   M. W. Roberts. "Birth of The Catalytic Concept (1800-1900)". Catalysis Letters, Vol. 67, 2000. 1-4.

[90]   James T. Richardson. "Principles of Catalyst Development". Springer-Verlag (USA) 1989.

[91]   Richard I. Masel. "Chemical Kinetics and Catalysis". John Wiley & Sons Inc. (Canada) 2001.

[92]   M. E. Davis and R. J. Davis. "Fundamentals of Chemical Reaction Engineering". McGraw-Hill Companies, Inc. (USA) 2003.

[93]   Ingeborg Solheim. "Reaction Mechanism of MnO and SiO_2 in SiMn Process: Method Development". SINTEF Project, No. 102010872-2. SINTEF, Trondheim (Norway), 2018.

[94]   M. Tangstad, B. Heiland, S. E. Olsen and R. Tronstad. "SiMn Production in a 150kVA Pilot Scale Furnace". The 9th International Ferroalloys Congress (INFACON 9), Quebec City, Jun. 2001. 401-406.

[95]   B. Monsen, M. Tangstad and H. Midtgaard. "Use of Charcoal in Silicomanganese Production". The 10th International Ferroalloys Congress (INFACON 10), Cape Town, Feb. 2004. 392-404.

[96]   X. Li and M. Tangstad. "The Influence of Sulphur Content on the Carbothermal Reduction of SiMn slag". SINTEF Project, No. 102001892-2. SINTEF, Trondheim (Norway), 2017.

[97]   Jafar Safarian. "Kinetics and Mechanisms of Reduction of MnO Containing Silicate Slags by Selected Forms of Carbonaceous Materials". PhD Thesis, Sept. 2007, Department of Materials Science and Engineering, Norwegian University of Science and Technology.

[98]   H. G. Lee and Y. K. Rao. "Rate of Decarburization of Iron-Carbon Melts: Part 1. Experimental Determination of the Effect of Sulfur". Metallurgical and Materials Transactions B, Vol. 13B, Sept. 1982. 403-409.

[99]   K. Nakashima and K. Mori. "Interfacial Properties of Liquid Iron Alloys and Liquid Slags Relating to Iron- and Steel-making Processes". ISIJ International, Vol. 32, No. 1, 1992. 11-18.

[100]   Y. Zhang and R. J. Fruehan. "Effect of Bubble Size and Chemical Reactions on Slag Foaming". Metallurgical and Materials Transactions B, Vol. 26B, Aug. 1995. 803-812.

[101]   Michael D. Pomeroy. "Decarburization Kinetics of Fe-C-S Droplets in Oxygen Steelmaking Slags". Master's Thesis, Aug. 2011, Department of Materials Science and Engineering, McMaster University.

[102]   K. Gu, N. Dogan and K. S. Coley. "The Influence of Sulfur on Dephosphorization Kinetics Between Bloated Metal Droplets and Slag Containing FeO". Metallurgical and Materials Transactions B, Vol. 48B, Oct. 2017. 2343-2353.

[103]   H. Eyring. "The Activated Complex in Chemical Reactions". The Journal of Chemical Physics, Vol. 3, Feb. 1935. 107-115.

[104]   K. J. Laidler and M. C. King. "Development of Transition-State Theory". The Journal of Physical Chemistry, Vol. 87 (15), Jul. 1983. 2657-2664.

[105]   D. G. Truhlar, B. C. Garrett and S. J. Klippenstein. "Current Status of Transition-State Theory". The Journal of Physical Chemistry, Vol. 100 (31), Aug. 1996. 12771-12800.

[106]   J. H. Espenson. "Chemical Kinetics and Reaction Mechanism". McGraw-Hill (USA) 2002.

[107]   P. Atkins, T. Overton, J. Rourke, M. Weller and F. Armstrong. "Shriver & Atkin's Inorganic Chemistry 5th Ed.". Oxford University Press 2010.

[108]   J. D. Atwood and T. L. Brown. "Cis Labilization of Ligand Dissociation. 3. Survey of Group G and 7 Six-coordinate Carbonyl Compounds. The Site Preference Model for Ligand Labilization Effects". Journal of the American Chemical Society, Vol. 98 (11). 3160-3166.

[109]   Margaret R. Wright. "Introduction to Chemical Kinetics". Wiley 2004.

Appendix A: Calculations of initial and pre-reduced charges

The calculation of mass balance between the initial amount of raw materials and slag/metal composition at 1600 °C is described in this section. An random amount of raw materials were initially considered in the mass balance. Then, according to the targeted slag (approximately 5 wt% MnO and 40 wt% SiO_2) and metal (approximately 18 wt% Si) compositions at 1600 °C, the input raw materials were adjusted. The calculation details of each charge type is shown in the following tables and equations. Note that the chemical composition of raw materials in **Table 3.1** are shown again for convenience.

Table 3.1: Chemical composition of industrial raw materials. Assmang ore and HC FeMn slag were used as manganese-bearing raw materials.

Material	MnO	MnO$_2$	SiO$_2$	Fe$_2$O$_3$	CaO	MgO	Al$_2$O$_3$	S	C	CO$_2$	H$_2$O	Total [wt%]
Assmang	32.69	33.22	5.77	15.06	6.26	1.1	0.26	0.16	0.27	3.52	1.55	99.86
Quartz	0.14	-	93.85	-	0.09	0.05	1.19	-	-	-	-	95.32
HCS*	35.23	-	25.45	-	18.45	7.53	12.3	0.46	0.46	-	2.2	102.08
Coke	0.04	-	5.6	0.86	0.42	0.22	2.79	0.4	87.68	-	15.5	113.51

* HCS: High Carbon FeMn Slag

A.1 Charge "As"

The initial raw materials for charge "As" was Assmang ore, quartz and coke. The amount of each raw material is shown in **Table A.1**.

Table A.1: Initial input of raw materials for charge "As". Note that each amount was randomly considered initially, but adjusted later according to slag and metal composition at 1600 °C.

	Assmang ore	Quartz	HC FeMn slag	Coke	Total [g]
Raw materials input	7	1.94	-	2.2	11.14

The amount of each slag component can be calculated by using the chemical compositions in **Table 3.1**, which is shown in **Table A.2**. Chemical compositions of only Assmang ore and quartz were considered and not coke.

Table A.2: Amount of chemical components of charge "As" according to **Tables 3.1** and **A.1**. Note that chemical components from coke were not included.

	MnO	MnO$_2$	SiO$_2$	Fe$_2$O$_3$	CaO	MgO	Al$_2$O$_3$	C	CO$_2$	H$_2$O	Total [g]
Chemical components	2.30	2.33	2.32	1.06	0.44	0.08	0.04	0.02	0.25	0.11	8.94

Then, the pre-reduced slag composition can be calculated. Complete pre-reduction of raw materials are assumed: All higher manganese oxides are reduced to MnO with CO gas, all iron oxides are reduced to

metallic iron with CO gas, all carbonates are decomposed and all moisture vaporized. The calculated pre-reduced slag and metal composition at 1200 °C is shown in **Tables A.3** and **A.4**.

Table A.3: Calculated pre-reduced slag composition of charge "As" at 1200 °C. Note that the primary slag at 1200 °C is not liquid but shows the initial composition.

Pre-reduced slag	MnO	SiO$_2$	CaO	MgO	Al$_2$O$_3$	Total
[g]	4.20	2.32	0.44	0.08	0.04	7.08
[wt%]	59.35	32.71	6.24	1.11	0.60	100

Table A.4: Calculated pre-reduced metal composition of charge "As" at 1200 °C. Note that the amount of carbon was calculated from **Equation [3]**, where carbon saturation was assumed.

Pre-reduced metal	Mn	Si	C	Fe	Total [g]
[g]	-	-	0.03	0.74	0.77
[wt %]	-	-	4.07	95.93	100

The initial raw materials input can be adjusted by calculating the slag and metal composition at 1600 °C with assumptions: The amount of unreducible oxides (CaO, MgO and Al$_2$O$_3$) is constant. The calculated slag and metal compositions are shown in **Tables A.5** and **A.6**.

Table A.5: Calculated slag composition of charge "As" at 1600 °C. Amount of CaO, MgO and Al$_2$O$_3$ is constant. Targeted slag (MnO and SiO$_2$) compositions are in bold.

Slag at 1600 °C		MnO	SiO$_2$	CaO	MgO	Al$_2$O$_3$	Total
[g]	After cal.	0.05	0.41	0.44	0.08	0.04	1.02
	Before cal.	**x**	**y**				x + y +0.56
[wt%]		**5**	**40**	43.19	7.66	4.16	100

Table A.6: Calculated metal composition of charge "As" at 1600 °C. Amount of manganese and silicon was calculated according to the reduced amount of MnO and SiO$_2$. Amount of iron is constant from the initial condition. Amount of carbon was also calculated using **Equation [3]** assuming carbon saturation. Targeted metal (Si) composition is in bold.

Metal at 1600 °C	Mn	Si	Fe	C	Total
[g]	3.21	0.89	0.74	0.12	4.96
[wt %]	64.75	**17.95**	14.91	2.39	100

A.2 Charge "As/HCS"

The mass balance calculation in charge "As/HCS" are similar with the methods and assumptions used in charge "As". The initial raw materials for charge "As/HCS" was Assmang ore, quartz, HC FeMn slag and coke. The amount of each raw material is shown in **Table A.7**.

Table A.7: Initial input of raw materials for charge "As/HCS". Note that each amount was randomly considered initially but adjusted later according to slag and metal composition at 1600 °C.

Raw materials input	Assmang ore	Quartz	HC FeMn slag	Coke	Total [g]
	4	1.69	4	2.5	12.19

The amount of each slag component in **Table A.7** can be calculated using the chemical compositions in **Table 3.1**, which is shown in **Table A.8**. Chemical compositions of only Assmang ore, quartz and HC FeMn slag were considered and not coke.

Table A.8: Amount of chemical components of charge "As/HCS" according to **Tables 3.1** and **A.7**. Note that chemical components from coke were not included.

Chemical components	MnO	MnO$_2$	SiO$_2$	Fe$_2$O$_3$	CaO	MgO	Al$_2$O$_3$	C	CO$_2$	H$_2$O	Total [g]
	2.70	1.33	2.90	0.60	0.98	0.34	0.52	0.03	0.14	0.15	9.69

Then, the pre-reduced slag composition can be calculated. Complete pre-reduction of raw materials are assumed: All higher manganese oxides are reduced to MnO with CO gas, all iron oxides are reduced to metallic iron with CO gas, all carbonates are decomposed and all moisture vaporized. The calculated pre-reduced slag and metal composition at 1200 °C is shown in **Tables A.9** and **A.10**.

Table A.9: Calculated pre-reduced slag composition of charge "As/HCS" at 1200 °C. Note that the primary slag at 1200 °C is not liquid but shows the initial composition.

Pre-reduced slag	MnO	SiO$_2$	CaO	MgO	Al$_2$O$_3$	Total
[g]	3.79	2.90	0.98	0.34	0.52	8.52
[wt%]	44.45	34.00	11.49	4.01	6.05	100

Table A.10: Calculated pre-reduced metal composition of charge "As/HCS" at 1200 °C. Note that the amount of carbon was calculated from **Equation [3]**, where carbon saturation was assumed.

Pre-reduced metal	Mn	Si	C	Fe	Total [g]
[g]	-	-	0.02	0.42	0.44
[wt %]	-	-	4.07	95.93	100

The initial raw materials input can be adjusted by calculating the slag and metal composition at 1600 °C with assumptions: The amount of unreducible oxides (CaO, MgO and Al_2O_3) is constant. The calculated slag and metal compositions are shown in **Tables A.11** and **A.12**.

Table A.11: Calculated slag composition of charge "As/HCS" at 1600 °C. Amount of CaO, MgO and Al_2O_3 is constant. Targeted slag (MnO and SiO_2) compositions are in bold.

Slag at 1600 °C		MnO	SiO_2	CaO	MgO	Al_2O_3	Total
[g]	After cal.	0.17	1.34	0.98	0.34	0.52	3.34
	Before cal.	**x**	**y**				x + y + 1.84
	[wt%]	**5**	**40**	29.32	10.23	15.54	100

Table A.12: Calculated metal composition of charge "As/HCS" at 1600 °C. Amount of manganese and silicon was calculated according to the reduced amount of MnO and SiO_2. Amount of iron is constant from the initial condition. Amount of carbon was also calculated using **Equation [3]** assuming carbon saturation. Targeted metal (Si) composition is in bold.

Metal at 1600 °C	Mn	Si	Fe	C	Total
[g]	2.81	0.73	0.42	0.10	4.06
[wt %]	69.10	**17.98**	10.41	2.51	100

A.3 Charge "HCS"

The mass balance calculation in charge "HCS" are similar with the methods and assumptions used in charges "As" and "As/HCS". The initial raw materials for charge "HCS" was quartz, HC FeMn slag and coke. The amount of each raw material is shown in **Table A.13**. Note that charge "HCS" lacked iron.

Table A.13: Initial input of raw materials for charge "HCS". Note that each amount was randomly considered initially but adjusted later according to slag and metal composition at 1600 °C.

Raw materials input	Assmang ore	Quartz	HC FeMn slag	Coke	Total [g]
	-	1.46	10	3	14.46

The amount of each slag component in **Table A.13** can be calculated using the chemical compositions in **Table 3.1**, which is shown in **Table A.14**. Chemical compositions of only quartz and HC FeMn slag were considered and not coke.

Table A.14: Amount of chemical components of charge "HCS" according to **Tables 3.1** and **A.13**. Note that chemical components from coke were not included.

Chemical components	MnO	MnO_2	SiO_2	Fe_2O_3	CaO	MgO	Al_2O_3	C	CO_2	H_2O	Total [g]
	3.47	0.00	3.94	0.00	1.82	0.74	1.23	0.04	0.00	0.22	11.46

Then, the pre-reduced slag composition can be calculated. Complete pre-reduction of raw materials are assumed: All higher manganese oxides are reduced to MnO with CO gas, all iron oxides are reduced to metallic iron with CO gas, all carbonates are decomposed and all moisture vaporized. The calculated pre-reduced slag and metal composition at 1200 °C is shown in **Tables A.15** and **A.16**.

Table A.15: Calculated pre-reduced slag composition of charge "HCS" at 1200 °C. Note that the primary slag at 1200 °C is not liquid but shows the initial composition.

Pre-reduced slag	MnO	SiO_2	CaO	MgO	Al_2O_3	Total
[g]	3.47	3.94	1.82	0.74	1.23	11.20
[wt%]	30.98	35.20	16.23	6.62	10.97	100

Table A.16: Calculated pre-reduced metal composition of charge "HCS" at 1200 °C. Note that the amount of carbon was calculated from **Equation [3]**, where carbon saturation was assumed.

Pre-reduced metal	Mn	Si	C	Fe	Total [g]
[g]	-	-	-	~ 0	~ 0
[wt %]	-	-	-	-	-

The initial raw materials input can be adjusted by calculating the slag and metal composition at 1600 °C with assumptions: The amount of unreducible oxides (CaO, MgO and Al_2O_3) is constant. The calculated slag and metal compositions are shown in **Tables A.17** and **A.18**.

Table A.17: Calculated slag composition of charge "HCS" at 1600 °C. Amount of CaO, MgO and Al_2O_3 is constant. Targeted slag (MnO and SiO_2) compositions are in bold.

Slag at 1600 °C		MnO	SiO_2	CaO	MgO	Al_2O_3	Total
[g]	After cal.	0.34	2.76	1.82	0.74	1.23	6.89
	Before cal.	**x**	**y**				x + y +
[wt%]		**5**	**40**	26.39	10.77	17.84	100

Table A.18: Calculated metal composition of charge "HCS" at 1600 °C. Amount of manganese and silicon was calculated according to the reduced amount of MnO and SiO_2. Amount of iron is constant from the initial condition. The amount of carbon was also calculated using **Equation [3]** assuming carbon saturation. Targeted metal (Si) composition is in bold.

Metal at 1600 °C	Mn	Si	Fe	C	Total
[g]	2.42	0.56	0.00	0.05	3.02
[wt %]	80.13	**18.37**	0.00	1.50	100

203

Appendix B: EPMA analyses of charges

The detailed EPMA analyses of the slag phase of charges "M1", "M2", "M3", "R1", "R2", "R3" … are described in this section. The average slag compositions for each phase were obtained by three analysis points.

B.1 Charge "M1"

The chemical analyses of slag phases of charge "M1" (Assmang ore + quartz + HC FeMn slag + coke) at 1250, 1400 and 1530 °C are shown in **Table B.1**.

Table B.1: Detailed chemical analyses of slag phases in charge "M1" according to Figure 4.4.

Position in Figure 4.4	Point	MnO	SiO$_2$	CaO	MgO	Al$_2$O$_3$	Total [wt%]	Temperature [°C]	Notes
A	1	95.6	0.4	2.5	0	0.7	99.2		White spherical (MnO)
	2	97.8	0.1	2.0	0.3	0.5	100.7		
	3	95.6	0.36	2.0	0.24	0.4	98.6		
B	1	42.8	48.6	7.8	0.6	0.1	99.9		Light grey (Slag)
	2	44.1	48.3	8.3	0.9	0.2	101.8	1250	
	3	43.1	49.2	7.9	0.8	0.2	101.2		
C	1	61.2	31.8	2.8	0.8	0.1	96.7		Dark grey (Slag)
	2	61.5	32.5	2.9	1.3	0	98.2		
	3	62.6	31.4	2.2	1.0	0	97.2		
D	1	51.3	38.9	9.2	0.7	1.3	101.4		
	2	50.0	39.3	8.5	0.4	1.1	99.3	1400	
	3	49.3	39.7	8.9	0.4	1.0	99.3		
E	1	50.1	42.3	8.1	1.0	1.3	102.8		De-focused* (Slag)
	2	50.0	43.3	7.9	1.4	1.2	103.8		
	3	49.5	42.9	7.5	1.0	1.1	102	1530	
F	1	50.1	42.0	8.3	1.4	1.6	103.4		
	2	48.6	43.1	8.0	1.3	1.0	102		
	3	49.6	42.8	7.5	1.0	1.1	102		

* 30 µm de-focus measured

B.2 Charge "M2"

The chemical analyses of slag phases of charge "M2" (Assmang ore + quartz + coke) at 1215, 1325, 1400, 1500, 1560 and 1610 °C are shown in **Table B.2**.

Table B.2: Detailed chemical analyses of slag phases in charge "M2" according to Figure 4.5.

Position in Figure 4.5	Point	MnO	SiO$_2$	CaO	MgO	Al$_2$O$_3$	Total [wt%]	Temperature [°C]	Notes
A	1	40.0	50.2	12.0	0.5	1.1	103.8	1215	Light grey phase (Slag)
	2	38.5	50.1	11.2	0.3	1.0	101.1		
	3	38.0	48.0	12.3	0.4	0.7	99.4		
B	1	59.6	33.0	3.5	0.6	0.1	96.8		Dark grey phases (Slag)
	2	60.6	32.1	3.4	1.0	0	97.1		
	3	59.9	31.0	3.1	0.9	0.1	95		
C	1	44.0	47.9	7.6	2.0	0	101.5	1325	Light grey phase (Slag)
	2	42.9	48.3	6.9	1.3	0.4	99.8		
	3	43.8	48.6	6.6	1.5	0.4	100.9		
D	1	59.4	33.0	2.1	1.9	0.2	96.6		Dark grey phases (Slag)
	2	58.9	32.1	2.8	2.0	0	95.8		
	3	60.3	31.6	2.6	1.5	0	96		
E	1	52.9	40.2	4.1	0.9	0.8	98.9	1400	Defocused* (Slag)
	2	54.1	42.0	4.0	0.8	1.0	101.9		
	3	53.3	42.0	3.3	0.5	0.5	99.6		
F	1	47.9	44.5	8.6	1.1	1.6	103.7	1500	
	2	48.4	45.1	9.0	1.0	2.3	105.8		
	3	48.7	44.2	8.9	1.0	2.4	105.2		

* 30 µm defocus measured

B.3 Charge "M3"

The chemical analyses of slag phases of charge "M3" (Assmang ore + quartz) at 1200, 1250, 1275, 1300, 1350 and 1400 °C are shown in **Tables B.3** and **B.4**.

Table B.3: Detailed chemical analyses of slag phases in charge "M3" at 1200 and 1250 °C according to Figure 4.6.

Position in Figure 4.6	Point	MnO	SiO$_2$	CaO	MgO	Al$_2$O$_3$	Total [wt%]	Temperature [°C]	Notes
A	1	0	100.2	0.1	0	0	100.3		Dark phase (Slag)
	2	0	98.3	0	0.1	0	98.4		
	3	0	98.9	0	0	0	98.9		
B	1	98.6	0.5	0.4	0.3	0	99.8		White spherical (MnO)
	2	99.1	0.8	0.2	0.4	0.1	100.6	1200	
	3	97.6	0.6	0.1	0.4	0	98.7		
C	1	51.2	38.8	7.5	0.8	1.2	99.5		Grey (Slag)
	2	50.2	37.9	8.3	1.3	2.0	99.7		
	3	49.9	40.0	7.1	0.5	1.1	98.6		
D	1	0	99.1	0.1	0.1	0.1	99.4		Dark (SiO$_2$)
	2	0.1	99.8	0	0	0	99.9		
	3	0	99.8	0.1	0	0	99.9		
E	1	99.1	0.6	0	0.4	0	100.1		White spherical (MnO)
	2	98.4	1.0	0.1	0.1	0.2	99.8		
	3	99.3	0.9	0.1	0.2	0	100.5	1250	
F	1	62.0	34.1	1.3	1.4	0.3	99.1		Light grey (Slag)
	2	63.0	35	1.9	1.8	0	101.7		
	3	61.9	34.4	1.4	1.0	0.2	98.9		
G	1	46.9	48.5	1.1	2.1	0	98.6		Dark grey (Slag)
	2	47.0	47.8	2.1	1.9	0.5	99.3		
	3	45.0	50.2	1.4	1.0	0.4	98		

Table B.4: Detailed chemical analyses of slag phases in charge "M3" at 1275, 1300, 1350 and 1400 °C according to Figure 4.7.

Position in Figure 4.7	Point	MnO	SiO$_2$	CaO	MgO	Al$_2$O$_3$	Total [wt%]	Temperature [°C]	Notes
A	1	0.1	99.2	0	0	0	99.3		Dark (SiO$_2$)
	2	0	98.9	0.1	0.1	0	99.1		
	3	0	99.3	0	0	0.1	99.4		
B	1	46.9	51.1	2.5	0.8	0	101.3		Dark grey (Slag)
	2	45.1	51.0	2.6	0.6	0.2	99.5		
	3	46.1	50.5	2.1	0.2	0.3	99.2		
C	1	62.6	35.2	1.4	0	0.1	99.3	1275	Light grey (Slag)
	2	60.1	34.6	1.5	0.5	0	96.7		
	3	62.0	39.9	1.5	0.3	0.2	103.9		
D	1	99.8	0.2	0	0.5	0	100.5		White spherical (MnO)
	2	98.9	1.0	0.3	0.5	0.1	100.8		
	3	97.8	0.7	0.3	0.1	0	98.9		
E*	1			Fe			100		White (Fe)
F	1	0.1	100.2	0	0	0	100.3		Dark (SiO$_2$)
	2	0.1	99.5	0	0	0	99.6		
	3	0	99.9	0.1	0	0	100		
G	1	44.1	50.6	4.8	1.1	0	100.6		Dark grey (Slag)
	2	43.2	50.6	4.8	1.5	0.2	100.3		
	3	43.7	50.2	4.9	1.1	0.3	100.2	1300	
H	1	62.3	35.8	2	1.5	0	101.6		Light grey (slag)
	2	61.1	35.0	1.8	1.4	0.1	99.4		
	3	60.0	36.0	1.7	1.4	0.1	99.2		
I	1	97.6	0	0	2.6	0	100.2		White spherical (MnO)
	2	97.1	0.1	0.1	2.5	0	99.8		
	3	96.5	0.2	0	3.0	0.2	99.9		
J	1	0	99.0	0.1	0	0	99.1		Dark (SiO$_2$)
	2	0	101	0.1	0.1	0	101.2		
	3	0.1	100.7	0	0	0	100.8		
K	1	46.2	49.8	1.1	1.5	0	98.6		Dark grey (Slag)
	2	45.2	50.3	1.3	2.4	0.1	99.3	1350	
	3	45.8	50.9	1.3	1.8	0.2	100		
L	1	60.2	36.2	1.0	1.0	0.1	98.5		Light grey (Slag)
	2	60.2	35.0	1.5	1.3	0	98		
	3	62.9	37.1	1.4	1.0	0	102.4		
M	1	0.1	99.0	0.1	0.1	0.1	99.4		Dark (SiO$_2$)
	2	0.2	99.9	0	0	0	100.1		
	3	0	102.9	0	0	0	102.9		
N	1	63.1	34.5	1.7	1.0	0	100.3		Light grey (Slag)
	2	62.0	34.0	2.2	1.2	0.1	99.5	1400	
	3	62.7	35.0	1.5	1.3	0	100.5		
O	1	48.5	45.6	4.4	1.0	0.7	100.2		Dark grey (Slag)
	2	48.5	45.8	4.4	1.0	0.8	100.5		
	3	47.6	45.9	3.9	1.4	1.0	99.8		

* Metal phase: Fe

B.4 Charges "R1", "R2" and R3"

The chemical analyses of slag phases of charges "R1" (Assmang ore + coke), "R2" (Assmang ore + quartz + coke) and "R3" (Assmang ore + quartz + HC FeMn slag + coke) at 1600 °C are shown in **Table B.5**.

Table B.5: Detailed chemical analyses of slag phases in charges "R1", "R2" and "R3" at 1600 °C.

Charge No.	Points	MnO	SiO_2	CaO	MgO	Al_2O_3	Total [wt%]	Particle sizes [mm]
R1.a	1	16.5	40.9	35.9	5.9	1.7	100.9	
	2	15.8	40.1	35.3	6.2	1.5	98.9	0.6 − 1.6
	3	16.5	40.7	36.2	5.5	1.4	100.3	
R1.b	1	20.5	40.6	33.8	3.9	1.6	100.4	
	2	20.7	40.9	33.1	4.0	1.4	100.1	4.0 − 6.3
	3	21.3	40.0	34.1	3.2	1.2	99.8	
R2.a	1							
	2			- Slag not observed -			-	0.6 − 1.6
	3							
R2.b	1	4.2	57.0	30.6	4.9	4.3	101	
	2	4.0	57.1	30.9	4.5	3.6	100.1	4.0 − 6.3
	3	3.6	57.6	30.0	4.0	3.9	99.1	
R3.a	1	10.1	49.3	24.3	5.0	12.5	101.2	
	2	9.3	50.1	24.0	5.8	11.5	100.7	0.6 − 1.6
	3	9.5	48.9	22.9	5.8	11.7	98.8	
R3.b	1	7.5	48.5	26.0	6.9	12.5	101.4	
	2	6.1	49.0	27.3	6.4	11.9	100.7	4.0 − 6.3
	3	6.8	49.0	26.5	5.7	12.0	100	

Appendix C: Mass change results of FeMn and SiMn charges

The mass change results of pre-reduction between 1500 and 1650 °C of FeMn and SiMn charges are shown in this section.

### C.1 Charges "R1", "R2" and "R3" (Pre-reduction)

The mass change results during the pre-reduction condition of charges "R1" (Assmang ore + coke), "R2" (Assmang ore + quartz + coke) and "R3" (Assmang ore + quartz + HC FeMn slag + coke) between 25 and 1200 °C are shown in **Figure C.1**. The mass changes of complete pre-reduction for charges "R1", "R2" and "R3" were approximately -21, -19 and -24 wt%, respectively.
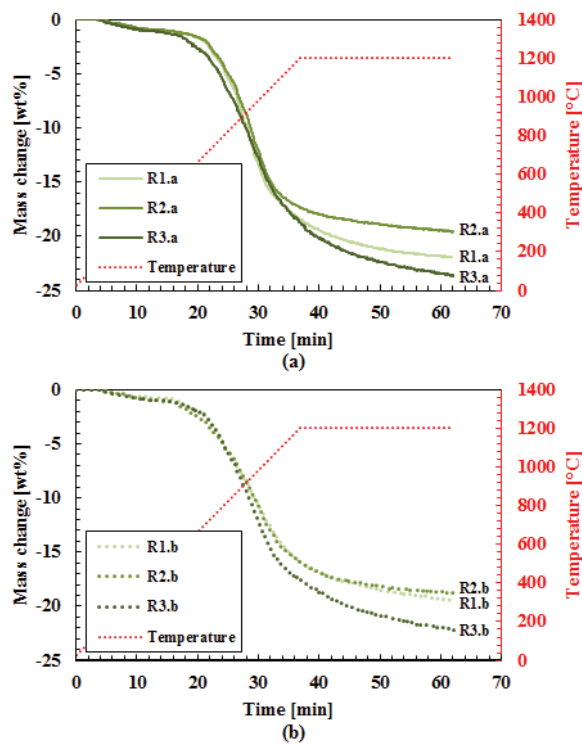
Figure C.1: Pre-reduction results of charges "R1", "R2" and "R3" with two different particle sizes, (a) 0.6 − 1.6 and (b) 4.0 − 6.3, between 0 and 1200 °C. Pre-reduction condition in this work was sufficient for near complete pre-reduction.

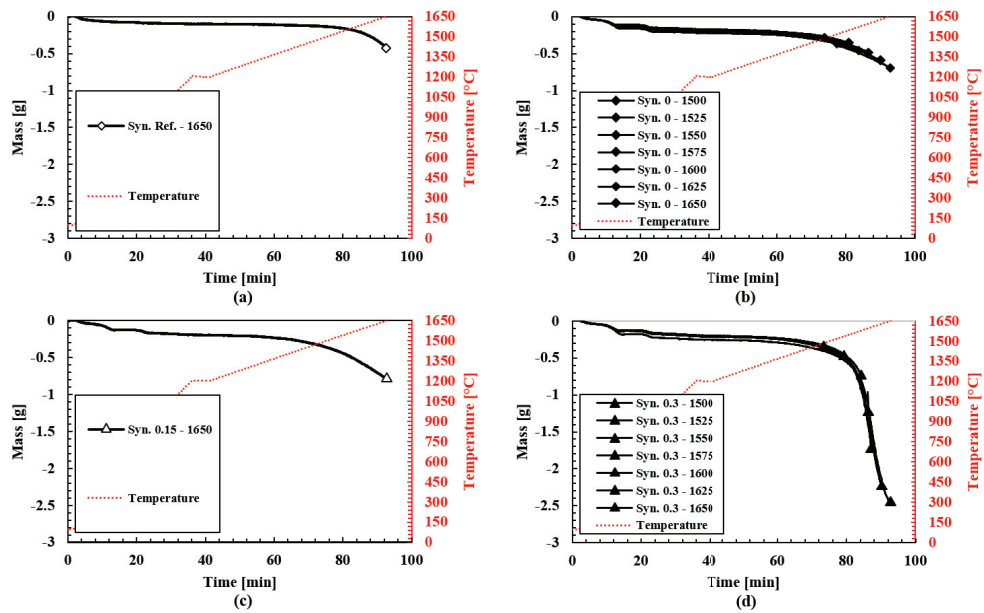**C.2 Charges "As", "As/HCS" and "HCS" (Pre-reduction)**

The individual mass change results of charges "As" (Assmang ore + quartz + coke), "As/HCS" (Assmang ore + quartz + HC FeMn slag + coke) and "HCS" (Assmang ore + quartz + HC FeMn slag + coke) between 25 and 1650 °C are shown in **Figure C.2**. The mass changes of complete pre-reduction for charges "As", "As/HCS" and "HCD" were approximately -1.1, -0.72 and -0.14 g, respectively.
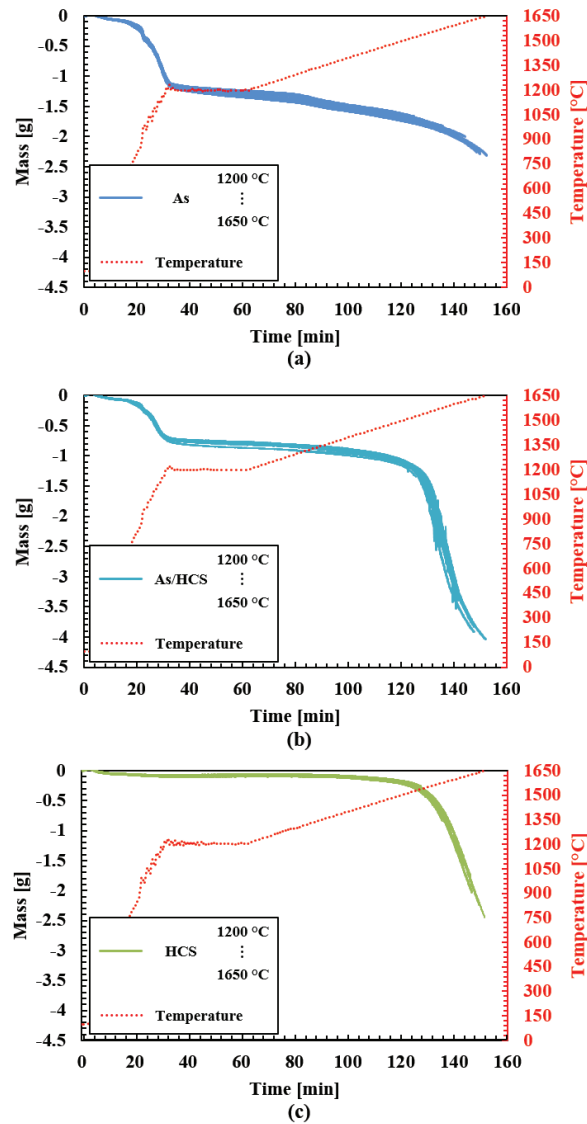
Figure C.2: Individual mass changes of charges (a) "As", (b) "As/HCS" and (c) "HCS" between 25 and 1650 °C. There were 16 experiments between 1500 and 1650 for each charge type.

C.3 Synthetic charges

The individual mass change results of synthetic charges with different amount of sulfur between 25 and 1650 °C are shown in **Figures C.3** and **C.4**. Note that pre-reduction was not required for synthetic charges

Figure C.3: Individual mass change results of charges (a) "Syn. Ref.", (b) "Syn. 0", (c) "Syn. 0.15" and (d) Syn. 0.3" between 25 and 1650 °C.
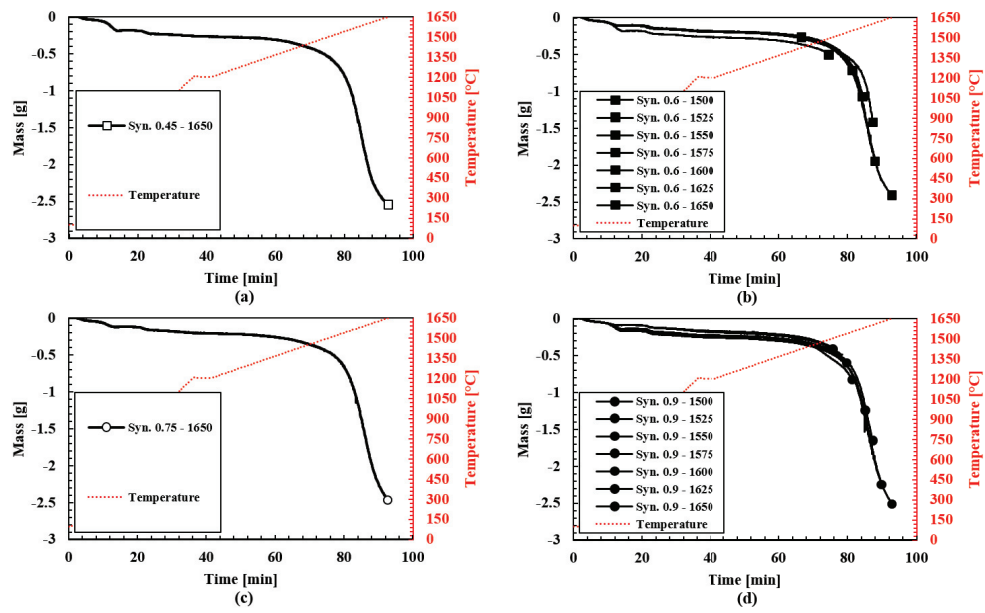
Figure C.4: Individual mass change results of charges (a) "Syn. 0.45.", (b) "Syn. 0.6", (c) "Syn. 0.75" and (d) Syn. 0.9" between 25 and 1650 °C.

Appendix D: BSE images of slag phases

The back scattered electron (BSE) images of the slag phase from charges "As", "As/HCS" (Assmang ore + quartz + HC FeMn slag + coke) and "HCS" (quartz + HC FeMn slag + coke) between 1500 and 1650 °C are shown in this section.
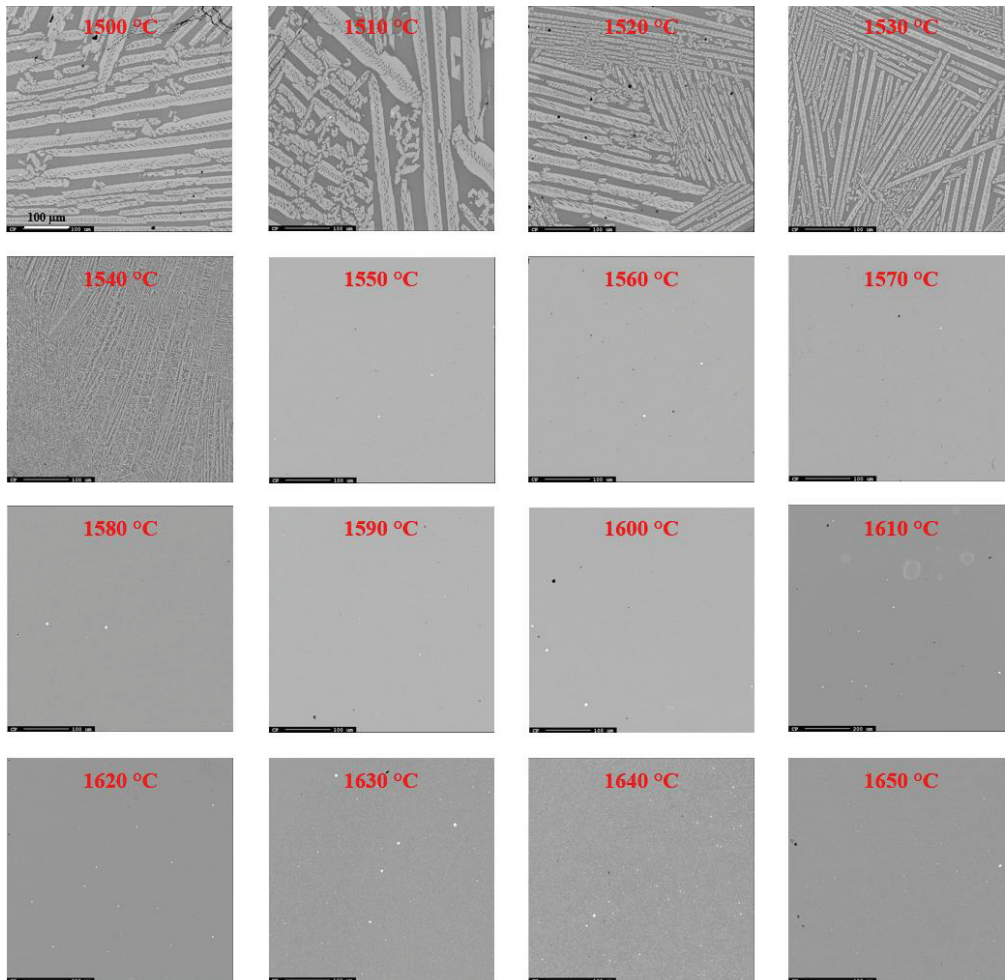
D.1 Charge "As"

The BSE images of charges "As" (Assmang ore + quartz + coke) between 1500 and 1650 °C, where the heating rate was + 4.5 °C/min, are shown in **Figure D.1**.
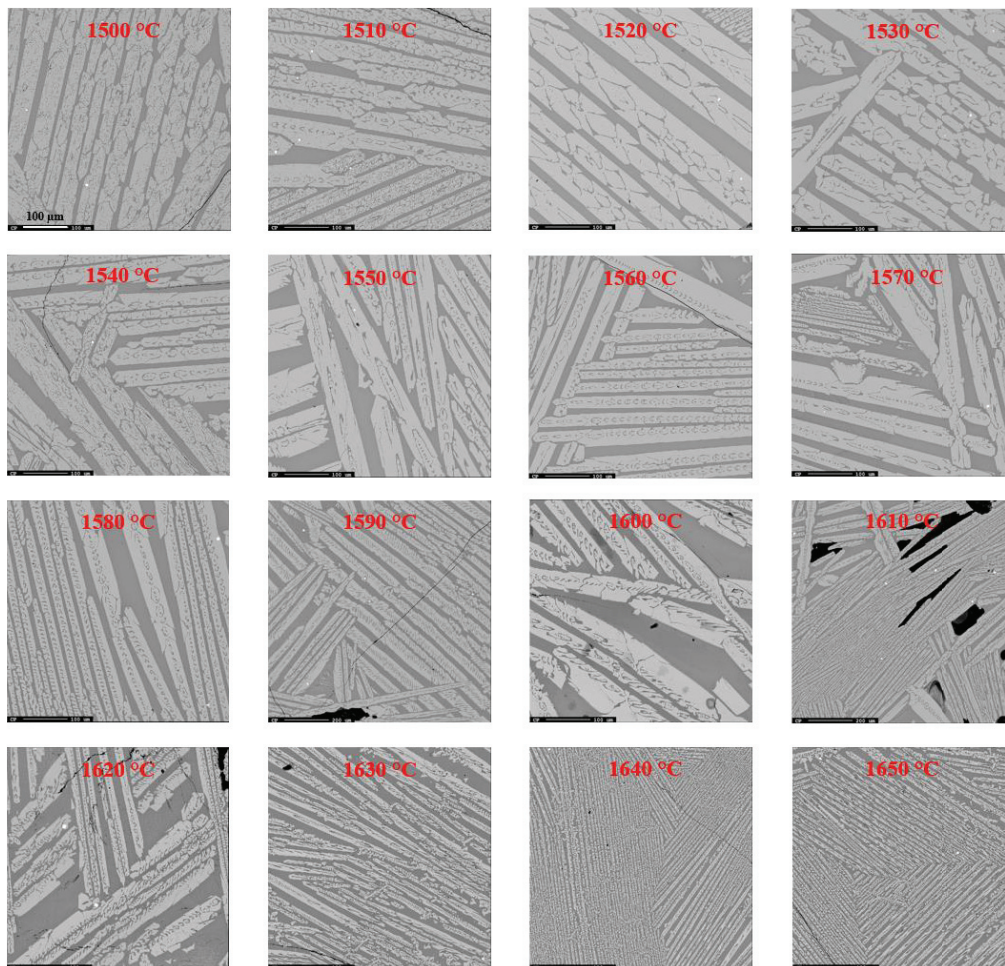
Figure D.1: BSE images of slag phase in charge "As" between 1500 and 1650 °C.

D.2 Charge "As/HCS"

The BSE images of charges "As/HCS" (Assmang ore + quartz + HC FeMn slag + coke) between 1500 and 1650 °C, where the heating rate was + 4.5 °C/min, are shown in **Figure D.2**.

Figure D.2: BSE images of slag phase in charge "As/HCS" between 1500 and 1650 °C**.**

D.3 Charge "HCS"

The BSE images of charges "HCS" (quartz + HC FeMn slag + coke) between 1500 and 1650 °C, where the heating rate was + 4.5 °C/min, are shown in **Figure D.3**.
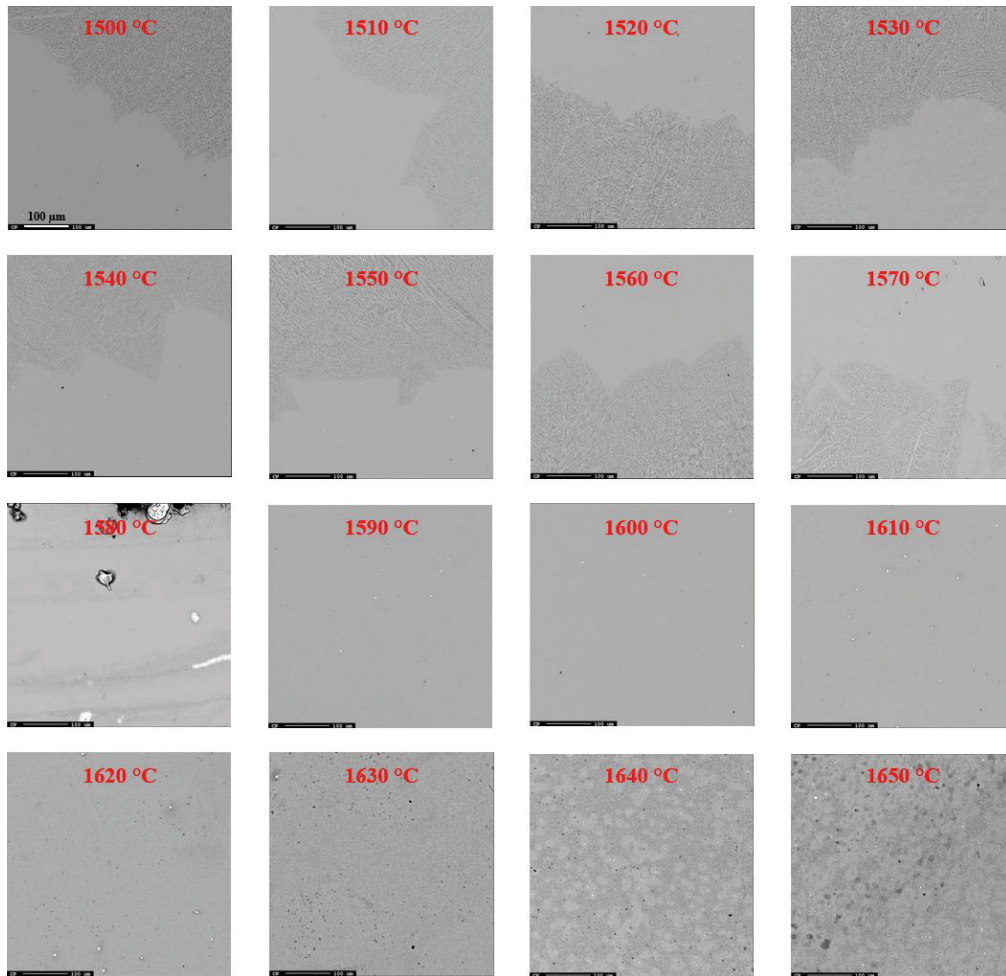
Figure D.3: BSE images of slag phase in charge "HCS" between 1500 and 1650 °C**.**

Appendix E: Calculated slag and metal compositions of charges

The details of calculated slag and metal compositions of charges "As", "As/HCS" and "HCS" are described in this section. The metal compositions were calculated based on the analyzed slag compositions from EPMA. It was assumed that the amount of unreducible oxides (CaO, MgO and Al_2O_3) were constant throughout the experiments. The calculated pre-reduced slag and metal compositions, **Tables A.3**, **A.4**, **A.9**, **A.10**, **A.15** and **A.16**, were used as reference compositions to calculated the slag composition in absolute amount (g). An example using the EPMA analysis of charge "As/HCS" at 1650 °C is shown in the following (**Tables E.1 – E.5**):

Table E.1: Calculated pre-reduced slag composition of charge "As/HCS" at 1200 °C.

Unit	Slag (Calculated)						Metal (Calculated)				
	MnO	SiO_2	CaO	MgO	Al_2O_3	Total	Mn	Si	Fe	C	Total
[wt%]	44.45	34.03	11.48	4.00	6.04	100	-	-	95.93	4.07	100
[g]	3.79	2.90	0.98	0.34	0.52	8.52	-	-	0.42	0.02	0.44

Table E.2: Measured slag composition of charge "As/HCS" at 1650 °C (Before calculations)

Unit	MnO	SiO_2	CaO	MgO	Al_2O_3	Total	Notes
[wt%]	4.88	43.90	26.54	7.06	13.84	96.23	EPMA
[g]	x	y	0.98	0.34	0.52	x + y + 1.84	Constant CaO, MgO and Al_2O_3

The following relation between MnO and SiO_2 in **Table E.2** needs to be satisfied:

$$\frac{x}{y} = \frac{MnO}{SiO_2} = \frac{4.88}{43.90} \approx 0.11$$

and

$$x = 0.11y$$

$$x + y = 0.11y + y = 1.11y$$

Then, the total amount (g) is

$$x + y + 1.84 = 1.11y + 1.84$$

The amount of SiO_2 can be calculated:

$$\frac{y}{1.11y + 1.84} \times 100 = 43.90$$

216

where

$$y \approx 1.57$$

and the following amount of MnO is

$$x \approx 0.18$$

Table E.3: Measured slag composition of charge "As/HCS" at 1650 °C (After calculations).

Unit	MnO	SiO$_2$	CaO	MgO	Al$_2$O$_3$	Total	Notes
[wt%]	4.88	43.90	26.54	7.06	13.84	96.23	EPMA
[g]	0.18	1.57	0.98	0.34	0.52	3.59	Constant CaO, MgO and Al$_2$O$_3$

Comparing the absolute amount of MnO and SiO$_2$ between the compositions at 1200 and 1650 °C, the amount of consumed MnO and SiO$_2$ is calculated:

$$MnO_{(Consumed)}: 3.79_{(1200\,°C)} - 0.18_{(1650\,°C)} = 3.61\ g$$

$$SiO_{2\,(Consumed)}: 2.90_{(1200\,°C)} - 1.57_{(1650\,°C)} = 1.33\ g$$

Then, the amount of manganese and silicon produced can be calculated from the molar relationship between slag (MnO: 70.94 g/mol, SiO$_2$: 60.08 g/mol) and metal (Mn: 54.94 g/mol, Si: 28.09 g/mol):

$$Mn_{(Produced)} = 3.61 \times \frac{54.94}{70.94} \approx 2.80\ g$$

$$Si_{(Produced)} = 1.33 \times \frac{28.09}{60.08} \approx 0.62\ g$$

which gives the metal composition in absolute amount in **Table E.4**.

Table E.4: Calculated metal composition of charge "As/HCS" at 1650 °C (Before calculations)

Unit	Mn	Si	Fe	C	Total	Notes
[wt%]	a	b	c	2.75	a +b +c + 2.75	C: Eq. [3]
[g]	2.80	0.62	0.42	ω	ω + 3.84	Constant Fe

The amount of saturated carbon was calculated from **Equation [3]** in **Section 2.1.2**:

$$C_{(Eq.??)} \approx 2.75\ wt\%$$

Then, the amount of carbon in absolute amount (g) can be calculated by the following relation:

$$C_{(Sat.)} = \frac{0.0275 \times 3.84}{1 - 0.0275} \approx 0.11\ g$$

Finally, **Table E.5** shows the completed slag and metal compositions of charge "As/HCS" at 1650 °C.

Table E.5: Calculated slag and metal compositions of charge "As/HCS" at 1650 °C

| Unit	Slag (EPMA: [wt%] / Calculated: [g])						Metal (Calculated: [g])				
	MnO	SiO$_2$	CaO	MgO	Al$_2$O$_3$	Total	Mn	Si	Fe	C	Total
[wt%]	4.88	43.90	26.54	7.06	13.84	96.23	70.88	15.66	10.71	2.75	100
[g]	0.18	1.57	0.98	0.34	0.52	3.59	2.80	0.62	0.42	0.11	3.95

Note that the calculated slag and metal compositions in other industrials ("As" and "HCS") and synthetic ("Syn. 0", "Syn. 0.3", "Syn. 0.6" and "Syn. 0.9") charges were also obtained by the same method.

Appendix F: The reduction paths of industrial SiMn Charges

The reduction paths of industrial SiMn charges, "As", "As/HCS" and "HCS", from two different heating rates (4.5 and 9 °C/min) are described in this section. Note that the kinetic parameters (activation energy and pre-exponential constant) obtained by the slower heating rate (4.5 °C/min) were applied to the faster heating rate (9 °C/min).

F.1 Charge "As"

The reduction path of charge "As" (Assmang ore + quartz + coke) between 1200 and 1650 °C is described in **Figure F.1**.
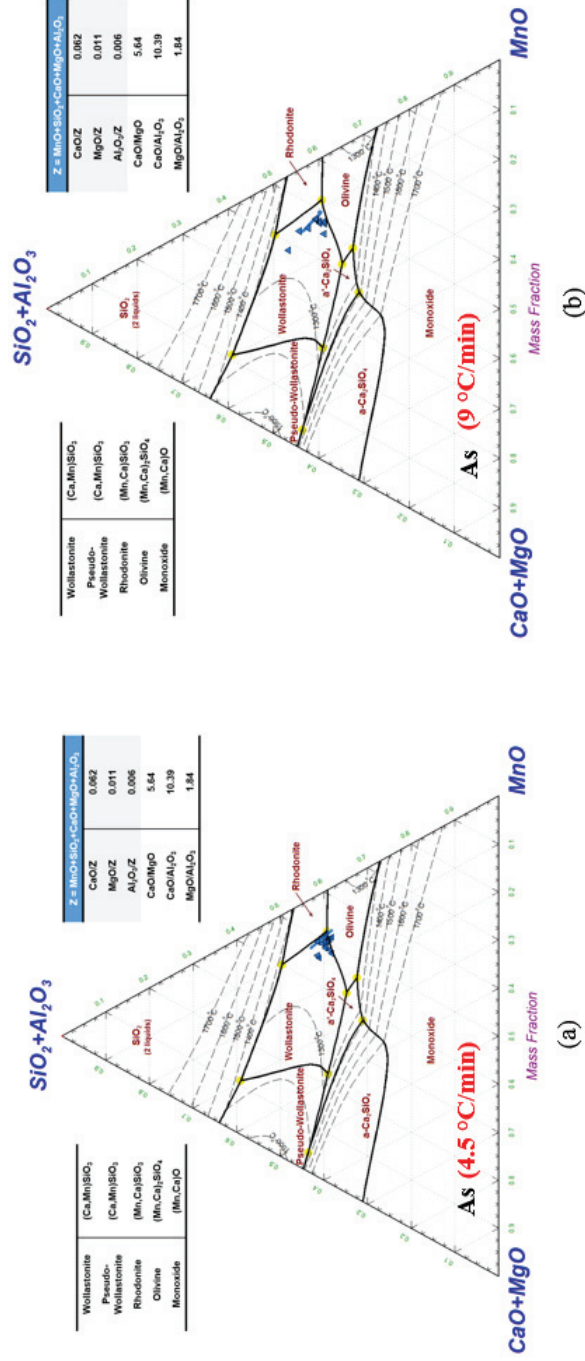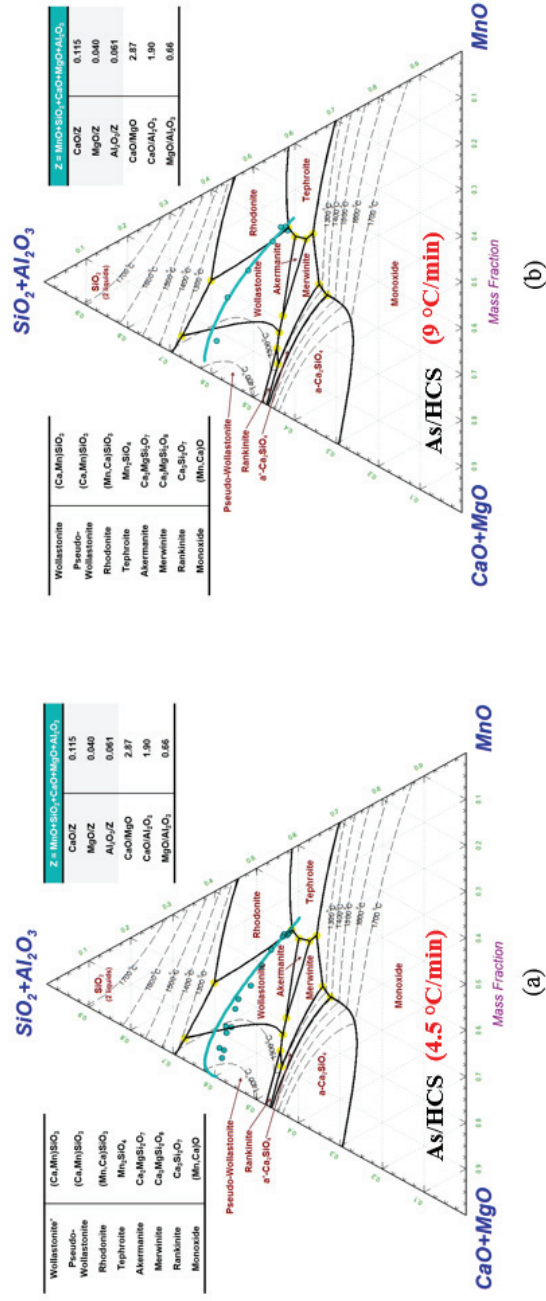

Figure F.1: Reduction path of charge "As" between 1200 and 1650 °C: Heating rate of (a) 4.5 °C/min and (b) 9 °C/min. Lines are the calculated reduction paths from the rate models, and symbols are the measured slag compositions from the experiments. Reduction path is meaningless due to the low reduction of MnO and SiO$_2$.

F.2 Charge "As/HCS"

The reduction path of charge "As/HCS" (Assmang ore + quartz + HC FeMn slag + coke) between 1200 and 1650 °C is described in **Figure F.2.**

Figure F.2: Reduction path of charge "As/HCS" between 1200 and 1650 °C: Heating rate of (a) 4.5 °C/min and (b) 9 °C/min. Lines are the calculated reduction paths from the rate models, and symbols are the measured slag compositions from the experiments. Comparison shows that the rate models were applicable to describe the reduction paths of MnO and SiO_2. Note that the discrepancy of Figure F.2 (a) at high temperatures is from the measurement uncertainties.

F.3 Charge "HCS"

The reduction path of charge "HCS" (quartz + HC FeMn slag + coke) between 1200 and 1650 °C is described in **Figure F.3.**
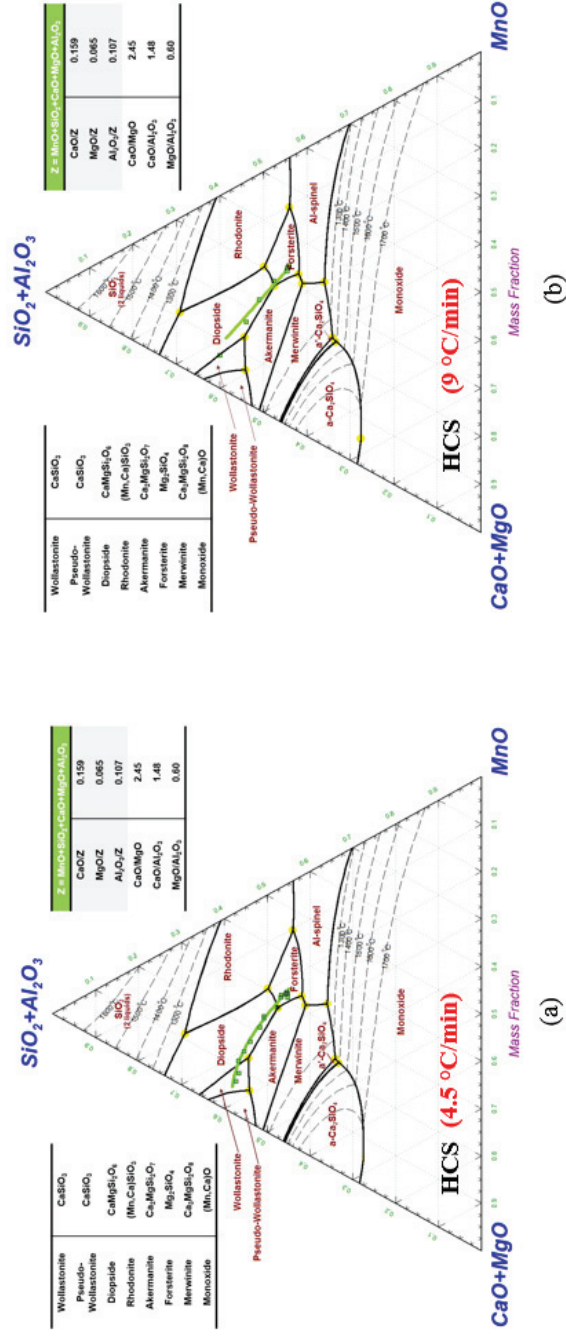

(a)

(b)

Figure F.3: Reduction path of charge "HCS" between 1200 and 1650 °C: Heating rate of (a) 4.5 °C/min and (b) 9 °C/min. Lines are the calculated reduction paths from the rate models, and symbols are the measured slag compositions from the experiments. Comparison shows that the rate models were applicable to describe the reduction paths of MnO and SiO₂.